Generation, evolution and detection of electron entanglement in nanostructures

A thesis presented

by

Elsa Prada

to the

Departamento de Física Teórica de la Materia Condensada

in partial fulfillment of the requirements

for the degree of

Doctor of Philosophy

in the subject of

Physics

Universidad Autónoma de Madrid

Madrid

February 2006

Thesis advisor
Fernando Sols

Author
Elsa Prada

Generation, evolution and detection of electron entanglement in nanostructures

Abstract

Non-locally spin-entangled electron pairs could be used for quantum communication purposes inside a future solid-state-based quantum computer. In this thesis we have addressed three important aspects related to them. First, we have studied the problem of how to generate such EPR-pairs. We have obtained a local tunneling Hamiltonian that permits to investigate transport through interfaces of arbitrary geometry. With it, we have analyzed the emission of two electrons forming a Cooper pair from a superconductor into two normal metals through two narrow tunneling contacts separated by a distance r. To overcome the problem of the quick decay of that current with r, we have proposed a device which makes use of normal and Andreev resonances in a superconducting-2DEG structure to generate divergent beams of nonlocally entangled electrons. In a second part, we have considered the problem of the evolution of those entangled pairs inside a nanostructure when they are subject to decoherence. We have modeled inelastic scattering by means of a phenomenological charge-conserving voltage probe model, conveniently generalized to deal with entangled states. Finally, we have investigated the problem of entanglement detection. We have looked into the violation of the Clauser-Horne inequality expressed in terms of the full electron counting statistics in a mesoscopic multiterminal conductor, finding that there exist parameters of the system for which violation holds for arbitrary strong decoherence. In order to be able to discriminate between singlet-entangled, triplet-entangled or polarized states in the presence of decoherence, we have analyzed the behaviour of shot-noise measurements in one of the outgoing leads of a beam splitter geometry.

Contents

List of Publications of this Thesis

Part of the contents of this work can be found in the following publications:

- E. Prada and F. Sols. *Entangled electron current through finite size normal-superconductor tunneling structures.* The European Physical Journal B **40**, 379 (2004).

- E. Prada, F. Taddei and R. Fazio. *Clauser-Horne inequality and decoherence in mesoscopic conductors.* Physical Review B **72**, 125333 (2005).

  Article selected for the October 3, 2005 issue of Virtual Journal of Nanoscale Science & Technology, Vol. 12, Issue 14 (2005).

  Article selected for the October 2005 issue of Virtual Journal of Quantum Information, Vol. 5, Issue 10 (2005).

- F. Taddei, L. Faoro, E. Prada and R. Fazio. *Clauser-Horne inequality for the full counting statistics.* New Journal of Physics **7**, 183 (2005).

- E. Prada and F. Sols. *Divergent beams of nonlocally entangled electrons emitted from hybrid normal-superconducting structures.* New Journal of Physics **7**, 231 (2005).

- P. San-Jose and E. Prada. *Effect of inelastic scattering on spin entanglement detection through current noise.* Sent to Phys. Rev. B. Preprint archive cond-mat/0601365.

Acknowledgments

I would like to express my deepest gratitude to my husband Pablo. Not only he helped me throughout all the process of this thesis with his sharp intuition in physics, but gave me constant support, specially in the difficult hours, and motivation. I want to sincerely thank my advisor Prof. Fernando Sols for several things. First, for introducing me in this fascinating field of solid state-based quantum information theory; second, for his keen intuition and enthusiasm when speaking about physics; and third, for his help and many wise advices not only in physics but in life in general. I also want to kindly thank Prof. Álvaro Martín Rodero for being my tutor at the Universidad Autónoma de Madrid when my advisor moved to the Universidad Complutense de Madrid in 2004. Besides, I deeply thank Prof. Rosario Fazio and Dr. Fabio Taddei, whom I admire and whom I had the opportunity to collaborate with at the Scuola Normale Superiore of Pisa. I moreover feel very grateful to Prof. Gerd Schön, who gave me the opportunity to finish my thesis in his group at the University of Karlsruhe and to continue my scientific career under his intelligent and determined supervision.

I would like to thank my parents Josefina and José Manuel with all my heart. They made it possible for me to study physics, to proceed towards a research carrier and, specifically, to be able to do all that feeling loved, happy and secure. I also want to thank my little son Adrián because, though he still doesn't know, he has helped me enormously with his happiness and unconditional love during the last part of this thesis, which has been the most fruitful one, surely because of the strength and joy he has given me.

Furthermore, I want to thank a number of people since, in one way or another, they helped me with my thesis and walked by my side part of the way. They are: Miguel Ángel Fernández, Miguel Rey, Ramón Aguado, Geli Vozmediano, Juana Martín, Pedro San José, Eduardo Elizalde, Carlos Sieiro, Christoph Simon, Alfredo Levy Yeyati, José González Carmona and Enrique García Michel.

Moreover, I feel grateful to Markus Buttiker, Carlo Beenakker and Denis Feinberg, who made constructive criticisms to my work.

Finally, I would like to acknowledge the following financial support: Post-graduate Studies Grant from the Universidad Autónoma de Madrid (from October 2000 to March 2001), FPU Grant from the Ministerio de Educación, Cultura y Deporte de España (from April 2001 to September 2002), FPI Grant from the Comunidad Autónoma de Madrid (from October 2002 to January 2005) and European Union - Marie Curie Research Training Networks contract (from February 2005 to present).

Note added after the PhD thesis defence (the 21st of April, 2006): I sincerely thank the members of my thesis board, Prof. Sebatián Vieira, Prof. Gerd Schön, Prof. Christoph Bruder, Prof. Alfredo Levy-Yeyati and Prof. Ramón Aguado, for being there and for their inspiring questions and comments.

To my husband Pablo and to my son Adrián.

To my parents Josefina and José Manuel.

To José Luis.

Chapter 1

Introduction

In quantum mechanics there exists a phenomenon with no classical counterpart whereby a system can be in a superposition of different states at the same time. Moreover, two or more quantum objects can be in a special type of superposition such that the state of the global system cannot be described as the product of the states of its different constituents, even though the individual objects may be spatially separated. These objects are then said to be mutually *entangled* [1, 2]. For example, it is possible to prepare two spin-1/2 particles in a single quantum state called a *singlet* state, such that when one is observed to be spin-up, the other one will always be observed to be spin-down and vice versa. As a result, measurements performed on one of the particles seem to be instantaneously influencing the other particle entangled with it, no matter how far away it is. This "spooky action at a distance", as Albert Einstein called it, is in contradiction with the intuitively obvious principle of *local realism*, which states that physical objects are influenced only by its immediate surroundings and that they must objectively have their properties already before these properties are observed. Schrödinger coined the term "entanglement" to describe this peculiar connection between quantum systems in 1935 [3]. Since then this concept has produced some of the most philosophically disturbing and entertaining questions about the interpretation of quantum mechanics and it is at the core of the quantum world weirdness.

But entanglement is not only of conceptual relevance. From the 1980s onwards, scientists began to think about the non-local correlations of entangled quantum states as a physical resource (like energy), which could open the door to problems untractable inside classical physics in an efficient way, like for example prime factorization of big numbers or the simulation of the dynamic of a quantum system. The new field of *Quantum Information* (QI) had emerged, and soon became the object of attention from different communities of physics, such as quantum optics, nuclear physics or condensed matter physics.

Nowadays there already exist several proposals to build some of the basic ingredients of the *quantum computer* hardware, such as quantum bits or *qubits*, which are

bits of information that are allowed to be in any state of a quantum two-level system. These state pairs might be two polarizations of a photon in an optical cavity, the excess of one nuclear spin state over another in a liquid sample in a nuclear magnetic resonance machine, the ground and excited states of an atom in a linear ion trap, or the spin up and down of an electron confined in a quantum dot, just to mention a few.

One of the requirements to build a quantum computer is that the chosen system can be scaled-up to contain a large number of qubits. In this respect, the schemes for quantum computation based on solid-state qubits are very promising. In particular, the use of the electron spin as the qubit within semiconductors seems a convenient option, since experiments have demonstrated very long lifetimes of electron spin, on the order of 100 nanoseconds [4, 5]. This means that spin transport can be coherent over long distances in semiconductors. Moreover, coherence times of electron spins confined in semiconductor quantum dots were found to be even larger [6, 7].

There is another important task for quantum computation, which belongs to the field of quantum *communication*, namely that of transmitting qubits between distant locations in a faithful way. One way to attain this is to implement the so-called *flying qubits*, which are qubits that can be conveniently moved from place to place [8]. In principle, the natural candidate for these moving qubits is the two polarization states of the photon. But, in order to avoid the problem of having to convert quantum information from spin to light and vice versa in a potentially spin-based quantum computer, it would be very desirable to be able to use mobile electrons as flying qubits. This is the reason why, since 1999, a great deal of theoretical proposals to design an *entangler*, i.e., a source of non-locally entangled pairs, have appeared inside the community of solid-state physics, mainly dealing with the electron spin degree of freedom. It is exactly in this field of knowledge where this thesis must be framed.

To sum up, the main motivation of this thesis has been to understand various properties of electron spin entanglement in nanostructures. Specifically, we have addressed some aspects of the following three important questions:

- How to generate non-local spin-entangled states in solid sate-based devices?
- How to describe its evolution subject to decoherence inside the nanostructure?
- How to detect that entanglement?

In order to elaborate on the description of the content of this thesis it is convenient at this point to give a series of definitions of some basic concepts in the field of QI theory. This is what we do in the next section. Some of those concepts come mainly from a different field from the one this work is devoted to and are not the main message nor the core of this thesis. They are simply useful to establish a common language and to give a broader spectrum to the non-expert reader of the sort of knowledge framework to which our work belongs. A reader already acquainted with

terms such as: qubit, EPR-state, Bell inequality, etc., can jump directly to Sec. 1.2, where we describe in more detail which are the specific problems we have addressed here. Apart from the problems derived from the quantum communication motivation, the dynamics of electron entanglement has stimulated our research into a number of other interesting condensed-matter problems, which we point out in Sec. 1.3. We finish this introduction with Sec. 1.4, where we describe the structure of this thesis.

1.1 Some basic concepts of Quantum Information theory

Here we briefly introduce some historical background and some definitions of the field of QI. This doesn't pretend to be an exhaustive list nor a formal description of the different subjects, but a modest summary of the main concepts that might help the non-expert reader to get an idea of the motivation and the jargon used in this thesis. Most of the definitions are taken from the Stanford Encyclopedia of Philosophy and from Wikipedia (the Internet free encyclopedia), sometimes literally.

1.1.1 Einstein-Podolsky-Rosen paradox

Quantum mechanics is probably one of the most beautiful and experimentally successful theories in scientific history, but also one of the most counterintuitive and challenging for the human reasoning, since it seems to violate some fundamental principles of classical physics we are so familiar with. Around 1927 a group of physicists, which included N. Bohr, W. Heisenberg and M. Born, made a proposal about how to interpret the mathematical formalism of quantum mechanics based in their study of the physics of atoms. Some of the concepts they considered were that the wave-function shouldn't be thought as a real object, but as a mathematical tool whose only physical meaning is our ability to calculate probabilities for the measurements out of it. Besides, the results of measurements are probabilistic not because they reflect our limited knowledge of some properties of the quantum objects, but because measurement outcomes are fundamentally indeterministic. They also discussed the problem of measurement. The asserted that the act of measurement causes an instantaneous "collapse of the wave function". This first general attempt to formulate a correct interpretation of quantum mechanics would be known as the *Copenhagen interpretation* [9–11].

In classical mechanics the state of a system can be described specifying a set of parameters, like for example the positions and momenta of all the particles comprising the system. The evolution of this system can be calculated according to some deterministic laws, in such a way that it is possible to know the value of all those parameters in a future time, and therefore completely characterize the properties of the system. Pauli referred to this way of describing the system as "detached observer"

idealization. Within the Copenhagen interpretation, such a description is not possible for quantum systems. Instead, the quantum state has to be described not only taking into account the properties of the system, but also the presence or action of an observer on it, as well as the outcomes of what has been observed in the past [11].

In 1935 A. Einstein, who rejected the orthodox Copenhagen interpretation of quantum mechanics, co-authored an article with his two postdoctoral research students B. Podolsky and N. Rosen, entitled: "Can Quantum Mechanical Description of Physical Reality Be Considered Complete?" [12]. In the modern version of this thought experiment, two observers, in our days commonly referred to as Alice and Bob (or A and B), perform independent measurements of spin on a pair of electrons in a spin singlet state. According to their reasoning, once Alice has measured her spin in one direction, Bob's measurement in the same direction is determined with certainty, whereas immediately before Alice's measurement Bob's outcome is only statistically determined. Thus, either the effects of measurement can travel from Alice to Bob instantly, or the quantum mechanical description of the those spins is an incomplete characterization of them. In order to avoid non-local, instantaneous "effects at a distance", they concluded that there have to be some unknown deterministic microscopic parameters not included in the theory that cause correlations between particles. The missing parameters are sometimes referred to as *hidden parameters* or *hidden variables* (although they didn't use this terminology). Soon, their paper became a centerpiece in the debate over the interpretation of the quantum theory, and would be referred to as Einstein-Podolsky-Rosen (EPR) paradox [13].

1.1.2 Bell inequalities

After the EPR article the credibility of quantum mechanics was left in an unsatisfactory position, since it seemed that it was either incomplete in the sense that it couldn't describe some elements of physical reality, or it violated the principle of finite propagation speed of physical effects. At that moment, most physicists attributed the puzzling features of entangled quantum states to Einstein's inappropriate "detached observer" view of physical theory and left the question aside. This was unfortunate, because the study of entanglement was ignored for thirty years until J. Bell's reconsideration and extension of the EPR argument in 1964 [1, 14].

Bell reopened the debate on the foundations of quantum mechanics examining the problem of entanglement in simpler systems than the EPR case: he considered correlations between two-valued observable quantities, like polarization or spin, of two separate systems in an entangled state. He derived an inequality based on Einstein's assumptions of "locality" and "realism", which was expressed in terms of joint probability distributions for the outcomes of measurements performed simultaneously in the two separate parts of the entangled state. The measurements were performed for different settings of the measurement apparatus (like, e.g., different polarizer angles). In this way, Bell showed that quantum statistical correlations between those proba-

bilities in different directions of the detectors lead to violation of the inequality. This is summarized in the so-called Bell's theorem: "No physical theory of local hidden variables can ever reproduce all of the predictions of quantum mechanics". The Bell inequality is therefore a test to distinguish quantum from classical correlations by comparing the correlation along different directions [15].

Bell test experiments to date have shown that, indeed, the inequalities of Bell's theorem are violated. This provides empirical evidence against local realism and proves the validity of quantum mechanics. Besides, the principle of special relativity is saved because, although the two entangled particles seem to be interacting across a space-like interval, no useful information is traveling between them, so causality cannot be violated through entanglement. The reason why it is impossible for Alice to pass information to Bob (or vice versa) faster than the speed of light has to do with the *no cloning theorem*, stated by Wootters, Zurek, and Dieks in 1982. This theorem forbids the creation of identical copies of an arbitrary "unknown" state without disturbing it. If Alice and Bob share an entangled pair and it were possible for Bob to clone his qubit many times, then Alice could send him bits of information in the following way. If Alice wanted to send a "1" to Bob, she would measure the spin of her particle in the z direction, collapsing Bob's state to either spin-up or down. If she wanted to send a "0", she would leave her qubit untouched. On his part, Bob would create several copies of his qubit and would measure the spin of each copy in the z direction. If all the measurements yielded the same result, he would know for sure that Alice had measured her spin, obtaining the bit of information "1". If he would measure half of the times up and half of the times down, Alice would have sent him a "0". But the fact is that, due to the existence of the no cloning theorem, it is impossible to make an statistical inspection of entangled quantum states [2, 16].

1.1.3 Quantum information

The general study of the information-processing capabilities of quantum systems is the subject of QI theory [17]. By definition, QI is physical information that is held in the "state" of a quantum system. Two quantum systems in an entangled state can be used as a quantum information channel to perform tasks which are impossible classically. For example, if Alice and Bob share two particles, which we call I (Alice's) and II (Bob's), in a *maximally* entangled state, it is possible for Alice to transfer exactly the state of a third particle she has, let us say, an atom in a complicated state she doesn't know, to Bob's particle II, which is at an arbitrarily distant location. To do this, Alice has to perform a *Bell measurement* over the atom she wants to "teleport" and her particle I of the entangled pair. After doing this measurement the atom to be sent has lost its former state, but the information of its initial state has not been destroyed, its has been transferred to particle II by virtue of the previously existing entanglement, but not completely. It is necessary that Alice communicates the outcome of her measurement to Bob classically (for example with a telephone call),

so that Bob can make a unitary operation onto his particle. After this he obtains the desired state. This phenomenon is known as *quantum teleportation* [18]. In 1993 C. H. Bennett et al. proposed a scheme that in principle could be used to teleport an object [19]. The scheme was experimentally verified by D. Bouwmeester et al. in 1997 using photons [20]. It is also possible to use entangled pairs in *quantum cryptography*, where entanglement is used to transmit signals that cannot be eavesdropped upon without leaving a trace.

Quantum information differs from classical information in several respects. For example, it cannot be read or duplicated without disturbance (no cloning theorem). Furthermore, since one system can exist in a superposition of many different states at once, it is possible to process quantum information in a "parallel" way, i.e., exponentially more efficiently than classical information. This permits to perform some difficult tasks in an "efficient" way, i.e., in a time that increases polynomially with the size of the problem. In contrast, these same tasks would be inefficient in a classical context, because they would demand a time which increases exponentially with the complexity of the problem. On the other hand, QI cannot be completely retrieved through measurements of the qubits or any other means. Therefore, this massive *parallelism* of quantum computations can only be exploited by the use of clever algorithms, adapted to the peculiarities of quantum mechanical laws.

Quantum information, and changes in quantum information, can be quantified by using a quantum analogue of the classical Shannon entropy, which is the Von Neumann entropy [17].

1.1.4 Qubit and ebit

The basic unit of quantum information is the quantum bit or *qubit*, which represents the amount of information that can be stored in a two-level quantum mechanical system. The term is due to Schumacher (1995) [21]. The state space of a single qubit can be represented geometrically by the two dimensional surface of a sphere. This essentially means that the single qubit space has two local degrees of freedom. Equivalently, an n-qubit register space has (roughly) 2^n continuous degrees of freedom. In contrast, the configuration space of a classical register is strictly discrete, and therefore infinitely smaller.

An arbitrarily large amount of classical information can be encoded in a qubit. This information can be processed and communicated but, because of the peculiarities of quantum measurement, the amount of information that can be retrieved from a single qubit is equal to one bit. It is in the processing of information (quantum computation) that a difference occurs.

An important distinguishing feature between a qubit and a classical bit is that multiple qubits can exhibit quantum entanglement. We say that two qubits in two spatially separated points A and B are entangled when their state cannot be prepared from a product state of the qubit in A and the qubit in B by means of local operations

in each qubit and classical communication of bits of information between them. Two qubits in a *maximally* entangled state are called entangled bit or *ebit*. The four basic pure entangled states which form the Bell basis are:

$$|\Psi_{Bell_1}\rangle = \frac{1}{\sqrt{2}}\left(|\uparrow\rangle_A|\downarrow\rangle_B - |\downarrow\rangle_A|\uparrow\rangle_B\right), \tag{1.1}$$

$$|\Psi_{Bell_2}\rangle = \frac{1}{\sqrt{2}}\left(|\uparrow\rangle_A|\downarrow\rangle_B + |\downarrow\rangle_A|\uparrow\rangle_B\right), \tag{1.2}$$

$$|\Psi_{Bell_3}\rangle = \frac{1}{\sqrt{2}}\left(|\uparrow\rangle_A|\uparrow\rangle_B - |\downarrow\rangle_A|\downarrow\rangle_B\right), \tag{1.3}$$

$$|\Psi_{Bell_4}\rangle = \frac{1}{\sqrt{2}}\left(|\uparrow\rangle_A|\uparrow\rangle_B + |\downarrow\rangle_A|\downarrow\rangle_B\right), \tag{1.4}$$

where the arrows $\uparrow, \downarrow$ represent, for instance, the spin-up and the spin-down states of an electron. One ebit is also the amount of information we need to exchange between two qubits in A and B to create an entangled state out of them.

Entanglement is a necessary ingredient of any quantum computation that cannot be simulated efficiently on a classical computer. A possible picture that helps to understand the power of quantum computing is that, by means of entanglement, a quantum computer performing a computation is in a superposition of many different classical computations, all of which proceed concurrently.

1.1.5 Quantum computers

A quantum computer (QC) [1, 22] is any physical device that makes direct use of entanglement to perform operations on data. Due to this, QC promise to increase greatly the efficiency of solving some problems with respect to the possibilities of classical computers. One of these problems is *integer factorization*. If a number has n bits (i.e., it is n digits long when written in the binary numeral system), then a QC with just over 2n qubits can use Shor's algorithm (1994) to find its factors. Another problem is called the *discrete log problem*. This ability would allow a QC to "break" many of the cryptographic systems in use today, in the sense that there would be a relatively fast (polynomial in n computation time) algorithm for solving the problem. Another interesting problem which could only be solved with a QC was proposed by Richard Feynman in 1982 [23]. It is the *simulation of the dynamics of quantum systems*. The dramatic advantage of QC is currently known to exist for only those three problems: factoring, discrete log, and quantum physics simulations. However, there is no proof that the advantage is real: it is still possible that an equally fast classical algorithm may be discovered, although it is considered unlikely. There is yet other problem where QC have a smaller, though significant (quadratic) advantage. It is quantum database search, and can be solved by *Grover's algorithm*. In this case the advantage is provable. This establishes beyond doubt that (ideal) quantum computers are potentially superior to classical computers [22].

One of the greatest challenges nowadays is to implement the basic quantum computational elements in a physical system and to demonstrate that they can be reliably and scalably controlled. Experiments have already been carried out in which quantum computational operations were executed on a very small number of qubits. In particular, in 2001 I. L. Chuang and his group performed the world's most complicated QC calculation to date, a 7-qubit computer (based on nuclear magnetic resonance on molecules in solution) that factorized the number 15 using Shor's algorithm [24].

How a quantum computer works

A classical computer has a memory made up of bits, where each bit holds either a one or a zero. This device computes by manipulating those bits, i.e. by transporting them from memory to *logic gates* and back. By "gates" is meant the set of transformations that make up a computation. The same philosophy applies to a QC, but with some differences. First, it contains a set of qubits. As we said before, a qubit can hold a one, a zero, or any superposition of both states. Therefore, if we have in memory a n-qubit register, the total state of the QC is a superposition of as many as 2^n states, each of them classically equivalent to a single list of n 1's and 0's. Like before, a QC operates by manipulating those qubits, but now it transports them from memory to *quantum logic gates* and back. Quantum logic gates act on qubits by applying unitary (reversible) transformations. Besides they work with superpositions, so they can perform multiple logic operations at the same time. For practical reasons, it is convenient to choose sets of *universal* quantum gates. These are sets of gates from which any computation can be constructed, or at least approximated as precisely as desired. Such a set allows one to perform any arbitrary calculation without inventing a new gate each time. It can be shown that all unitary quantum operations on an n-qubit register that one could think of, can be implemented by combinations of a single-qubit unitary gate (a rotation) and a two-qubit controlled-NOT gate. The concept of a universal quantum computer was first proposed in 1985 by D. Deutsch. Another important difference with respect to a classical computer is that quantum computations are probabilistic. In a QC, at the end of the calculation a measurement is performed on the n-qubit register. By the laws of quantum mechanics, that measurement will yield a random n-bit string and will destroy the stored state as well. In order to be able to use a QC to get the solution of a desired calculation, the computation has to be designed in such a way that the probability distribution of the measured output string is skewed in favour of the correct value of the function. Thus, generally one has to repeat the computation several times and choose the value that has come out with higher probability [22, 25].

Requirements of a quantum computer

There exists some requisites for a successful implementation of a QC. D. DiVincenzo listed the following requirements for a practical QC [22, 26]:

- the qubits have to be able to be initialized to arbitrary values,
- quantum gates have to work faster than decoherence time,
- there must exist a universal set of quantum gates,
- the qubits have to be read easily, and
- it has to be scalable, i.e., it has to be possible to enlarge the device to contain many qubits while still adhering to all requirements described above.

Apart from these five QC criteria, there also exist two QC networkability criteria, which are two "desiderata" that are important for performing quantum communication tasks [8]. They are:

- the ability to inter-convert stationary and flying qubits, and
- the ability to faithfully transmit flying qubits between specified locations.

Proposals for quantum computers

Many setups have been proposed for the hardware of a QC arising from different fields of research. Some of them are:

- Trapped ion QC → The earliest proposal using these systems came from J. I. Cirac and P. Zoller in 1995 [27]. Ions, or charged atomic particles, can be confined and suspended in free space using electromagnetic fields. They are then said to be "trapped" in magnetic traps. Qubits are stored in stable electronic states of each ion, and QI can be processed and transferred through the collective quantized motion of the ions in the trap (interacting through the Coulomb force). Lasers are applied to induce coupling between the qubit states (for single qubit operations) or coupling between the internal qubit states and the external motional states (for entanglement between qubits). The fundamental operations of a QC have been demonstrated experimentally with high accuracy in trapped ion systems, and a strategy has been developed for scaling the system to arbitrarily large number of qubits by shuttling ions in an array of ion traps. Nevertheless, ion trap computers are limited in speed by the vibration frequency of the modes in the trap.

- Cavity quantum electrodynamics (CQED)-based QC → This term refers to the coherent interaction of a material qubit (such as a trapped atom or semiconductor dot system) with the quantized (usually single photon) field of a optical or microwave resonator. To achieve coherent dynamics with just a single photon and atom, a small, extremely low-loss build-up cavity is used to enhance the electric field per photon such that the coherent Rabi frequency of the atom-field interaction is faster than the spontaneous emission rate of the atom or the decay rate of the field in the cavity. The first proposal of this kind was done by P. Domokos et al. in 1995 where Rydberg atoms and a superconducting millimeter-wave cavity were used [28].

- Nuclear magnetic resonance (NMR) on molecules in solution-based QC → Nuclear spins of molecules in a solution serve as qubits. The nuclear spins can interact with each other, be programmed by radio frequency pulses and be detected by NMR instruments similar to those commonly used in hospitals and chemistry labs. The first proposal for this kind of systems came from A. Gershenfeld and I. L. Chuang in 1997 [29]. As a result of several significant experiments, NMR has become the most popular component in quantum hardware architecture. Nevertheless, NMR devices have an exponential attenuation of signal to noise as the number of qubits in a system increases.

- Superconductor-based QC (charge-based or flux-based QC) → Solid-state implementations of a QC would be a highly desirable achievement, particularly nanometre-scale electronic devices, since these could be easily embedded in electronic circuitry and scaled up to provide the large numbers of qubits required for useful computations. Among the first proposals for solid-state quantum computing were qubits based on superconducting Josephson junctions, proposed by A. Shnirman, G. Schön and Z. Hermon in 1997 [30–32]. In this proposal two kinds of devices have been suggested, based on either charge or phase (flux) degrees of freedom. Single- and two-qubit quantum manipulations can be controlled by gate voltages in one case and by magnetic fields in the other case. Both kinds of devices can be fabricated with present technology. There are two major problems that must be solved before these devices can be used for quantum information processing, decoherence times and the readout of the final state of the system [31, 32].

- Quantum dot electron spin-based QC → In 1998 D. Loss and D. P. DiVincenzo opened up the field of spin-based solid-state quantum computation by proposing the spin of an electron trapped in a quantum dot as the qubit [8, 33]. Spin-based quantum computation relies on qubit-qubit interactions to implement two-qubit gates where the charged spin qubits can interact with each other via the Coulomb exchange interaction. The major drawback of this proposal is the decoherence of the spin qubits due to interactions with the environment.

- Optic-based QC → One of the earliest proposals for quantum computation is based on implementing a quantum bit with two optical modes of a photon. The proposal is appealing because of the ease with which photon interference can be observed. But the need for qubit-qubit interactions represents a major drawback because photons do not ordinarily interact; nonlinear optical media can mediate photon-photon interaction, but it is technically difficult to make these perform with the required strength. However, E. Knill et al. showed in 2001 that efficient quantum computation is possible using linear optics, using only beam splitters, phase shifters, single photon sources and photo-detectors. This method exploits feedback from photo-detectors and is robust against errors from photon loss and detector inefficiency [34]. Nevertheless, free-photon quantum computation schemes are so far only nearly deterministic (i.e., the quantum gates operate with less than 100% success).

- Free electron QC → Qubit-qubit interactions are, in principle, a crucial ingredient for quantum computation. Most of the proposals and experiments rely on controlled qubit-qubit interactions to implement universal two-qubit gates. Nevertheless, Beenakker et al. [35] showed in 2004 that projective measurements together with single spin rotations on electron spin flying qubits can yield efficient and deterministic quantum computation. In this way no qubit-qubit interaction is needed, and thus free-electron quantum computation is possible. To overcome a theorem that seemed to preclude efficient quantum computation with free electrons, these authors used the fact that charge measurements do not affect the spin qubit. However, this proposal, which contains a spin-polarizing beam-splitter, is not yet experimentally accessible.

1.1.6 Decoherence

For a QC to work it is necessary that the operations performed by the gates during a calculation are unitary, that is, reversible. Besides, the states that are often used as the input of those gates have to arrive there effectively in a specific superposition of states or in an entangled state. However, in the real world there are interactions that break the coherent state in which the components of a QC need to remain in order to fulfil those operations. In general, it is very difficult to shield these devices completely from extrinsic and intrinsic sources of decoherence, and so far QC have only solved trivial problems. For the typical systems proposed as candidates for quantum computing, the decoherence times vary from nanoseconds to seconds. It is necessary for a calculation to be done successfully that the time required to do it be much smaller than the decoherence time, at least without employing *quantum error correction*. The *error rate* is precisely defined as the ratio of the operation time to the decoherence time. If the error rate is small enough, it is possible to use quantum error correction, which corrects errors due to decoherence. An often cited (but rather

arbitrary) figure for maximum error rate in each gate is 10^{-4}. This implies that each gate must be able to perform its task 10000 times faster than the decoherence time of the system [22].

1.2 The problems treated in this thesis

As we already mentioned at the beginning of this introduction, in the last seven years there has been a frenetic activity inside the field of solid-state-based flying qubits. The study of how to create and measure non-locally entangled particles has attracted the interest of physicists for its potential use in quantum communication tasks, like quantum teleportation or quantum cryptography. Furthermore, a proposal to build a free electron quantum computer with flying qubits already exists in the literature [35]. Here we describe our contribution to the field together with previous proposals that motivated our work and some new ideas from other groups.

1.2.1 Non-local entanglement generation in solid state devices

An entangler is a device which serves as a source of non-locally entangled states. In the recent years there has been a large amount of proposals to build such a device within a solid-state medium.

One possibility is using conventional superconductors as a natural source of spin entangled electron pairs that may be injected into normal or ferromagnetic metals [36–57]. In order to obtain the needed spacial separation of the two electrons when they are extracted from the superconductor several mechanisms have been proposed, like spin and energy filters [41, 46, 49], two quantum dots [38, 49, 53], the use of Luttinger-liquid leads [45, 47] or Coulomb blockade from the finite resistance leads [50]. Our proposed mechanism, as we will show below, is an angular filter [54].

Other than through the use of superconductors, many other ways to generate these EPR states have been proposed: by means of a magnetic impurity [58], through a single dot [59], from biexcitons in double quantum dots [60], through a triple dot [61], using chaotic quantum dots [62], from Coulomb scattering in a two-dimensional electron gas [63] or between static and flying qubits in a carbon nanotube [64, 65], using voltage pulses [66], through a nano-mechanical oscillator [67] or from buckling nanobars [68].

Within the set of mechanisms for generating pairs of entangled qubits there is a group where no interactions are needed to create them (in all the cases cited above some kind of electron-electron interaction was always present, like the phonon-mediated pairing interaction in the superconductor, or the Coulomb interaction in the quantum dot, etc.). In the absence of interactions it is still possible to entangle

the spin degree of freedom [69–71], or the orbital degree of freedom [62, 72–74]. For a recent review on electron-hole entanglement free of interactions see Ref. [75].

As we explain in the following section, in this thesis we have focused on the study of a superconductor as a source of entangled pairs. In our case, the degree of freedom which is entangled is the spin. Spin entanglement is much less sensitive to decoherence than orbital entanglement, simply because most external degrees of freedom couple to the orbital degree of freedom of the electron rather than to its spin.

Our proposals

We have studied two types of entanglers in which the source of non-locally entangled pairs is a BCS conventional superconductor.

In the first work [51], which is described in detail in Chapter 2, we were inspired by the 2001 article of Recher, Sukhorukov, and Loss [38]. There we theoretically investigate the simultaneous emission of two electrons from a three-dimensional (3D) superconductor into two different normal metals at low temperatures and voltages (this process is usually called "crossed Andreev reflection"). These electrons, which form a Cooper pair inside the superconductor, lose the superconductor correlations when they jump into the normal metals (we disregard proximity effect), but the singlet spin-entanglement between them holds when they are in the two distant metallic wires, thus constituting an ebit of information. In order to describe the tunneling current from a finite size interface such as the one formed by the 3D superconductor and the two distant contacts attached to it, we have obtained a local tunneling Hamiltonian involving the normal derivatives of the electron fields in each electrode (instead of the commonly used but erroneous one that is proportional to the fields). We find that, as a function of the distance r between contacts, the entangled current is cut off by an exponential decay with the superconductor coherence length [38], and further modulated by a geometrical prefactor ($\sim 1/r^4$) which makes the probability to extract entangled pairs to decay quickly on the scale of the Fermi wavelength. Therefore, in this work we conclude that the requirement of physical separation between the contacts attached to the superconductor is a severe limitation in practice. We note that, if the tunneling matrix elements are assumed to be momentum independent [38], then the geometrical prefactor decays more leniently with distance ($\sim 1/r^2$). There have been some ideas in the literature to try to improve this decaying prefactor. Within the context of momentum-independent tunneling models, the power law changes if the superconductor is low (d) dimensional [45, 49], or diffusive [48, 52], yielding r^{-d+1} and r^{-1}, respectively. It remains to be investigated how that behaviour changes when more realistic tunnel matrix elements are employed.

To overcome the shortcomings caused by the need to emit the pair of entangled electrons from distant points, we propose a different experimental setup [54], analyzed in detail in Chapter 3, in which the emitter is again a BCS superconductor. The idea behind it is to transmit both electrons through the same spatial region but

inducing them to leave in different directions. To attain this we propose the use of normal and Andreev resonances in normal-superconducting structures. Resonant levels are tuned to selectively transmit electrons with specific values of the momentum perpendicular to the interface, thus fixing the magnitude of the exit angle. When the normal metal is a ballistic two-dimensional electron gas (2DEG), the proposed scheme guarantees arbitrarily large spatial separation of the entangled electron beams emitted from a finite interface. We have performed a quantitative study of the linear and nonlinear transport properties of some suitable structures, taking into account the large mismatch in effective masses and Fermi wavelengths. Numerical estimates confirm the feasibility of the proposed beam separation method. Besides, the type of structures needed for this kind of device seems to be within the reach of current experimental expertise [76, 77].

1.2.2 Evolution of entangled states in nanostructures: decoherence

In real systems electrons are unavoidably coupled to external degrees of freedom. As a result, dephasing (term we will normally use if energy is conserved) or decoherence (in general) takes place, thereby reducing and eventually destroying entanglement. Understanding the consequences of this phenomenon is an important issue.

For spin entanglement, the spin-orbit interaction and the hyperfine interaction with nuclear spins are effective mechanisms of dephasing and relaxation. For a review on decoherence of electron spins confined to quantum dots in the context of the Loss-DiVincenzo proposal [33] see Ref. [8].

For orbital entanglement, the electromagnetic fluctuations caused by other charges lead to decoherence (or to dephasing if the fluctuations are slow enough). Various phenomenological methods have been developed to treat its effect in transport through mesoscopic conductors. In Refs. [73,74,78,79] the effect of dephasing was mimicked by introducing in the density matrix of the electronic entangled states a phenomenological parameter which suppressed its off-diagonal elements. In Refs. [72, 80] dephasing was introduced averaging over an uniform distribution of random phase factors accumulated in each edge channel of the quantum Hall bar. In Refs. [81, 82], which actually describe exactly nonequilibrium radiation acting on the system, dephasing was induced by a classical fluctuating potential. In Ref. [83], dephasing was treated as random fluctuations of the phase of propagating modes through the conductor. These two last methods have been recently applied to full counting statistics (FCS) in Refs. [84, 85].

It is also possible to treat decoherence phenomenologically as due to the presence of additional fictitious reservoirs or voltage probes attached to the mesoscopic conductor under study. This method, which mimics the effect of inelastic processes, was

introduced by Büttiker twenty years ago [86,87]. The advantage of this model resides in the fact that inelastic, phase randomization processes are implemented within an elastic, time-independent scattering framework. Ideally, a voltage probe is an infinite impedance terminal with zero net current flow, i.e. any electron leaving the conductor through the probe is thermalized by dissipation and immediately fed back into the conductor. Early theory [87] used these dissipative voltage probes as simple means to investigate the transition from quantum coherent conduction to the classical series addition of resistances. Later on, it was generalized to include instantaneous current conservation [88]. Moreover, it was realized that, theoretically, dissipation at a probe can be suppressed by demanding that each electron exiting into the probe is replaced by an electron incident from the probe at the same energy [89, 90]. Such a dephasing probe can serve as a simple model to describe dephasing in mesoscopic conduction processes. Alternatively, it is a good model for a real infinite-impedance voltage probe, a common component of many mesoscopic devices.

Voltage and dephasing probes also play an important role in the investigation of noise and current correlations in mesoscopic conductors [85, 88–94]. The validity of the model has been widely discussed (for a review see Ref. [95]), in general finding good qualitative agreement with microscopic models [96–99] and experiments [100, 101], although in certain systems failing at a quantitative level [82]. Recently it was demonstrated to become equivalent to microscopic phase averaging techniques at the FCS level in some limits and setups [102]. Besides, recently it has been used to model spin-flip scattering and decoherence in chaotic quantum dots [103, 104].

Nevertheless, the problem of how to apply such decoherence model to the particularly interesting case of nonlocally entangled input currents had not been previously discussed to the best of our knowledge. This is what we have done [93, 94] and what we summarize below.

Phenomenological model for inelastic scattering

In Ref. [93] we treat the effect of inelastic scattering, as produced by the presence of additional fictitious reservoirs [86,87], over a pair of non-locally entangled electron states and its consequences for detection of entanglement. Decoherence is parameterized by an inelastic scattering probability α and it affects both the spin and the energy degrees of freedom. However, in this work, which is presented here in Chapter 4, we don't consider instantaneous conservation of the current that flows in and out of the external reservoir, but we set it to zero only on average. In this sense we are not describing a true voltage probe attached to the system, since by definition it should have an infinite impedance an therefore zero instantaneous net current flow through it.

We have solved this problem in Ref. [94], where we develop a modification of the fictitious voltage probe model generalized to include instantaneous current conservation in the presence of arbitrary incoming entangled states. Our generalization

is specifically targeted towards the computation of the FCS of a generic mesoscopic conductor and, by using a different voltage probe for each spin, we conserve spin but not the energy degree of freedom. This problem is described in detail in Chapter 5. Let us add here that, in our method, a sequential scattering approximation is implicit. If we wanted to describe only dephasing, i.e, phase memory loss without exchange of energy, then different energies would decouple in the elastic scattering problem and we could treat each energy separately. But in the presence of inelastic scattering this is not possible anymore. In order to deal with this, instead of using the energy representation, what we do is to use the wave packet representation, in which localized electrons arrive at the voltage probe at fixed times. In this language, an electron that in the absence of inelastic scattering would arrive to a detector at a time τ_i, in the presence of inelastic scattering is delayed and arrives at a later one $\tau_i + \delta t$, which is equivalent to energy relaxation. Moreover, in our calculation we ignore the wave packet overlap, this is, we divide the time in slices Δt in such a way that each particle group scatters through the system completely before the next one comes. What we suggest is that the contribution coming from this overlap is negligible in the long time limit. We don't prove this statement, we just justify it by obtaining with our method exactly the same analytical expressions for current and all cumulants (for the characteristic function) as with the Langevin semiclassical approximation [88] in a series of systems without incident entanglement. Inelastic scattering is specifically taken into account in our model through the memory that a quantum counter Q we introduce in the voltage probe keeps of each event. It works in such a way that it tends to counteract the excess or absence of particles the probe got in the previous event, therefore modeling charge relaxation. Thus, this counter correlates one slice Δt with the following one and so on. With this model we try to phenomenologically characterize the inelastic scattering produced onto the electrons by an external dissipative bath (not electron-electron interaction).

1.2.3 Detection of entanglement

Besides its generation, a crucial issue is that of the detection of entanglement. By means of a beam-splitter, entanglement can be detected in transport through an analysis of current noise [105–107] or higher cumulants (FCS) [94, 108]. Furthermore, the presence of entanglement can be revealed by analyzing Bell inequalities and quantities like concurrence [109], which have been expressed in terms of zero-frequency charge- and spin-current noise [41, 46, 72, 73, 110–112]. Violation of a Bell inequality implies that there exist quantum correlations between the detected particles that cannot be described by any local hidden variables theory. In the same spirit as it was done for the noise, in Ref. [113] a Clauser-Horne (CH) inequality [1] [115, 116] was derived for the FCS.

[1] Given the conditions $|x|, |x'|, |y|, |y'| \leq 1$, the the so-called CH (or CH74) inequality is derived from the algebraic inequality $-1 \leq xy - xy' + x'y + x'y' - x' - y \leq 0$. In reality, there is an infinite

Clauser-Horne inequality and shot noise in a beam splitter

In Refs. [93, 117] we analyze the effect of decoherence on the violation of the CH inequality, when it is expressed in terms of the FCS, in a mesoscopic multiterminal conductor. There, the setup consists of an entangler, whose existence is assumed, that emits a flux of entangled electrons into two conductors characterized by a scattering matrix and subject to decoherence (as explained in the previous subsection). Given a certain average number of incoming entangled electrons, we evaluate the CH inequality as a function of the numbers of detected particles and of the various quantities characterizing the scattering matrix. When decoherence is turned on, we show that the amount of violation of the CH inequality is effectively reduced. Interestingly we find that, by adjusting the parameters of the system, there exists a protected region of values of the detected particles for which violation holds for arbitrary strong decoherence. This work is presented here in Chapter 4.

In Chapter 5 we present the results of Ref. [94]. There we analyze the robustness of the entanglement detection scheme through a beam-splitter geometry proposed in Ref. [106], in the presence of spin-conserving inelastic scattering and finite backscattering for various incoming non-locally entangled current states. We find that, unlike elastic orbital dephasing [73], the action of inelastic processes in the beam-splitter cannot be neglected, since it directly affects the underlying physical mechanism of the detector, which is the fact that two electrons with equal quantum numbers cannot be scattered into the same quantum channel (Pauli blocking). If energy is not conserved, such antibunching mechanism is no longer perfect, and the entanglement detection scheme has to be revised. However, we find that the detection of entanglement through shot noise measurements remains possible even under very relaxed conditions for imperfections in the beam-splitter device and substantial inelastic scattering (up to 50%).

1.3 Other motivations and contributions of this thesis

Along with the main motivation of this thesis, which is the study of quantum communication problems in solid-state devices, we have faced other interesting topics inside the field of Condensed Matter physics. We provide here with a brief summary of other contributions we have made in this thesis and other tools we have used:

- Probably the most important technical contribution of this thesis is the study we have done in Chapter 2 of a local tunneling Hamiltonian that permits to investigate transport through interfaces of arbitrary geometry and potential

hierarchy of such Bell type inequalities, which can basically be classified by specifying the type of correlation experiments they deal with [114].

barrier shapes [51]. We prove that, in a 3D or 2D heterostructure, the bilinear momentum dependence of the low-energy tunneling matrix element translates into a real space Hamiltonian involving the normal derivatives of the electron fields in each electrode. We also derived this form from a tight-binding description. Besides we show that, in a ballistic metal, the neglect of the momentum dependence of tunneling causes the violation of unitarity and leads to the wrong thermodynamic (broad interface) limit, among other inconsistencies. This local Hamiltonian has been recently used in other interesting problems, like in the work "Quantum charge fluctuations in a superconducting grain" by M. Houzet, D. A. Pesin, A. V. Andreev and L. I. Glazman [118], and in the work "Weak Localization in Metallic Granular Media" by Y. M. Blanter, V. M. Vinokur and L.I. Glazman [119], both of them in 2005.

- Also in Chapter 2 we have studied the angular distribution of electron current flowing through tunneling normal metal-superconductor (NS) and normal metal-normal metal (NN) interfaces of circular shape and finite radius. In the case of the Andreev current through a NS contact, we have computed the angular correlations between the entangled electron beams emitted through the finite size interface and show how they are lost as the interface radius becomes small.

- We have rigorously established the physical equivalence between Cooper pair emission and Andreev reflection of an incident hole in a NS interface, noting that they emerge from different choices of the chemical potential respect to which quasiparticles in the normal metal are defined, μ_S in the standard Bogoliubov - de Gennes picture, and μ_N in the scenario which contemplates the spontaneous emission of two electrons (Chapter 2).

- In Chapter 3 we have studied resonant transport through double barriers in superconductor metal-semiconductor nanostructures when there exists a large mismatch in effective masses and Fermi wavelengths. We have found zero bias and finite bias peaks in the differential conductance vs. applied voltage which are not symmetric under reversal of voltage sign.

- We have employed the FCS as the observable quantity to test the violation of the CH inequality. In particular, we consider the joint probability distribution $P(Q_1, Q_2)$ for transferring a number of Q_1 and Q_2 electronic charges into two different leads over an observation time t. The electron counting is performed using spin-selective counters, which are spin filters without backscattering (Chapter 4).

- Following the idea of Ref. [106], in Chapter 5 we have used a local spin-rotation in one lead of a beam-splitter geometry patterned onto a 2DEG. The spin-rotation is implemented theoretically by the addition of backgates above and

below a certain section of the lead. Applying a voltage across these backgates the structure inversion asymmetry of the 2DEG is enhanced, inducing a strong Rashba spin-orbit coupling in that region of the 2DEG in a tunable fashion without changing the electron concentration. This in turn gives rise to a precession of the spin around an in-plane axis perpendicular to the electron momentum, resulting in a tunable spin rotation of a certain angle after crossing the region with backgates. This mechanism permits to distinguish between different entangled and polarized incoming states due to switching from bunching to antibunching signatures in shot noise measurements [106].

- Also in Chapter 5 we have generalized the voltage probe phenomenological model of inelastic scattering to obtain the FCS of non-locally entangled particles traversing a mesoscopic conductor.

1.4 Structure of this thesis

This thesis is organized in the following way: It contains four chapters, the first two of them, Chapters 2 and 3, are devoted to the question: *How to generate non-locally spin-entangled electrons using hybrid normal-superconducting structures?*; and the other two chapters, Chapters 4 and 5, to the questions: *How to describe the evolution of non-locally entangled states in the presence of inelastic scattering?*, and *How to detect non-local entanglement and how to discriminate between different incoming entangled states and non-entangled ones?* Each chapter has a self-contained introductory section to the specific problem it deals with (where many references to related works in the field are given), some new results we have obtained, and a conclusive summary at the end. Besides, a section devoted to "Related experiments" is included at the end of each chapter. Due to the novelty of the problems considered in this thesis, our theoretical studies have not been targeted to describe an already pre-existing experiment; at most, to trigger the interest of some experimental groups on the realization of the proposed devices. Nevertheless, with the passing of the years there have appeared in the literature some related experiments to some of the problems treated here which are not so far from the specific devices we had studied. This is for example the case of the work "Experimental Observation of Bias-Dependent Nonlocal Andreev Reflection" by S. Russo, M. Krough, T. M. Klapwijk and A. F. Morpurgo in 2005 [120], which is described in Chapter 2, or the experiment "Shot-noise and conductance measurements of trasparent superconductor/two-dimensional electron gas junctions", by B.-R. Choi et al. in 2005 [76], described in Chapter 3. Other experiments are relevant to us simply because they confirm the experimental accessibility of some quantities we use in our theory. This is the case of the FCS for electrons of Chapter 4, whose experimental accessibility is not so far away according to the work "Current measurement by real-time counting of single electrons" by J. Bylander, T. Duty and P. Delsing in 2005 [121]. Finally, we have transferred to the

appendices some of the more lengthy discussions and computations that could have otherwise distracted from the main discourse.

Chapter 2

Entangled electron current through finite size NS tunneling structures

In this chapter we investigate theoretically the simultaneous tunneling of two electrons from a superconductor into a normal metal at low temperatures and voltages. Such an emission process is shown to be equivalent to the Andreev reflection of an incident hole. We obtain a local tunneling Hamiltonian that permits to investigate transport through interfaces of arbitrary geometry and potential barrier shapes. We prove that the bilinear momentum dependence of the low-energy tunneling matrix element translates into a real space Hamiltonian involving the normal derivatives of the electron fields in each electrode. The angular distribution of the electron current as it is emitted into the normal metal is analyzed for various experimental setups. More importantly for current research on quantum information devices, in the case of a two-point interface we calculate the nonlocally entangled current stemming from processes in which each electron leaves the superconductor through a different orifice. We find that, as a function of the distance between openings, it is cutoff by an exponential decaying with the superconductor coherence length and, due to a geometrical prefactor, it decays quickly on the scale of the Fermi wave length. Finally, we show that, in a full three-dimensional problem, the neglect of the momentum dependence of tunneling causes the violation of unitarity and leads to the wrong thermodynamic (broad interface) limit, among other inconsistencies.

The contents of this chapter were published in Eur. Phys. J. B **40**, 379 (2004), by E. Prada and F. Sols.

2.1 Introduction

The electric current through a biased normal-superconductor (NS) interface has for long been the object of extensive theoretical and experimental attention [122–125]. Recently, new interest in this classic problem has been spurred by the possibility of

using conventional superconductors as a natural source of entangled electron pairs that may be injected into a normal or ferromagnetic metal [36–46,48–50,52,53,56,126] and eventually used for quantum communication purposes. Clearly, the efficient and controlled emission of electron singlet pairs into normal metals or semiconductor nanostructures requires a deeper understanding of the underlying transport problem than has so far been necessary. In particular, it is of interest to investigate how the entangled electron current depends on various parameters such as the shape and size of the NS interface as well as the potential barrier profile experienced by the tunneling electrons. A preliminary focus on tunneling interfaces seems adequate, both because such interfaces are amenable to a simpler theoretical study and because the low electric currents which they typically involve will facilitate the control of individual electron pairs.

In the light of this new motivation, which shifts the attention onto the fate of the emitted electron pairs, it seems that the picture of Andreev reflection, which so far has provided an efficient book-keeping procedure, has reached one of its possible limits. When dealing with finite size tunneling contacts, the Hamiltonian approach is more convenient than the calculation of the scattering wave functions, since it does not require to solve the diffraction problem to find the conductance. Moreover, it is hard to see how problems such as the loss of nonlocal spin correlations among distant electrons emitted from a common superconducting source can be analyzed in terms of Andreev reflected holes in a way that is both practical and respectful to causality. While an Andreev description may still be practical in situations involving multiple electron-hole conversion, the fate of the quasiparticles in the outgoing scattering channels will have to be investigated in terms of a two-electron (or two-hole) picture if one is interested in studying nonlocal correlations in real time.

In the last few years, several authors [37–40, 42, 43, 45, 48–50, 52, 53, 56] have addressed the emission of electron pairs through two distant contacts in a language which explicitly deals with electrons above the normal Fermi level. The mechanism that describes this current is usually addressed in the literature as crossed Andreev reflection effect (CARE). Here we investigate the emission of electron pairs from a superconductor into a normal metal through tunneling interfaces of different geometrical shapes and potential barriers. With this goal in mind, we devote Sec. 2.2 to rigorously establish the equivalence between the pictures of two-electron emission and Andreev reflection of an incident hole. We argue extensively that each picture reflects a different choice of chemical potential for the normal metal, a point also noted in Ref. [73] . After a precise formulation of the problem in Sec. 2.3, we derive a real space tunneling Hamiltonian in Sec. 2.4 that accounts for the fact that electrons with different perpendicular energy are transmitted with different probability through the interface. In Sec. 2.5 we study the structure of the perturbative calculation that, for vanishing temperatures and voltages, will yield the electron current to lowest order in the tunneling Hamiltonian. Sec. 2.6 concerns itself with the angular dependence of the current through a broad NS interface, providing the connection with calcula-

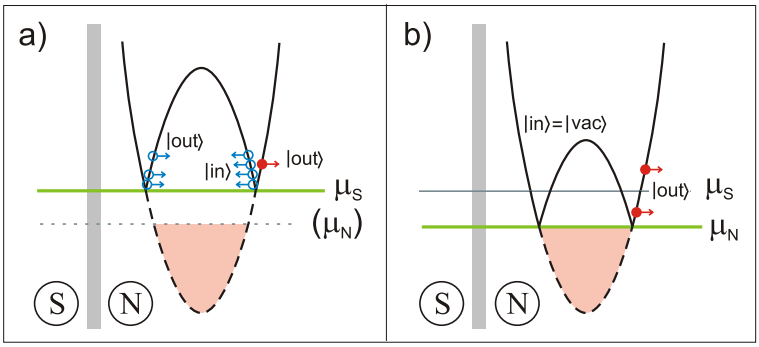

Figure 2.1: Hole Andreev reflection vs two-electron emission: (a) When μ_S is used as the reference chemical potential both in S and N, a typical scattering process at the NS tunneling interface for $eV \equiv \mu_S - \mu_N > 0$ is that of incoming holes with energies between μ_S and $\mu_S + eV$ that are most often normally reflected and only rarely Andreev reflected. (b) If, alternatively, μ_N is used to define quasiparticles in N, the many incoming or outgoing holes are viewed as a vacuum of quasiparticles. The outgoing electron generated in a rare Andreev reflection event appears now as a spontaneously emitted electron above μ_S. Such an event causes an outgoing hole state to be empty. This is now perceived as the emission of a second electron with energy between μ_N and μ_S. Tracking the spin and the momentum component parallel to the interface leads to the picture of two electrons emitted with opposite spin and with opposite parallel momenta.

tions based on the standard quasiparticle scattering picture [127, 128]. In Sec. 2.7 we investigate the tunneling current through a circular NS interface of arbitrary radius, paying attention not only to the total value of the current but also to its angular distribution and to the underlying two-electron angular correlations. We also investigate how the thermodynamic limit is achieved for broad interfaces. Sec. 2.8 deals with the electron current through an interface made of two distant small holes, focussing on the distance dependence of the contribution stemming from nonlocally entangled electrons leaving through different holes. In Sec. 2.9 we investigate the commonly used energy-independent hopping model and prove that it violates unitarity, leads to a divergent thermodynamic limit, and yields a wrong distance dependence for the current contribution coming from nonlocally entangled electrons. In Sec. 2.10 we comment on some very recent experiments related to the observation of nonlocal Andreev current [120, 129, 130]. A concluding summary is provided in Sec. 2.11.

2.2 Two-electron emission vs. Andreev reflection

In a biased NS tunneling interface in which e.g. the superconductor chemical potential is the greatest, one expects current to be dominated by the injection of electron

pairs from the superconductor into the normal metal if the voltage difference V and the temperature T are sufficiently low, single-electron tunneling being forbidden by the energy required to break a Cooper pair. Specifically, one expects two-electron tunneling to dominate if $k_BT, eV \ll \Delta$, where Δ is the zero-temperature superconductor gap. Simple and unquestionable as this picture is, it is not clear how it can be quantitatively described within the popular Bogoliubov - de Gennes (BdG) quasiparticle scattering picture [124, 131, 132]. While it leaves the BCS state unchanged, the emission of two electrons into the normal metal involves the creation of two quasiparticles, something that is not possible within the standard BdG formalism, where the quasiparticle number is a good quantum number and the quasiparticle scattering matrix is thus unitary. The conservation of quasiparticle current is a consequence of the implicit assumption contained in the conventional BdG scheme that the reference chemical potential used to identify quasiparticles in the normal metal is the superconductor chemical potential μ_S. However, as shown below, one does not need to be constrained by such a choice.

In the mean field description of inhomogeneous superconductivity provided by the BdG formalism, the Hamiltonian is given by

$$H = E_0 + \sum_{n\sigma} \varepsilon_n \gamma^\dagger_{n\sigma} \gamma_{n\sigma}, \tag{2.1}$$

where E_0 is the condensate energy and $\gamma^\dagger_{n\sigma}$ creates a quasiparticle of energy ε_n, spin quantum number σ and wave function $[u_n(\mathbf{r}), v_n(\mathbf{r})]$ satisfying the BdG equations

$$\begin{bmatrix} H_0 - \mu_S & \Delta \\ \Delta^* & -H_0^* + \mu_S \end{bmatrix} \begin{bmatrix} u_n \\ v_n \end{bmatrix} = \varepsilon_n \begin{bmatrix} u_n \\ v_n \end{bmatrix}, \tag{2.2}$$

where $H_0 = -\hbar^2\nabla^2/2m + U$ is the one-electron Hamiltonian. In the standard convention, one adopts solutions such that $\varepsilon_n - \mu_S > 0$. However, a fundamental property of the BdG equations [131,133,134] is that, for every quasiparticle n, σ of energy $\varepsilon_n > \mu_S$, there exists another solution n', σ' with spin $\sigma' = -\sigma$, energy $\varepsilon_{n'} = -\varepsilon_n + 2\mu_S < \mu_S$ and wavefunction $(u_{n'}, v_{n'}) = (-v_n^*, u_n^*)$. These two solutions are not independent, since creating quasiparticle n, σ is equivalent to destroying quasiparticle $n', -\sigma$ [134]. More specifically, $\gamma^\dagger_{n\downarrow} = \gamma_{n'\uparrow}$, and $\gamma_{n\uparrow} = -\gamma^\dagger_{n'\downarrow}$.

In the case of a normal metal, where quasiparticles are pure electrons or pure holes, the above property implies that creation of a quasiparticle of energy $\varepsilon_n > \mu_S$ and wave function $(0, v_n)$ (i.e. a pure hole) corresponds to the destruction of a quasiparticle of energy $\varepsilon'_n = 2\mu_S - \varepsilon_n < \mu_S$ and wave function $(-v_n^*, 0)$ (i.e. a pure electron). If $v_n(\mathbf{r}) \sim \exp(i\mathbf{k}_h \cdot \mathbf{r})$, the existence of a hole of momentum $\mathbf{k}_h$, with $k_h < k_F$, and energy $\varepsilon > \mu_S$ corresponds to the absence of an electron in the state of wave function $v_n^*(\mathbf{r}) \sim \exp(-i\mathbf{k}_h \cdot \mathbf{r})$ with energy $\varepsilon' = 2\mu_S - \varepsilon < \mu_S$.

In a biased NS tunneling structure, the normal metal has a different chemical potential $\mu_N = \mu_S - eV$. Without loss of generality, we may assume $\mu_N < \mu_S$. If

we release ourselves from the standard BdG constraint of using μ_S as the reference chemical potential even on the normal side, a clearer picture is likely to emerge. We may decide that, in the energy range $\mu_N < \varepsilon' < \mu_S$, we switch to the opposite convention for the identification and labeling of quasiparticles. In other words, we decide to use μ_N as the reference chemical potential. Translated to the example of the previous paragraph, we pass to view the occupation of the hole-type quasiparticle state of wave function $(0, v_n)$ and energy $\varepsilon > \mu_S$ as the emptiness of the electron-type quasiparticle state of wave function $(-v_n^*, 0)$ and energy $\varepsilon' < \mu_S$. Conversely, the absence of quasiparticles in $(0, v_n)$ is now viewed as the occupation of $(-v_n^*, 0)$, i.e. as the existence of an electron with wave function $-v_n^*(\mathbf{r})$ and energy ε' between μ_N and μ_S.

The consequences that this change of paradigm has on the way we view transport through an NS interface can be more clearly appreciated in Fig. 2.1. In the standard BdG picture represented in Fig. 2.1(a), with μ_S as the reference chemical potential, the "in" state is that of many holes impinging on the NS interface from the N side, with energies between μ_S and $\mu_S + eV$. Since ours is a tunneling structure, normal reflection is the dominant scattering channel and only one hole is Andreev reflected as an electron (quasiparticle transmission is precluded at sufficiently low temperatures and voltages). Thus the "out" state is that of many holes and only one electron moving away from the surface, all with energies also between μ_S and $\mu_S + eV$, since quasiparticle scattering is elastic. Given the unitary character of quasiparticle scattering in the BdG formalism, the existence of an outgoing electron requires the outgoing hole quasiparticle state at the same energy to be empty, due to the incoming hole that failed to be normally reflected. The absence of such an outgoing hole is clearly shown in Fig. 2.1(a).

If we now shift to μ_N as the reference chemical potential, the picture is somewhat different. The many impinging holes on the surfaces are now viewed as the absence of quasiparticles, i.e. the "in" state is the vacuum of quasiparticles. The one electron that emerged from a rare Andreev process continues to be viewed as an occupied electron state, shown above μ_S in Fig. 2.1(b). The many outgoing holes of the BdG picture are again viewed as an absence of quasiparticles. The *second outgoing electron* that is needed to complete the picture of two-electron emission corresponds to the empty outgoing hole state of the BdG picture which originates from the *hole that failed to be normally retro-reflected*. It is shown in Fig. 2.1(b) with energy between μ_N and μ_S. As is known from the theory of quasiparticle Andreev reflection, the outgoing electron of Fig. 2.1(a) follows the reverse path of the incident hole (conjugate reflection). Therefore the two electrons in Fig. 2.1(b) have momenta with opposite parallel (to the interface) components and the same perpendicular component, i.e. they leave the superconductor forming a V centred around the axis normal to the interface. Conservation of the spin quantum number through the barrier completes the picture of two electrons emitted into the normal metal in an entangled spin singlet

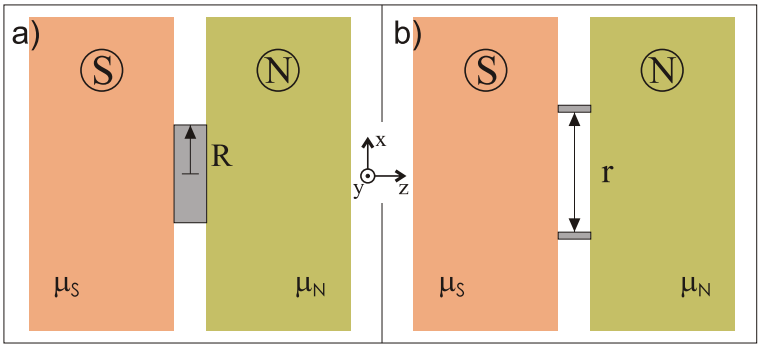

Figure 2.2: Schematic lateral view of the NS tunneling structures studied in this paper: (a) circular interface of arbitrary radius R and (b) interface made of two small holes at a distance r from each other. The rest of the NS interface is assumed to be opaque.

state [1].

In summary, we have rigorously established the equivalence between the pictures of Andreev reflection and two-electron emission, noting that they emerge from *different choices of the chemical potential* to which quasiparticles in the normal metal are referred, μ_S in the standard BdG picture, and μ_N in the scenario which contemplates the spontaneous emission of two electrons. For simplicity, and because it better fits our present need, we have focussed on the case of a tunneling structure. However, the essence of our argument is of general validity. Here we just note that, in the opposite case of a transmissive NS interface [124,135], the same argument applies if, exchanging roles, Andreev reflection passes to be the rule while normal reflection becomes the exception. In that case, charge accumulation and its accompanying potential drop, which are generated by normal reflection [136], will be essentially nonexistent.

2.3 Formulation of the problem

As has been said, an extensive body of literature has been written on the various aspects of electron transport through a NS interface [36,38,39,41,45,46,48,50,122–128, 131–134,136–140]. Generally those works have focussed on the case of broad interfaces or point contacts [132, 139]. Our goal here is to analyze the current of spin entangled Cooper pairs from a BCS bulk superconductor into a bulk normal metal through an arbitrarily shaped insulating junction in the tunnel limit. Apart from the desire to explore novel types of NS structures, we are also motivated by the need to investigate in depth the two-electron emission picture, which is likely to be useful in the design

[1]Note here, nevertheless, that the BdG picture doesn't account for the singlet entanglement of the two emitted electrons.

of quantum communication devices. We wish to consider explicitly geometries of the sort depicted in Fig. 2.2, i.e. a 2D planar interface of arbitrary radius R, presented in Fig. 2.2(a), and two small orifices separated by a distance r, shown in Fig. 2.2(b). It is assumed that, outside the designed region, the interface is opaque to the flow of electrons. For simplicity, both the normal and the superconducting electrodes are taken to be ballistic. An advantage of the tunneling regime is that the proximity effect may be neglected, i.e. we assume that the gap function drops sharply at the NS interface and that self-consistency in the gap may be safely neglected [134]. Another benefit is that we deal at most with two chemical potentials, since the low scale of tunneling currents guarantees that the normal metal is close to equilibrium [136] and that no phase slips develop within the superconductor [141]. Inelastic processes at the interface will also be ignored [142].

We are interested in a conventional (s-wave) superconductor because it may act as a natural source of spin-entangled electrons, since its electrons form Cooper pairs with singlet spin wave functions and may be injected into a normal metal. The superconductor, which is held at a chemical potential μ_S, is weakly coupled by a tunnel barrier to a normal metal which is held at μ_N. By applying a bias voltage $V = (\mu_S - \mu_N)/e$ such that $eV > 0$, transport of entangled electrons occurs from the superconductor to the normal metal. We focus on the regime $k_B T \ll eV \ll \Delta$. Since $\delta \equiv \Delta/E_F \sim 10^{-4}$ in a conventional superconductor, rearrangement of the potential barrier due to the voltage bias can be also neglected. However, the effect of a finite, small δ will often be tracked because pairing correlations (and thus nonlocal entanglement) decays on the scale of the coherence length ξ_0, which is finite to the extent that Δ is nonzero. For convenience, we assume that the superconductor normal-state properties (m, k_F, etc.) are the same as for an ordinary metal.

We will use a tunneling Hamiltonian approach and explicitly consider the emission of two electrons from the superconductor, a viewpoint that will be mandatory in contexts where the late evolution of correlated electron pairs in the normal metal is to be investigated.

2.4 Three-dimensional tunneling Hamiltonian

The Bardeen model for electron tunneling [143] assumes that a system made up of two bulk metals connected through an insulating oxide layer can be described by the Hamiltonian

$$H = H_L + H_R + H_T \,. \tag{2.3}$$

Here H_L and H_R are the many-body Hamiltonians for the decoupled (i.e. unperturbed) electrodes, the superconductor being on the left and the normal metal on the right. The connection between both electrodes is described by the tunneling term H_T

(see e.g. Ref. [144]):

$$H_T = \sum_{\mathbf{kq}\sigma} T_{\mathbf{kq}}\, c^\dagger_{\mathbf{k}\sigma}\, c_{\mathbf{q}\sigma} + \text{H.c.} \tag{2.4}$$

Here $c^\dagger_{\mathbf{k}\sigma}$ is the creation operator in the normal metal of the single-particle state of orbital quantum number $\mathbf{k}$ and spin σ, whereas $c_{\mathbf{q}\sigma}$ destroys state $\mathbf{q},\sigma$ in the superconductor and $T_{\mathbf{kq}}$ is the matrix element connecting both states. We assume a perfect interface defined by a square barrier $U(\mathbf{r},z) = U_0\Theta(z+w/2)\Theta(w/2-z)$ (hereafter $\mathbf{r}$ refers to the in-plane coordinate).

If $\chi_{\mathbf{q}}(\mathbf{r},z)$ are the left-side stationary waves for a potential step $U_L(\mathbf{r},z) = U_0\Theta(z+w/2)$ and $\chi_{\mathbf{k}}(\mathbf{r},z)$ behaves similarly for $U_R(\mathbf{r},z) = U_0\Theta(w/2-z)$, Bardeen [143] showed

$$T_{\mathbf{kq}} = \frac{-\hbar^2}{2m}\int d\mathbf{r}\,\left[\chi^*_{\mathbf{k}}(\mathbf{r},z)\frac{\partial}{\partial z}\chi_{\mathbf{q}}(\mathbf{r},z) - \chi_{\mathbf{q}}(\mathbf{r},z)\frac{\partial}{\partial z}\chi^*_{\mathbf{k}}(\mathbf{r},z)\right]_{z=z_0}, \tag{2.5}$$

where z_0 lies inside the barrier, i.e. $J_{\mathbf{kq}}(\mathbf{r},z_0) \equiv (i/\hbar)T_{\mathbf{kq}}$ is the matrix element of the z component of the current operator (current density integrated over coordinate $\mathbf{r}$). [2] Due to charge conservation, $J_{\mathbf{kq}}$ is independent of the choice of point $z_0 \in [-w/2, w/2]$. The unperturbed wave functions are of the form

$$\chi_{\mathbf{k}}(\mathbf{r},z) = \frac{e^{i\mathbf{k}_\parallel\mathbf{r}}}{\sqrt{A}}\varphi_{k_z}(z), \tag{2.6}$$

where the exact shape of $\varphi_{k_z}(z)$ depends on the barrier height. Thus,

$$T_{\mathbf{kq}} = \frac{\tau}{\sqrt{\Omega_L\Omega_R}N(0)}\,\delta(\mathbf{k}_\parallel - \mathbf{q}_\parallel)\,L(k_z,q_z)\,. \tag{2.7}$$

Hereafter, the volume of each metal $\Omega_{L,R}$ is taken equal to $\Omega = AL$, A being the area of the interface and L the length of each semi-infinite metal. $N(0)$ is the 3D one-spin electronic density of states of the normal metal at the Fermi level: $N(0) = k_F^3/4\pi^2E_F$. We define the *transparency* of the barrier as

$$\tau \equiv 4\sqrt{\frac{E_F}{U_0}}e^{-p_0 w}\,, \tag{2.8}$$

where $p_0 \equiv \sqrt{2mU_0}/\hbar$. In the particular case $p_0 w \gg 1$ and $E_F \ll U_0$, τ coincides with the probability amplitude that an electron with perpendicular energy $E_z = E_F$ traverses the barrier. $L(k_z,q_z)$ in Eq. (2.7) captures the dependence of the hopping energy on the z momentum component. Some authors take it as constant, but we shall argue in Sec. 2.9 that its k_z, q_z dependence is crucial for a sound description of 3D transport problems.

[2] Note that $T_{\mathbf{kq}}$ has energy units.

For a square barrier, we may define $u \equiv U_0/E_F$, $\varrho_z \equiv q_z/k_F$, $\kappa_z \equiv k_z/k_F$, and write

$$L(k_z, q_z) = k_z\, q_z\, a(\kappa_z, \varrho_z)\, \exp\left\{p_0 w\left[1 - a(\kappa_z, \varrho_z)\right]\right\}, \tag{2.9}$$

where

$$a(x, y) \equiv [b(x) + b(y)]/2\,, \tag{2.10}$$

$$b(x) \equiv \sqrt{1 - x^2/u}\,. \tag{2.11}$$

For high barriers ($u \to \infty$) we have $a(x) \to 1$. Then,

$$T_{\mathbf{kq}} \simeq \frac{\tau}{\Omega N(0)}\, \delta(\mathbf{k}_\parallel - \mathbf{q}_\parallel)\, k_z\, q_z\,. \tag{2.12}$$

If we make $U_0 \to \infty$ while keeping the electron transmission probability finite, we are implicitly assuming that the barrier becomes arbitrarily thin ($w \to 0$), i.e. we are taking it to be of the form $V(z) = H\delta(z)$, as popularized in Ref. [124]. On the other hand, since the height of the barrier is judged in relation to the perpendicular energy $E_z \leq E_F < U_0$, it is clear that, given U_0 and w, Eq. (2.12) becomes correct for sufficiently small k_z, q_z. In other words, $T_{\mathbf{kq}}$ behaves identically for $u \to \infty$ or $k_z, q_z \to 0$. As a consequence, such bilinear dependence of $T_{\mathbf{kq}}$ for sufficiently small k_z, q_z may be expected to hold for arbitrary barrier profiles within the tunneling regime. We note that Eq. (2.12) differs from the result obtained in Ref. [145] for the low energy hopping.

2.4.1 Validity of the tunneling Hamiltonian model: momentum cutoff

We wish to quantify the idea that a perturbative treatment of Bardeen's tunneling Hamiltonian is valid only when it involves matrix elements between weakly coupled states [143, 146].

The transmission probability for a low energy electron incident from the left can be written

$$T(E_z) = W_{\mathbf{q}}/J_{\mathbf{q}}\,, \tag{2.13}$$

where $J_{\mathbf{q}}$ is the current probability carried by the incoming component of the stationary wave $\mathbf{q}$ (note that it has units of inverse time), and

$$W_{\mathbf{q}} = \frac{2\pi}{\hbar} \sum_{\mathbf{k}} |T_{\mathbf{kq}}|^2 \delta(E_{\mathbf{k}} - E_{\mathbf{q}}) \tag{2.14}$$

is the tunneling rate. Using Eqs. (2.7) and (2.9), Bardeen's theory yields

$$T(E_z) = 16 \frac{E_z}{U_0} \left(1 - \frac{E_z}{U_0}\right) e^{-2p_z w}\,, \tag{2.15}$$

where $p_z = \sqrt{2m(U_0 - E_z)}/\hbar$. On the other hand, an exact calculation using matching of wave functions [147] gives for a square barrier and for $E_z < U_0$

$$T^{exact}(E_z) = \left[\cosh^2(p_z w) + \frac{1}{4}\frac{(U_0 - 2E_z)^2}{U_0 E_z - E_z^2}\sinh^2(p_z w)\right]^{-1}, \tag{2.16}$$

which recovers the tunneling result (2.15)[3] if we make the approximation

$$\sinh(p_z w) \approx \cosh(p_z w) \approx e^{p_z w}/2\,. \tag{2.17}$$

Thus we adopt as a criterion of the validity of Bardeen's approximation that Eq. (2.17) holds within a certain accuracy, which from (2.15), implies $T(E_F) \ll 1$. This defines an upper energy cutoff E_c in the various sums over electron states, which is the maximum energy for which the approximation (2.17) is valid. For the square barrier, $E_c \simeq U_0 - \hbar^2/2mw^2$.

For processes described by amplitudes which are first order in H_T, and as long as U_0 is high enough compared to E_F to fulfill condition (2.17) for all relevant E_z, all electron momenta lie within the applicability of the tunnel limit and we may use the tunneling Hamiltonian safely. That is the case of the tunnel current through a NN interface or the quasiparticle tunnel current through a NS interface.

The situation is different for Andreev transport through a NS interface, since it requires the coherent tunneling of two electrons. Then, the leading contribution to the tunneling amplitude is quadratic in H_T and the final transmission probability is sensitive to the existence of intermediate virtual states where only one electron has tunneled and a quasiparticle above the gap has been created in the superconductor. Unlike the weighting factors of the initial and final states, which are controlled by the Fermi distribution function, the contribution of the virtual intermediate states decays slowly with energy and the cutoff E_c may be reached. In Sec. 2.5 we show that there are two cases where the cutoff can be safely neglected, namely, the limit of high barrier ($u \gg 1$) and the limit of small gap ($\delta \ll 1$).

2.4.2 Tunneling Hamiltonian in real space

One of our main goals is to investigate transport through tunneling interfaces of arbitrary shape [149] that are otherwise uniform. For that purpose we need a reliable tunneling Hamiltonian expressed in real space. Our strategy will be to rewrite Eq. (2.4) as an integral over the infinite interface and postulate that a similar Hamiltonian, this time with the integral restricted to the desired region, applies to tunneling through the finite-size interface. The discontinuity between the weakly transparent interface and the completely opaque region causes some additional scattering in the

[3]The low-energy linear dependence $T(E_z) \sim E_z$ and the related bilinear dependence $T_{\mathbf{kq}} \sim k_z q_z$ is implicit in Ref. [148]. We note, however, that here we find perfect agreement between Bardeen's perturbative method and the exact results in the tunneling limit.

electronic wave functions that enter the exact matrix element. However, this effect should be negligible in the tunneling limit. In fact, we provide in Appendix A an independent derivation of the continuum results shown in this section, which starts from a discrete tight-binding Hamiltonian.

Thus, in (2.4) we introduce the transformations

$$c^{\dagger}_{\mathbf{k}\sigma} = \int_A d\mathbf{r} \int dz\ \chi_{\mathbf{k}}(\mathbf{r},z)\ \psi^{\dagger}_N(\mathbf{r},z;\sigma) \tag{2.18}$$

$$c_{\mathbf{q}\sigma} = \int_A d\mathbf{r} \int dz\ \chi^{*}_{\mathbf{q}}(\mathbf{r},z)\ \psi_S(\mathbf{r},z;\sigma) \tag{2.19}$$

where the wave functions $\chi_{\mathbf{q}}$ and $\chi_{\mathbf{k}}$ are, respectively, solutions of H_L and H_R and are given in (2.6). $\psi^{\dagger}_N(\mathbf{r},z;\sigma)$ and $\psi_S(\mathbf{r},z;\sigma)$ are the field operators in the normal and superconducting metals.

Invoking Eq. (2.7) and the completeness of plane waves in the x,y plane [which yields a term $\delta(\mathbf{r}-\mathbf{r}')$], we obtain

$$H_T = \sum_{\sigma} \frac{\tau}{4\pi^2 N(0)} \int_A d\mathbf{r} \int dz' \int dz\ \widetilde{L}(z,z')\ \psi^{\dagger}_N(\mathbf{r},z;\sigma)\,\psi_S(\mathbf{r},z';\sigma) + \text{H.c.}\,, \tag{2.20}$$

where

$$\widetilde{L}(z,z') = \frac{1}{L_z} \sum_{k_z,q_z>0} \varphi_{k_z}(z)\,\varphi^{*}_{q_z}(z')\,L(k_z,q_z)\,. \tag{2.21}$$

Since the initial Hamiltonian (2.4) connects states which overlap in a finite region below and near the barrier, it is logical that the real space Hamiltonian (2.20) is non-local in the z-coordinate. An interesting limit is that of a high and (to keep transmission finite) thin barrier, i.e. the delta barrier limit. Then, the perpendicular wave functions can be precisely written

$$\varphi_{k_z}(z) = \sqrt{2/L}\sin(k_z z), \quad z \geq 0 \tag{2.22}$$

and similarly for the left electrode. We introduce such wave functions in Eq. (2.21) and invoke the identity (hereafter $L \to \infty$)

$$\frac{1}{L}\sum_{k_z>0} k_z \sin(k_z z) = -\delta'(z), \tag{2.23}$$

where the volume per orbital in k_z-space is π/L. Then, to leading order in $u^{-1} \ll 1$, Eq. (2.20) yields

$$H_T = \sum_{\sigma} \frac{\tau}{8\pi^2 N(0)} \int_A d\mathbf{r}\ \left.\frac{\partial \psi^{\dagger}_N(\mathbf{r},z;\sigma)}{\partial z}\right|_{z\to 0^+} \left.\frac{\partial \psi_S(\mathbf{r},z';\sigma)}{\partial z'}\right|_{z'\to 0^-} + \text{H.c.} \tag{2.24}$$

If we replace the thermodynamic area A by a specific finite area, the real space Hamiltonian (2.24) can be used to describe tunneling through interfaces of arbitrary shape. As we have said, in Appendix A we provide an alternative derivation which makes Eq. (2.24) appear as the natural continuum limit of the hopping Hamiltonian in a regularized tight-binding representation. We note that the tunneling Hamiltonian (2.24) may also be obtained if the r.h.s. of Eq. (2.22) is replaced by a plane wave representation.

From Eq. (2.24) we conclude that apparently reasonable choices of local tunneling Hamiltonian such as those $\propto \int \psi_S^\dagger \psi_N$ lead to unphysical results in 3D. This point will be discussed in depth in Sec. 2.9.

To describe tunneling in real space, rather than starting from Hamiltonian (2.20), or its limiting version (2.24), it is more convenient in practice to go back to Eq. (2.7) and make the replacement $\delta(\mathbf{k}_\parallel - \mathbf{q}_\parallel) \to (2\pi)^{-2} \int_A d\mathbf{r}\, e^{i(\mathbf{k}_\parallel - \mathbf{q}_\parallel)\cdot\mathbf{r}}$, with A finite. Then Eqs. (2.20) and (2.21) may equivalently be written

$$H_T = \sum_{\mathbf{kq}\sigma} \frac{\tau (2\pi)^{-2}}{N(0)\Omega} \int_A d\mathbf{r}\, e^{i(\mathbf{k}_\parallel - \mathbf{q}_\parallel)\cdot\mathbf{r}} L(k_z, q_z) c_{\mathbf{k}\sigma}^\dagger\, c_{\mathbf{q}\sigma} + \text{H.c.} \tag{2.25}$$

If we make $L(k_z, q_z) = k_z q_z$, it is easy to prove that (2.25) becomes (2.24).

2.5 Perturbative calculation of the stationary current

Following Ref. [38], we write the stationary electron current from the superconductor to the normal metal as

$$I_{\text{NS}} = 2e \sum_{if} W_{fi}\, \rho_i\,, \tag{2.26}$$

where W_{fi} is the transition rate at which *two* electrons tunnel from the superconductor into the normal metal, and ρ_i is the stationary occupation probability for the entire system to be in the state $|i\rangle$. We calculate the transition rate with a T-matrix approach [150],

$$W_{fi} = \frac{2\pi}{\hbar} \left|\langle f|\, \hat{T}(\varepsilon_i)\, |i\rangle\right|^2 \delta(\varepsilon_f - \varepsilon_i)\,. \tag{2.27}$$

The T-matrix can be written as a power series in the tunnel Hamiltonian H_T,

$$\hat{T}(\varepsilon) = H_T + H_T \sum_{n=1}^{\infty} [G_0(\varepsilon) H_T]^n \tag{2.28}$$

where $G_0(\varepsilon) = (\varepsilon - H_0 + i0^+)^{-1}$ is the retarded Green function for the decoupled system.

At zero temperature the initial state is $|i\rangle = |\mathrm{F}\rangle \otimes |\mathrm{BCS}\rangle$, where $|\mathrm{F}\rangle$ is the filled Fermi sea ground state of the normal metal and $|\mathrm{BCS}\rangle$ is the BCS ground state of the superconductor. The state $|i\rangle$ is the vacuum of quasiparticles if these are referred to μ_S in the superconductor and to $\mu_N = \mu_S - eV$ in the normal metal (see Sec. 2.2). In the final state

$$|f\rangle = \frac{1}{\sqrt{2}}(c^\dagger_{\mathbf{k}_1\uparrow} c^\dagger_{\mathbf{k}_2\downarrow} - c^\dagger_{\mathbf{k}_1\downarrow} c^\dagger_{\mathbf{k}_2\uparrow})|i\rangle\,, \tag{2.29}$$

i.e. the superconductor remains unperturbed within the BCS description, since an entire Cooper pair has been removed, and two singlet-correlated electrons hover above the normal Fermi sea [4]. In the ensuing discussion we take $\varepsilon_i = 2\mu_S \equiv 0$.

Since we wish to focus on the regime $k_B T \ll eV \ll \Delta$, single electron emission is forbidden due to energy conservation, because it requires the breaking of a Cooper pair. Therefore, to leading order in H_T, we may approximate

$$\hat{T}(0) \approx T'' \equiv H_T\, G_0\, H_T \tag{2.30}$$

and so we write

$$\langle f|\hat{T}(0)|i\rangle = \frac{1}{\sqrt{2}}\,\langle (c_{\mathbf{k}_2\downarrow} c_{\mathbf{k}_1\uparrow} - c_{\mathbf{k}_2\uparrow} c_{\mathbf{k}_1\downarrow})\, T''\rangle\,. \tag{2.31}$$

We insert a complete set of single-quasiparticle (virtual) states, i.e.

$$\mathbb{1} = \sum_{\mathbf{k}\mathbf{q}\sigma\sigma'} \gamma^\dagger_{\mathbf{q}\sigma} c^\dagger_{\mathbf{k}\sigma'} |i\rangle\langle i| c_{\mathbf{k}\sigma'} \gamma_{\mathbf{q}\sigma}\,,$$

between the two H_T in (2.30) and we use the fact that the resulting energy denominator $|i0^+ - \xi_{\mathbf{k}} - E_{\mathbf{q}}| \approx |E_{\mathbf{q}}|$, since $\xi_{\mathbf{k}} \equiv \hbar^2 k^2/2m - \mu_N \to 0$ when $eV \to 0$. To see this, one must note that the energy conservation implies $\varepsilon_f = \varepsilon_i$; therefore, $\varepsilon_f = \xi_{\mathbf{k}_1} + \xi_{\mathbf{k}_2} - 2eV = 2\mu_S = 0$. Thus, when $eV \to 0$, one may write $\xi_{\mathbf{k}_1} \approx -\xi_{\mathbf{k}_2} \approx 0$. We also make use of $u_{\mathbf{q}} v_{\mathbf{q}} = u_{-\mathbf{q}} v_{-\mathbf{q}}$ for a s-wave superconductor [5]. Finally, we get

$$\langle f|\hat{T}(0)|i\rangle = 2\sqrt{2}\langle c_{\mathbf{k}_2\uparrow} c^\dagger_{\mathbf{k}_2\uparrow} c_{\mathbf{k}_1\downarrow} c^\dagger_{\mathbf{k}_1\downarrow}\rangle \sum_{\mathbf{q}} \frac{\langle c_{\mathbf{q}\uparrow} c_{-\mathbf{q}\downarrow}\rangle}{E_{\mathbf{q}}} T_{\mathbf{k}_1\mathbf{q}} T_{\mathbf{k}_2,-\mathbf{q}} \tag{2.32}$$

where $E_{\mathbf{q}} = [(\hbar^2/2m)^2(q^2 - k_F^2)^2 + \Delta^2]^{1/2}$ is the quasiparticle energy and $F_{\mathbf{q}} \equiv \langle c_{\mathbf{q}\uparrow} c_{-\mathbf{q}\downarrow}\rangle$ is the condensation amplitude in the state $\mathbf{q}$ [131].

At zero temperature we have $F_{\mathbf{q}} = \Delta/2E_{\mathbf{q}}$. Thus, in the summation of Eq. (2.32), the contribution of high energy virtual states is weighted by the Lorentzian $F_{\mathbf{q}}/E_{\mathbf{q}}$,

[4] Note that, as defined in Eq. (2.29), the final state $(\mathbf{k}_1, \mathbf{k}_2)$ is identical to the state $(\mathbf{k}_2, \mathbf{k}_1)$. Thus, when summing over final states, one must avoid double counting. Specifically, in Eq. (2.26), $\sum_f$ is to be understood as $\frac{1}{2}\sum_{\mathbf{k}_1,\mathbf{k}_2}$, where $\sum_{\mathbf{k}_1,\mathbf{k}_2}$ is an unrestricted sum over indices $\mathbf{k}_1, \mathbf{k}_2$.

[5] If we had considered a final state $\langle f|$ with an entangled spin triplet pair over the normal Fermi sea (instead of a singlet), this property of the BCS coherence factors $u_{\mathbf{q}}$ and $v_{\mathbf{q}}$ would have made the matrix element of Eq. (2.31) identically zero.

of width Δ and centred around E_F. We already mentioned in the previous section the need for a high-energy cutoff E_c to prevent the inclusion of states for which the tunneling approximation is not valid. However, in the limit $\Delta/E_F \to 0$, the Lorentzian distribution becomes a delta function and the results are independent of the cutoff, which can be safely taken to infinity. A similar situation is found in the limit $U_0 \gg E_F$, for which the sum in Eq. (2.32) converges before reaching the energy E_c above which Bardeen's approximation is no longer valid. In any of these two limits ($\Delta/E_F, E_F/U_0 \ll 1$), it is correct to take $E_c \to \infty$.

2.6 Total current and angular distribution through a broad interface

The current through a NS junction is most easily calculated when the interface section is much bigger than λ_F. We shall refer to it as the broad interface or thermodynamic limit. Its detailed understanding is of interest for later reference in the investigation of finite size interfaces. For $k_BT \ll eV \ll \Delta$, the set of equations in the previous section yields

$$I_{\rm NS} = I_V \frac{\tau^4}{2} \int_0^{\pi/2} d\theta \, \sin\theta \, g(\theta) \,, \tag{2.33}$$

where $g(\theta)$ is the angular distribution (θ being the angle between the outgoing electron momentum and the direction normal to the interface) and

$$I_V \equiv \frac{1}{2} e^2 \, VN(0) \, v_F \, A = J_V A \,, \tag{2.34}$$

with V the applied voltage, A the interface area, and v_F the Fermi velocity. Eq. (2.34) may be written as $I_V = (2e^2/h)NV$, where $N = Ak_F^2/4\pi$ is the number of transverse channels that fit in an interface of area A. Thus, I_V can be interpreted as the current that would flow through a transmissive [$T(E_z) = 1$ for all E_z] normal-normal interface with the same area and subject to the same voltage bias. The τ^4 dependence of $I_{\rm NS}$ reflects the simultaneous tunneling of two electrons.

Using the previous definition $\varrho_z \equiv q_z/k_F$, the angular distribution for the current through an arbitrary square barrier is [6]

$$\begin{aligned} g(\theta) &= 2\cos^3\theta \, e^{2p_0 w[1-b(\cos\theta)]} \\ &\times \left[\frac{2}{\pi} \int_0^{\varrho_c} d\varrho_z \, \frac{\delta}{(\varrho_z^2 - \cos^2\theta)^2 + \delta^2} \, \varrho_z^2 \, \left[a(\varrho_z, \cos\theta)\right]^2 \, e^{p_0 w[1-b(\varrho_z)]} \right]^2 , \end{aligned} \tag{2.35}$$

[6] A study of the angular dependence of Andreev reflection in the broad interface limit has been presented in Ref. [151]. However, it is restricted to a delta barrier interface and considers the case where N is a doped semiconductor.

where $\varrho_c = \sqrt{E_c/E_F}$ is the cutoff and the functions a and b were defined in Eqs. (2.10) and (2.11).

For $\delta \to 0$, we have

$$\lim_{\delta\to 0}\int_0^{\varrho_c} d\varrho\, \frac{\delta}{(\varrho^2-x^2)^2+\delta^2}\, \varrho\, f(\varrho) = \frac{\pi}{2}\, f(x)\,, \tag{2.36}$$

if, as is the case, $\varrho_c > 1 \geq |x|$. Therefore, in the limit $\delta \to 0$, Eq. (2.35) yields

$$g(\theta) = 2\, e^{4p_0 w[1-b(\cos\theta)]}[b(\cos\theta)]^4 \cos^5\theta\,. \tag{2.37}$$

For large barriers ($u \gg 1$) and finite δ we find (with $\varrho_c \to \infty$)

$$\begin{aligned} g(\theta) &= \cos^5\theta + \cos^3\theta\sqrt{\cos^4\theta+\delta^2} && (2.38)\\ &= 2\cos^5\theta\left[1+\mathcal{O}(\delta^2)\right]. && (2.39)\end{aligned}$$

Combining Eqs. (2.33) and (2.38), we obtain for the total current

$$\begin{aligned} I_{\rm NS} &= \frac{1}{12} I_V \tau^4 \left[1+(1+\delta^2)^{3/2}-\delta^3\right] && (2.40)\\ &= \frac{1}{6} I_V \tau^4 \left[1+\mathcal{O}(\delta^2)\right]. && (2.41)\end{aligned}$$

However, if the cutoff ϱ_c remains finite, Eq. (2.41) must be replaced by

$$I_{\rm NS} = \frac{1}{6} I_V \tau^4 \left[1 - \frac{24}{5\pi}\frac{\delta}{\varrho_c} + \mathcal{O}(\delta^2)\right], \tag{2.42}$$

i.e. a finite cutoff qualitatively affects the leading low-δ dependence of $I_{\rm NS}$.

The underlying physics goes as follows. The product of hopping matrix elements appearing in (2.32) satisfies

$$T^*_{\mathbf{k_1 q}} T^*_{\mathbf{k_2},-\mathbf{q}} \propto k_{1z}\, k_{2z}\, q_z^2\, \delta(\mathbf{k}_{1\|}+\mathbf{k}_{2\|})\delta(\mathbf{k}_{1\|}-\mathbf{q}_{\|})\,. \tag{2.43}$$

Thus, when crossing the barrier, electrons forming a Cooper pair of momenta $(\mathbf{q}, -\mathbf{q})$ undergo the following process: Their opposite interface-parallel momenta are conserved ($\mathbf{k}_{1\|} = \mathbf{q}_{\|}$ and $\mathbf{k}_{2\|} = -\mathbf{q}_{\|}$). By contrast, one of their perpendicular momentum components (more specifically, the negative one pointing away from the interface) is reversed so that both electrons enter the normal metal with perpendicular momenta $k_{1z}, k_{2z} > 0$. In the limit of $eV \to 0$ the modulus difference between k_{1z} and k_{1z} is negligible. This means that the electron current through a broad interface will propagate into the normal lead in the form of two rays which are symmetric with respect to the direction normal to the interface. Due to axial symmetry, g is only a function of the zenithal angle $\theta \in [0, \pi/2]$.

The normalized angular distributions for several barrier heights are depicted in Fig. 2.3 in the limit $\delta \to 0$. The lowest barrier which we have considered has $u = 1.1$.

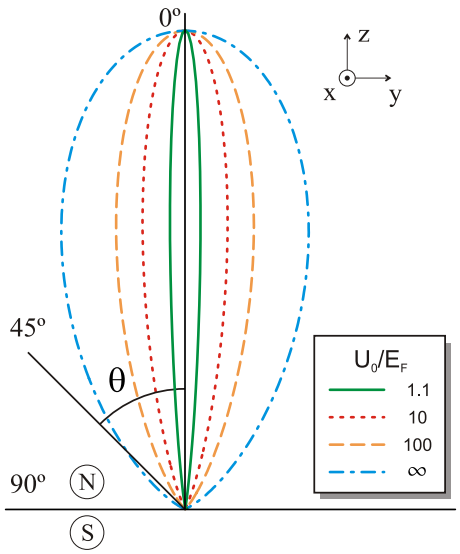

Figure 2.3: Angular dependence of the normalized tunnel current ranging from $U_0/E_F \to \infty$ for the outer $(\cos^5\theta)$ curve to $U_0/E_F = 1.1$ for the inner one. Finite barriers have a width $w = 5\lambda_F$. Observe how the angular distribution focalizes around the perpendicular direction as the barrier hight decreases.

This means that, for a typical value of $E_F = 5$ eV, the difference between the height of the barrier and the Fermi energy is 0.5 eV, i.e. large enough to ensure that the junction operates in the tunneling regime. In particular, following the arguments of Subsec. 2.4.1, in this case the error incurred by using the tunneling approximation of Eq. (2.15) instead of the exact one of Eq. (2.16) is less than $2 \times 10^{-7}\%$ for the worst case on normal incidence to the interface. In Fig. 2.3, finite-height barriers are taken to have a width $w = 5\lambda_F$. For large U_0 we reproduce the analytical $\cos^5\theta$ behaviour given in Eq. (2.39). As the barrier height decreases, the angular distribution becomes more focussed in the forward direction because transmission is more sensitive to the perpendicular energy. Thus, the relative fraction of Fermi surface electrons crossing the interface with E_z close to the highest value E_F increases. That majority of transmitted electrons have low parallel momenta and, accordingly, a characteristic parallel wave length much larger than λ_F. We will see later that this perpendicular energy selection bears consequences on the length scale characterizing the dependence of the total current on the radius of the interface.

In general, knowledge of the current angular distribution is physically relevant, as one is ultimately interested in directionally separating the pair of entangled electron beams for eventual quantum information processing. To acquire a more complete picture, we may compare the previous results with the case of a NN interface. In that

case the total tunnel current is

$$I_{\rm NN} = I_V \tau^2 \int_0^{\pi/2} d\theta \, \sin\theta \, g(\theta) \,, \tag{2.44}$$

where I_V is given in Eq. (2.34) and, for large u,

$$g(\theta) = 2\cos^3\theta \,. \tag{2.45}$$

Thus we see that electron transport through a tunneling NN interface also exhibits focussing which is however less sharp than in the NS case [see Eq. (2.39)]. The term τ^2 in Eq. (2.45) reflects the dominance of single-electron tunneling at the NN interface. Finally, we may compare Eqs. (2.39) and (2.45) with the $\cos\theta$ distribution law exhibited by electron current in the bulk of a disordered wire [7].

2.6.1 Connection with the multi-mode picture

We could have derived the angular distributions in Eqs. (2.33), (2.39), (2.44) and (2.45) following the scattering theory of conduction in normal [152–154] and normal-superconducting [138] multichannel wires. For an NN interface in the zero temperature limit and for a small applied voltage, the Landauer-Büttiker formalism gives us the relation between conductance and transmission probabilities at the Fermi energy

$$G_{\rm NN} = \frac{2e^2}{h} {\rm Tr}[t^\dagger(E_F) t(E_F)] = \frac{2e^2}{h} \sum_{n=1}^{N} T_n = \frac{2e^2}{h} \sum_{n,m} T_{n,m}^{RL} \,. \tag{2.46}$$

Here, the matrix t is the off-diagonal block of the scattering matrix describing the scatterer, and T_n ($n = 1, 2, ...N$) are the eigenvalues of the transmission matrix $t^\dagger t$ at the Fermi energy. Since the trace of $t^\dagger t$ is a basis invariant expression, it is possible to express the conductance in terms of the transmission probabilities $T_{mn}^{RL} = |s_{{\rm RL},mn}|^2$, where s is the scattering matrix, for carriers incident in channel n in the left lead L and transmitted into channel m in the right lead R. In this basis the Hamiltonians of the left and right leads (the reservoirs) are diagonal, and the conductance can be expressed like in the last equality in Eq. (2.46). In the case of a broad interface whose dimensions equal those of the reservoirs, which is the one we are considering here, since the parallel momentum to the interface $\mathbf{k}_{||}$ is a conserved quantity, it already represents the set of eigen-channels of our problem. Therefore, in order to calculate the conductance of Eq. (2.46), we can consider the transmission probability through a square barrier of Eq. (2.15). We replace $T_n \to T(E_z)$. For $E_z/U_0 \ll 1$ we have

$$T(E_z) = 16 \frac{E_z}{U_0} e^{-2p_0 w} = \tau^2 \frac{E_z}{E_F} \,, \tag{2.47}$$

[7] There, under the constraint of a given total current, entropy is maximized by the electron system adopting a displaced Fermi sphere configuration which exactly yields the $\cos\theta$ law.

thus $T(E_z) \propto E_z \propto \cos^2\theta$. Moreover, the sum over transverse modes can be replaced by an integration over the zenithal angle, $\sum_n \to \text{cnst.} \times \int_0^{\pi/2} d\theta \sin\theta\cos\theta$. Altogether, the angular distribution follows exactly the $\cos^3\theta$ law expressed in Eq. (2.45).

A similar line of argument can be made for the Andreev current through a NS interface, whose conductance according to Beenakker's formula is given by[8]

$$G_{\rm NS} = \frac{2e^2}{h} \sum_{n=1}^{N} \frac{2\,T_n^2}{(2-T_n)^2}\,. \tag{2.48}$$

In the tunneling limit one has $T_n \ll 1$ and G_{NS} can thus be approximated as

$$G_{\rm NS} \simeq \frac{2e^2}{h} \sum_{n=1}^{N} \frac{T_n^2}{2}\,. \tag{2.49}$$

Arguing as we did for the NN conductance, it follows that $g(\theta) \propto \cos^5\theta$, which confirms Eq. (2.39). Therefore, in the tunneling limit there is a one to one correspondence between the conductance calculated with the Bardeen's Hamiltonian through the T-matrix approach and the scattering formalism of Landauer-Büttiker and Beenakker. We note here that, in Refs. [132, 138], the *Andreev approximation* was made whereby all the momenta involved are assumed to be equal to k_F. In our language, this corresponds to taking $\delta \to 0$ in Eq. (2.35) and thereafter.

Finally, comparison of Eqs. (2.46) and (2.49) also illuminates the contrast between the factor $\tau^4/2$ in Eq. (2.33) and the factor τ^2 in Eq. (2.44).

2.6.2 Universal relation between NN and NS tunneling conductances

In the case of a normal interface with high barrier, the total current can be integrated to yield

$$I_{\rm NN} = \frac{I_V \tau^2}{2} = \left(\frac{2e^2}{h}\right)\frac{\tau^2}{2} NV\,. \tag{2.50}$$

Thus $\tau^2/2$ is the average transmission per channel in a $3D$ geometry [9]. In one dimension ($N = 1$) one has $I_{\rm NN}^{1D} = (2e^2/h)V\tau^2$. Eqs. (2.34), (2.40), and (2.50)

[8] As noted in Ref. [132], the equivalence invoked in Eq. (2.46) between the sum of eigenvalues and the sum of modal transmission probabilities is no longer applicable in Eq. (2.48) because of its nonlinearity.

[9] Together with the factor appearing in the definition (2.34), this factor 1/2 yields the 1/4 geometrical correction given by Ref. [155] and cited in Ref. [124]. We emphasize however that such 1/4 correction applies only to the normal conductance, as derived in Ref. [155], but not to the NS interface where, rather, the correct geometrical correction is 1/12, as implicitly noted in Eqs. (2.34) and (2.42).

suggest the universal relation

$$\frac{I_V I_{\rm NS}}{(I_{\rm NN})^2} = \frac{G_V G_{\rm NS}}{(G_{\rm NN})^2} = \frac{2}{3}\,, \tag{2.51}$$

where $G_i = I_i/V$ $(i = \mathrm{V}, \mathrm{NS}, \mathrm{NN})$. Eq. (2.51) indicates that knowledge of $G_{\rm NS}$ and $G_{\rm NN}$ may allow us to infer G_V and, from (2.34), the *effective area* of a tunneling interface.

2.6.3 Comparison with the quasiparticle scattering method

Blonder et al. [124] studied transport through a one-dimensional NS interface modeled by a delta-barrier one-electron potential $[U(z) = H\delta(z)]$ by solving for the quasiparticle scattering amplitudes. If the dimensionless parameter $Z = mH/\hbar^2 k_F$ is employed to characterize the scattering strength of the barrier, the tunneling limit corresponds to $Z \gg 1$, for which they obtained $I_{\rm NS}^{\rm 1D} = I_V/Z^4$ assuming $k_B T \ll eV \ll \Delta \ll E_F$ (i.e. a low-transmission regime in which Andreev reflection is the only charge-transmitting channel). Later, Kupka generalized the work of Ref. [124] to investigate the sensitivity of Andreev and normal reflection to the thickness of the barrier [127] and to the presence of a realistic 3D geometry [128]. For the case of a broad interface in the tunneling limit he obtained $I_{\rm NS}^{\rm 3D} = I_V/6Z^4$. Therefore, Kupka found a result identical to Eq. (2.41) (to zeroth order in δ) with τ replaced by $1/Z$. In fact, it is easy to see that, in the case of a delta-barrier with $Z \gg 1$, the transparency defined in Sec. 2.4 is precisely $\tau = 1/Z$. Therefore, comparison of Eqs. (2.39) and (2.41) with the results of Ref. [128] completes the discussion of Sec. 2.2 by establishing the *quantitative equivalence* between the pictures of quasiparticle Andreev reflection and two-electron (or two-hole) emission. We note that, in Refs. [124, 127, 128], the Andreev approximation ($\delta \to 0$) was made.

2.7 Current through a circular interface of arbitrary radius

In this section we investigate transport through a circular NS tunneling interface of arbitrary radius. The setup is as depicted in Fig. 2.2(a). To make the discussion more fluent, lengthy mathematical expressions have been transferred to Appendix B, leaving here the presentation of the main results, which include some analytical expressions for the limit of small gap and high barrier.

2.7.1 Total current

The most general expression for the current is given in Eq. (B.1). Below we focus on the limit $\delta, u^{-1} \ll 1$. We find three regimes of interest, depending on the value of

R/λ_F.

Small radius ($R \ll \lambda_F$)

This limit is not physically realizable, at least with current materials. However, it is interesting for two reasons. First, it yields a radius dependence that directly reflects the entangled nature of the electron current. Second, it can be used as a unit of current such that, when referred to it, calculated currents have a range of validity that goes well beyond the geometrical model here considered. That permits a direct comparison between different theoretical models and experimental setups.

For $k_F R \ll 1$ we obtain

$$I(R) \simeq I_0 \equiv \frac{2\pi}{6^4} J_V \tau^4 k_F^6 R^8. \tag{2.52}$$

This R^8 behaviour is easy to understand. To compute the current we must square the matrix element between the initial and the final state, i.e. the Cooper pair hopping amplitude. The tunneling of each electron involves an integral over the interface, which for $k_F R \ll 1$ contributes a factor R^2 to the amplitude, regardless of the incident angle. The Cooper pair amplitude becomes $\sim R^4$, which leads to the R^8 behaviour for the probability.

It is interesting to compare the R^8 law here derived with, e.g. the R^4 behaviour of the NN tunnel current ($u \gg 1$), namely,

$$I_0 \simeq \frac{\pi}{9} J_V \tau^2 k_F^2 R^4 \,, \tag{2.53}$$

or with the R^6 dependence for the transmission of photons through a circular aperture [156].

Eqs. (2.52) and Eq. (2.53) yield the following relation for the narrow interface conductances:

$$G_{\rm NS} = \frac{h}{4e^2} G_{\rm NN}^2 \;\; (R \to 0) \;. \tag{2.54}$$

It is important to note that Eq. (2.54) still applies if both conductances are replaced by their momentum-independent counterparts.

In Fig. 2.4 we plot the current density as a function of the interface radius. Dots represent the exact calculation taken from Eqs. (B.3) and (B.5), which we have been able to evaluate numerically for $u \to \infty$ (up to $R = 1.65\lambda_F$) and $u = 10$ (up to $R = 3\lambda_F$), while solid lines are obtained from a large-radius approximation described in Appendix B. For $u = 1.1$ convergence problems prevent us from presenting numerically exact results. We find that the small-radius approximation ($\sim R^8$) is correct within 1% accuracy up to $R \sim 0.1\lambda_F$. Above that value it overestimates the current.

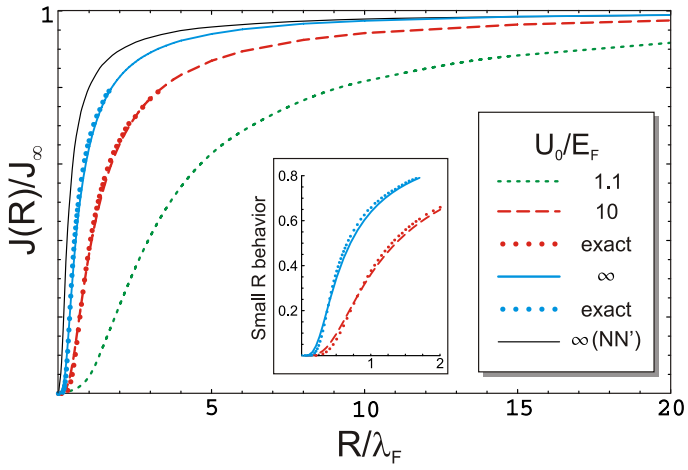

Figure 2.4: Radial dependence of the normalized NS Andreev tunnel current through a circular interface of radius R for different barrier heights. $J(R) \equiv I(R)/\pi R^2$ and J_∞ is the current density in the thermodynamic limit. Finite barriers have a width $w = 5\lambda_F$. Everywhere $\Delta/E_F \ll 1$ is taken. Dots correspond to numerically exact results. Solid lines are computed with an approximation described in Appendix B which becomes exact for $R/\lambda_F \gg 1$. The inset magnifies results for small R.

Intermediate radius ($\lambda_F < R < \infty$)

In this region no analytical expression for the current is possible. Above $R \approx 2\lambda_F$ even the numerical calculation of Eq. (B.5) (which presumes $\delta, u^{-1} \ll 1$) is difficult, since for large radii we cannot compute five strongly oscillating nested integrals. A set of two approximations which reduces the number of nested integrals from five to three is discussed in Appendix B and expressed in Eqs. (B.6) and (B.8).

In Fig. 2.4 we plot $I(R)/I(R \to \infty)$, which is the total current normalized to the thermodynamic limit expression (2.33) with A in Eq. (2.34) replaced by πR^2. For finite barriers, $w = 5\lambda_F$ has been taken. A free parameter has been adjusted to fit the numerically exact result in the region where it is available. As explained in Appendix B, such a scheme is particulary well suited for moderate-to-large radius values. The inset of Fig. 2.4 shows that, as expected, the approximation fails for small values of R, where it yields an R^4 behaviour instead of the correct R^8 law, thus overestimating the current.

Here we wish to remark that, unlike in the case of a clean NS point contact [132, 138], the radial current dependence shows *no structure of steps and plateaus* as more channels fit within the area of the interface. This is due the fact that we operate in the tunneling regime, which decreases the height of the possible steps and, more importantly, to the strongly non-adiabatic features of the structure along the z-direction.

Large radius ($R \to \infty$)

While a numerically exact calculation is already nonfeasible for R a few times λ_F, the approximation described in Appendix B becomes increasingly accurate for large R. This allows us to conveniently investigate how the broad interface limit is recovered [see Eqs. (2.33) and (2.41)]. Such a limit is characterized by $I(R)$ growing with R^2, i.e. proportionally to the area, a behaviour also shown by the NN conductance. Convergence to the thermodynamic limit is much slower for low barriers than for large barriers. The reason has to do with *focussing*. The wave length of the characteristic energies $E_\parallel = E - E_z$ determines the length scale over which the relative phase between distant hopping events varies appreciably. This is the distance over which multiple hopping points (which play the role of multiple "Feynman paths") cancel destructively for large radius interfaces. As discussed in the previous section, low barriers are more energy selective, making most of the electrons leave with E_z close to E_F and thus with small $E_\parallel$. As a consequence, saturation to the large radius limit is achieved on the scale of many times λ_F. By contrast, high barriers are less energy selective and give a greater relative weight to electrons with low E_z and high $E_\parallel$. A large fraction of the electrons has a short parallel wave length. This explains why, for high barriers, the large R behaviour is reached on a short length scale.

2.7.2 Length scales in the thermodynamic limit

It is known that pairing correlations between electrons decay exponentially on the scale of the coherence length $\xi_0 = \lambda_F/\pi^2\delta$. This fact is reflected by the exponential factors contained in the integrands of the equations for $I(R)$ in Appendix B. Thus one might expect that the thermodynamic limit relies on such a decay of correlations.

The following argument might seem natural. The double integral over the interface of area A may be viewed as an integral of the two-electron centre of mass, which yields a factor A, and an integration over the relative coordinate, which is independent of A due to a convergence factor which expresses the loss of pairing correlations. The final current would grow as $I \sim A\xi_0^2 \sim A/\delta^2$. However, as discussed in the previous subsection, the thermodynamic limit is achieved on a much shorter scale, namely, the Fermi wave length. If an electron leaves through point $\mathbf{r}_1$ one may wonder what is the contribution to the amplitude stemming from the possibility that the second electron leaves through $\mathbf{r}_2$, eventually integrating over $\mathbf{r}_2$. Eq. (2.25) suggests that the amplitude for two electrons leaving through $\mathbf{r}_1$ and $\mathbf{r}_2$ will involve the sum of many oscillating terms with different wave lengths, the shortest ones being $\sim \lambda_F$. This reflects the interference among the many possible momenta that may be involved in the hopping process. Such an interference leads to an oscillating amplitude which decays fast on the scale of λ_F, rendering the exponentially convergent factor irrelevant. Thus, in the thermodynamic limit the current tends to a well defined value for $\xi_0 \to \infty$ ($\delta \to 0$). In Appendix B we provide a more mathematical discussion of this result.

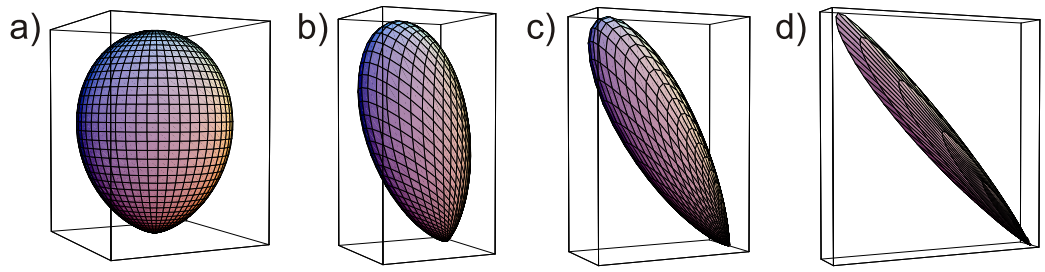

Figure 2.5: Angular correlation profile (in arbitrary units) of the conditional probability distribution $P(\Omega|\Omega_0)$ that, in a given tunneling event, an electrons goes into Ω if the other electron has gone into Ω_0. Here we plot $P(\Omega|\Omega_0)$ as a function of Ω for fixed $\Omega_0 \equiv (\theta_0, \phi_0) = (\pi/4, 0)$. From left to right the radii are: $R = 0.01, 0.5, 1, 3\lambda_F$. Observe that, as R increases, the angular dependence of the second electron tends to be the conjugate of the first one, i.e. the distribution becomes peaked around $\Omega = (\pi/4, \pi)$. Note also that, for small R, $P(\Omega|\Omega_0)$ becomes $\propto \cos^2\theta$ regardless of Ω_0.

One may also investigate the first correction for small, finite δ. As indicated in Eqs. (2.40) and (2.41), it increases the current. However, in the presence of a finite cutoff ($\varrho_c < \infty$), a nonzero value of δ generates the opposite trend. As discussed in Appendix B, at tiny relative distances between hopping points ($|\mathbf{r}_1 - \mathbf{r}_2| \lesssim \delta\lambda_F$), the amplitude increases considerably. A finite upper momentum cutoff rounds the physics at short length scales, thus eliminating such a short-distance increase. The result is that, with a finite cutoff, the first correction to the $\delta = 0$ limit is a decreasing linear term in δ, as revealed in Eq. (2.42).

2.7.3 Angular distribution and correlation

We have computed the conditional probability distribution $P(\Omega|\Omega_0)$ for an electron to be emitted into $\Omega \equiv (\theta, \phi)$ given that the other electron is emitted in a fixed direction Ω_0. Such a distribution is shown in Fig. 2.5 for $\Omega_0 = (\pi/4, 0)$. We observe that, for large R/λ_F, the angular distribution of the second electron is quite focussed around $\Omega = (\pi/4, \pi)$, which is mirror-symmetric to Ω_0 [see Fig. 2.5(d)]. As R/λ_F decreases, the angular correlation between electrons disappears and, as a function of Ω, $P(\Omega|\Omega_0)$ becomes independent of the given value of Ω_0. In particular it tends to $\sim \cos^2\theta$ [see Fig. 2.5(a)].

We may also study the probability distribution that one electron is emitted into direction Ω regardless of the direction chosen by the other electron. This amounts to the calculation of an effective $g(\theta)$ for a finite radius interface to be introduced in an equation like Eq. (2.33) to compute the current (by symmetry, such a distribution is independent of ϕ). As expected, one finds such effective angular distribution to be $\sim \cos^5\theta$ for large R [see Eq. (2.39)], which contrasts with the sharp Ω-dependence of

the conditional angular distribution $P(\Omega|\Omega_0)$ for given Ω_0.

For small R, the effective $g(\theta)$ goes like $\cos^2\theta$, i.e. it becomes identical to $P(\Omega|\Omega_0)$. This coincidence reflects the loss of angular correlations. The $\cos^2\theta$ behaviour may be understood physically as stemming from a random choice of final $\mathbf{k}_\parallel$, which yields a $\cos\theta$ factor (since $|\mathbf{k}_\parallel| = k_F \sin\theta$), weighted by a $\cos\theta$ reduction accounting for the projection of the current over the z direction. An equivalent study for a NN interface yields also $g(\theta) \propto \cos^2\theta$. Thus we see that the loss of angular correlations after transmission through a tiny hole makes the NN and NS interfaces display similar angular distributions.

The crossover from $g(\theta) \propto \cos^2\theta$ to $\cos^5\theta$ as R increases involves a decrease of the width $\Delta\theta$ of the angular distribution. A detailed numerical analysis confirms this result but reveals that $\Delta\theta$ is not a monotonically decreasing function of R (not shown).

2.8 Nonlocal entanglement in a two-point interface

Let us turn our attention to a tunneling interface consisting of two small holes, as depicted in Fig. 2.2(b). By "small" we mean satisfying $R/\lambda_F \ll 1$. This is the limit in which the detailed structure of a given hole is not important and the joint behaviour of the two holes is a sole function of their relative distance r and the current that would flow through one of the holes if it were isolated. We expect the conclusions obtained in this section to be applicable to similar interfaces made of pairs of different point-like apertures such as, e.g. two point-contacts or two quantum dots weakly coupled to both electrodes [38].

The current through a two-point interface has three contributions. One of them is the sum of the currents that would flow through each hole in the absence of the other one. Since the two orifices are assumed to be identical we refer to it as $2I_0$, where I_0 is given in Eq. (2.52). This contribution collects the events in which the two electrons tunnel through the same opening. A second contribution $I_e(r)$ comes from those events in which each electron leaves through a different hole. This is the most interesting contribution since it involves two non-locally entangled electrons forming a spin singlet. The third contribution, $I_i(r)$, accounts for the interference between the previous processes.

If we write

$$I = 2I_0 + I_e(r) + I_i(r)\,, \tag{2.55}$$

we obtain for the entangled current in the high barrier limit

$$I_e(r) = 18I_0[B^2(k_F r) + F^2(k_F r)B^2(k_F r)]\,, \tag{2.56}$$

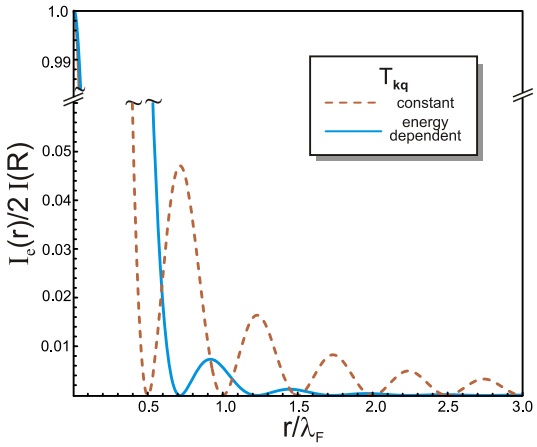

Figure 2.6: Current density through a two-point interface stemming from non-locally entangled electron pairs, as a function of the distance between points. The dashed line corresponds to the current obtained using an energy-independent hopping approximation whereas in the solid line the correct momentum dependence has been taken into account.

where $B(x)$ is defined in Eq. (B.10) and

$$F(x) = 3\,\frac{\sin x - x\cos x}{x^3}\,. \tag{2.57}$$

For $\delta \ll 1$, and noting that we are not interested in tiny distances $r \lesssim \delta\lambda_F$, we can write

$$I_e(r) = 2I_0[F^2(k_F r) + F^4(k_F r)]e^{-2r/\pi\xi_0}\,. \tag{2.58}$$

This is a fast decay because of the geometrical prefactor, which goes like r^{-4} for $k_F r \gg 1$. For instance, $I_e(\xi_0)/I_e(0) \sim 10^{-15}$, with data taken from Al ($\xi_0 \simeq 10^3\lambda_F$). For possible comparison with other tunneling models it is interesting to write the entangled conductance $G_e(r) \equiv I_e(r)/V$ in terms of the normal conductance through one narrow hole, $G_{\rm NN}$. Using Eq. (2.54), we obtain

$$G_e(r) = \frac{h}{2e^2}G_{\rm NN}^2\,[F^2(k_F r) + F^4(k_F r)]e^{-2r/\pi\xi_0}\,. \tag{2.59}$$

To keep track of the interference terms, it is convenient to adopt a schematic notation whereby $H_T = t_a + t_b$ is the tunneling Hamiltonian through points a and b. Then one notes that, as obtained from Eqs. (2.26), (2.27) and (2.30), the total current can be symbolically written as $I \sim |(t_a + t_b)(t_a + t_b)|^2$. In this language $I_0 \sim |t_a t_a|^2$. The F^2 term in (2.58) corresponds to $\sim |t_a t_b|^2 + |t_b t_a|^2$, while the F^4 term stems from the interference $\sim (t_a t_b)(t_b t_a)^* + \text{c.c.}$ Altogether, $I_e(r) \sim |t_a t_b + t_b t_a|^2$.

The interference current may be divided into two contributions,

$$I_i = I_{i1} + I_{i2}\ , \tag{2.60}$$

corresponding to the different types of outgoing channel pairs which may interfere. The first contribution stems from the interference between both electrons leaving through point a and both electrons leaving through point b, $I_{i1} \sim (t_a t_a)(t_b t_b)^* + \text{c.c.}$ One obtains

$$I_{i1}(r) = 2I_0 F^2(k_F r) \ . \tag{2.61}$$

$I_{i2}(r)$ comes from the interference between the channel in which the two electrons leave through the same hole and that in which they exit through different openings, $I_{i2}(r) \sim (t_a t_a)(t_a t_b)^* + \text{c.c.}$, plus three other equivalent contributions, altogether summing

$$I_{i2}(r) = 8I_0 F^2(k_F r) e^{-r/\pi\xi_0} \ . \tag{2.62}$$

In the hypothetical case where orifices a and b are connected to different normal electrodes [e.g. when an opaque barrier divides into two halves the normal metal of Fig. 2.2(b)], the interference contributions (2.61) and (2.62) would be absent. Then one would have $I = 2I_0 + I_e(r)$. Furthermore, if any mechanism prevents the two electrons from leaving through the same opening (like, e.g. by means of two quantum dots weakly coupled to the orifices and properly engineered [38]), then $I = I_e(r)$.

2.9 Failure of the momentum-independent hopping approximation

It has been common in the literature on the tunneling Hamiltonian to assume that the tunneling matrix elements appearing in (2.4) are independent of the perpendicular momenta $k_z q_z$ (see, for instance, Ref. [144]). Below we show that, for three-dimensional problems, such an assumption is unjustified and leads to a number of physical inconsistencies [10].

For simplicity we focus on the high barrier limit. To investigate the consequences of the momentum-independent hopping approximation, we replace Eq. (2.12) by

$$T_{\mathbf{kq}} = \frac{\tau}{\Omega N(0)} \delta(\mathbf{k}_\parallel - \mathbf{q}_\parallel)\, k_F^2 \,, \tag{2.63}$$

i.e. we change $k_z q_z$ by k_F^2.

Broad interface. For a large NS junction, we find that the total current in units of I_V diverges ($x \equiv \cos\theta$):

$$I_{\rm NS} = \tau^4 I_V \int_0^1 \frac{dx}{x} \, \frac{x^2 + \sqrt{x^4 + \delta^2}}{2(x^4 + \delta^2)} \to \infty \,, \tag{2.64}$$

[10] We do not rule out, however, that the errors derived from the use of Eq. (2.63) may cancel in the calculation of some physical quantities such as e.g. the ratio between the critical current and the normal conductance of a superconducting tunnel junction [144, 157].

i.e. $I_{\rm NS}$ grows faster than A for $A \to \infty$. Eq. (2.64) is the analogue of Eqs. (2.33) and (2.38), where $I_{\rm NS} \sim \int_0^1 dx\,(x^5 + x^3\sqrt{x^4+\delta^2})$.

A different divergence occurs for a broad NN tunnel junction:

$$I_{\rm NN} = 2\tau^2 I_V \int_0^1 \frac{dx}{x} \to \infty\,, \tag{2.65}$$

which contrasts with the finite integral $I_{\rm NN} \sim \int_0^1 dx\, x^3$ obtained from inserting (2.45) into (2.44).

Local Hamiltonian. If one attempts to derive the real space tunneling Hamiltonian with the assumption (2.63), one obtains an expression identical to that in Eq. (2.20) with $\widetilde{L}(z,z')$ replaced by

$$\widetilde{M}(z,z') = \frac{k_F^2}{L_z}\sum_{k_z,q_z} \varphi_{k_z}(z)\,\varphi^*_{q_z}(z')\,. \tag{2.66}$$

As in Sec. 2.4, we use stationary waves for $\varphi_{k_z,q_z}(z)$. Invoking the identity

$$\sum_{k_z>0} \sin(k_z z) = \mathcal{P}\frac{1}{z} \tag{2.67}$$

we obtain

$$H_T = \sum_\sigma \frac{\tau k_F^2}{2\pi^4 N(0)} \int d\mathbf{r} \int_{-L}^0 \frac{dz}{z} \int_0^L \frac{dz'}{z'}\, \psi^\dagger_N(\mathbf{r},z;\sigma)\psi_S(\mathbf{r},z';\sigma) + \text{H.c.}\,, \tag{2.68}$$

where the reference to the principal value has been removed because, in the tunneling limit, the fields vanish linearly at the origin.

If we had chosen plane wave functions for φ_{k_z,q_z} in Eq. (2.66), we would have obtained a different Hamiltonian, namely,

$$H_T = \sum_\sigma \frac{\tau k_F^2}{8\pi^2 N(0)} \int d\mathbf{r}\, \psi^\dagger_N(\mathbf{r},0;\sigma)\psi_S(\mathbf{r},0;\sigma) + \text{H.c.}\,, \tag{2.69}$$

which is some times proposed in the literature (see e.g. Ref. [39]). This situation, whereby plane-wave and stationary-wave representations lead to different, both unphysical, local Hamiltonians contrasts with the scenario obtained with the right matrix element. As noted in Sec. 2.4, the more physical choice (2.12) leads in both representations (plane and stationary waves) to the correct local Hamiltonian (2.24). The fact that Eq. (2.63) leads to a wrong real space Hamiltonian which, moreover, depends on the choice of representation, may be viewed as further proof of the inadequacy of the energy-independent hopping model.

Thermodynamic limit. For a NS interface with $\delta \to 0$, a dimensional analysis for $A \to \infty$ suggests that the total current $I_{\rm NS}$ diverges non-thermodynamically like $\sim A^2$. For a NN interface, we find the divergence $A \ln A$.

Unitarity. The divergences expressed in Eqs. (2.64) and (2.65), as well as the related anomalous thermodynamic behaviour, could have been anticipated by noting that, if $T_{\mathbf{kq}}$ is assumed to be independent of energy, then Eq. (2.15) must be multiplied by $(E_F/E_z)^2$. As a result, the transmission probability at energy E_z, which should stay smaller than unity, grows instead as $T(E_z) \sim E_z^{-1}$ for $E_z \to 0$. Such a violation of unitarity necessarily generates a divergent current in the broad interface limit for both NN and NS interfaces.

Nonlocally entangled current. Finally, we note that, using (2.63), the nonlocally entangled current through two distant points is

$$\tilde{I}_e(r) = 2\,\tilde{I}_0[\tilde{F}^2(k_F r) + \tilde{F}^4(k_F r)]e^{-2r/\pi\xi_0}\,, \tag{2.70}$$

where

$$\tilde{F}(x) = \frac{\sin x}{x}\,, \tag{2.71}$$

with the tildes generally referring to the momentum-independent approximation. Here, $\tilde{I}_0 = 81 I_0$ is the current through one narrow hole. Correspondingly, the entangled conductance $G_e(r)$ is written like in Eq. (2.59) with $F(k_F r)$ replaced by $\tilde{F}(k_F r)$.

Comparison of Eqs. (2.58) and (2.70) indicates that the r-dependence of the geometrical prefactor is markedly different: For growing r, the nonlocally entangled current decays much more slowly (r^{-2}) than its momentum-dependent counterpart (r^{-4}). It is interesting to compare the ratios $\lambda(r) \equiv I_e(r)/I_e(0)$ and $\tilde{\lambda}(r) \equiv \tilde{I}_e(r)/\tilde{I}_e(0)$. While $\lambda(0) = \tilde{\lambda}(0) = 1$ by construction, the ratio $\lambda/\tilde{\lambda}$ becomes $\sim 6 \times 10^{-4}$ and 2×10^{-7} for $r/\lambda_F = 20$ and 10^3, respectively.

Interference terms. As expected from the comparison of Eqs. (2.58) and (2.70), the interference contributions are identical to those discussed in the previous section with $F(k_F r)$ replaced by $\tilde{F}(k_F r)$ in Eqs. (2.61) and (2.62).

Generality of the model. An important question is whether our results for the entangled and interference currents through pairs of tiny geometrical holes apply to other, more realistic pairs of small interfaces such as two point contacts or two quantum dots [38]. The fact that the decay with distance of the entangled current reported in Refs. [37–39, 42–45, 48, 50] follows the same law as Eqs. (2.70) and (2.71) (except for the $\tilde{F}^4$ term there neglected), suggests that such is indeed the case. Below we prove this expectation.

Due to Eq. (2.25), the sum in Eq. (2.32) involves

$$\sum_{\mathbf{q}} \frac{u_{\mathbf{q}} v_{\mathbf{q}}}{E_{\mathbf{q}}} q_z^2 e^{-i\mathbf{q}_\parallel\cdot(\mathbf{r}_1-\mathbf{r}_2)}\,. \tag{2.72}$$

This sum over $\mathbf{q}$ is clearly affected by the presence of the q_z^2 factor, yielding a result $\propto F(k_F r)$, with $r = |\mathbf{r}_1 - \mathbf{r}_2|$. In the momentum-independent hopping approximation, q_z^2 is replaced by k_F^2, rendering the sum $\propto \tilde{F}(k_F r)$. In fact, the two functions are related:

$$\frac{\partial^2}{\partial z^2}\tilde{F}(k_F\sqrt{r^2+z^2})\bigg|_{z=0} = \frac{1}{3}k_F^2 F(k_F r)\ . \tag{2.73}$$

We note that the distance dependence is determined by the properties of the superconductor and not by those of the normal electrode. If a quantum dot mediates between the superconductor and the normal metal, then an effective hopping must be introduced in (2.72) which, however, does not add any new momentum dependence [see Eq. (11) of Ref. [38]]. Departure from the specific type of contact here considered will translate only into a different value of I_0, the distance dependent prefactor remaining identical. We notice, however, that the preceding discussion is restricted to the case where quasiparticle propagation is ballistic in both electrodes, i.e. we neglect the effect of impurities, additional barriers or close boundaries [158].

2.10 Related experiments

As explained in the introduction of this chapter, interest has been created, in the context of solid state physics, over the possibility of building up a source of nonlocal entangled electrons, which is usually called an *entangler*. In this sense, some very recent experiments have dealt with the idea of extracting singlet-entangled Cooper pairs from a superconductor with two normal metals attached to it at a certain distance [120, 129, 130].

In our work in this thesis we have considered 3D ballistic semi-infinite metals. In Sec. 2.8 we found that the current steaming from two distant tunneling contacts from a superconductor is cut off by a decaying exponential with the superconductor coherence length and further modulated by a geometrical prefactor which decays quickly at scales of the Fermi wave length. This problem was also encountered by other theoretical works, although in a less pessimistic fashion due to the use of the momentum-independent tunneling Hamiltonian [38, 39, 42, 43, 45, 48–50, 52]. In any case, some theoretical groups realized that the spatial dependence of the geometrical prefactor with the distance r between the two normal leads attached to the superconductor could be improved, i.e., made less decaying with r, if the dimensionality of the superconductor was reduced [45, 49, 50] or it was considered to be in the diffusive regime [48, 52]. These results motivated the experimental search for crossed Andreev or *entangled* non-local current.

In the work called "Experimental Observation of Bias-Dependent Nonlocal Andreev Reflection" by S. Russo, M. Krough, T.M. Klapwijk and A.F. Morpurgo in 2005 [120], the authors consider two normal electrodes (made of Al) connected via two extended tunnel barriers to one common superconducting electrode (made of Nb),

which is diffusive and has a coherence length of $10-15$ nm. The superconductor has a film shape, and the separation between the two tunnel barriers is determined by the thickness of the superconducting layer. The mechanism they use to detect CARE is the following: through one of the tunneling contacts ($J1$) they inject current into the superconductor below the gap, and the other contact ($J2$) is used as a voltage probe. As holes have the opposite charge of electrons, holes undergoing nonlocal Andreev reflection (AR) generate a voltage difference across $J2$ that has opposite sign to that observed when the superconductor is in the normal state ($T > T_c^S$). In this kind of setup another process competing with nonlocal AR is possible: electrons injected from $J1$ can be transmitted into $J2$ without being converted into holes. This process in called elastic cotanneling (EC), and it produces a voltage across $J2$ which has the same sign as that observed when the superconductor is in the normal state. Therefore, applying a voltage V_{dc} across the first junction $J1$, which generates a current into the superconductor, and measuring the nonlocal voltage V^{nl} across the other junction $J2$ while maintaining the superconductor at ground, they can know if the underlying process is dominated by CARE or by EC depending on the obtained sign of V^{nl} (or if the two processes cancel each other resulting in $V^{nl} = 0$). What they observed was that, at bias below the Thouless energy (E_{Th}) of the superconducting layer, the sign was the same as the sign of V_{dc}, indicating that EC dominates. At energies above the E_{Th} the sign was negative, opposite to that of V_{dc}, indicating the occurrence of CARE. They also measure how, increasing the width of the superconductor and therefore the distance between $J1$ and $J2$, both signals get strongly suppressed in absolute value. This very nice, clean and well explained experiment confirms the possibility of using a superconductor as an entangler. At the end of the article the authors themselves point out that the results they find have not yet been explained theoretically. To their believe, Coulomb interaction may play an important role in this problem. Let us add here that R. Mélin in a recent paper [56] has tried to explain this experiment by means of the weak localization contribution using a tight-binding description of the metals. Although he finds a change of sign in the crossed resistance between elastic cotunneling at low voltages and weak localization at higher voltage, the appearance of a voltage scale related to the superconductor Thouless energy is left as an open question.

Another experimental setup was considered in the work "Evidence of Crossed Andreev Reflection in Superconductor-Ferromagnet Hybrid Structures" by D. Beckmann, H.B. Weber and H.v. Löhneysen in 2004 [129]. There the superconductor is made of Al and has a dirty-limit coherence length of $200-300$ nm. Several ferromagnetic wires (presenting parallel or antiparallel orientation of their magnetizations) are connected by point contacts to the aluminum bar at different distances. Considering couples of wires, if the two contacts are spin polarized, EC and CAR are favourable for parallel and antiparallel alignment, respectively. At low temperatures and voltages well below the gap they measure a spin-dependent nonlocal resistance which decays on a smaller length scale than the normal-state spin-valve signal, signalling the pres-

ence of subgap transport. They propose a superposition of CAR and EC processes as the origin of the observed nonlocal resistance difference at temperatures well below T_c^S. Nevertheless, Ref. [120] considers that only the sign of V_{dc} corresponding to EC was indeed observed in this work.

Finally, we just mention that a high-T_c superconductor has also been used, in particular in the 2005 work called "Signature of a crossed Andreev reflection effect (CARE) in the magnetic response of $YBa_2Cu_3O_{7-\delta}$ junctions with the itinerant ferromagnet $SrRuO_3$", by P. Aronov G. and Koren [130].

2.11 Conclusions

We have investigated the electron current through a NS tunneling structure in the regime $k_BT \ll eV \ll \Delta$ where Andreev reflection is the dominant transmissive channel. We have rigorously established the physical equivalence between Cooper pair emission and Andreev reflection of an incident hole. A local tunneling Hamiltonian has been derived by properly truncating that of an infinite interface in order to describe tunneling through an arbitrarily shaped interface. Such a scheme has been applied to study transport through a circular interface of arbitrary radius and through an interface made of two tiny holes. In the former case, the angular correlations between the two emitted electrons have been elucidated and shown to be lost as the interface radius becomes small. We have also investigated how the thermodynamic limit is recovered, showing that, due to the destructive interference between possible exit points, it is achieved for radii a few times the Fermi wave length. For the case of a two-point interface, we have calculated the nonlocally entangled current stemming from processes in which each electron leaves the superconductor through a different orifice. We have found that, as a function of the distance between openings, such an entangled current decays quickly on the scale of one Fermi wave length. The interference between the various outgoing two-electron channels has also been investigated and shown to yield contributions comparable to the nonlocally entangled current. We have found that, in a three-dimensional problem, it is important to employ hopping matrix elements with the right momentum dependence in order to obtain sound physical results in questions having to do with the local tunneling Hamiltonian (whose correct form has also been obtained from a tight-binding description), the thermodynamic limit, the preservation of unitarity, and the distance dependence of the nonlocally entangled current through a two-point interface. An important virtue of the method here developed is that it enables the systematic study of Cooper pair emission through arbitrary NS tunneling interfaces. Besides, it can be used as an starting point for more sophisticated and realistic theoretical models where the metals are in the diffusive regime or Coulomb interactions are taken into account, as suggested by related experiments.

Chapter 3

Divergent beams of nonlocally entangled electrons emitted from resonant NS structures

In this chapter we propose the use of normal and Andreev resonances in normal-superconducting (NS) structures to generate divergent beams of nonlocally entangled electrons. Resonant levels are tuned to selectively transmit electrons with specific values of the perpendicular energy, thus fixing the magnitude of the exit angle. When the normal metal is a ballistic two-dimensional electron gas (2DEG), the proposed scheme guarantees arbitrarily large spatial separation of the entangled electron beams emitted from a finite interface. We perform a quantitative study of the linear and non-linear transport properties of some suitable structures, taking into account the large mismatch in effective masses and Fermi wavelengths. Numerical estimates confirm the feasibility of the proposed beam separation method.

The contents of this chapter were published in New J. Phys. **7**, 231 (2005), by E. Prada and F. Sols.

3.1 Introduction

The goal of using entangled electron pairs for the processing of quantum information poses a technological challenge that requires novel ideas on electron quantum transport. As mentioned in the previous chapter, it has been proposed that a conventional superconductor is a natural source of entangled electrons which may be emitted into a normal metal through a properly designed interface [37–40,42,43,45,48–53,56] . At low temperatures and voltages, the electric current through a NS interface is made exclusively of electron Cooper pairs whose internal singlet correlation may survive for some time in the context of the normal metal. The emission of two correlated electrons from a superconductor into a normal metal is often described as the Andreev

reflection [122] of an incident hole which is converted into an outgoing electron. The equivalence between the two pictures has been rigorously proved in Refs. [51,73,159].

The need for spatial separation of the entangled beams has motivated the search for schemes that constrain (or at least allow) the two pair electrons to be emitted from different locations at the NS interface [38]. In the conventional picture where quasiparticle scattering is unitary, that process is viewed as the absorption of a hole and its subsequent reemission as an electron from a distant point. Such a crossed Andreev reflection (CAR) has been observed experimentally [120, 129, 130].

The requirement of physical separation is a severe limitation in practice, since pairing correlations decay with distance. As a consequence, the current intensity of nonlocally entangled electrons decreases with the distance r between the two emitting points. There is an exponential decay on the scale of the superconductor coherence length which reflects the short-range character of the superconductor pairing correlations [38, 51]. A more important limitation in practice comes from the prefactor, which, besides oscillating on the scale of the superconductor Fermi wavelength, decreases algebraically with distance. In the tunneling limit, and for a ballistic 3D superconductor, the decay law is r^{-2}, if the tunneling matrix elements are assumed to be momentum independent [38], or r^{-4}, if proper account is taken of the low-momentum hopping dependence [51,118]. Within the context of momentum-independent tunneling models, the power law changes if the superconductor is low (d) dimensional [45,49], or diffusive [48,52], yielding r^{-d+1} and r^{-1}, respectively. It remains to be investigated how that behaviour changes when more realistic tunnel matrix elements are employed [51, 118] and when geometries other than planar or straight boundaries are considered.

In this chapter we propose an experimental setup that would guarantee long term separation of correlated electron pairs without the shortcomings caused by the need to emit the pair electrons from distant points. The idea is *to transmit both electrons through the same spatial region but inducing them to leave in different directions.* In a ballistic normal metal such as a 2DEG, that divergent propagation guarantees the long term separation of the entangled electrons at distances from the source much greater than the size of the source.

To force the pair electrons to leave in different directions, we propose to exploit the formation of resonances in a properly designed NS interface. These could be one-electron (normal) resonances, such as those found in double-barrier structures [160] (SININ structure), or two-electron (Andreev) resonances such as the de Gennes – Saint-James resonances appearing in structures with one barrier located on the normal metal side at some distance from the transmissive SN interface (SNIN structure) [77, 161–164]. Those quasi-bound states have it in common that, in a perfect interface, they select the perpendicular energy of the exiting electrons while ensuring the conservation of the momentum parallel to the interface. At low voltages and temperatures, this also determines the parallel energy, given that the total energy of the current contributing electrons is constrained to lie close to the normal Fermi level.

Altogether, this mechanism fixes the magnitude of the exit angle, since the parallel momenta of the pair electrons are opposite to each other and both remain unchanged during transmission through the perfect interface. Thus the electron velocities form a V-shaped beam centred around the perpendicular axis.

The type of structures which are needed seems to be within the reach of current experimental expertise. In the last fifteen years, several groups have built a variety of hybrid superconductor-semiconductor (SSm) structures [77, 120, 164–170]. More recently, some experimental groups [76,171,172] have investigated transport through SSm structures where Sm is a 2DEG on a plane essentially perpendicular to the superconductor boundary. In such setups, the SN interface lies at the one-dimensional (1D) border of the two-dimensional (2D) ballistic metal. If two parallel straight-line barriers were drawn in that structure, one along the SN interface and another one at some distance within N, then the experimental scenario considered in this article would be reproduced. A three-dimensional (3D) version of the same structure, in which Sm would be 3D and the interface would be 2D, of the type reported in Ref. [164], would also produce divergent electron beams. These, however, would be emitted into a 3D semiconductor, where it may be more difficult to pattern suitable detectors.

Once the two electrons propagate in the ballistic 2DEG, their motion can be controlled by means of existing techniques. For instance, they can be made to pass through properly located narrow apertures, such as those used in electron focusing experiments [173]. For quantum information processing, their spin component in an arbitrary direction could eventually be measured by using the Rashba effect [174,175] to rotate the spin before electrons enter the spin filter [176]. Then one could attempt to measure Bell inequalities [41, 46, 72, 73, 93, 113, 117, 177]. Alternatively, one may measure electric current cross-correlations [36,52,79,105,178] to indirectly detect the presence of singlet spin correlations.

In Sec. 3.2 we describe the model we have adopted for our calculations. Two important features are the offset between the conduction band minima and the difference in the effective masses of S and Sm. Both effects have been analyzed by Mortensen *et al.* [151] in the context of SIN structures, with N a 3D semiconductor. In Sec. 3.3 we focus on the linear regime and calculate the zero bias conductance using the multimode formula derived by Beenakker [138]. There we investigate the angular distribution of the outgoing electron current and observe how it is indeed peaked around two symmetric directions. Sec. 3.4 is devoted to the nonlinear regime [179], where the voltage bias may be comparable to the superconductor gap. We find divergent beams again, this time with new features caused by the difference between the electron and hole wavelengths. By plotting the differential conductance, we relate our work to the previous literature on SN transport and note the presence of a reflectionless tunneling zero bias peak [164, 166, 180], as well as the existence of de Gennes – Saint-James resonances. In Sec. 3.5 we discuss how the need to have a broad perfect interface, as required for parallel momentum conservation, can be reconciled with the

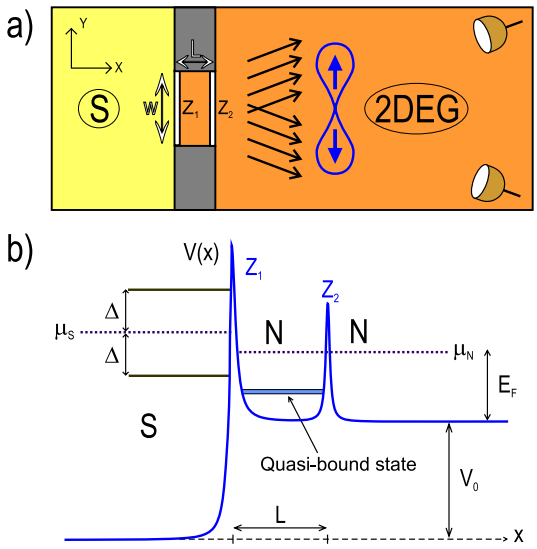

Figure 3.1: (a) Schematic representation of the SN structure considered in this chapter. S is a conventional superconductor; N is a two-dimensional electron gas. Energy selection in the x direction by the resonance structure limits current flow to two divergent beams of entangled electrons. (b) One-electron potential profile in the x direction. Quasi-bound electron states form due to multiple reflection by two barriers of strength Z_1 and Z_2.

interface finite size which is needed for the eventual spatial separation of the emerging beams. Some comments on experiments that use the type of structures needed for our proposal are made in Sec. 3.6. We conclude in Sec. 3.7.

3.2 The model

We wish to investigate the role of resonances in the angular distribution of the normal current in suitably designed SSm interfaces. A prototypical structure is shown in Fig. 3.1(a), where the 2DEG forms an angle with the planar boundary of a superconductor, similar to the setup built in Ref. [76].

In the present analytical and numerical work we consider a semi-infinite ballistic 2DEG (hereafter also referred to as N) lying in the half-plane $x > 0$. We assume a perfect interface, so that the one-electron potential is independent of y. Specifically, $V(x)$ is taken of the form

$$V(x) = -V_0\Theta(-x) + H_1\delta(x) + H_2\delta(x - L). \tag{3.1}$$

Here, V_0 accounts for the large difference between the widths of the S and N conduction bands. If $E_F = \hbar^2 k_F^2/2m$ and $E'_F = \hbar^2 k_F'^2/2m'$ are N and S Fermi energies, respectively, one typically has $E'_F \sim V_0 \gg E_F \gg \Delta$, where Δ is the zero-temperature

superconducting gap. We assume that the bulk parameters change abruptly at $x = 0$. The structure contains two delta barriers, located at the SN interface and at a distance L from it within the N side. Their reflecting power is measured by the dimensionless parameters Z_1 and Z_2, defined as $Z_1 = H_1/\hbar\,(v_F v'_F)^{1/2}$ and $Z_2 = H_2/\hbar v_F$. The effective mass m, the Fermi wavevector k_F, and the Fermi velocity v_F are those of the normal 2DEG, while m', k'_F, and v'_F correspond to a conventional superconductor.

It was shown in Chapter 2 [51] that the picture of two-electron emission and hole Andreev reflection are equivalent. For computational purposes, we employ here the standard Andreev picture whereby all quasiparticles have positive energy ($\varepsilon > 0$), with the quasiparticle energy origin given by μ_S. However, in our discussion we will occasionally switch between the two images. An important feature is that the absence of a hole at $\varepsilon > 0$ in the Andreev scenario corresponds to the presence of an electron at $-\varepsilon < 0$ in the two-electron picture [51].

In a transport context, the superconductor and normal metal chemical potentials differ by $\mu_S - \mu_N = eV$, where V is the applied bias voltage. In the Andreev picture, one artificially takes μ_S as the reference chemical potential for labeling quasiparticles and the imbalance eV is accounted for by introducing an extra population of incoming holes with energies between 0 and eV [124, 137].

An apparent shortcoming of the Andreev picture is that it does not show explicitly that the emitted electron pairs are internally entangled. In this respect, we may note the following remarks: (i) the two-electron hopping matrix element (2.31) of Eq. (2.27) vanishes when the spin state of the final state (2.29) in the N side is a triplet (instead of a singlet) [38]; (ii) an analytical study of transport through a broad SN interface based on a two-electron tunneling picture [51] (with the final state explicitly entangled) gives results identical to those obtained within an Andreev description [128]; (iii) entanglement in the outgoing electron pairs has been explicitly proven in the general tunneling case [159]; and (iv) transport across the SN structure is spin independent and thus must preserve the internal spin correlations of the emitted electron pair [181]. Moreover, using full counting statistics Samuelsson [182] has shown that current through an SN double-barrier structure is carried by correlated electron pairs.

To compute the current, we must sum over momenta parallel to the interface, which on the N side take values $-k_F < k_y < k_F$. For the purposes of solving the one-electron scattering problem, we assume that the superconductor is also two-dimensional. Due to the mismatch in effective masses, the perpendicular energy is not conserved (refraction). The conserved quantum numbers are the parallel momentum ($k_y = k'_y$) and the total energy ($E_x + E_y = E'_x + E'_y - V_0 = E$, with $E_x \neq E'_x$ and $E_y \neq E'_y$).

For a given k_y, the energy available for perpendicular motion in the normal side is $E_x = E - \hbar^2 k_y^2/2m$, where E is the electron total energy. As a consequence, for each k_y the picture depicted in Fig. 3.1(b) holds provided that the μ_N is replaced by

an effective value [151]

$$\mu_N(k_y) = \mu_N - \hbar^2 k_y^2/2m, \tag{3.2}$$

which is matched to $\mu_S(k_y) = \mu_S - \hbar^2 k_y^2/2m'$, with $\mu_S(k_y) - \mu_N(k_y)$ not equal to eV but bigger[1]. In this case, the resonant level must lie between the effective chemical potentials in order to have current.

Beenakker [138] has computed the SN zero bias conductance for an interface with many transverse modes. Mortensen *et al.* [151] have adapted the work of Ref. [124] to account for the full 3D motion through a perfect, 2D SSm interface, where the effective masses and the Fermi wavelengths of N and S may differ widely. Lesovik *et al.* [179] have generalized the work of Ref. [138] to the nonlinear case where eV may be comparable to Δ. They have applied their results to structures displaying quasiparticle resonances. Here we combine the work of these previous three references. Specifically, we investigate the transport properties of an SN interface for *arbitrary bias* V between 0 and Δ. We consider structures displaying *resonances* due to multiple quasiparticle reflection, and allow for a *large disparity between the* S *and* N *bulk properties*. Most importantly, we calculate the *angular distribution* of the pair electron current emitted into the semiconductor. Another novel feature is that the semiconductor we consider is a 2DEG whose plane forms an angle with the superconductor planar boundary, so that the SN interface is formed by a straight line.

3.3 Zero bias conductance

The zero bias conductance is defined as

$$G(0) \equiv \lim_{V\to 0} dI/dV, \tag{3.3}$$

where I is the total current at voltage bias V. For an SN interface [138],

$$G(0) \equiv \frac{4e^2}{h} \sum_{\nu=1}^{N} \frac{T_\nu^2}{(2-T_\nu)^2}\,, \tag{3.4}$$

where $\{T_\nu\}$ are the eigenvalues of the one-electron transmission matrix through the scattering region between the two contacts as if both metals were in the normal state. They are evaluated at total energy $E = \mu_N \simeq \mu_S \equiv \mu$. N is the number of transverse channels available for propagation in the normal electrode at energy μ. For a perfect interface, the index ν runs over the possible values of k_y. Thus, when needed, we make the replacement $\sum_\nu \to (w/2\pi)\int dk_y$, where $w \to \infty$ is the interface length. The minimum energy required for propagation in mode ν, referred to the bottom of the conduction band, is $E_\nu \equiv E_y = \hbar^2 k_y^2/2m$.

[1] With the notation we will introduce in the next section, where $m = r_k/r_v m'$ (see Sec. 3.3), we have $\mu_S(k_y) - \mu_N(k_y) = eV + E_y - E_y' = eV + (1 - r_k/r_v)\, E_y$.

In general, we consider throughout this chapter the following values for the parameters of our system. The ratios between the Fermi wavevectors and Fermi velocities in N and S are, respectively, $r_k \equiv k_F/k'_F = 0.007$ and $r_v \equiv v_F/v'_F = 0.1$ (GaAs values), which imply that $m = (r_k/r_v)m' = 0.07m_e$. The semiconductor conduction band width is taken $E_F = k_B \times 100$ K ≈ 8.62 meV, which gives $E'_F = E_F/(r_k r_v) \approx 12.31$ eV. Moreover, $\lambda_F \approx 50$ nm and $\lambda'_F \approx 0.35$ nm.

In the linear regime, the total energy is restricted to be at μ. Therefore we can write for the superconductor side: $\mathbf{k}' = (k'_x, k'_y) = k'_F(\cos\theta', \sin\theta')$, and for the normal metal side: $\mathbf{k} = (k_x, k_y) = k_F(\cos\theta, \sin\theta)$, being θ the angle between the N wave vector $\mathbf{k}$ and the normal to the interface, and θ' the angle between the S wave vector $\mathbf{k}'$ and the same normal. Since translational invariance symmetry holds along y direction, we have $k_y = k'_y$. This implies that the angle in the superconductor side can be expressed in terms of the angle in the normal side: $\sin\theta' = r_k \sin\theta$ and $\cos\theta' = \sqrt{1 - r_k^2 \sin^2\theta}$. Then, only the running value of k_y determines the exit angle

$$\theta \equiv \arctan\left(k_y/k_x\right), \tag{3.5}$$

since k_x and k_y must satisfy $k_x^2 + k_y^2 = k_F^2$. Therefore, Eq. (3.4) may be written as

$$G(0) = \int_{-\pi/2}^{\pi/2} d\theta \; G(0,\theta), \tag{3.6}$$

with $G(0,\theta)$ properly defined as the *angular distribution* of the zero bias conductance.

We can express $G(0,\theta)$ in terms of the transmission through the double barrier system:

$$G(0,\theta) = \cos\theta \frac{T(\theta)^2}{[2 - T(\theta)]^2}, \tag{3.7}$$

where

$$T(\theta) = \frac{T_1(\theta)T_2(\theta)}{1 + R_1(\theta)R_2(\theta) + 2\sqrt{R_1(\theta)R_2(\theta)}\cos[\beta_1(\theta) + \phi_2(\theta) - 2k_F L\cos\theta]}. \tag{3.8}$$

Defining $\Gamma(\theta) \equiv \cos\theta/cos\theta'$ [151], we have for the first barrier (which connects the superconducting metal properties with the normal metal ones)

$$T_1(\theta) = \left[1 + Z_1^{\text{eff}}(\theta)^2\right]^{-1} \tag{3.9}$$

and $R_1(\theta) = 1 - T_1(\theta)$, where

$$Z_1^{\text{eff}}(\theta) \equiv \sqrt{\Gamma(\theta)\left(\frac{Z_1}{\cos\theta}\right)^2 + \frac{\left[\Gamma(\theta)r_v - 1\right]^2}{4\Gamma(\theta)r_v}}. \tag{3.10}$$

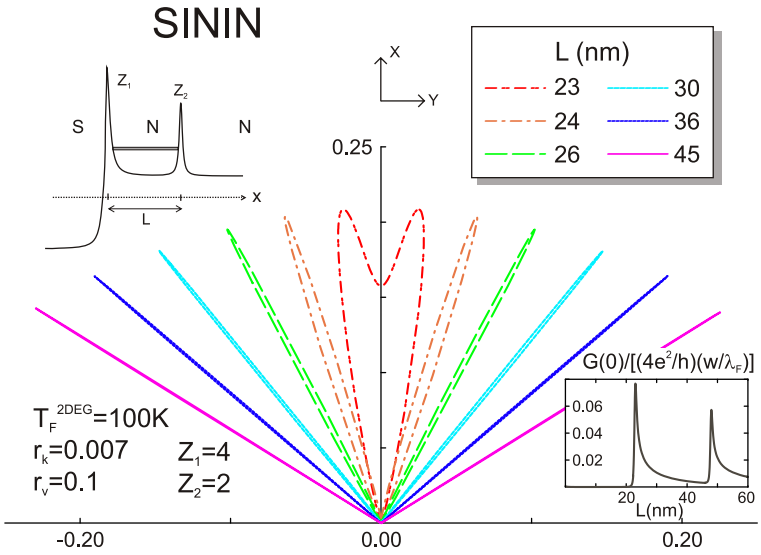

Figure 3.2: Normalized angular distribution of the zero bias conductance for several values of the interbarrier distance L. The barrier strengths are $(Z_1, Z_2) = (4, 2)$. Upper inset: schematic representation of the perpendicular potential profile. Lower inset: total conductance, normalized to half the maximum possible conductance, as a function of L. See main text for the meaning of other parameters.

Furthermore, the phase of the reflection probability amplitude from the left side is

$$\beta_1(\theta) = \arctan\left\{\frac{1}{\sqrt{r_v}}\frac{Z_1}{\cos\theta} + \frac{[1-\Gamma(\theta)^2 r_v^2]\cos\theta}{4\Gamma(\theta)^2\sqrt{r_v^3 Z_1}}\right\}. \tag{3.11}$$

On the other hand, for the second barrier we simply have

$$T_2(\theta) = \left[1 + \left(\frac{Z_2}{\cos\theta}\right)^2\right]^{-1}, \tag{3.12}$$

$R_2(\theta) = 1 - T_2(\theta)$ and $\phi_2(\theta) = \arctan(Z_2/\cos\theta)$.

In Fig. 3.2, we show $G(0,\theta)$ for several values of the interbarrier distance L, on a structure with potential barriers of strength $Z_1 = 4$ and $Z_2 = 2$ located at $x = 0$ and L, respectively. It is divided by $4e^2 w/h\lambda_F$ (λ_F being the N Fermi wavelength), which is half the maximum possible value of $G(0)$ (obtained when $T_\nu = 1$ for all ν or $T(\theta) = 1$ for all θ).

The presence of quasi-bound states located between the two barriers yields a structure of resonance peaks in the one-electron transmission probability $T(\theta)$ as a function of θ. We also note that the small value of r_k will cause important internal reflection of the electrons within the superconductor. As a result, only S electrons very close to normal incidence will have a chance to be transmitted into N. Once in

N, they may leave with much larger angles. Specifically, as we already pointed out, one has $\sin\theta' = r_k \sin\theta$ (Snell law). For the parameters considered in this work, only electrons arriving from S within $\Delta\theta'/2 = \arcsin(r_k) \simeq 0.4$ degrees of normal incidence are transmitted through the normal-state structure.

As L increases, the position of the resonant levels is lowered. In Fig. 3.2, the values of L are chosen such that only the lowest resonant level plays a role. This allows us to investigate the effect of a resonant level at perpendicular energy (on the N side) $E_x = E_R \lesssim \mu$, which appears as a peak in T_ν as a function of θ. This occurs for $\theta = \theta_R$ satisfying

$$\mu - E_y(\theta_R) = E_R \ . \tag{3.13}$$

For the shortest interbarrier distance displayed ($L = 23$ nm), the structure of $G(0,\theta)$ begins to reveal the presence of a resonance just below E_F. The trend towards a bifurcation of the conductance angular distribution becomes clearer for larger values of L. As discussed before, the presence of a sharp resonance only permits the transmission of electrons with perpendicular energy E_x close to E_R. This fixes the value of k_x at $k_x = k_R$ and, with it, the magnitude of the exit angle

$$\theta_R = \arctan\left(\sqrt{(k_F/k_R)^2 - 1}\right). \tag{3.14}$$

For a given linewidth Γ of the one-electron resonance, the corresponding spread of the angular distribution is

$$\Delta\theta \simeq \frac{\Gamma}{E_F \sin(2\theta_R)}, \tag{3.15}$$

Thus, the angular width has a minimum at $\theta_R = \pi/4$, as in fact revealed by the narrower spikes in Fig. 3.2.

The lower-right inset of Fig. 3.2 shows the total conductance [see Eq. (3.6)] as a function of the interbarrier distance. It is normalized to half its maximum possible value. For small L, the lowest resonance lies at $E_R > \mu$, which blocks current flow. As L is increased, E_R decreases and the lowest resonance becomes available for transport ($E_R < \mu$). Then $G(0)$ shows a rapid increase followed by a decaying tail. The effect is so marked that, if we attempt to plot $G(0,\theta)$ for e.g. $L = 22$ nm (just below the smallest shown value), the resulting curve is invisible on the scale of Fig. 3.2. As L increases further, a second resonance becomes available for transmission and the wide spikes due to the the first resonance coexist with the new, more centred lobes which in turn tend to bifurcate as L increases even more (not shown).

The decay of $G(0)$ for $L > L_R$ (where L_R is the interbarrier distance at which $E_R = \mu$) goes like $L^{-1/2}$ because it reflects the 1D nature of the transverse density of states. This can be proved by noting that Eq. (3.4) can be written as

$$G(0) = \frac{4e^2}{h} \sum_\nu A_\nu, \tag{3.16}$$

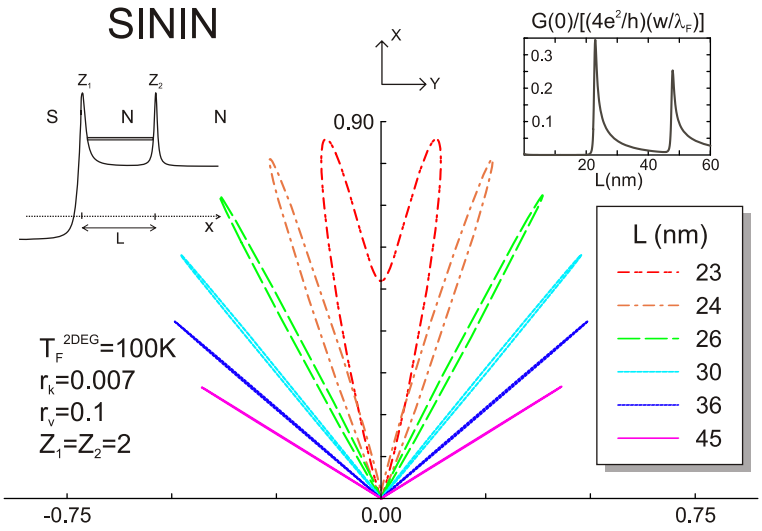

Figure 3.3: Same as Fig. 3.2, for $(Z_1, Z_2) = (2, 2)$.

where $A_\nu = T_\nu^2/(2 - T_\nu)^2$ is the probability for Andreev reflection in mode ν at total energy μ, which corresponds to quasiparticle energy $\varepsilon = 0$. Because of the normal resonance, both T_ν and A_ν are strongly peaked around the value of θ_R satisfying (3.13). Thus we may approximate $A_\nu \simeq a\delta(\mu - E_\nu - E_R)$, where a is an appropriate weight. Then $G(0)$ becomes

$$G(0) \simeq \frac{4e^2}{h} aD(\mu - E_R), \tag{3.17}$$

where $D(\epsilon) \equiv \sum_\nu \delta(\epsilon - \epsilon_\nu)$ is the transverse density of states. On this energy scale, E_R is a smooth function of L, so that it can be approximated as $E_R \simeq \mu - b(L - L_R)$, with $b > 0$. Then Eq. (3.17) yields $G(0) \propto D(b(L - L_R)) \sim (L - L_R)^{-1/2}$, as observed in the inset of Fig. 3.2. Such a manifestation of the transverse density of states in the total transport properties is characteristic of structures which select the energy in the propagation perpendicular to the plane of the heterostructure [183]. The foregoing argument allows us to predict that, for a 3D structure, the total conductance will display steps as a function of L, since then $D(\epsilon)$ will be constant (not shown).

Figs. 3.3 and 3.4 show $G(0, \theta)$ for setups identical to that of Fig. 3.2, except for Z_1 taking values 2 and 0, respectively, Z_2 remaining fixed at 2. The building of SSm interfaces with small Z_1 seems feasible with the doping techniques implemented in Refs. [164, 166, 169].

As in Fig. 3.2, the electron flow is channeled through well-defined resonances in the x direction, again giving rise to divergent beams in the N electrode. At first sight it may seem surprising that for $Z_1 = 0$ one still finds peaks in the angular distribution, since they reveal a structure in the transmission $T(\theta)$ that is not expected from a single barrier of strength Z_2. However, when $Z_1 = 0$, there is still some normal reflection at

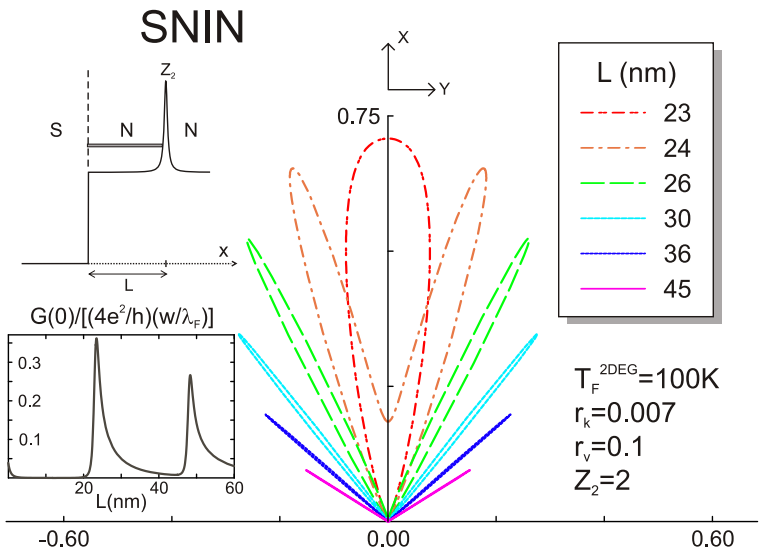

Figure 3.4: Same as Fig. 3.2, for $(Z_1, Z_2) = (0, 2)$.

$x = 0$ due to the large mismatches $E'_F \gg E_F$ and $m' \gg m$ [see Eq.(3.10)].

In Fig. 3.3, μ stays slightly above E_R for $L = 23$ nm. The details of reflection at the interface cause some shift in the detailed position of the resonances. For $Z_1 = 0$ (Fig. 3.4), the resonant level E_R at that particular interbarrier distance is exactly at μ, as revealed by the absence of splitting in $G(0, \theta)$. If, by decreasing L, E_R were taken considerably above μ, then the forward lobe of Fig. 3.4 would be sharply reduced. This general property was already noted in the discussion of Fig. 3.2 and its inset.

3.4 Nonlinear transport: spectral conductance

We have seen so far that, in the zero bias limit, the peaks in the angular distribution directly reflect the structure of (normal) resonances in $T(\theta)$ as a function of θ (or T_ν as a function of ν), since this determines $G(0)$ through Eq. (3.4). As V becomes nonzero and comparable to Δ, new resonances appear which are a direct manifestation of Andreev reflection occurring at nonzero quasiparticle energies. Such Andreev resonances have been discussed, for instance, in Refs. [162–164, 179]. Below we present a brief description that suits our present needs and which complements the discussion given by Lesovik *et al.* [179].

We restrict our study to the case $0 < |eV| < \Delta$. We focus for simplicity on the spectral conductance $G_s(\varepsilon, V)$, i.e. we don't take into account the contribution to the total differential conductance coming from the derivative with respect to V of

$G_s(\varepsilon, V)$ itself [2]. From Ref. [179], we have that [3], for $0 < |\varepsilon| < \Delta$,

$$G_s(\varepsilon, V) = \frac{4e^2}{h} \sum_{\nu} g_\nu(\varepsilon, V), \tag{3.18}$$

$$g_\nu(\varepsilon, V) \equiv \frac{T_\nu(\varepsilon) T_\nu(-\varepsilon)}{1 + R_\nu(\varepsilon) R_\nu(-\varepsilon) - 2\sqrt{R_\nu(\varepsilon) R_\nu(-\varepsilon)} \cos\left[\varphi_\nu(\varepsilon) - \varphi_\nu(-\varepsilon) - 2\vartheta(\varepsilon)\right]}. \tag{3.19}$$

Here, $g_\nu(\varepsilon, V)$ is the Andreev reflection probability for a quasiparticle of energy ε incoming in mode ν, with $|\varepsilon| < |eV|$ (by convection, the energy is measured with respect to the chemical potential in the superconductor). It is determined by $T_\nu(\pm\varepsilon)$, which is defined as the one electron transmission probability of the scattering region between the two metals as if both of them were in the normal state, $R_\nu(\pm\varepsilon) = 1 - T_\nu(\pm\varepsilon)$, $\vartheta(\varepsilon) \equiv \arccos(\varepsilon/\Delta)$, and $\varphi_\nu(\pm\varepsilon)$, which is the phase of the reflection amplitude for an electron (positive sign) or a hole (negative sign) impinging from the S side on the disordered region between the metals. The last term in the denominator describes the crucial scattering process which involves twice the propagation between the disorder region and the NS interface, once as an electron and a second time as a hole.

Now the wave vectors in the N and S side differ from those given in Sec. 3.3 because, for finite ε, we assume

$$k_x(\pm\varepsilon) = k_F \cos\theta \sqrt{1 + \frac{eV \pm \varepsilon}{E_F \cos^2\theta}} \tag{3.20}$$

and

$$k'_x(\pm\varepsilon) = k'_F \cos\theta' \sqrt{1 \pm \frac{\varepsilon}{E'_F \cos^2\theta'}} = \frac{k_F \cos\theta}{r_k \Gamma(\theta)} \sqrt{1 \pm \frac{\varepsilon\, r_k r_v \Gamma(\theta)^2}{E_F \cos^2\theta}}. \tag{3.21}$$

Note that we have included eV in the expression for $k_x(\pm\varepsilon)$, i.e., we implicitly assume that the applied bias shifts the bottom of the conduction band in the left electrode by an amount eV while keeping its bandwidth constant, as expected from electrostatic arguments [4]. We also note that the way to include the angular dependence in the

[2] Note that, when G_s depends on V, the differential conductance is $\frac{dI}{dV}\big|_V = G_s(eV, 0) + 2V \partial_V G_s(\varepsilon, V)|_{\varepsilon=eV, V=0} + \dots$.

[3] We note that, in order to get these expressions for the spectral conductance in Ref. [179], the Andreev approximation at the transparent NS interface in done, which treats the the wave numbers k_x and k'_x in the phase factors of the single-particle excitations only to zeroth order. This implies that incoming electrons are purely reflected into holes and viceversa.

[4] As a result, the potential profile and the scattering probabilities depend on the applied voltage, which will yield asymmetric I-V curves as we will see later on in this section. Such a scenario differs from that where the applied bias is assumed to introduce only an excess or defect of electron density in one the electrodes against the background of a fixed one-electron potential. In this latter case, no term eV would appear in Eq. (3.20) and symmetric I-V curves would be obtained.

previous wave vectors is in accordance with Ref. [151] and the references cited therein [5].

We notice the symmetry $G_s(\varepsilon, V) = G_s(-\varepsilon, V)$ and the fact that, through (3.20) and (3.21), the transmission $T_\nu(\varepsilon)$ or $T(\varepsilon, \theta)$ does depend on V. In practice, we are only interested in the case $\varepsilon = eV$. Thus, hereafter we refer to both G_s and g_ν as functions of a single argument ε which is to be identified with eV in the sense indicated in Eqs. (3.18) and (3.19).

Like in Sec. 3.3, we express Eq. (3.18) in terms of the *angular distribution of the spectral conductance*, $G_s(\varepsilon, \theta)$, which is defined to yield

$$G_s(\varepsilon) = \int_{-\pi/2}^{\pi/2} d\theta \; G_s(\varepsilon, \theta) = \int_{-\pi/2}^{\pi/2} d\theta \cos\theta \, g(\varepsilon, \theta), \tag{3.22}$$

where $g(\varepsilon, \theta)$ is given in Eq. (3.19) with the transmissions, reflections and phases depending on the variables ε and θ through Eqs. (3.20) and (3.21). Their specific expressions are now more complicated than those needed in the linear regime of Sec. 3.3, so we don't show them here.

The structure of the angular distribution of the conductance reflects that of $g(\varepsilon, \theta)$ as a function of θ, which generally reveals a complex and rich behaviour, since it is determined by the combined role of the product $T(\varepsilon, \theta)T(-\varepsilon, \theta)$ and the cosine term in (3.19). Below we discuss some general trends.

First we note that $g_\nu(0) = T_\nu^2(0)/[2 - T_\nu(0)]^2$, with $T_\nu(0)$ computed for $eV = 0$, which is consistent with Eq. (3.4). Now, for $|\varepsilon| < \Delta$, if the one-electron (normal) resonance occurs at a perpendicular energy $E_x = E_R$ satisfying $\mu_N - E_F < E_R < \mu_S$, there is always a transverse mode $k_y(\theta)$ for which

$$\mu_S - E_y(\theta_R^+) + \varepsilon = E_R, \tag{3.23}$$

i.e. such that $T(\varepsilon, \theta)$ presents a peak at $\theta = \theta_R^+(\varepsilon)$. Correspondingly, a peak at $\theta = \theta_R^-(-\varepsilon)$ appears in $T(-\varepsilon, \theta)$, for which

$$\mu_S - E_y(\theta_R^-) - \varepsilon = E_R. \tag{3.24}$$

As a function of $\theta > 0$ (the analysis is identical for $\theta < 0$, since the current is symmetric with respect to $\theta = 0$), the phases $\varphi(\pm\varepsilon, \theta)$ undergo an abrupt change at

[5] Note that Mortensen et al. don't consider a voltage difference eV in their expressions for the wave vectors. Besides, since they use a "matching of wave functions" technique to calculate the NS current (à la BTK [124]), the normal component to the interface of the S wave vector (what they call $k^\pm$), depends on Δ, the superconducting gap. This is not so in our case because, for us, all wave vectors correspond to the metals in the normal state. The dependence with Δ in our case is collected in $\vartheta(\varepsilon)$. In particular, it is possible to get the results for the Andreev reflection probability found in Ref. [151] through Eqs.(3.18) and (3.19), if the only dependence with ε considered is in $\vartheta(\varepsilon)$. This correspond to make the Andreev approximation not only at the transparent NS interface, but also at the disordered region.

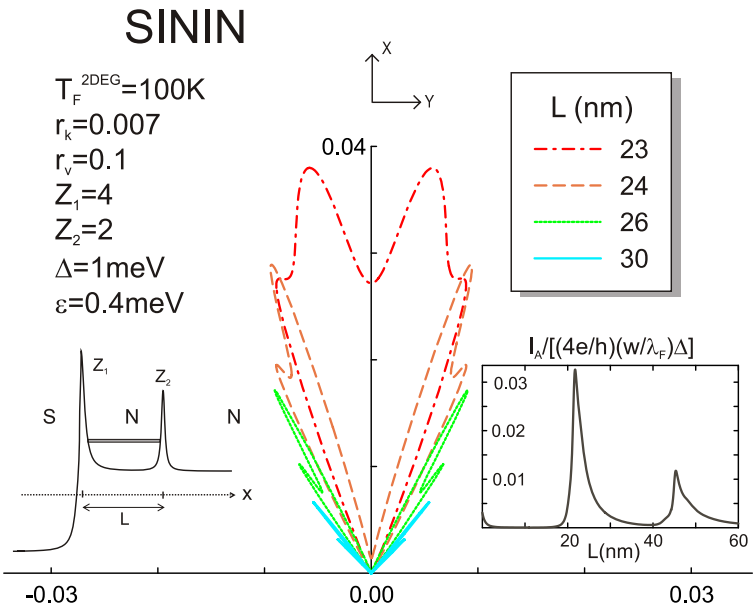

Figure 3.5: Normalized angular distribution of the spectral conductance evaluated at $\varepsilon = 0.4$ meV, for several values of the interbarrier distance L. The superconductor gap is $\Delta = 1$ meV. Barrier strengths are $(Z_1, Z_2) = (4, 2)$. Left inset: schematic representation of the perpendicular potential profile. Right inset: total current, integrated over angles and energies (up to Δ), normalized to half its maximum possible value, as a function of L.

$\theta_R^{\pm}(\pm\varepsilon)$, so that the cosine term goes quickly through two maxima at or near those values of the angle [6]. In the case of $(Z_1, Z_2) = (4, 2)$, the maxima never approaches one except for energies close to Δ. Nevertheless, for $(Z_1, Z_2) = (0, 2)$ the maxima in general reach the unity. As we will comment later, this is related to the difference between normal and Andreev resonances. Moreover, for $(Z_1, Z_2) = (4, 2)$, the maxima of $G_s(\varepsilon, \theta)$ follow in general the maxima of $T(\varepsilon, \theta)$ and $T(-\varepsilon, \theta)$ as a function of θ. However, for $(Z_1, Z_2) = (0, 2)$, the maxima of $G_s(\varepsilon, \theta)$ follow in general the maxima of the cosine term $\cos[\varphi(\varepsilon, \theta) - \varphi(-\varepsilon, \theta) - 2\vartheta(\varepsilon)]$. In both cases this translates into pairs of close lying peaks in the conductance angular distribution.

Figs. 3.5-3.7 show the value of $G_s(\varepsilon, \theta)$ normalized to $4e^2 w/h\lambda_F$ for structures with $(Z_1, Z_2) = (4, 2)$ and $(0, 2)$, the former being considered for two different combination of ε and Δ. As L increases, the value of E_R decreases and sinks below μ_S. This generates maxima in the angular distribution in the manner discussed above.

At zero temperature, and for $eV > 0$, $G_s(\varepsilon)$ can be understood as the contribution

[6] This is always the case for $(Z_1, Z_2) = (4, 2)$ (except for vanishing ε where the cosine is equal to $-1 \forall \theta$), but in the case of $(Z_1, Z_2) = (0, 2)$ and small (nonvanishing) energies ε compared to Δ, the cosine only presents one peak, whereas for $\varepsilon \to \Delta$, the inner peak spreads forming a plateau for angles between zero and θ_R^- approximately.

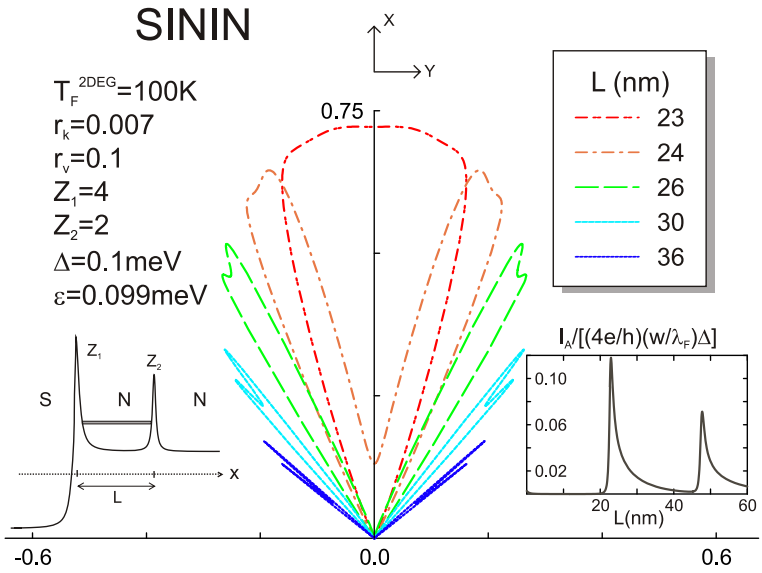

Figure 3.6: Same as Fig. 3.5, for $\Delta = 0.1$ meV and $\varepsilon = 0.099$ meV.

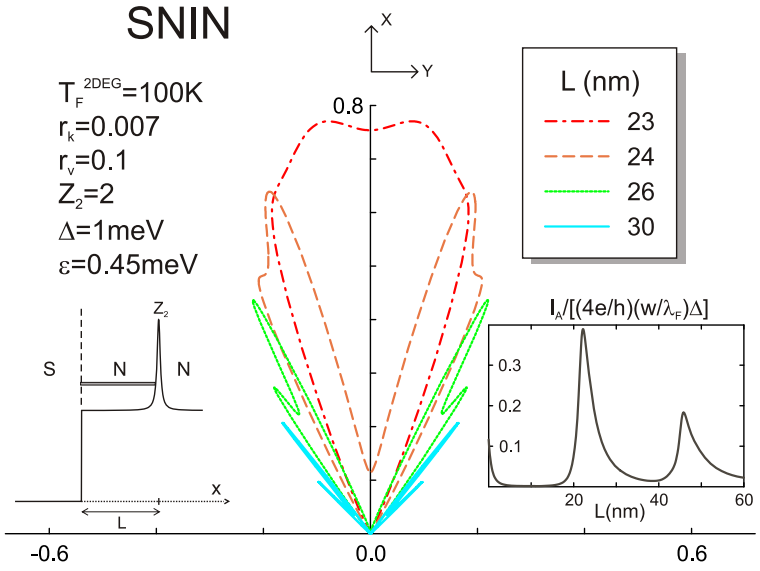

Figure 3.7: Same as Fig. 3.5, for $(Z_1, Z_2) = (0, 2)$ and $\varepsilon = 0.45$ meV.

to the total current stemming from electron pairs emitted into the normal metal with total energies $\mu_S \pm \varepsilon$. The two electrons leaving the superconductor have identical $|k_x|$ (which is selected by the resonance) and slightly different total energy (see below). Thus they do not point exactly in the same direction, i.e. the V which they form upon emission is not exactly centred around the normal axis. By symmetry, for each pair in which e.g. the upper electron is emitted towards the right (and the lower one to the left), there is another pair solution in which the upper electron travels to the left (and the lower one to the right). When plotting the total differential conductance, the two asymmetric Vs appear as a single V whose lobes are double peaked.

We note here that, in the contribution to $G_s(\varepsilon)$ as defined in Eqs. (3.18) and (3.19) [or in Eq. (3.22)], $T_\nu(-\varepsilon)$ is identical to the T_ν appearing in the zero voltage limit discussed in the previous section [see $k_x(-\varepsilon)$ in Eq. (3.20), where $eV - \varepsilon = 0$ when $\varepsilon = eV$], i.e. $\theta_R^-(-\varepsilon) = \theta_R$ as defined in (3.13) if we identify $\mu_N \equiv \mu$. This implies that, in the double-peaked lobes, the inner peak points in the same direction as the single-peaked lobe of the linear ($V = 0$) limit, a result which is independent of the sign of eV. Besides we have that $E_x(\pm\varepsilon, V) = E_F \cos^2\theta + eV \pm \varepsilon$, which we can consider a function of a single argument since we are considering that $\varepsilon = eV$. At the resonance we have $E_x(\varepsilon) = E_x(-\varepsilon) = E_R$, therefore $k_x[\varepsilon, \theta_R^+(\varepsilon)] = k_x[-\varepsilon, \theta_R^-(\varepsilon)]$, while $E_y[\theta_R^+(\varepsilon)] = E_y[\theta_R^-(\varepsilon)] + 2eV$. Thus, at a given ε, peaks in the angular distribution occur near θ_R^+ and θ_R^-. Both have the same perpendicular momentum, but the latter has lower parallel kinetic energy.

The fact observed in Figs. 3.5-3.7 that the inner peak displays a larger current density is due to the asymmetric character of the peaks in $T(\pm\varepsilon, \theta)$ as a function of θ, which ultimately reflects the greater efficiency with which close-to-normal emission electrons contribute to the electric current.

The insets of Figs. 3.5-3.7 show the total current (integrated over θ and ε) as a function of L. It is given by the expression

$$I_A = \int_0^\infty d\varepsilon \, \frac{1}{e} \left[f(\varepsilon - eV) - f(\varepsilon + eV) \right] G_s(\varepsilon, V). \tag{3.25}$$

In this case, V in Eq. (3.19) is fixed to the value of Δ and ε is integrated over the energy window left by the difference of Fermi distribution functions at zero temperature. As for the zero bias conductance, the total current reveals a succession of maxima followed by an inverse square root decay law that mirrors the transverse density of states (see discussion in the previous section).

Fig. 3.8 shows the total spectral conductance for voltages below the gap. This type of curves has been the object of preferential attention in the previous literature on NS transport. By presenting them here, we make connection with that preexisting body of knowledge, in particular with the experimental and theoretical works of Refs. [164] and [179], respectively. The forthcoming remarks are intended to complement that discussion and to provide a self-contained, unified picture of the work presented here.

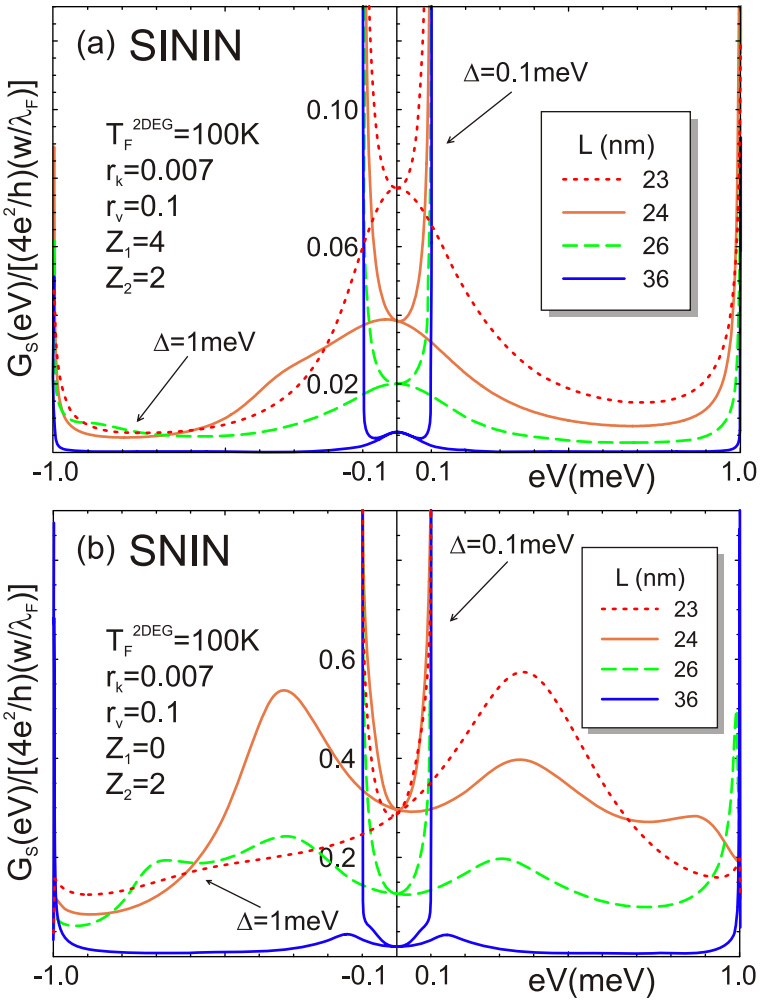

Figure 3.8: Subgap spectral conductance (integrated over angles), normalized to half its maximum possible value, for four values of the interbarrier distance L, two values of the superconductor gap Δ, and two values of the strength Z_1 of the barrier located right at the SN interface.

The asymmetry observed in $G_s(eV)$ as a function of eV is due to the general characteristic that $G_s(\varepsilon, V) \neq G_s(-\varepsilon, -V)$ which, in our case, comes from the fact that (3.20) depends on V in such a way that $k_x(\varepsilon, V) \neq k_x(\varepsilon, -V)$. [7] When we integrate over angles to get the spectral conductance $G_s(eV)$ of Eq. (3.22) [or (3.18)], for $V > 0$ our integration interval is $\theta \in [-\pi/2, \pi/2]$. However, for $V < 0$, the interval is $\theta \in [-\arccos(\sqrt{2|eV|/E_F}), \arccos(\sqrt{2|eV|/E_F})]$, which comes from the fact that, in Eq. (3.20), θ must be such that $E_F \cos^2\theta - eV - \varepsilon \geq 0$. [8] This ultimately reflects the finiteness of the normal bandwidth, since the greater is E_F, the smaller is the contribution to the conductance of angles between $\arccos(\sqrt{2|eV|/E_F})$ and $\pi/2$ and, therefore, the smaller is the asymmetry. Asymmetric curves are displayed in Ref. [76] and have been pointed out in Ref. [179] (see also references therein). Let us add here that if we had consider that the applied bias does not change the bottom of the conduction band, then no term eV would appear in Eq. (3.20) and symmetric I-V curves would be obtained. The important message is that, in systems with relative small bandwidths, and especially for low perpendicular energies, transport properties are sensitive to the details of the voltage drop. A realistic, model-independent calculation would have to include, self-consistently, the electrostatic effect that the local rearrangement of electron density has on the effective one-electron potential. In what follows, we focus on the behaviour for $eV > 0$.

Both in Figs. 3.8(a) and (b) we present two groups of curves, corresponding to a small and a large gap. The barrier parameters of Fig. 3.8(a) are the same as those of Figs. 3.5 and 3.6 , namely, $(Z_1, Z_2) = (4, 2)$. Although Figs. 3.5 and 3.6 already exhibit Andreev features such as the double-peaked lobes in $G_s(\varepsilon, \theta)$, these are washed out when the angular variable is integrated to yield the total spectral conductance $G_s(\varepsilon = eV)$, as shown by the single peaked curves obtained for the same value of the gap as in Fig. 3.5 ($\Delta = 1$ meV), or by the absence of peaks for the parameters of Fig. 3.6 ($\Delta = 0.1$ meV). The curves for $\Delta = 1$ meV display a clear zero bias conductance peak (ZBCP) whose height is determined by the structure of the normal properties [see Eq. (3.4)]. As ε increases above zero, both electron and hole (or both the upper and lower energy emitted electrons) may benefit from the low-lying normal resonance ($E_R < \mu_S$) as long as $\varepsilon < \Gamma$, where Γ is the linewidth of the normal resonance. When

[7] In order to have symmetry in the current-voltage characteristics under reversal of voltage, i.e. $G(\varepsilon, V) = G(-\varepsilon, -V)$, it is necessary that $G(\varepsilon, V)$ be independent of voltage. In that case $G_s(\varepsilon) \mid_{\varepsilon = eV} = dI/dV \mid_V$ and the differential conductance in invariant under sign reversal of the voltage.

[8] Of course we know that for Eqs. (3.19) and (3.18) to hold it is necessary that the Andreev approximation at the transparent NS interface can be made. Therefore, the condition $E_x \gg \varepsilon, \Delta$ must be satisfied [in order to simplify the BdG equations by linearizing the dispersion relations around $k_x(0)$ and $k'_x(0)$]. This implies that, in principle, we are not sure how correctly we are treating grazing angles on the interface or, in other words, that the approximation becomes inaccurate for angles in the vicinity of $\theta \sim \pi/2$. Nevertheless, according to Ref. [151], numerical estimates suggest that the approximation is reasonable even for semiconductors, which have much lower Fermi energies as compared to those of normal metals.

$\varepsilon > \Gamma$, it is not possible to channel both electrons through the same resonance and the contribution to the conductances decreases. On closer inspection, one finds that the width of the ZBCP is indeed determined by the normal resonance width, but not by that appearing in the perpendicular transmission $T_\nu(\varepsilon)$ (viewed as a function of ε). Rather, it essentially mirrors the width of the numerator in Eq. (3.19). This is the product $T_\nu(\varepsilon)T_\nu(-\varepsilon)$ evaluated at $\theta_R(\varepsilon = 0)$ and viewed also as a function of ε, i.e., for electrons leaving in the direction of maximum current flow (at exit angle $\theta = \theta_R$). [9]

A general property of SN interfaces with a single barrier right at the interface is that Andreev reflection probability tends to unity as $|\varepsilon| \to \Delta$ [124]. However, we find that this is generally not the case for a double barrier interface. For $Z_1 = 4$ (and also for $Z_1 = 0$), we do notice that sharp peaks in $G_s(\varepsilon)$ form just below the gap for some values of L, so close to it that they can be observed only through a magnification of Fig. 3.8. Due to this tendency to acquire large values near the gap, $G_s(\varepsilon)$ goes through a minimum at finite ε if the width of the ZBCP is smaller than the gap. This is the case shown in Fig. 3.8(a) for $\Delta = 1$ meV. For a smaller gap ($\Delta = 0.1$ meV), the value of $G_s(0)$ remains unchanged but there is no room for $G_s(\varepsilon)$ to display a minimum between 0 and Δ.

Being $Z_1 = 0$ more transmissive (although not entirely because of the reflection at the potential step; see Sec. 3.3), Fig. 3.8(b) displays Andreev resonance features that do survive upon integration over angles. For $\Delta = 1$ meV and $L = 23$ nm, one observes a peak at finite energies that adds to the overall ZBCP. (We will call these kind of peaks FBCP, finite bias conductance peak) [10]. As L increases, the inner Andreev peak evolves towards zero energy. At larger distances ($L = 36$ nm), the lowest Andreev resonance can only be hinted at as a shoulder in the plot for $\Delta = 0.1$ meV. We also note that, for $L = 24$ and 26 nm, a second Andreev resonance becomes visible close to the gap edge. However, due to the involved interplay between the transmission probabilities and the cosine term appearing in Eq. (3.19), this second peak does not appear to follow a simple monotonic trend.

The formation of FBCP can be qualitatively understood in the following way. Andreev resonances are characteristically given by the condition [179]

$$\cos\left[\varphi(\varepsilon,\theta) - \varphi(-\varepsilon,\theta) - 2\vartheta(\varepsilon)\right] = 1 \ , \tag{3.26}$$

because when this condition is satisfied for a given ε and a given θ, the denominator in Eq. (3.19) is minimum so that $g(\varepsilon,\theta)$ is maximum. As we noticed before, for $(Z_1, Z_2) = (4, 2)$, Eq. (3.26) only happens for $\varepsilon \to \Delta$. Nevertheless, when $Z_1 = 0$

[9] According to Ref. [179], the width of the ZBCP is of the order of the Thouless energy, which can be defined for ballistic systems with appropriate boundary conditions [184]. The boundary condition in our case is the double barrier.

[10] We want to make the observation that, if the Andreev approximation was made not only at the NS transparent interface but also at the disordered region, no such structure as ZBCP or FBCP could develop in G_s as a function of ε.

there is always a certain region of values of ε (whose width is the width of the FBCP) for which the cosine of Eq. (3.19) is one or remains close to one for a certain window of values of $\theta \geq 0$, and for a symmetric window with respect to $\theta = 0$ for $\theta \leq 0$. Integration over these θ windows translates into a big contribution to $G_s(\varepsilon)$. In the case of the first FBCP (the one with smaller $\varepsilon = eV$ for each L), those "plateaus" in the behaviour of the cosine as a function of θ occur around $\pm\theta_R$ [see Eq. (3.13)]. Besides, they are wider for values of L for which the resonance is at $E_R \lesssim \mu_S$ (where the current is carried by electrons moving perpendicular to the interface), and get reduced as L increases. This is why peaks are bigger for values of $L = 23$ nm and 24 nm than for $L = 26$ nm or 36 nm. The formation of the second FBCP comes from the transformation of the previous "plateaus" into depressions and the appearance of another "plateau" between the previous ones for θ values around zero. This mechanism usually occurs for a small region of values of ε close to the gap energy.

3.5 Discussion

So far we have assumed that the SN interface is infinitely long ($w \to \infty$). This has allowed us to treat k_y as a continuous, conserved quantum number, which considerably simplifies the transport calculation. Of course, the idea of an infinite interface is at odds with the primary motivation of our work, which is to propose a method to spatially separate mutually entangled electron beams. Below we argue that, fortunately, only a moderately long interface is needed in practice.

For simplicity, we focus our discussion on the low voltage limit, where the total energy can be assumed to be sharply defined. Then the width $\Delta\theta$ of the angular distribution is due only to the uncertainty in the parallel momentum Δk_y. This in turn is closely connected to Δk_x through the relation $k_x \Delta k_x = k_y \Delta k_y$, since total energy uncertainty is zero. There are two contributions to the momentum uncertainty: the nonzero width of the resonance in the perpendicular transmission and the finite length of the SN interface. Thus we may estimate

$$\Delta k_y \simeq \frac{m\Gamma}{\hbar^2 k_y} + \frac{1}{w} \, . \tag{3.27}$$

This translates into an angular width

$$\Delta\theta \simeq \frac{\Gamma}{E_F \sin(2\theta_R)} + \frac{1}{k_F w \cos\theta_R} \, . \tag{3.28}$$

The actual angular width of $G_s(0,\theta)$ is actually a bit smaller, since the present estimate is based on one-electron considerations, while the relevant angular distribution is determined by Eq. (3.4). We neglect this difference for the present simple estimates.

Eq. (3.28) contains two contributions. The first term is determined by the normal resonance and is responsible for the width of the angular distributions plotted in Figs.

3.2-3.4 (with $w \to \infty$). Our main concern here is that the second contribution, that which stems from the finiteness of the aperture, does not contribute significantly.

A strict criterion may be that the interface finite length should not modify the intrinsic angular width ($\hbar v_F \sin\theta_R / w \ll \Gamma$), which everywhere has been assumed to be small enough to allow for narrow divergent beams. A more lenient criterion is that, regardless of the specific value of Γ, the finite aperture should not generate an excessively broad angular distribution. For typical cases this amounts to requiring $k_F w \gg 1$ (for a discussion see Fig. 5 in Ref. [51]). For the bandwidth which we have assumed ($E_F/k_B = 100$ K) and an effective mass of $m = (r_k/r_v)m' = 0.07m_e$, where m_e is the bare electron mass, we have $\lambda_F = 2\pi/k_F \sim 50$ nm. So apertures greater than a few hundred nanometres seem desirable to keep the angular uncertainty within acceptable bounds.

Another source of angular spreading is interface roughness, with a characteristic length scale l. However, it should not pose a fundamental problem as long as $l \gg \lambda_F$, so that a structure of intermediate width could be designed satisfying $l \gg w \gg \lambda_F$.

For the difference in velocity direction to translate into spatial separation, it is necessary that the spin detectors are placed sufficiently away from the electron-emitting SN interface. Of course, the needed distance depends also on the exit angle θ_R. For a convenient value of $\theta_R \sim \pi/4$, simple geometrical considerations suggest that, unsurprisingly, the distance d from the detector to the centre of the SN interface must be greater than its width w. Since elastic mean free paths in a 2DEG can be made as high as $l_e \sim$100 μm, there seems to be potentially ample room for building structures satisfying $\lambda_F \ll w \ll d \ll l_e$. Such devices would display well-defined divergent current lobes which could be detected (and, eventually, manipulated) at separate locations before the directional focusing is significantly reduced by elastic scattering.

3.6 Related experiments

To the best of our knowledge, there are no experiments that implement the kind of system we have proposed and analyzed theoretically here. Nevertheless, there already exist in the literature quite similar experimental devices to the one we consider [76, 77, 164, 172, 185] and that, with little changes, could serve to test our proposal. Here we talk briefly about a couple of those experiments.

In the work called "Shot-noise and conductance measurements of transparent superconductor/two-dimensional electron gas junctions" by B. -R. Choi et al. in 2005 [76], a 3D superconducting injector made of Nb is put in contact with a 2DEG formed between layers of InGaAs and InAlAs. The superconductor forms an angle of 30 deg to the 2D plane of the high-mobility electron gas. The Fermi wavelength of electrons in the N side is $\lambda_F = 18nm$ (which corresponds to a $T_F^{2DEG} = 770K$), and the superconducting gap is $\Delta = 1.14meV$. Since the motivation of the authors is to use such a structure to pattern a three terminal beam-splitter geometry onto the

2DEG and measure shot noise and cross-correlators, they engineer a highly transparent S-N interface. In our proposal, we would rather need a tunneling interface there. It is remarkable that, after creating a long 1D superconductor-2DEG interface and by means of e-beam lithography, they reduce it to submicron dimensions (containing 20 conducting channels approximately). In this way, the top-view of their device is very similar to our Fig. 3.1(a), except for the lack of the two tunneling barriers. We also note here that the plot they present of voltage dependent differential resistance [dV/dI(V)] is clearly asymmetrical with respect to zero voltage, although for voltages bigger than the superconducting gap. Other experimental works that obtain asymmetric current-voltage characteristics can be found in Refs. [186, 187].

Double barrier structures are considered in the work "Resonant transport in Nb/GaAs/AlGaAs heterostructures: Realization of the de Gennes-Saint-James model" by F. Giazotto et al. in 2001 [77], and in the later extended paper "Coherent transport in Nb/delta-doped-GaAs hybrid microstructures" by F. Giazotto, P. Pingue and F. Beltram in 2003 [164]. The authors report experimental observation of de Gennes–Saint-James-type resonances in a microstructure consisting of a Nb/GaAs/AlGaAs/GaAs hybrid heterojunction. This corresponds to a SNIN structure where the N's are semiconductors. The thickness of the GaAs epylayer sandwiched between the superconductor and the insulator was selected in order to have a single quasibond state below the superconducting gap. There is no 2DEG here and the interfaces between metal and semiconductors are two dimensional, which is different from our setup, but the philosophy of the resonant structure they implement is similar to ours, and consequently they measure zero-bias and finite-bias conductance peaks vs voltage. Moreover, the values of the parameters they have (for barrier heights, distance between interfaces, effective mass, etc.) are also very similar to ours.

3.7 Conclusions

We have investigated theoretically the possibility of creating resonant NS structures where the two electrons previously forming a Cooper pair in the superconductor are sent into different directions within the normal metal. The central idea relies on the design of a structure that is transparent only to electrons with perpendicular energy within a narrow range of a resonant level. Since the total energy lies close to the Fermi level, such a filtering of the electron perpendicular energy translates into *exit angle selection*.

Electrons from a conventional superconductor are known to be correlated in such a way that electrons moving at similar speeds in opposite directions tend to have opposite spin. At low temperatures and voltages, electron flow from the superconductor to the normal metal is entirely due the transmission of correlated electron pairs. These have both opposite spin and opposite parallel (to the interface) momentum, while possessing the same total energy. If the exit angle is selected by filtering

the perpendicular momentum, the current in the normal metal is formed by two narrow, mutually singlet entangled electron beams which point in different directions and which spatially separate from each other at distances from the source much greater than the width of the source.

The trick of exit angle selection is intended to facilitate a neat observation of nonlocal entanglement between electron beams, and this work has been devoted to proposing a specific implementation of that idea. One cannot help noting, however, that such a selection of the outgoing direction might not be totally essential. If we content ourselves with measuring anticorrelated low-energy spin fluctuations over mesoscopic length scales, it may just be sufficient to place the two spin detectors symmetrically around the interface at a sufficient distance and angle, very much like in the setup of Fig. 3.1(a) but with a conventional, non angle-selecting SN tunnel interface. If their motion between the emitter and the detector is ballistic, electrons arriving at each detector have, on average, opposite parallel momentum and opposite spin (angular anticorrelation has been explicitly shown in Ref. [51] for a broad perfect interface). The boundaries of the 2DEG might conceivably be designed to optimize such correlations. The outcome is that electrons arriving at each detector will exhibit a degree of nonlocal spin-singlet correlations that could be measured.

Altogether, we conclude that a ballistic two-dimensional electron gas provides an ideal scenario to probe nonlocal entanglement between electrons emitted from a distant, finite-size interface with a superconductor. If that interface is formed by a resonant structure that selects the perpendicular energy and thus the magnitude of the electron exit angle, nonlocal spin correlations will be clearly observed if the outgoing beams are directed towards suitably placed detectors.

Chapter 4

Clauser-Horne inequality and decoherence in mesoscopic conductors

In this chapter we analyze the effect of decoherence on the violation of the Clauser-Horne (CH or CH74) inequality for the full electron counting statistics in a mesoscopic multiterminal conductor. Our setup consists of an *entangler* that emits a flux of entangled electrons into two conductors characterized by a scattering matrix and subject to decoherence. Loss of phase memory is modeled phenomenologically by introducing fictitious extra leads. The outgoing electrons are detected using spin-sensitive electron counters. Given a certain average number of incoming entangled electrons, the CH inequality is evaluated as a function of the numbers of detected particles and of the various quantities characterizing the scattering matrix. When decoherence is turned on, we show that the amount of violation of the CH inequality is effectively reduced. Interestingly we find that, by adjusting the parameters of the system, there exists a protected region of Q values for which violation holds for arbitrary strong decoherence.

The contents of this chapter were published in Phys. Rev. B **72**, 125333 (2005), by E. Prada, F. Taddei and R. Fazio; and in New J. Phys. **7**, 183 (2005), by F. Taddei, L. Faoro, E. Prada and R. Fazio.

4.1 Introduction

Entanglement [14] is probably the most important resource for the implementation of quantum computation and quantum communication protocols [188]. Since recently, most of the work on entanglement has been carried out in optical systems using photons [189], cavity QED systems [190], and ion traps [191]. Solid state systems, however, are a very attracting arena of research in quantum information [32, 33, 192]

because, in perspective of future applications, they should allow for scalability and integration. In this light, a number of different realizations of entangled electrons have since been proposed: hybrid normal-superconducting structures [38, 41, 46, 50, 51, 53, 73, 79], superconductor-carbon nanotubes systems [45, 47, 49], quantum dots in the Coulomb blockade regime [33, 59, 61], chaotic quantum dots [62], Kondo-like impurities [58], quantum Hall bar systems [72, 74, 111, 193, 194], Coulomb scattering in 2D electron gas [195].

Besides its generation, a crucial issue is that of the detection of entanglement. By means of a beam-splitter, entanglement can be detected in transport through an analysis of current noise [105] or higher cumulants [108]. Furthermore, the presence of entanglement can be revealed by analyzing the Bell inequality and quantities like concurrence [109], which have been expressed in terms of zero-frequency charge and spin-current noise [41, 46, 72, 73, 110–112]. Violation of a Bell inequality implies that there exist quantum correlations between the detected particles that cannot be described by any local hidden variables theory. In the same spirit as it was done for the noise, in Ref. [113] a Clauser-Horne(CH) inequality [115,116] was derived for the Full Counting Statistics (FCS) of electrons and its properties were discussed [1]. In particular, it was found that the maximum violation of the CH inequality for electrons in the Bell state simply scales as the inverse of the number of injected particles. It was also found that the CH inequality is violated for a superconducting hybrid structure and, more interestingly, for a three terminal fully normal device.

In real systems electrons are unavoidably coupled to the electromagnetic environment. As a result dephasing or decoherence takes place, thereby reducing and eventually destroying entanglement. Understanding their consequences is an important issue. In Refs. [73,74,78,79] the effect of dephasing was mimicked by introducing in the density matrix of the electronic entangled states a phenomenological parameter which suppresses its off-diagonal elements. By properly choosing the transmission probability of beam-splitters or tunnel barriers, violation of Bell inequality was found even for "strong" dephasing. In Refs. [72,80] dephasing was introduced averaging over an uniform distribution of random phase factors accumulated in each edge channel of the quantum Hall bar. If the two edge channels are mixed by the tunnel barrier, no violation was reported for "strong" dephasing. The effect of decoherence and relaxation has also been analyzed using a Bloch equation formalism in Ref. [107].

In the present work we analyze the CH inequality for the FCS [113] in the presence of decoherence. We consider the prototype setup depicted in Fig. 4.1, consisting of a generic entangler connected to two conducting wires. Entangled electrons injected in the two leads are detected by performing spin-selective counting along a given local quantization axis. The entangled electrons are subject to decoherence while travers-

[1] Recently in the literature there have been proposals to measure the FCS [J. Tobiska, and Yu. V. Nazarov, Phys. Rev. Lett. 93, 106801 (2004); J. P. Pekola, Phys. Rev. Lett. 93, 206601 (2004)] and a first experiment has been performed (only in the tunneling limit at present [J. Bylander, T. Duty, and P. Delsing, Nature 434, 361 (2005)]).

ing the conductors (thus before reaching the detectors) [2]. Various phenomenological methods have been developed to treat decoherence in transport through mesoscopic conductors. In Refs. [81, 82], which actually describe exactly nonequilibrium radiation acting on the system, dephasing is induced by a classical fluctuating potential. In Ref. [83], dephasing is treated as random fluctuations of the phase of propagating modes through the conductor. Both methods have been recently applied to FCS in Refs. [84, 85]. In this chapter decoherence is introduced as due to the presence of additional fictitious reservoirs along both wires. This method, which mimics the effect of inelastic processes, was introduced by Büttiker [86, 87] in terms of fictitious extra leads. The advantage of this model resides in the fact that inelastic, phase randomization processes are implemented within an elastic, time-independent scattering problem. In the rest of the paper we shall refer to decoherence as to the effect produced by such fictitious additional leads.

As expected, we find that decoherence suppresses the violation of the CH inequality, though leaving unchanged the range of angles for which violation occurs. In particular, the value of the maximum violation is suppressed more rapidly as compared with the absence of decoherence (exponentially with the square root of the number of injected electrons instead of algebraically). Importantly, by studying the CH inequality as a function of the number of transmitted electrons, there exist values of such quantity that are more protected against decoherence.

The paper is organized as follows: In Sec. 4.2 we described in detail the mesoscopic system we are considering to test the violation of the CH inequality together with the phenomenological model of decoherence. Sec. 4.3 is devoted to the formulation of the CH inequality for the FCS within the scattering approach and to the analysis of the no-enhancement assumption (Sec. 4.3.1). The results are presented in Sec. 4.4, where a systematic analysis of the violation of the CH inequality against all the parameters of the device is addressed. A concluding summary is provided in Sec. 4.6.

For completeness, we include in Sec. 4.4.1 the results relative to an asymmetric setup, whereby decoherence occurs only in one of the two wires. In Appendix C.1 and C we collect, respectively, the expressions of the expectation values and the different probability distributions.

4.2 Description of the system

We consider the setup illustrated in Fig. 4.1. It consists of an entangler, two conducting wires and two spin-selective counters. The entangler, on the left-hand-side, is a device that produces pairs of electrons, with energy $E < \mu_{\rm L}$, in a maximally spin entangled state (Bell state). On the right-hand-side of Fig. 4.1 the electron counting is performed in leads 1 and 2 (at equal electrochemical potential $\mu_{\rm R}$) for

[2]Note that we make use of the CH inequality as a tool to detect the persistence of entanglement in the presence of decoherence processes, given an injected entangled state (whose existence is assumed).

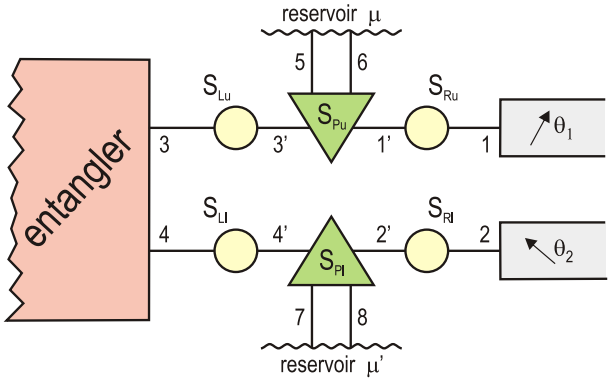

Figure 4.1: Idealized setup for testing the CH inequality for electrons in a solid-state environment in the presence of decoherence. It consists of three parts: An entangler that produces pairs of spin-entangled electrons exiting from terminals 3 and 4. Two conductors that connect these terminals with exiting leads 1 and 2, and two analyzers. The conductors are described by the elastic scattering matrices $S_{\rm Lu}, S_{\rm Ru}, S_{\rm Ll}$ and $S_{\rm Rl}$, and the inelastic ones $S_{\rm Pu}$ and $S_{\rm Pl}$. These last ones can simulate phenomenologically the presence of decoherence through the coupling via two leads $(5, 6$ and $7, 8)$ to two additional reservoirs of chemical potentials μ and μ'. Electron counting is performed in leads 1 and 2. Finally, θ_1 and θ_2 are the angles at which the spin-quantization axis are oriented.

electrons with spin aligned along the local spin-quantization axis at angles θ_1 and θ_2 (spin-selective counters). As a convention we say that the analyzer is not present when the electron counting is spin-insensitive (electrons are counted irrespective of their spin direction). Since we assume no back-scattering from counters to the entangler, the particles which are not counted are lost and hence there is no communication between the two detectors. Leads 3 and 4 of the entangler are connected to exit leads 1 and 2 through two conductors, where inelastic processes are introduced through the fictitious lead model of Büttiker [196]. Let us analyze in detail the upper wire (see Fig. 4.1) which connects the emitting lead 3 with the exiting lead 1. The conductor consists of three scattering regions. The elastic scatterer connecting lead 3 to 3' is described by the matrix

$$\hat{S}_{\rm Lu} = \begin{pmatrix} \check{r} & \check{t}' \\ \check{t} & \check{r}' \end{pmatrix} = \begin{pmatrix} r_\uparrow & 0 & t'_\uparrow & 0 \\ 0 & r_\downarrow & 0 & t'_\downarrow \\ t_\uparrow & 0 & r'_\uparrow & 0 \\ 0 & t_\downarrow & 0 & r'_\downarrow \end{pmatrix}. \tag{4.1}$$

[The index L (R) stands for Left (Right) elastic scatterer, while P stands for Probe scatterer; u (l) refers to the upper (lower) wire.] Here r_σ (t_σ) is the probability amplitude for an incoming particle with spin σ from lead 3 to be reflected (transmitted

into lead 3'). For a normal single-channel wire we set $t_\sigma = t'_\sigma = \sqrt{T_0}$, and $r_\sigma = r'_\sigma = i\sqrt{1-T_0}$, where T_0 is the transmission probability. Inelastic scattering is introduced by plugging in an additional reservoir of chemical potential μ with an energy- and spin-independent scattering matrix

$$\bar{S}_{\rm Pu} = \begin{pmatrix} \check{0} & \sqrt{1-\alpha}\,\check{1} & \sqrt{\alpha}\,\check{1} & \check{0} \\ \sqrt{1-\alpha}\,\check{1} & \check{0} & \check{0} & \sqrt{\alpha}\,\check{1} \\ \sqrt{\alpha}\,\check{1} & \check{0} & \check{0} & -\sqrt{1-\alpha}\,\check{1} \\ \check{0} & \sqrt{\alpha}\,\check{1} & -\sqrt{1-\alpha}\,\check{1} & \check{0} \end{pmatrix}, \tag{4.2}$$

represented by a triangle in Fig. 4.1. For the sake of clarity, we have denoted by a check ($\check{}$), a caret ($\hat{}$) and an overbar ($\bar{}$), respectively, (2×2), (4×4) and (8×8) matrices. In Eq. (D.1) $\check{1}$ and $\check{0}$ are, respectively, unit and zero (2×2)-matrices in the spin space, and $(1-\alpha)$ is the probability for transmitting a particle between leads 3' and 1'. The coupling parameter ranges from $\alpha = 0$, when no particles are transmitted into leads 5 and 6 from leads 3' and 1', to $\alpha = 1$, when no particles are transferred between leads 3' and 1'. A third elastic scatterer, described by a matrix $\hat{S}_{\rm Ru}$, connects lead 1' to lead 1. The conductor is therefore described by the matrix $\hat{S}_{13}$ defined as $\hat{S}_{13} = \hat{S}_{\rm Ru} \otimes \bar{S}_{\rm Pu} \otimes \hat{S}_{\rm Lu}$, where the notation $\otimes$ stands for the scattering matrix composition (elimination of internal current amplitudes) [197]. For simplicity, we shall assume that $\hat{S}_{\rm Ru} = \hat{S}_{\rm Lu}$.

Due to the presence of the additional reservoir, particles propagating through lead 3 are transmitted partially to lead 1 and partially to leads 5 and 6 (see Fig. 4.1). The additional reservoir, however, can transfer itself particles to lead 1 and 3. As a result, only a fraction of the particles arriving in lead 1 comes from *coherently* transmitted ones sent in from lead 3, with probability

$$T_{13} = \frac{T_0^2(1-\alpha)}{[1+(1-T_0)(1-\alpha)]^2}. \tag{4.3}$$

Another fraction, the *incoherent* contribution, comes from the additional reservoir through leads 5 and 6, with probability

$$T_{15} + T_{16} = \frac{T_0\alpha}{1+(1-T_0)(1-\alpha)}. \tag{4.4}$$

The presence of the extra reservoir mimics the fact that the current flowing through the conductor is partially composed of particles (the *incoherent* fraction) which have lost phase memory while traversing it. For $\alpha = 0$ all particles are coherently transmitted and $T_{15} + T_{16} = 0$, while for $\alpha = 1$ all particles are transferred incoherently and $T_{13} = 0$. For $\alpha = 0$, the overall transmission probability through the conductors is given by $T = T_0^2/(2-T_0)^2$. In the rest of the paper we will refer to α as to the *decoherence rate*.

The chemical potential μ of the additional reservoir is set in such a way that no net current flows in or out of the reservoir ($I_5 + I_6 = 0$). This constraint is enforced only on average. An instantaneous current in or out the additional reservoir is then allowed [86–88, 95], and a non-fluctuating chemical potential μ is assumed (for this reason the additional terminal does not behave as a voltage probe).

A similar description applies to the lower wire connecting lead 4 with lead 2, so that the scattering matrix of the conductor is defined as $\hat{S}_{24} = \hat{S}_{\mathrm{Rl}} \otimes \bar{S}_{\mathrm{Pl}} \otimes \hat{S}_{\mathrm{Ll}}$, where, for simplicity, we set $\hat{S}_{\mathrm{Rl}} = \hat{S}_{\mathrm{Ll}}$. If the angles θ_1 and θ_2 of the analyzers are parallel to each other and in the absence of spin mixing processes, the total matrix of the system can be written as

$$\bar{S} = \begin{pmatrix} \hat{S}_{13} & \hat{0} \\ \hat{0} & \hat{S}_{24} \end{pmatrix} . \tag{4.5}$$

The general scattering matrix relative to non-collinear angles $\bar{S}_{\theta_1,\theta_2}$ is obtained from $\bar{S}$ by rotating the spin quantization axis independently in the two conductors (note that this is possible because the two wires are decoupled) [198]: $\bar{S}_{\theta_1,\theta_2} = \bar{\mathcal{U}}\bar{S}\bar{\mathcal{U}}^{\dagger}$, where $\bar{\mathcal{U}}$ is the rotation matrix given by

$$\bar{\mathcal{U}} = \begin{pmatrix} \check{1} & \check{0} & \check{0} & \check{0} \\ \check{0} & \check{U}_{\theta_1} & \check{0} & \check{0} \\ \check{0} & \check{0} & \check{1} & \check{0} \\ \check{0} & \check{0} & \check{0} & \check{U}_{\theta_2} \end{pmatrix} , \tag{4.6}$$

and

$$\check{U}_{\theta} = \begin{pmatrix} \cos\frac{\theta}{2} & \sin\frac{\theta}{2} \\ -\sin\frac{\theta}{2} & \cos\frac{\theta}{2} \end{pmatrix} . \tag{4.7}$$

For simplicity, we further assume that the two conductors are equal and that they are subjected to the same degree of decoherence, so that $\hat{S}_{13} = \hat{S}_{24}$. For this reason the chemical potentials of the additional reservoirs are identical. It is interesting to notice that decoherence processes in the two wires are, in some sense, "uncorrelated", meaning that we have imposed that the currents flowing through the fictitious leads vanish separately in the two reservoirs. (Correlations can be introduced, for example, by imposing $I_5 + I_6 + I_7 + I_8 = 0$.) In the symmetrical setup we are considering here, $\mu = \mu_{\mathrm{R}} + (\mu_{\mathrm{L}} - \mu_{\mathrm{R}})/2$. In the rest of the paper we consider the case in which all the reservoirs are at zero temperature.

The incoming state of the system $|\psi\rangle$ depends on whether the energy of electrons falls within the range $\mu_{\mathrm{R}} < E < \mu$ or $\mu < E < \mu_{\mathrm{L}}$:

$$|\psi\rangle = \begin{cases} |\psi_{\mathrm{B}}\rangle & \mu < E < \mu_{\mathrm{L}} \\ |\psi_{\mathrm{S}}\rangle & \mu_{\mathrm{R}} < E < \mu \end{cases} , \tag{4.8}$$

where

$$|\psi_{\mathrm{B}}\rangle = \frac{1}{\sqrt{2}} \left[a^{\dagger}_{3\uparrow}(E) a^{\dagger}_{4\downarrow}(E) \pm a^{\dagger}_{3\downarrow}(E) a^{\dagger}_{4\uparrow}(E) \right] |0\rangle , \tag{4.9}$$

and

$$|\psi_{\rm S}\rangle = \frac{1}{\sqrt{2}}\left[a^\dagger_{3\uparrow}(E)a^\dagger_{4\downarrow}(E) \pm a^\dagger_{3\downarrow}(E)a^\dagger_{4\uparrow}(E)\right]\prod_{n=5,6,7,8} a^\dagger_{n\uparrow}(E)a^\dagger_{n\downarrow}(E)\,|0\rangle\,. \tag{4.10}$$

In Eqs. (4.9) and (4.10) $a^\dagger_{i\sigma}(E)$ is the creation operator for a propagating electron in lead i with spin σ at energy E. The upper sign refers to the case in which the incoming state is a spin triplet and the lower sign to the spin singlet. Electrons with energy between μ and $\mu_{\rm L}$ are exiting leads 3 and 4 of the entangler in a superposition of spin $\uparrow$ and $\downarrow$ states. For energies between $\mu_{\rm R}$ and μ electrons are also injected from the additional leads (with indexes 5, 6, 7 and 8) in a factorized state. Note that this occurs only in the presence of decoherence, i.e. for $\alpha \neq 0$.

By setting $\mu_{\rm R} = 0$ and $\mu_{\rm L} = eV$, the total current flowing in lead 1, calculated using the Landauer-Büttiker formalism [152] in the linear response regime, is given by

$$I_1 = e^2V/h(T_{13} + T_{15} + T_{16}). \tag{4.11}$$

Although the coherent part of the current decreases with α, the total current increases with it (except for $T = 1$, where it remains constant and equal to e^2V/h). We would like to mention that this is a special feature of the model of decoherence we are using, not to be expected in general.

4.3 CH inequality for the full counting statistics

The quantity employed in the formulation of the CH inequality, as derived in Ref. [113], is the joint probability $P(Q_1, Q_2)$ for transferring a number of Q_1 and Q_2 electronic charges into leads 1 and 2 over an observation time t. The CH inequality is based on the hypothesis that the outcome of a measurement could be accounted for by a local hidden variable theory. The test of the CH inequality proceeds as follows. The entangler is switched on during an observation time t (where the minimum t is the inverse of the measuring device bandwidth) in which it emits an average number M of pairs of entangled electrons. After traversing the conductors (and being affected by inelastic scattering) the electrons are counted in both terminals 1 and 2. The experiment is then repeated to get single terminal and joint terminal probability distributions that Q_1 particles arrive into analyzer 1 and Q_2 particles arrive into analyzer 2 (along a local spin-quantization axis or independently of it) with $Q_1+Q_2 \leq 2M$.

The CH inequality for the FCS reads [113]

$$\begin{aligned}\mathcal{S}_{\rm CH} &= P^{\theta_1,\theta_2}(Q_1,Q_2) - P^{\theta_1,\theta_2'}(Q_1,Q_2) + P^{\theta_1',\theta_2}(Q_1,Q_2) + P^{\theta_1',\theta_2'}(Q_1,Q_2)\\ &- P^{\theta_1',-}(Q_1,Q_2) - P^{-,\theta_2}(Q_1,Q_2) \leq 0.\end{aligned} \tag{4.12}$$

The possible violation, or the extent of it, also depends on Q_1 and Q_2. $P^{\theta_1,\theta_2}(Q_1,Q_2)$ is the joint probability in the presence of two analyzers, where Q_1 electrons are counted in lead 1 along θ_1 direction and Q_2 are counted in lead 2 along θ_2. $P^{\theta_1,-}(Q_1,Q_2)$ is the corresponding joint probability when one of the two analyzers has been removed. The same notation will be used for single terminal probability distributions: $P^{\theta_i}(Q_i)$ in the presence of an analyzer and $P(Q_i)$ if no analyzer is present. Eq. (4.12) holds for all values of Q_1 and Q_2 which satisfy the *no-enhancement assumption*:

$$P^{\theta_i}(Q_i) \leq P(Q_i). \tag{4.13}$$

The joint probability distribution for transferring $Q_{1\sigma}$ electrons with spin σ in lead 1, $Q_{2\sigma}$ electrons with spin σ in lead 2 and so on is given by

$$P(Q_{1\uparrow},Q_{1\downarrow},Q_{2\uparrow},\ldots) = \frac{1}{(2\pi)^{2n}}\int_{-\pi}^{+\pi} d\lambda_{1\uparrow}d\lambda_{1\downarrow}d\lambda_{2\uparrow}\ldots\ \chi(\vec{\lambda_\uparrow},\vec{\lambda_\downarrow})\ e^{i\vec{\lambda_\uparrow}\cdot\vec{Q_\uparrow}}\ e^{i\vec{\lambda_\downarrow}\cdot\vec{Q_\downarrow}}, \tag{4.14}$$

where $\chi(\vec{\lambda_\uparrow},\vec{\lambda_\downarrow})$ is its characteristic function that can be expressed within the scattering approach.

For long measurement times t, the total characteristic function χ is the product of contributions from different energies, so that

$$\chi(\vec{\lambda_\uparrow},\vec{\lambda_\downarrow}) = e^{\frac{t}{h}\int dE\ \log\chi_E(\vec{\lambda_\uparrow},\vec{\lambda_\downarrow})}. \tag{4.15}$$

The energy-resolved characteristic function for the transfer of particles at a given energy E in a structure attached to n leads can be written as [199–201]

$$\chi_E(\vec{\lambda_\uparrow},\vec{\lambda_\downarrow}) = \langle \prod_{j=1,n} e^{i\lambda_{j\uparrow}\hat{N}_I^{j\uparrow}} e^{\lambda_{j\downarrow}\hat{N}_I^{j\downarrow}} \prod_{j=1,n} e^{-i\lambda_{j\uparrow}\hat{N}_O^{j\uparrow}} e^{-i\lambda_{j\downarrow}\hat{N}_O^{j\downarrow}} \rangle\,, \tag{4.16}$$

where the brackets $\langle ... \rangle$ stand for the quantum statistical average over the thermal distributions in the leads. Assuming a single channel per lead, $\hat{N}_{O(I)}^{j\sigma}$ is the number operator for outgoing (incoming) particles with spin σ in lead j and $\vec{\lambda_\uparrow}$, $\vec{\lambda_\downarrow}$ are vectors of n real numbers, one for each open channel. In terms of outgoing (incoming) creation operator $\hat{\phi}_{j\sigma}^\dagger$ ($\hat{a}_{j\sigma}^\dagger$), which are linked by the total scattering matrix of the system S, the number operators can be expressed as

$$\hat{N}_I^{j\sigma} = \hat{a}_{j\sigma}^\dagger \hat{a}_{j\sigma}; \qquad \hat{N}_O^{j\sigma} = \hat{\phi}_{j\sigma}^\dagger \hat{\phi}_{j\sigma}. \tag{4.17}$$

At zero temperature, the statistical average over the Fermi distribution function in Eq. (4.16) simplifies to the expectation value calculated over the state $|\psi\rangle$ defined in Eq. (4.8). The interval of integration in Eq. (4.15) can be separated in two energy ranges, namely $E < \mu$ and $\mu < E < eV$. Since, in the limit of a small voltage bias V, χ_E is energy-independent, Eq. (4.15) can be approximated to

$$\chi(\vec{\lambda_\uparrow},\vec{\lambda_\downarrow}) \simeq \left[\chi_0^{\mathrm{S}}(\vec{\lambda_\uparrow},\vec{\lambda_\downarrow})\right]^{M_\mu}\left[\chi_0^{\mathrm{B}}(\vec{\lambda_\uparrow},\vec{\lambda_\downarrow})\right]^{M-M_\mu}, \tag{4.18}$$

where $M_\mu = \mu t/h$ and $M = eVt/h$.

According to Eq. (4.14), both single terminal and joint probability distributions require the computation of multidimensional integrals, which can only be performed numerically. In Appendix C it is shown that the various probability distributions needed to evaluate the CH inequality can be expressed in a differential form, more suitable for numerical evaluation. All the expectation values needed for the calculations are collected in Appendix C.1. Since the two wires are decoupled and there are no spin-flip processes, the joint probabilities with a single analyzer are factorized:

$$\begin{aligned} P^{\theta_1,-}(Q_1,Q_2) &= P^{\theta_1}(Q_1)P(Q_2), \\ P^{-,\theta_2}(Q_1,Q_2) &= P(Q_1)P^{\theta_2}(Q_2). \end{aligned} \tag{4.19}$$

Rotational invariance makes $P^{\theta_1,-}(Q_1,Q_2)$ and $P^{-,\theta_2}(Q_1,Q_2)$ independent of the angle of the analyzers, while $P^{\theta_1,\theta_2}(Q_1,Q_2)$ depends on the angles only through the combination $\frac{\theta_1 \pm \theta_2}{2}$ (upper sign for triplet and lower sign for singlet), so that we can define $P_{1,2}^{\frac{\theta_1\pm\theta_2}{2}}(Q_1,Q_2) \equiv P^{\theta_1,\theta_2}(Q_1,Q_2)$ and $P_{1,-}(Q_1,Q_2) \equiv P^{\theta_1,-}(Q_1,Q_2)$. As a result, the CH inequality depends only on three angles $\theta_a \equiv \theta_1 \pm \theta_2$, $\theta_b \equiv \theta_2 \pm \theta_1'$ and $\theta_c \equiv \theta_1' \pm \theta_2'$ ($\theta_d = \theta_1 \pm \theta_2'$ is a linear combination of the other three: $\theta_d = \theta_a + \theta_b + \theta_c$). Since $P^{\theta_1,\theta_2}(Q_1,Q_2)$ is an even function of $\frac{\theta_1\pm\theta_2}{2}$, in order to find maximal violations we can restrict the evaluation of the CH inequality to the following set of angles: $\theta_a = \theta_b = \theta_c = \theta_d/3 \equiv 2\Theta$. (This is found by imposing that positive contributions to $\mathcal{S}_{\rm CH}$ are maximum while negative contributions are minimum.) The quantity $\mathcal{S}_{\rm CH}$, characterizing the CH inequality, will therefore depend on a single angle Θ, on the decoherence strength α and on the value of the transmitted charge Q_1 and Q_2. As a result, the CH inequality takes the simplified form

$$\mathcal{S}_{\rm CH} = 3P_{1,2}^{\Theta}(Q_1,Q_2) - P_{1,2}^{3\Theta}(Q_1,Q_2) - P_{1,-}(Q_1,Q_2) - P_{-,2}(Q_1,Q_2) \leq 0. \tag{4.20}$$

Without loss of generality we can choose $\sigma = \sigma' = \uparrow$. The other cases can be recovered by rotating the polarizers an angle π.

4.3.1 No-enhancement assumption

As mentioned above, the CH inequality can be derived under the no-enhancement assumption, Eq. (4.13). Such a condition is trivially true when a single particle is transmitted, $Q = 1$: The presence of an analyzer can only decrease the counting probability [115]. However, when many particles are transmitted, $Q > 1$, the no-enhancement assumption is a relationship between distribution probabilities that is not, in general, satisfied for all values of Q.

We remind that in the absence of decoherence [113], for given M and Q, the no-enhancement assumption in one of the two leads is satisfied only within a range of values of T below certain threshold $T_{\max}(M,Q)$. In the case of different numbers of

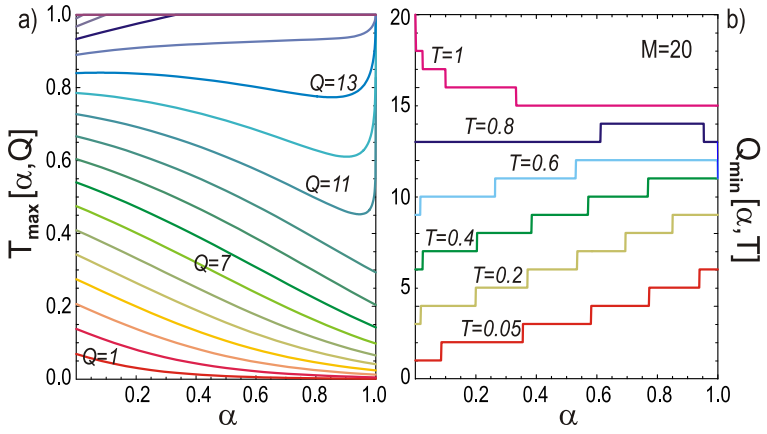

Figure 4.2: a) Maximum value of the transmission, $T_{\max}$, allowed by the no-enhancement assumption as a function of decoherence rate α for $M = 20$ emitted pairs and for the different values of Q. b) Minimum allowed number of transmitted particles $Q_{\min}$ for a fixed wire transmission as a function of the decoherence rate.

transmitted particles in lead 1 and 2 ($Q_1 \neq Q_2$), the maximum allowed transmission probability must be taken to be the minimum between $T_{\max}(M, Q_1)$ and $T_{\max}(M, Q_2)$, according to our assumption of identical wires.

The no-enhancement assumption is affected by decoherence as a consequence of the fact that single terminal probabilities, with or without analyzer, depend on α. More precisely, the no-enhancement assumption in one of the two leads is satisfied for transmissions up to a threshold value which is now a function of α: $T_{\max}(\alpha, M, Q)$. Unlike the ideal case, for $\alpha \neq 0$ it is not possible to find an analytical expression for $T_{\max}$. In Fig. 4.2a $T_{\max}$ is plotted as a function of α for $M = 20$ and all values of Q from 1 to 20. One can see that $T_{\max}$ monotonically decreases with α for values of $Q \lesssim M/2$ and monotonically increases for large values of Q. For intermediate values of Q, $T_{\max}$ decreases up to values of α close to one and then rapidly increases reaching one when $\alpha = 1$. This behaviour is specific of the fictitious lead model and reflects the fact that both the average total current [Eq. (4.11)], related to $P(Q)$, and the average spin-polarized current, related to $P^{\theta}(Q)$, are increasing functions of α. Indeed, as a consequence of a finite α, the two distributions shift to larger values of Q, as it would happen for an enhanced effective transmission probability. Its maximum allowed value by the no-enhancement assumption is therefore reached for a smaller T. As a consequence $T_{\max}$ must decrease with α. This argument is not valid when $T_{\max} \simeq 1$ at $\alpha = 0$, since the average currents do not change appreciably with α and only the peculiar shape of the distributions matters. We define

$$T_{\max}(\alpha, M, Q_1, Q_2) = \mathrm{Min}[T_{\max}(\alpha, M, Q_1), T_{\max}(\alpha, M, Q_2)]. \tag{4.21}$$

Alternatively, given a wire with a fixed transmission T, the no-enhancement assumption is verified for values of Q bigger than or equal to a certain value $Q_{\min}(\alpha, M, T)$.

For $\alpha \neq 0$, the behaviour of $Q_{\min}$ is shown in Fig. 4.2b for $M = 20$ and for different transmissions. We observe that it increases (step-wise, since only integer values of the number of particles are permitted) as a function of the decoherence rate for almost every transmission T, except for those close to unity, for which it decreases. The behaviour for small values of T can still be understood in terms of the average current increase with α. For $T = 1$, being $Q_{\min} = M$ at $\alpha = 0$, decoherence can only cause a decrease.

4.4 Results

In the present section we shall discuss how the CH inequality of Eq. (4.20) is affected by the presence of decoherence. There are some general characteristics of the behaviour of $\mathcal{S}_{\rm CH}$ that were already found in the absence of decoherence [113] that hold also for finite α [3]. The most relevant are the following:

- $\mathcal{S}_{\rm CH}$ is always symmetric as a function of Θ around $\Theta = \pi/2$;
- for given M, Q_1 and Q_2 the maximum violation always occurs for transmission equal to $T_{\max}(\alpha, M, Q_1, Q_2)$.

In Fig. 4.3, $\mathcal{S}_{\rm CH}$ is plotted as a function of the angle Θ for $M = 20$ and $Q_1 = Q_2 = 8$. The three curves refer, respectively, to $\alpha = 0$ (solid line), $\alpha = 0.3$ (dashed line) and $\alpha = 0.5$ (dotted line), each one calculated for the corresponding $T = T_{\max}$ reported in the label box. The plot shows that the CH inequality is violated within a certain window of values of Θ. The violation is suppressed with increasing decoherence rate, but occurs for the same range of angles. This is due to the following properties of the joint probabilities, which hold at $T = T_{\max}$ for all values of α: i) $P_{1,2}^{\pi/4}(Q_1, Q_2) = P_{1,2}^{3\pi/4}(Q_1, Q_2) = P_{1,-}(Q_1, Q_2)$, as a consequence $\mathcal{S}_{\rm CH}(\Theta = \pi/4, 3\pi/4) = 0$; and ii) $P_{1,2}^{\Theta}(Q_1, Q_2) \geq P_{1,2}^{3\Theta}(Q_1, Q_2)$, $P_{1,-}(Q_1, Q_2)$, $P_{-,2}(Q_1, Q_2)$ for $\pi/4 \leq \Theta \leq 3\pi/4$. We checked that by reducing T from $T_{\max}$, but keeping α constant, both the window of angles where violation is present and its amount are decreased. Note that between $\Theta = 0$ and $\pi/2$, there is always an angle for which $\mathcal{S}_{\rm CH}$ is maximum, we shall denote it by $\Theta_{\rm best}(\alpha, M, Q_1, Q_2)$. For given α, M, Q_1 and Q_2, the maximum violation occurs at $T_{\max}$ and $\Theta_{\rm best}$.

We now analyze the maximum violation of the CH inequality for a given M with $T = T_{\max}$ and $\Theta = \Theta_{\rm best}$ as a function of Q_1, Q_2 and α. In Fig. 4.4 we show four density plots of $\mathcal{S}_{\rm CH}$ in the (Q_1, Q_2) plane for different values of decoherence rate and $M = 20$. In the gray scale white corresponds to $\mathcal{S}_{\rm CH} = 0$ and black to its

[3] In particular, if the entangler is substituted with a source that emits factorized states, the CH inequality is never violated for any decoherence rate. This is simply due to the fact that two terminal joint probability distributions are given by the product of single terminal probability distributions, thus making the CH inequality always equal to zero.

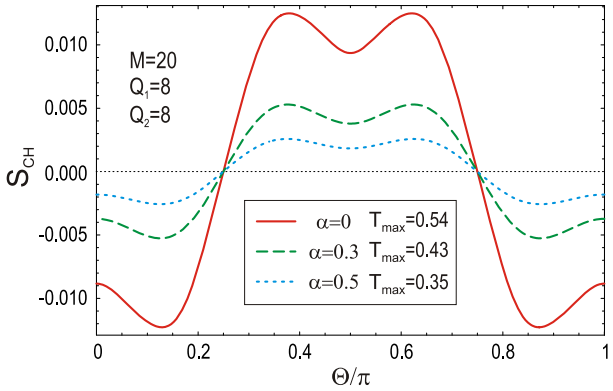

Figure 4.3: The quantity $\mathcal{S}_{\rm CH}$ is plotted as a function of Θ for $M = 20$, $Q_1 = Q_2 = 8$ and different decoherence rates at the corresponding maximum allowed transmissions. In particular, for $\alpha = 0$ (solid line) $T_{\rm max} = 0.54$, for $\alpha = 0.3$ (dashed line) $T_{\rm max} = 0.43$ and for $\alpha = 0.5$ (dotted line) $T_{\rm max} = 0.35$. The amount of violation of the CH inequality decreases with α, whereas the range of angles for which violation occurs does not change. We call $\Theta_{\rm best}$ the angle corresponding to the maximum violation.

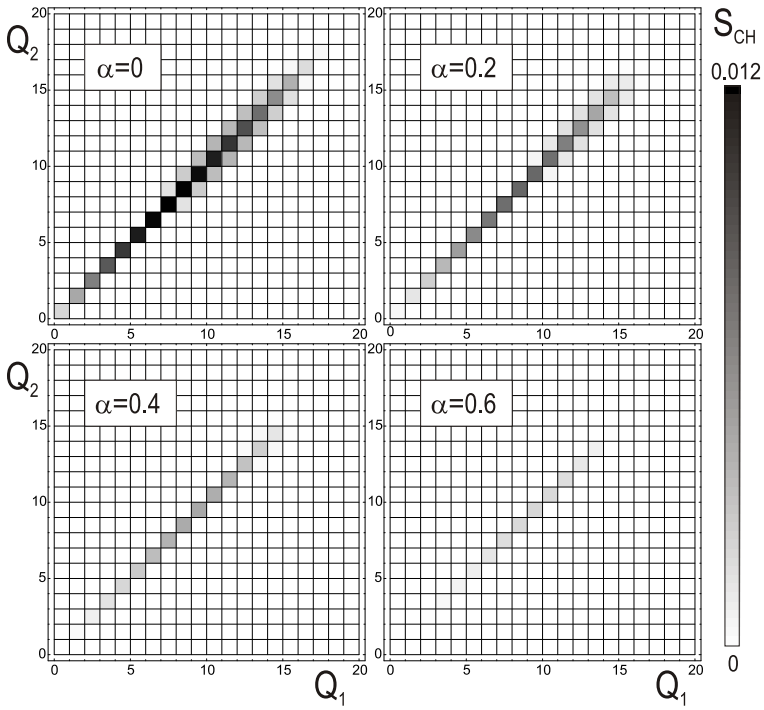

Figure 4.4: Density plots of the maximum value of $\mathcal{S}_{\rm CH}$, evaluated at $T = T_{\rm max}(\alpha, Q_1, Q_2)$ and $\Theta = \Theta_{\rm best}(\alpha, Q_1, Q_2)$, in the (Q_1, Q_2) plane for $M = 20$ relative to four different values of decoherence ($\alpha = 0$, 0.2, 0.4, 0.6). $\mathcal{S}_{\rm CH} \simeq 0.012$ is the maximum violation for $M = 20$ found in the absence of decoherence.

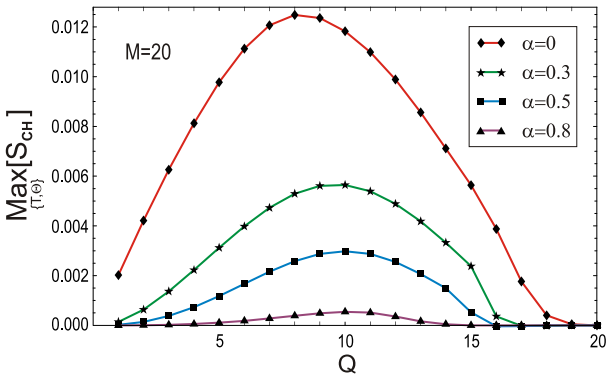

Figure 4.5: Maximum value of the quantity $\mathcal{S}_{\rm CH}$ ($T = T_{\rm max}$ and $\Theta = \Theta_{\rm best}$) as a function of Q for $M = 20$ and different values of decoherence: $\alpha = 0$, 0.3, 0.5, 0.8. The largest violation always occurs in the absence of decoherence and, for a given Q, violation is reduced monotonically with α. The position where the maximum occurs, $Q_{\rm best}$, slightly increases with α. At $Q = Q_{\rm best}$, $T_{\rm max} = 0.54$ for $\alpha = 0$, $T_{\rm max} = 0.59$ for $\alpha = 0.3$, $T_{\rm max} = 0.52$ for $\alpha = 0.5$ and $T_{\rm max} = 0.39$ for $\alpha = 0.8$.

maximum value taken in the absence of decoherence. When $\alpha = 0$, the CH inequality is strongly violated for diagonal terms of the distribution (where $Q_1 = Q_2$). However, some weaker violations are also possible for $Q_1 \neq Q_2$, though they tend to disappear with increasing α. By increasing the values of α the plots show that the maximum violation of the CH inequality decreases rapidly: for $\alpha = 0.6$ we get only 16% of the largest value reached at $\alpha = 0$. The behaviour of the CH inequality is symmetrical with respect to the exchange of Q_1 with Q_2 for any rate of decoherence. In Fig. 4.5 we report the section of the plots in Fig. 4.4 along the diagonal of the (Q_1, Q_2)-plane. The four curves are relative to $\alpha = 0$, 0.3, 0.5 and 0.8 and $M = 20$. Several observations are in order. If we denote with $Q_{\rm best}$ the position of the maximum of a curve, for all values of decoherence rate $Q_{\rm best} \sim M/2$, more precisely, $Q_{\rm best} = 8$ for $\alpha = 0$ and $Q_{\rm best} = 10$ for all other curves. This slight increase of $Q_{\rm best}$ with α is due to the fact that an increase in decoherence is accompanied by a slight enhancement of the average current [Eq. (4.11)] flowing through the wires (as mentioned at the end of Sec. 4.2). This is, however, a specific feature of the model of decoherence we are considering. Note furthermore that, as decoherence gets stronger, the range of values of Q for which violation takes place shrinks.

We now discuss the violation of the CH inequality as a function of α and M at $T = T_{\rm max}$, $\Theta = \Theta_{\rm best}$ and $Q = Q_{\rm best}$. In Fig. 4.6 the ratio $s \equiv \mathcal{S}_{\rm CH}(\alpha, M)/\mathcal{S}_{\rm CH}(0, M)$ at $T_{\rm max}, \Theta_{\rm best}$ and $Q_{\rm best}$ (i. e. the quantity $\mathcal{S}_{\rm CH}$ normalized to its value in the absence of decoherence) is reported in a three-dimensional plot as a function of α and the number of emitted pairs M. The most interesting feature is that such a ratio decays more rapidly with α as M is increased. This means that decoherence is more disruptive, as far as detection of entanglement is concerned, for long measuring times (i.e. large

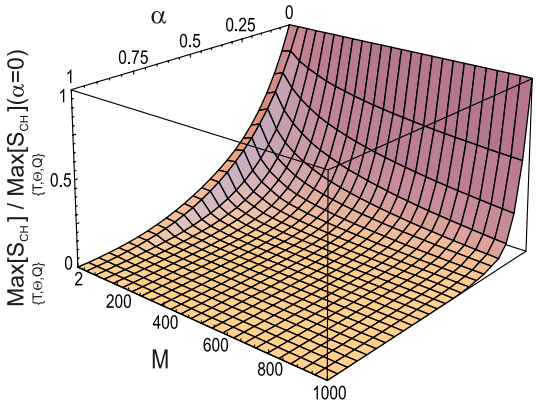

Figure 4.6: $\mathcal{S}_{\rm CH}$, normalized to its value in the absence of decoherence and calculated at $T = T_{\rm max}$, $\Theta = \Theta_{\rm best}$ and $Q = Q_{\rm best}$, is plotted as a function of decoherence rate α and number of injected entangled pairs M. Longer measuring times (i.e. larger values of M) make decoherence more effective, that is, make the detection of entanglement more difficult.

M). As an example, for $M = 1000$ the extent of the violation is reduced by 80% at $\alpha = 0.1$. More precisely, for values of M larger than 30, we find that the normalized $\mathcal{S}_{\rm CH}$ follows the law:

$$s \sim \frac{\sinh[K(1-\alpha)^{b\sqrt{M}}]}{\sinh(K)}, \tag{4.22}$$

with $K = 7.26$ and $b = 0.076$.

Another interesting aspect is related to $Q_{\rm best}$ which, as mentioned above, only slightly increases with α for all values of M. As M is increased, the value of $Q_{\rm best}$, for a given α, does not increase proportionally to M, but very much slowly and surprisingly remains of the order of 10 for $M = 1000$ (see Fig. 4.7). For $\alpha = 0$ this can be understood as follows. On the one hand, one expects $Q_{\rm best}$, corresponding to the largest $\mathcal{S}_{\rm CH}$, to be about the position of the maximum of joint probability distributions, which can be assumed to be equal to the product MT. On the other hand, $T_{\rm max}$ is a decreasing function of M, in fact it decays as $1/M$ [113]. The product $MT_{\rm max}$ is therefore expected to be a constant. Indeed, it is possible to show, in the large M expansion, that $Q_{\rm best} \sim MT_{\rm max}$ for $\alpha = 0$ and $Q_{\rm best} \sim M\sqrt{T_{\rm max}}$ for $\alpha \neq 0$, while $T_{\rm max} \sim 1/M$ for $\alpha = 0$ and $T_{\rm max} \sim 1/M^2$ for $\alpha \neq 0$. As a result, $Q_{\rm best}$ is roughly constant as a function of M and α [4].

The final point we address is the maximum decoherence rate, that we denote by $\alpha_{\rm max}$, for which there is still violation of the CH inequality as a function of $Q \equiv Q_1 = Q_2$. In Fig. 4.8 we plot $\alpha_{\rm max}$ as a function of Q for $M = 20$ at $T = T_{\rm max}$ and $\Theta = \Theta_{\rm best}$.

[4]More precisely, for large M, $Q_{\rm best}$ is implicitly given by the equation: $Q_{\rm best} = \tilde{Q}[\alpha, T_{\rm max}(\alpha, M, Q_{\rm best})]$, where $\tilde{Q}[\alpha, T] = M[\sqrt{T}\alpha(2-\alpha) + T(2-2\alpha+\alpha^2)]/[2 + (\sqrt{T}-1)\alpha]^2$ is the position of the maximum of the distribution in the large M approximation.

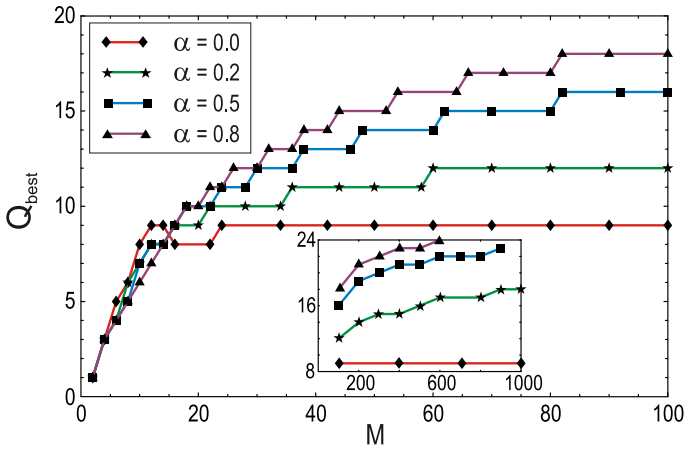

Figure 4.7: $Q_{\rm best}$ is plotted as a function of M for different values of decoherence rate ($\alpha = 0$, 0.2, 0.5 and 0.8). In the inset, curves are shown over an extended range, up to $M = 1000$. For a given α, with increasing M the value of $Q_{\rm best}$ increases very slowly remaining of the order of 10.

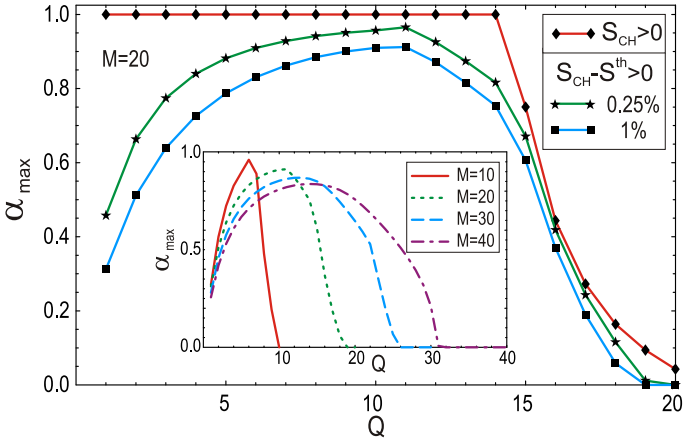

Figure 4.8: Maximum value ($\alpha_{\rm max}$) of the decoherence parameter for which there is still violation of the CH inequality as a function of Q for $M = 20$. The line with ♦ represents $\alpha_{\rm max}(Q)$ with $\mathcal{S}_{th} = 0$: from $Q = 1$ to $Q = 14$ violation is found for any decoherence rate. The line with ★ is instead computed using a threshold $\mathcal{S}_{th}$ which corresponds to 0.25% of the maximum violation value for $\alpha = 0$, and the line with ■ using $\mathcal{S}_{th}$ corresponding to 1%. The latter threshold is used in the inset where $\alpha_{\rm max}(Q)$ is plotted for $M = 10$, 20, 30 and 40. Interestingly we found that there is a value $\bar{Q}$ that is more robust against decoherence. In particular, $\bar{Q} = 6$ for $M = 10$, $\bar{Q} = 11$ for $M = 20$, $\bar{Q} = 13$ for $M = 30$ and $\bar{Q} = 14$ for $M = 40$. With increasing M, $\alpha_{\rm max}$ diminishes slowly.

The line with the symbol ♦ shows that violation of the CH inequality is found for any rate of decoherence for $Q = 1$ to $Q = 14$ and thereafter $\alpha_{\max}$ decreases sharply. Nevertheless, the extent of violation for α close to 1 is almost negligible for most of $1 \leq Q \leq 14$. One can therefore introduce a small positive threshold $\mathcal{S}_{\rm th}$ which defines the violation as: $\mathcal{S}_{\rm CH} < \mathcal{S}_{\rm th}$. The line with ★ refers to a threshold of 0.25% of the maximum value of $\mathcal{S}_{\rm CH}$ at $\alpha = 0$ ($\mathcal{S}_{\rm th} = 3 \times 10^{-5}$ for $M = 20$), and the line with ■ to a 1% ($\mathcal{S}_{\rm th} = 1.2 \times 10^{-4}$ for $M = 20$). The latter percentage is used for the thresholds of the plots in the inset of Fig. 4.8, where $\alpha_{\max}$ is plotted for $M = 10$, 20, 30 and 40. It is shown that there are values of Q that are more resistent to decoherence, i. e. for which violation survives for larger decoherence rates. In the caption of Fig. 4.8, the most protected value against decoherence is denoted with $\bar{Q} \equiv Q_{\rm best}(\alpha_{\max})$.

4.4.1 Asymmetric setup: one additional reservoir

It is interesting to consider the case in which decoherence affects the two wires differently. In this appendix we study the case when decoherence affects only one of the two conductors, i.e. in the presence of a single additional fictitious reservoir, for example, in the upper branch, as depicted in Fig. 4.9a. Being T_0 the transmission of the elastic scatterers in the upper conductor, we choose the transmission of the lower conductor to be equal to $T = T_0^2/(2 - T_0)^2$, in order for the two conductors to have the same conductance in the absence of decoherence. Fig. 4.9b shows the density plot of the maximum value of $S_{\rm CH}$ (with $T = T_{\max}$ and $\Theta = \Theta_{\rm best}$) as a function of Q_1 and Q_2, for $M = 20$, $\alpha = 0.4$ (left) and $\alpha = 0.6$ (right). In the presence of decoherence the maximum violation is not achieved on the diagonal ($Q_1 = Q_2$), i.e. the behaviour of $S_{\rm CH}$ is not symmetrical anymore with respect to Q_1 and Q_2. This is due to the fact that, as we have seen above, the overall current increases with α so that it is more likely to transmit a larger number of particles in the conductor subjected to decoherence. Another difference with respect to the case with two additional reservoirs is that the suppression of the violation by α is less pronounced.

The asymmetry found in the behaviour of the density plots of Fig. 4.9(b) must not be confused with the asymmetry we would obtain in a setup without decoherence but with conductors of different resistance [system sketched in Fig. 4.10(a)]. In this case, by applying separately the no enhancement assumption to the two conductors, large violations occur in a vast region of the (Q_1, Q_2)-plane, as shown in Fig. 4.10(b). Interestingly, we note that one would get large violations of the CH inequality for $Q_1 \neq Q_2$. However, this asymmetry would not come from the fact that entanglement is weakened by decoherence in only one wire.

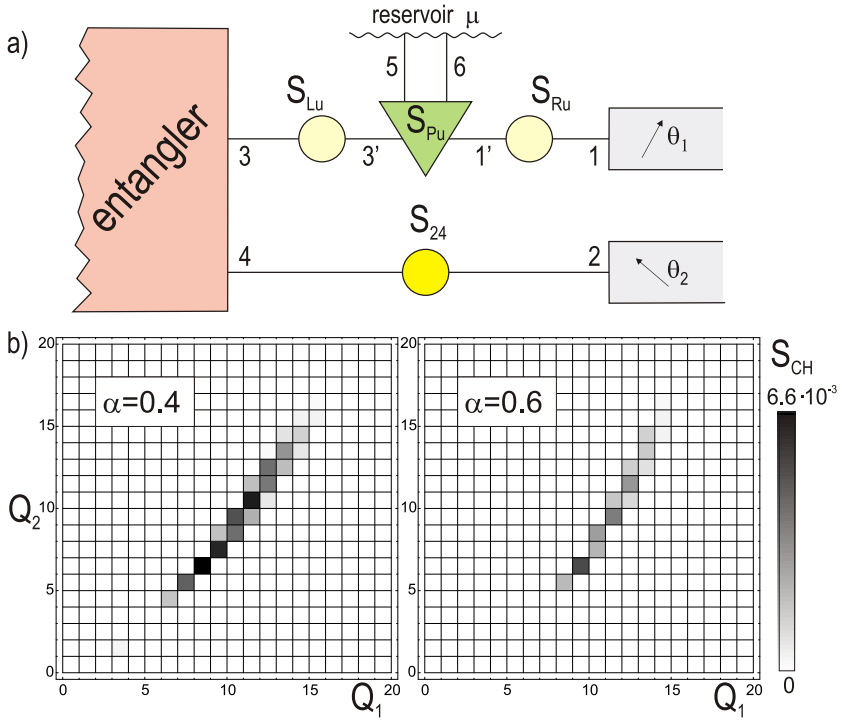

Figure 4.9: a) Idealized setup with a single additional reservoir in the upper branch of the system. Scattering matrices are chosen so that, in the absence of decoherence, the two conductors have equal transmission. b) Density plot of the maximum value of $\mathcal{S}_{\rm CH}$ in the (Q_1, Q_2)-plane for $M = 20$ and for $\alpha = 0.4$ (left) and $\alpha = 0.6$ (right). As decoherence increases, the maximum violation is not achieved on the diagonal, but is shifted towards the right-bottom part of the plane ($Q_1 > Q_2$). This occurs because only the current flowing through the conductor affected by decoherence is modified. Furthermore, the suppression of the violation by α is less pronounced with respect to the case with two additional reservoirs. For example, for $\alpha = 0$ we find $\mathrm{Max}[\mathcal{S}_{\rm CH}] = 0.012$ achieved at $(Q_1 = 8, Q_2 = 8)$. For $\alpha = 0.2$ and one additional reservoir we have $\mathrm{Max}[\mathcal{S}_{\rm CH}] = 0.0089$ reached at $(8, 7)$, whereas for two additional reservoirs we get $\mathrm{Max}[\mathcal{S}_{\rm CH}] = 0.0074$ at $(9, 9)$. For $\alpha = 0.4$ and one additional reservoir, $\mathrm{Max}[\mathcal{S}_{\rm CH}] = 0.0066$ at $(9, 7)$, and with two additional reservoirs, $\mathrm{Max}[\mathcal{S}_{\rm CH}] = 0.0042$ at $(10, 10)$. Finally, for $\alpha = 0.6$ and one additional reservoir, $\mathrm{Max}[\mathcal{S}_{\rm CH}] = 0.0046$ at $(10, 7)$, and with two additional reservoirs, $\mathrm{Max}[\mathcal{S}_{\rm CH}] = 0.0020$ at $(10, 10)$.

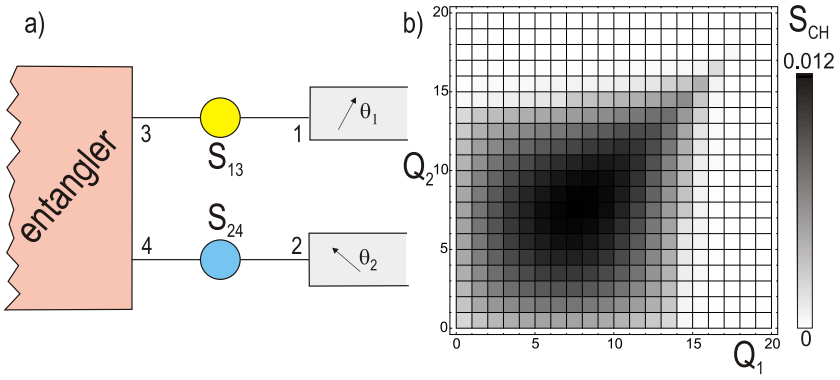

Figure 4.10: a) Idealized setup with no decoherence but differently transmitting upper and lower conductors. b) The density plot of the maximum value of the quantity $\mathcal{S}_{\rm CH}$ is shown in the (Q_1, Q_2)-plane for $M = 20$.

4.5 Related experiments

Bell inequalities have been tested experimentally many times over the last thirty years using photons. Although some experimental assumptions have been made, the results are considered reasonably conclusive, and thus, are in general thought to have confirmed quantum theory and shown results that cannot be explained under local hidden variable theories. Some of these well known experiments are: the one by Freedman and Clauser in 1972 [202] (where they violate Freedman's inequality, a variant on the CH74 inequality); the ones by Aspect and his team at Orsay in 1981 [203] and 1982 [204,205] (where they used calcium cascade sources, and violated the CH74 and the CHSH inequalities); the one by Tittel and his group in Geneva in 1998 [206] (where they showed that distance did not destroy the "entanglement", since light was sent in fibre optic cables over distances of several kilometres before it was analyzed); and the one by Weihs [207] and his team at Innsbruck in 1998, lead by Zeilinger (where they improved Aspect's of 1982 and violated the CHSH inequality by over 30 standard deviations) [208].

As far as we know, Bell test experiments have not been carried out with electrons, neither when they are formulated in terms of zero-frequency current crossed correlators, nor when expressed in terms of the FCS, where "coincidence counts" are needed.

So much for the Bell inequalities, but even the measurement of the FCS for electrons is only a recent achievement. Theoretical proposals to measure the FCS were suggested in 2004 in Refs. [209, 210], where the use of threshold detectors based on Josephson junctions were proposed. Then, in 2005, an experiment called "Current measurement by real-time counting of single electrons" was performed by J. Bylander, T. Duty and P. Delsing [121]. In this work the authors managed to count electrons one by one, although only in the tunneling limit, by means of a microelectronic cir-

cuit with a chain of islands connected by small tunnel junctions. Later in 2005, a preprint by S. Gustavsson et al. has appeared in the cond-mat archive called "Counting statistics of single-electron transport in a quantum dot" [211]. Here the authors claim to have measured the FCS of current fluctuations in a semiconductor quantum dot by real-time detection of single electron tunneling using a nearby quantum point contact.

4.6 Conclusions

In this chapter we have studied the effect of decoherence on the violation of the CH (or CH74) inequality formulated in terms of the FCS [113]. The system under investigation (Fig. 4.1) consists of an idealized entangler connected, through a pair of identical mesoscopic wires, to spin-selective counters. We have assumed that decoherence, which occurs equally but independently in the two conductors, is produced by the presence of additional fictitious reservoirs according to the phenomenological model of Büttiker [86, 87]. Decoherence is parameterized by the rate α.

As expected, decoherence gives rise to suppression of the violation of the CH inequality. The extent of such a suppression has been analyzed as a function of the parameters which characterize the system, namely, the transmission T of the wires, the angle between analyzers Θ, the number of injected entangled pairs M and the number of transmitted particles Q_1 and Q_2 in the counters. First we have discussed the *no-enhancement assumption*, a condition that needs to be satisfied in both leads 1 and 2 in order for the CH inequality to hold. We have found that such condition, in a given lead, is verified for all transmission T up to some maximum value $T_{\max}$ which depends on Q, M and, of course, α. In particular, $T_{\max}$ decreases with the decoherence rate up to some value of Q and thereafter increases. The main results can be summarized as follows:

- Maximal violation, even in the presence of decoherence, occurs at the largest allowed transmission $T = T_{\max}$ and for $Q_1 = Q_2$ (it disappears very rapidly when $Q_1 \neq Q_2$).

- As long as $T = T_{\max}$, the angle range of the analyzers for which violation takes place does not depend on the decoherence rate, though the extent of violation decreases with α.

- In the absence of decoherence, the maximum violation of the CH inequality was proved to decay as $1/M$ [113]. Here we have found that, for finite α, the parameter $\mathcal{S}_{\rm CH}$ decreases exponentially with $\sqrt{M}$, more precisely as $[f(\alpha)]^{-\sqrt{M}}/M$, i.e. decays both with increasing M and α.

- The value of Q for which maximum violation occurs is virtually independent of

M, which means that the largest violations appear for relatively small numbers of transmitted particles, even at large observation times.

- Interestingly, we have found that the largest decoherence rate for which the CH inequality is violated (within a given small tolerance) presents a maximum as a function of Q. This means that there exist numbers of transmitted charges which are more protected against decoherence, i.e. the influence of the environment is less disruptive as far as the violation of CH inequality is concerned.

Although in this work decoherence is assumed to be produced by the presence of additional reservoirs, other different sources of decoherence are possible in mesoscopic systems. We believe that this model captures the main effects of decoherence, as far as violations of the CH inequality in a mesoscopic system is concerned, and that the results found in this work may be useful to design the best experimental conditions.

Since real systems cannot be perfectly shielded from the environment, the issues analyzed in this work seem adequate not only from a fundamental point of view, but also in what it might contribute to the understanding of the properties of lossy quantum channels. For the future it would be interesting to apply our method to realistic systems, like normal or superconducting beam splitters.

Chapter 5

Effect of inelastic scattering on spin entanglement detection through current noise

In this chapter we study the effect of inelastic scattering on the spin entanglement detection and discrimination scheme proposed by Egues, Burkard and Loss [Phys. Rev. Lett. 89, 176401 (2002)]. The finite-backscattering beam splitter geometry is supplemented by a phenomenological model for inelastic scattering, the charge-conserving voltage probe model, conveniently generalized to deal with entangled states. We find that the behaviour of shot-noise measurements in one of the outgoing leads remains an efficient way to characterize the nature of the non-local spin correlations in the incoming currents for an inelastic scattering probability up to 50%. Higher order cumulants are analyzed, and are found to contain no additional useful information on the spin correlations. The technique we have developed is applicable to a wide range of systems with voltage probes and entanglement.

The contents of this chapter can be found in the preprint archive cond-mat/0601365, by P. San-Jose and E. Prada.

5.1 Introduction

Electron spin has various crucial properties that make it an ideal candidate for a robust carrier of quantum entanglement in solid state systems. Its typical relaxation and dephasing times can be much larger than any other electronic timescale [212,213], in particular in semiconductor heterostructures, where its controlled manipulation begins to be a reality [7]. This makes electron spin very valuable not only in the context of spintronics [214], but also in the path to a scalable realization of a potential quantum computer.

Moreover, the possibility of demonstrating non-local quantum entanglement of

massive particles such as electrons is of conceptual relevance in itself, since it is at the core of the quantum world weirdness. Quantum optics are far ahead in this respect, and present technology can already entangle [215], teleport [20] or otherwise manipulate quantum mechanically [190] the polarization state of photons, and even commercial solutions have been developed [216] for completely secure cryptographic key exchange via optical quantum communication.

In the context of solid state the equivalent feats are far away still, due to the additional difficulties imposed mainly by the fact that massive particles such as electrons suffer from interactions with their environment, which can be in general avoided in the case of photons. This in turn leads to strong decoherence effects, which degrades the entanglement transportation. Sometimes these disruptive effects can be minimized in the case of electron spin with the proper techniques [7]. Still, the problem of controlled spin manipulation and spin detection are two great hurdles to be tackled in the long path to spin-based quantum computation [33]. The main difficulty in the manipulation problem is that all the operations available in usual electronics address electron charge, being completely independent of the electron's spin, unless some additional mechanism involving, e.g., external magnetic fields [214, 217], ferromagnetic materials [218], or spin-orbit coupling [219, 220] are relevant. Such mechanisms usually correlate spin states to charge states, which allows to manipulate and detect the charge states via more conventional means.

Several recent theoretical works have specifically studied the influence of an electromagnetic environment [75, 78, 80] and the decoherence through inelastic processes [93, 117] on orbital and spin-entangled states, such as those that are the subject of the present work. Generally, in all of those cases some type of spin filter was necessary to measure Bell inequalities, which makes their experimental realization rather challenging.

Another interesting possibility to manipulate and detect spin states with electrostatic voltages is through Pauli blocking, which appears as a spin-dependent 'repulsion' between two electrons due to Pauli exclusion principle, as long as the two electrons share all the remaining quantum numbers. This peculiarity is therefore specific of fermions, and has no analog in quantum optics. An example of the potential of such approach was illustrated in Ref. [105]. It relied on the use of the mentioned Pauli blocking mechanism in a perfect four-arm beam splitter supplemented by the bunching (antibunching) behaviour expected for symmetric (antisymmetric) spatial two-electron wavefunctions. This was done through the analysis of current noise [105], cross-correlators [79], and FCS [108]. It was also shown that it is possible to distinguish between different incoming entangled states [79, 106]. In Ref. [106] it was demonstrated how the shot noise of (charge) current obtained in one of the outgoing leads was enough to measure the precise entangled state coming in through the two input arms, and to distinguish it from a classical statistical mixture of spin states. Finite backscattering and arbitrary mixtures in the spin sector were also considered in Ref. [107], with a focus on the entanglement content and its detection. Two chan-

nel leads and microscopic description of the spin-orbit interaction were also recently analyzed [221].

In this work we will analyze the robustness of the entanglement detection scheme proposed in Ref. [106] in the presence of spin-conserving inelastic scattering and finite beam-splitter backscattering for various entangled current states. Although the spin sector is not modified by scattering, inelastic scattering changes at least the energy quantum number of the scattered electrons, and since Pauli exclusion principle does no longer apply to electrons with different energy, we should expect such inelastic processes to degrade the performance of the detection scheme. From a complementary point of view, viewing the entangled electron pairs as wavepackets localized in space, it is clear that inelastic scattering will cause delays between them that will in general make them arrive at the detectors at different times, thereby lifting the Pauli blocking imposed by their spin correlations [1]. Moreover, as noted in Ref. [107], the presence of backscattering introduces spurious shot noise that is unrelated to the entanglement of the source. Assuming known backscattering but, in general, unknown inelastic scattering rate, we show that the scheme remains valid in certain range of parameter space, and point to a modified data analysis to extract the maximum information out of local shot noise measurements. We further study the information that may be extracted from higher order cumulants of current fluctuations.

We will work within the scattering matrix formalism, and to describe inelastic scattering we will employ a modification of the fictitious voltage probe phenomenological model [86,87,95] generalized to include instantaneous current conservation [88] in the presence of entangled states. This approach relies on phenomenological arguments and defines a scattering probability α that is used to parameterize inelastic effects. Elastic scattering has also been formulated within this language [89]. The validity of the model has been widely discussed, in general finding good qualitative agreement with microscopic models [96–99] and experiments [101]. Recently it was demonstrated to become equivalent to microscopic phase averaging techniques at the FCS level in some limits and setups [102] (clarifying some apparent discrepancies with classical arguments [82]). Also recently, it has been applied to study the effect of spin relaxation and decoherence in elastic transport in chaotic quantum dots [103, 104]. The scheme remains attractive as a first approximation to inelastic (or elastic) processes. Alternatively, it is a good model for a real infinite-impedance voltage probe, a common component of many mesoscopic devices. The generalization we present here is specifically targeted towards the computation of the FCS of mesoscopic systems with inelastic scattering and incoming scattering states with arbitrary entanglement properties. The problem of how to apply such decoherence model to the particularly interesting case of non-locally entangled input currents has not been previously discussed to the best of our knowledge, except in Ref. [93] (presented here in Ch. 4,

[1] Note that this argument also applies to elastic scattering as long as no energy filters are present before the scatterer. Otherwise, mere elastic delay effects will be irrelevant [79], and only inelastic scattering will break Pauli blocking.

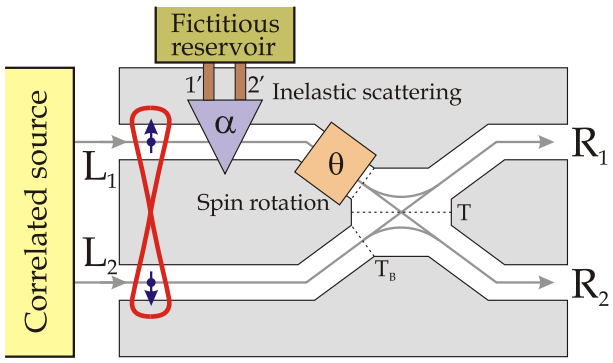

Figure 5.1: The beam splitter geometry fed with pairwise non-locally entangled electron currents or polarized currents. The action of the spin rotation via Rashba spin-orbit coupling in one of the input leads changes noise in the output leads dramatically. Inelastic transport is modeled between the entangler and the spin rotation region by means of one or more fictitious probes. Shot noise measured in terminal R_1 as a function of θ can be used to detect the nature of the incoming electron correlations.

where current conservation was not taken fully into account.

This chapter is organized as follows. In Sec. 5.2 we discuss the beam-splitter device as an entanglement detector in the presence of inelastic scattering. In Sec. 5.3 we give a short account of the technique we will employ to compute the FCS. Further details on our implementation of the fictitious probe scheme can be found in Appendix D. The analysis of the obtained results for the operation of the device are explained in Sec. 5.4. Finally, a summarized conclusion is given in Sec. 5.6.

5.2 Beam-splitter device with inelastic scattering

The system we will study is depicted in Fig. 5.1. It is an electronic beam splitter patterned on a two-dimensional electron gas (2DEG) with two (equal length) incoming and two outgoing arms, such that the transmission probability between the upper and the lower arms is T. The beam splitter is assumed to have also a finite backscattering amplitude whereby electrons get reflected back into the left leads with probability $1-T_B$. We have considered two possibilities for backscattering: the technically simpler case without cross reflection, for which electrons scatter back always into their original incoming leads, and which we will term *simple* backscattering; and the fully symmetric case, whereby the probability of going from any upper lead to any lower lead remains T, be it on the left or the right, which we will call *symmetric* backscattering. This distinction is only relevant when there is a finite inelastic scattering on the leads, and both give very similar results in any case, so we will

focus mainly in the simple backscattering case [2]. Other authors [221] have previously studied the effect of backscattering in this geometry, although considering that only the electrons in the lead with the backgates can backscatter, whereas in our case the two incoming leads are equivalent (the scattering occurs in the beamsplitter). The effect, as we shall see, is however qualitatively equivalent to their result, which is that backscattering effectively reduces the oscillation amplitude of noise with the spin rotation angle.

We connect the right arms to ground and the two incoming arms to a reservoir that emits non-local spin-correlated electron pairs, biased at a voltage $-V$. For definiteness we choose these pairs so that the $\hat{z}$ spin component of the electron coming at a given time through lead L_1 is always opposite to that of the corresponding electron coming simultaneously through lead L_2. They could be or not be entangled, depending on the characteristics of the source and the leads from source to splitter. Time coincidence of pairs is assumed to within a timescale τ_Δ that is shorter than any other timescale in the system, such as $\Delta t \equiv h/eV$. This implies two constraints. On the one hand, if the source is an entangler such as e.g. that of Ref. [38], this would mean that the superconductor emitting the correlated pairs has a large gap Δ as compared to the bias voltage. On the other hand, the length of the leads connecting the entangler to the beam-splitter device should be of equal length to within $v_F \Delta t$ accuracy.

A local spin-rotation in lead L_1 is implemented by the addition of backgates above and below a section of lead L_1. Applying a voltage across these backgates the structure inversion asymmetry of the 2DEG is enhanced, inducing a strong Rashba spin-orbit coupling in that region of the 2DEG in a tunable fashion without changing the electron concentration [222]. This in turn gives rise to a precession of the spin around an in-plane axis perpendicular to the electron momentum, which we chose as the $\hat{y}$ axis, resulting in a tunable spin rotation of an angle θ around $\hat{y}$ after crossing the region with backgates.

The idea behind this setup is that the spin rotation can change the symmetry of the spatial part of the electron pair wavefunction, thus affecting the expected shot noise in the outgoing leads, which is enhanced for even and suppressed for odd spatial wavefunctions. The switching from bunching to antibunching signatures in the shot noise as a function of θ is enough to identify truly entangled singlets in the incoming current. Likewise, a θ independent shot noise is an unambiguous signal of a triplet incoming current, since a local rotation of a triplet yields a superposition of triplets, preserving odd spatial symmetry and therefore, antibunching. A current of statistically mixed anticorrelated electron spins can also be distinguished from the entangled cases from the amplitude of the shot noise oscillations with θ. Thus, this

[2] Admittedly, in a realistic system there could be a finite probability that a backscattered particle be scattered back onto the system, which would probably give further corrections. We neglect these contributions for simplicity, although they could easily be included (in the limit of small induced delay) into the total scattering matrix by assuming a contact between the entangler and the system of finite transparency.

device was proposed as a realizable entanglement detector through local shot noise measurements [106, 107, 221].

As discussed in the introduction of this chapter, inelastic scattering due to environmental fluctuations could spoil the physical mechanism underlying this detector, which is Pauli exclusion principle, and should therefore be expected to affect its performance in some way. The implementation of inelastic scattering in ballistic electron systems can be tackled quite simply on a phenomenological level through the addition of fictitious reservoirs within the scattering matrix formalism [95]. The necessary generalization to deal with entangled currents and a simple scheme to derive the FCS in generic systems with additional fictitious probes is presented in Appendix D. We model spin-conserving inelastic scattering by the addition of two fictitious probes (one for spin-up and another for spin-down) in lead L_1, depicted as a single one in Fig. 5.1. We have numerically checked that the addition of another two fictitious probes in lead L_2 gives very similar results for the shot noise through the system, so we will take only two in the upper arm for simplicity. This is also physically reasonable if we consider only decoherence due to the backgates deposited on the upper arm to perform the local Rashba spin-rotation, which provide a large bath of external fluctuations that can provide much more effective inelastic scattering. The parameter that controls the inelastic scattering probability is $\alpha \in [0, 1]$, being $\alpha = 1$ the completely incoherent limit.

In the following analysis we will inject into the input arms of the device currents with different types of initial non-local electron-pair density matrix,

$$\begin{aligned}\hat{\rho} = &\frac{1}{2}\left(|L_1\uparrow; L_2\downarrow\rangle\langle L_1\uparrow; L_2\downarrow| + |L_1\downarrow; L_2\uparrow\rangle\langle L_1\downarrow; L_2\uparrow|\right) \\ &+\frac{\beta}{2}\left(|L_1\downarrow; L_2\uparrow\rangle\langle L_1\uparrow; L_2\downarrow| + |L_1\uparrow; L_2\downarrow\rangle\langle L_1\downarrow; L_2\uparrow|\right), \end{aligned} \tag{5.1}$$

namely, i) statistical mixtures of up and down classically correlated electrons (diagonal density matrix, $\beta = 0$), which we will also call spin-polarized currents, ii) EPR-type singlet spin-entangled pure states ($\beta = -1$), and iii) idem with $m_s = 0$ triplet states ($\beta = 1$). We will use subindexes s, t, and m to denote the pure singlet, pure $m_s = 0$ triplet and statistically mixed incoming states. Note that this expression refers to pairs of electrons that arrive at the same time at the device, so that this density matrix is actually expressed in a localized wavepacket basis.

Our goal is to ascertain to what extent, for a splitter transmission T, a finite backscattering $1 - T_B$ and finite and unknown amount of inelastic scattering α in the input leads, the shot noise in one of the output arms (R_1) as a function of rotation angle θ could still be used to demonstrate the existence or not of initial entanglement, and that way provide a means to distinguish truly quantum-correlated states from statistically correlated ones (unentangled).

5.3 The technique

In Appendix D we give a detailed account of the method we have used, which can be employed to compute the FCS of a generic mesoscopic conductor with instantaneous current conservation (on the scale of the measuring time) in the attached voltage probes, and quantum entanglement in the incoming currents. A sequential scattering approximation is implicit, which however yields the correct $\omega = 0$ current fluctuations in known cases with inelastic scattering, see e.g. Appendix D.2. We summarize here the main points as a general recipe for practical calculations.

Given a certain mesoscopic system with a number of biased external leads connected to reservoirs, one should add the desired voltage probes to model inelastic scattering (or real probes), and perform the following steps to compute the long-time FCS of the system:

(i) Define the (possibly entangled) incoming states in the external leads for a single scattering event without the probes,

$$|in\rangle = R[\{\hat{a}^+\}]|vac\rangle. \tag{5.2}$$

Here $R[\{\hat{a}^+\}]$ is an arbitrary combination of creation operators a_n^+ of incoming electrons (in the localized wavepacket basis) acting on the system's vacuum. In our case it would create state (5.1).

(ii) Add the N two-legged voltage probes (one channel per leg) with individual scattering matrices as in Eq. (D.1), and compute the total S-matrix of the multiterminal system, S_{nm}. Note that $S_{nm}(t,t')$ in our temporal basis is assumed to be constant, i.e., independent of t, t', which corresponds to an energy independent scattering matrix in an energy basis.

(iii) Define outgoing electron operators $\hat{b}_n^+ = \sum_m S_{nm}\hat{a}_m^+$. To implement instantaneous current conservation we expand our Hilbert space with N integer slave degrees of freedom $\vec{Q} = \{Q_i\}$, which result in the following outgoing state after one scattering event,

$$|out;\vec{Q}\rangle \equiv R[\{\hat{b}^+\}]\prod_i^N \left[\hat{b}^+_{p_i;1'}\hat{b}^+_{p_i;2'}\right]^{g(Q_i)/2}|vac\rangle. \tag{5.3}$$

These Q_i are counters of total charge accumulated in the probes. The notation here is that $\hat{b}^+_{p_i;l}$ creates the scattered state resulting from an electron injected through leg $l = \{1', 2'\}$ of the two-legged probe i. $g(Q)$ encodes the response of the probe to a certain accumulated charge Q. The specific form of $g(Q)$ is not essential as long as it tends to compensate for any charge imbalance in the probe. One convenient choice is given in Eq. (D.15), which yields in our setup a minimal tripled-valued fluctuation interval of $Q_i \in [-1, 1]$. Note also that state $|out;\vec{Q}\rangle$ in the above equation is nothing but $U_{\Delta t}|\phi_j^e\vec{Q}\rangle$ of Appendix D.

(iv) Compute the $3^N \times 3^N$ $\overline{W}$ matrix

$$\overline{W}_{\vec{Q}_b\vec{Q}_a}(\vec{\lambda}) = \langle out;\vec{Q}_a|\hat{P}_{\vec{Q}_b}\hat{\chi}_j(\vec{\lambda})|out;\vec{Q}_a\rangle, \tag{5.4}$$

which we write in terms of the moment generating operator $\hat{\chi}_j = e^{i\sum_n \lambda_n(\hat{N}_n^{\rm out}-\hat{N}_n^{\rm in})}$, where $\hat{N}$ are the number operators of electrons in event j. The operator $\hat{P}_{\vec{Q}_b}$ projects onto the subspace of electron states that have a total of $Q_{bi}-g(Q_{ai})$ particles scattered into probe i, i.e., states in which the probe i has gone from Q_{ai} to Q_{bi} excess electrons. If the incoming state is not a pure state, one should perform the statistical averaging over the relevant $|out;\vec{Q}\rangle$ states at this point.

(v) Compute the resulting long-time *current* moment generating function $\chi_I(\vec{\lambda})$ by taking the maximum eigenvalue of matrix $\overline{W}$. The charge generating function $\chi(\vec{\lambda})$ is obtained simply by taking the power M of $\chi_I(\vec{\lambda})$, cf. Eq. (D.17), where $M = eVt/h$ is the average number of emitted pairs from the source after an experiment time t at a bias V.

We make use of this method in our particular system by setting a single counting field λ on output lead $R1$, where we wish to compute current fluctuations. This way we derive results for χ_I and current cumulants [see Eqs. (D.18) and (D.19)] from the corresponding $\overline{W}$ matrix (5.4) for the different types of injected currents of Eq. (5.1).

While explicit expressions for the current cumulant generating function $\log\chi_I(\lambda)$ are in general impossible due to the large dimensions of the $\overline{W}$ matrix (9×9 in this case), it is always possible to write χ_I in an implicit form that is just as useful to sequentially compute all cumulants, namely, the eigenvalue equation

$$\det\left[\overline{W}(\lambda) - \chi_I(\lambda)\mathbf{1}\right] = 0, \tag{5.5}$$

supplemented by the condition $\chi_I(0) = 1$. By differentiating this equation around $\lambda = 0$ a number of times and using (D.18), one can obtain the various zero-frequency current cumulants on arm $R1$.

In the next section, instead of giving the general expression of $\overline{W}$, which is rather large, we provide the explicit expressions for χ_I and shot noise obtained in various useful limiting cases, together with plots of the first cumulants in the $\{T, T_B, \alpha, \theta\}$ parameter space.

5.4 Results

In this section we will analyze the performance of the beam splitter device of Fig. 5.1 as a detector of quantum correlations in the incoming currents through the shot noise or higher current cumulants induced in arm R_1. We will first make connection with the results in the literature [106] by computing the shot noise in an elastic splitter, and then we will generalize them to finite inelastic scattering probabilities and finite backscattering. We will thus establish tolerance bounds for such imperfections in the detector. Finally, we will address the question of whether the measurement of higher order current cumulants could improve the tolerance bounds of the device.

5.4.1 Shot noise

In the elastic transport limit $\alpha = 0$ and with arbitrary intralead backscattering strength $1 - T_B$, the following expression for the shot noise is obtained,

$$S = \frac{e^3|V|}{h} T_B \left[1 - T_B + (1-\beta) T_B T (1-T)(1+\cos\theta)\right], \tag{5.6}$$

where constant β corresponds to the different types of incoming current, cf. Eq. (5.1). Note that this expression holds for simple or symmetric backscattering (as defined in Sec. 5.2). As shown by Eq. (5.6), for $\alpha = 0$ the amplitude of the θ dependence is enough to distinguish between the different types of states, if T and T_B are known. As could have been expected, the triplet current noise ($\beta = 1$) is θ independent, since the local spin rotation only transforms the $m_s = 0$ triplet to a different superposition of the other triplet states, none of which can contribute to noise since each electron can only scatter into different outgoing leads due to the Pauli exclusion principle.

However, in the presence of a strong coupling to the environment, $\alpha = 1$, the shot noise behaves very differently. Due to the complete incoherence of scattering, which changes the orbital quantum numbers of the incoming states, the bunching-antibunching switching disappears. Therefore S_s, S_t and S_m become equal and θ independent. In particular, for simple backscattering we have

$$\begin{aligned} S_s = \quad S_t \quad = S_m = \frac{e^3|V|}{h} \frac{T_B}{(1+T_B)^3} \big[1 + 2T_B^2 T(1-T) \\ -T_B(1+3T^2-6T) - T_B^3 T^2 (2+T_B)\big]. \end{aligned} \tag{5.7}$$

These features are illustrated for $T_B = 1$ and $T = 1/2$ in Fig. 5.2, where we have plotted the current shot-noise in lead R_1, normalized to the constant e^3V/h [3], as a function of the spin rotation angle θ and the decoherence parameter α. Note that for $\alpha = 1$ (and without backscattering), Eq. (5.7) reduces to $S_s = S_t = S_m = (e^3V/h)T(1-T)$, which is 1/4 in normalized units. The cosine-type dependence of the current noise with θ, $S(\theta) = S(\pi) + \Delta S \cos^2(\theta/2)$, where $\Delta S = S(\theta = 0) - S(\theta = \pi)$, holds for any value of $\alpha < 1$ in the singlet and polarized cases. The oscillation amplitude of the noise for the singlet case is always twice the oscillation amplitude of the polarized one. In contrast, the triplet shot noise (and all higher cumulants for that matter) remains always θ independent for any α and T_B.

Since our aim in this study is to find a way to distinguish between the different incoming states of Eq. (5.1), we will disregard from now on the trivial case of the triplet current, which is easily detectable by its θ-independence, and focus entirely on the distinction between the singlet and mixed state cases. In these two cases, when $T_B < 1$, the oscillatory behaviour with θ remains, although it is no longer

[3] The shot noise normalized to e^3V/h is in fact the Fano factor since the total current is $I_{R_1} = e^2|V|T_B/h$.

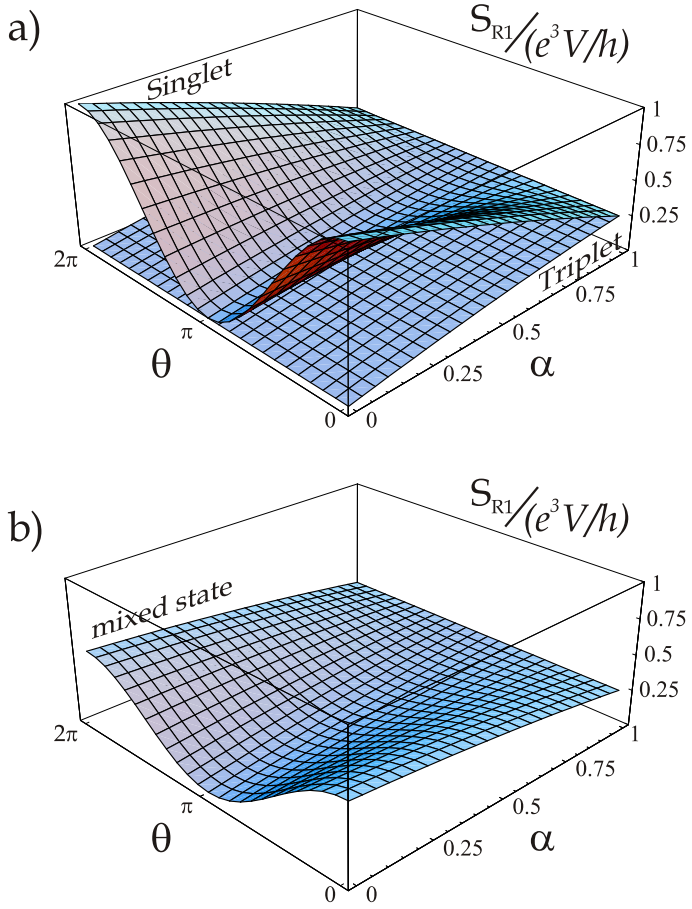

Figure 5.2: In the upper plot (a) we represent the current shot-noise in units of e^3V/h in lead $R1$ for the singlet and $m_s = 0$ triplet incoming states, as a function of spin rotation angle θ and decoherence strength α. The same for the polarized spin state case is presented in the lower plot (b). Inter-lead transmission probability between upper and lower arms T is fixed to 0.5, and no backscattering ($T_B = 1$) is assumed.

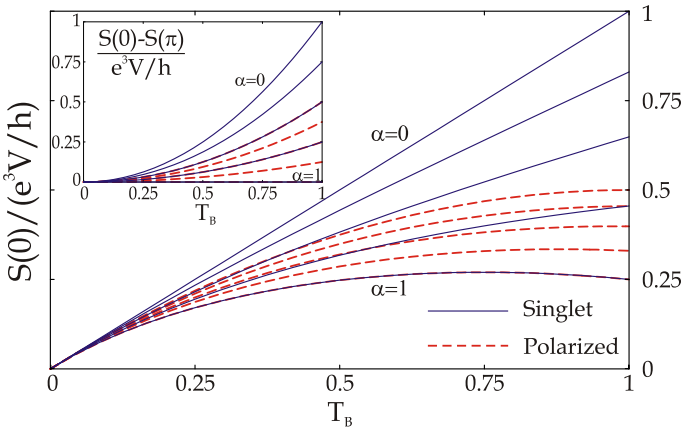

Figure 5.3: Normalized value of shot-noise in lead R_1 at zero spin rotation angle as a function of beam splitter transmission T_B for $T = 0.5$. Solid (blue) lines correspond to singlet incoming current whereas dashed (red) lines account for the polarized one. In both cases, different values of inelastic scattering probability have been considered, from $\alpha = 0$ (upper curves) to $\alpha = 1$ (lower curves) in steps of 0.25. Inset: the same for the oscillation amplitude with θ of the shot-noise.

purely sinusoidal. Besides, its oscillation amplitude quickly decreases with increasing backscattering, making the entanglement detection scheme harder. However, we will now show that, knowing only the value of the shot-noise at zero spin rotation angle (or alternatively the amplitude ΔS), it is possible to distinguish between the different incoming states for not-too-strong decoherence.

5.4.2 Robust entanglement detection scheme

Tuning once again the beam splitter to the symmetric $T = 1/2$ point, which turns out to be the optimum point of operation for entanglement detection, we notice from Fig. 5.2 that the analysis of the θ dependence of the shot-noise at an arbitrary and unknown value of α indeed precludes from a clear distinction of the singlet and mixed state cases.

A more complete picture can be obtained by plotting the value of the shot-noise at $\theta = 0$ in the interval $\alpha \in [0, 1]$ as a function of T_B. This is done in Fig. 5.3 for the case of simple backscattering. Solid (blue) lines correspond to singlet incoming current, and dashed (red) lines to the polarized one. Moreover, the upper curve in both sets of curves accounts for the case of $\alpha = 0$, and for the next ones the value of the inelastic scattering parameter increases, in steps of 0.25, until $\alpha = 1$ for the lower curves (which coincide for both the entangled and polarized cases). The same analysis can be done for the behaviour of the amplitude ΔS as a function of T_B, as shown in the inset of Fig. 5.3 (given also for simple backscattering). In this latter case, the

amplitudes for both the singlet and the polarized currents have in fact a very simple analytical form, the singlet case ranging from T_B^2 to 0 and the polarized one from $T_B^2/2$ to 0 as we sweep from $\alpha = 0$ to $\alpha = 1$. Therefore, we see how the θ-independent background noise introduced by the finite backscattering in the main plot of Fig. 5.3, which could in principle degrade the performance of the entanglement detector as mentioned in Ref. [107], can be filtered out by measuring the amplitude ΔS. We also note that if a symmetric backscattering is considered, the resulting curves for Fig. 5.3 are qualitatively the same, and therefore it does not affect the above discussion.

We can observe in both plots of Fig. 5.3 that if α is unknown, as it is usually the case in an experiment, the classical and quantum currents are distinguishable from a single noise measurement (or two in the case of the inset) only if its value is found to lie outside of the overlapping region between the two sets of curves. According to this model, this should always happen for values of inelastic scattering smaller than at least one half. In the case of the main figure, even higher values of α can be distinguished for values of T_B close to one. In any case, the values of α for which the noise measurement is no longer able to distinguish a singlet entanglement from a statistically mixed case are rather high, $\alpha \in [0.5, 1]$. This means that, in a realistic situation where decoherence is not too high, shot-noise measurements remain enough for determining if the source feeding the beam-splitter is emitting entangled or statistically mixed states.

5.4.3 Higher order cumulants

We could ask whether it is possible to distinguish between incoming singlet-entangled and polarized currents for a wider range of parameters α by analyzing higher order cumulants. The short answer is 'no'.

As we did for the noise in Fig. 5.2, we can plot the angular dependence of the third moment, the skewness, for different values of inelastic scattering parameter α. This is shown in a 2D plot in the inset of Fig. 5.4(b) for $T = 0.5$ and $T_B = 1$. As before, solid (blue) lines and dashed (red) lines correspond to spin singlet-entangled and polarized incoming currents, respectively. Now we find that the behaviour of skewness with θ is not monotonous as α varies. For $\alpha = 0$ and for $\alpha = 1$ at $T_B = 1$ the third cumulant is zero for every angle both for entangled and for mixed states (the probability distribution of the current is symmetric for those parameters as was previously noted in the $\alpha = 0$ case in Ref. [108]). Moreover, this means that the skewness is not a good entanglement detector for a near perfect beam splitter, nor when the inelastic scattering in strong. For intermediate values of decoherence, still at $T_B = 1$, the skewness oscillates with the spin rotation angle and its oscillation amplitude, $\langle\langle I^3\rangle\rangle(\theta = 0) - \langle\langle I^3\rangle\rangle(\theta = \pi)$, has a maximum around $\alpha \approx 0.5$. This oscillation range is depicted in the main plots of Fig. 5.4 as a function of the transmission between left and right arms T_B (where simple backscattering has been considered). Several values of the inelastic parameter are differentiated using different shades of

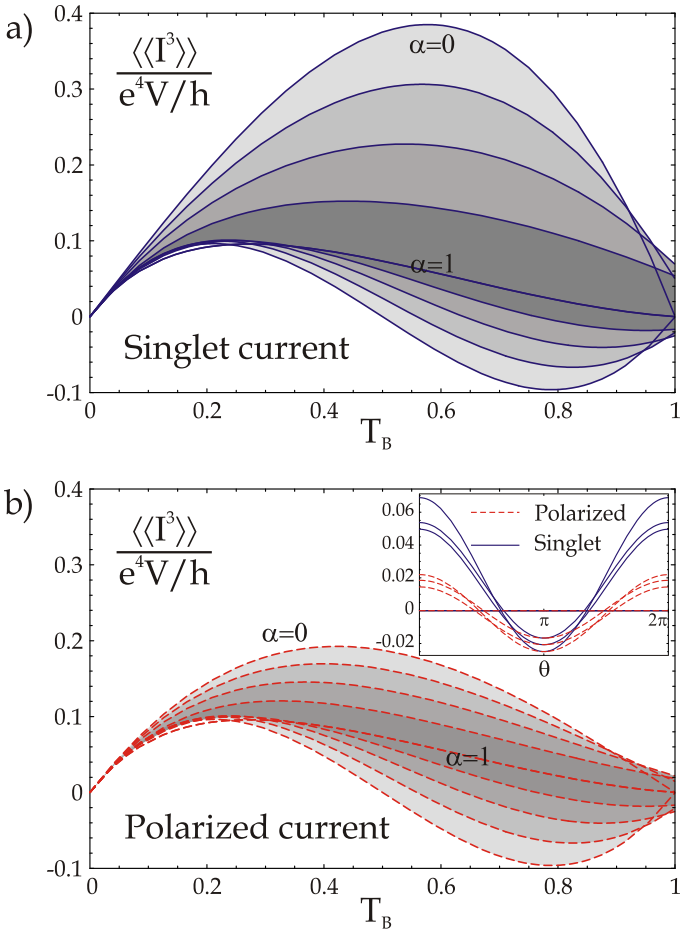

Figure 5.4: Oscillation range with angle θ of the skewness in lead R_1, in units of e^4V/h, as a function of beam-splitter transmission between left and right arms T_B. T is fixed to the optimal point $T = 0.5$. Different oscillation ranges for different values of inelastic scattering are indicated by different shades of grey, ranging from pale gray for $\alpha = 0$ to dark gray for $\alpha = 1$ in steps of 0.25. The case of singlet-entangled incoming current is considered in plot (a), whereas in plot (b) the incoming current is in a polarized state. The actual oscillation of skewness with Rashba spin rotation angle for entangled current (solid blue lines) and polarized current (dash red lines) is plotted in the inset of figure (b) (see main text).

grey, ranging from pale gray for $\alpha = 0$ to dark gray for $\alpha = 1$ in steps of 0.25. The main features can be summarized as follows. First, both for the entangled and the polarized current, the broadest oscillation range occurs for $\alpha = 0$ (being bigger for the singlet-entangled case). Second, for $\alpha = 1$ the oscillation amplitude in both cases is zero, although the skewness remains finite and positive (shifting from a Gaussian to a Poissonian distribution of current as T_B goes from 1 to 0). For T_B smaller than 0.9 approximately, the behaviour of the oscillation range is monotonous with α, it simply decreases with it. For small values of T_B, the skewness coincides with the shot-noise, which is expected since the probability distribution for a tunnel barrier recovers a Poisson distribution, even in the presence of inelastic scattering. In general, the sign of the skewness is reversed in a wide range of parameters by tuning the spin rotation θ.

Concerning our entanglement detection motivation, comparing Fig. 5.4(a) and 5.4(b) we find that the third cumulant doesn't provide any further information in our search of a way to distinguish between entangled and non-entangled incoming states. For T_B of the order of 0.9 and above, due to the non-monotonous behaviour of the oscillation range with α, the skewness of our beam splitter setup can hardly be used as a detector of entanglement at all. For smaller values of T_B, we are able to discriminate between different currents in the same range of inelastic scattering parameter α as we could with the noise, this is, from zero decoherence to roughly $\alpha = 0.5$.

We have also analyzed further cumulants, whose behaviours with T_B and θ get more intricate as the order of the cumulant increases, and have found the same qualitative result. Either they are not useful tools for entanglement detection or the range of parameters α and T_B is not improved from what we find with the shot-noise measurements.

5.5 Related experiments

Traditionally, transport experiments on small electronic devices have dealt with time averaged quantities like conductance. In the recent years and seeking for supplementary information about electronic transport, a number of experiments have considerer temporal fluctuations of the current [95]. Non-equilibrium noise has been widely explored to determine, for example, the effective charge of carriers [223–226] or to study the transmission properties of quantum coherent devices such as quantum point contacts [227, 228], diffusive wires [229], or chaotic cavities [230]. The third moment of the voltage fluctuations in a conductor has also been measured experimentally, for the first time, by B. Reulet, J. Senzier and D. E. Prober in the work called "Environmental effects in the third moment of voltage fluctuations in a tunnel junction" [231], in 2003. In particular, they measured the skewness on nonsuperconducting tunnel junctions, and they found that the measurements were significantly

affected by the electromagnetic environment of the sample.

Also current-current correlations between different leads in multiterminal devices have been measured. Negative correlations due to the Pauli exclusion principle have been observed in distinct experiments, like fermionic Hanbury Brown and Twiss experiments [232–234].

In this section we describe briefly the experiment "Positive cross correlations in a normal-conducting fermionic beam splitter", by S. Oberholzer et al in 2006 [101]. In this work the authors investigate a three terminal beam-splitter structure implemented in a normal-conducting fermionic electron gas in the quantum Hall regime. They measure the cross correlations between the current fluctuations in the two exit leads and find that they can be negative, zero, or even positive, depending on the scattering mechanism within the device. In particular, positive sign occurs due to interaction between different edge states by means of an extra voltage probe attached at the middle of the device. The positive sign does not reflect the statistics of the fermionic particles which usually antibunch. Due to this result, the authors warn that the observation of positive correlations in fermionic systems can be interpreted as a sign of entanglement only if effects such as the one they present can be ruled out. We have focussed our attention in this experiment for various reasons. On the one hand, they are implementing a fermionic beam-splitter. Besides, they are introducing in their device a real voltage probe to produce inelastic scattering. Those things make connection to our work in this chapter (although the experimental setup and the motivation are different). On the other hand, although positive cross correlations have been predicted by various theoretical works (using e.g. entanglers), they had not been seen before in mesoscopic devices, which makes this work an important contribution.

5.6 Conclusions

In this work we have analyzed the effect of inelastic scattering, modeled by spin-current conserving voltage probes, on entanglement detection through a beam-splitter geometry. We have shown that, unlike elastic orbital dephasing [73], the action of inelastic processes in the beam-splitter cannot be neglected, since it directly affects the underlying physical mechanism of the detector, which is the fact that two electrons with equal quantum numbers cannot be scattered into the same quantum channel. If energy is not conserved, such antibunching mechanism is no longer perfect, and the entanglement detection scheme has to be revised.

However, we have found that detection of entanglement through shot noise measurements remains possible even under very relaxed conditions for imperfections in the beam-splitter device and substantial inelastic scattering. Even if a reliable microscopic description of inelastic processes is not available, the present analysis suggests that the detection scheme is robust for inelastic scattering probabilities up to 50%.

We have also shown that higher current cumulants do not contain more infor-

mation about the entanglement of the incoming currents than the shot noise. We have analyzed in particular the skewness of current fluctuations, finding that finite backscattering and inelastic scattering strongly affect the asymmetry of current fluctuations. In particular, a positive skewness is developed as the beam splitter transparency is lowered.

Finally, we have developed a novel way to implement current conservation in voltage probe setups when the incoming currents are non-locally entangled, which can be applied to a wide variety of problems where entanglement is key.

Appendix A

Tunneling Hamiltonian in real space: discrete vs. continuum limit

In Chapter 2 we derived a local tunneling Hamiltonian (2.24) starting from the Bardeen model for electron tunneling [143]. This formalism, which is based on the tunneling approximation, has been sometimes criticized or called into question. That is why, in this Appendix, we want to derive (and therefore, justify) the same kind of Hamiltonian starting from a different point of view. We will consider a tight-binding discrete formalism, where the shape and validity of the hopping Hamiltonian is out of question, and we will find the very dependence with momentum and space of Hamiltonians of Eqs. (2.4), (2.12) and (2.24), taking the continuous space limit. This means that, if in the discrete limit the hopping Hamiltonian depends on the creation and destruction second-quantization operators at the last sites connecting two chains, in the continuum limit this behaviour will translate into normal derivatives of the field operators at the boundaries where the barrier is located.

Take a discrete chain made of N sites with period a described by the Hamiltonian

$$H_0 = -t \sum_{i=1}^{N-1} c_{i+1}^\dagger c_i + \text{H.c.}, \tag{A.1}$$

where $t = \hbar^2/2ma^2 > 0$ is the hopping parameter that yields an effective mass m in the continuum limit.

The eigenstates of this chain are of the form

$$|\phi_n\rangle = \left(\frac{2}{N+1}\right)^{1/2} \sum_{i=1}^{N} \sin(k_n z_i) c_i^\dagger |\text{vac}\rangle, \tag{A.2}$$

where $z_i = ia$ and $k_n = \pi n/a(N+1)$ with $i, n \in [1, N]$. The eigenvalues are

$$E_n = -2t\cos(k_n a). \tag{A.3}$$

The basis set $\{|\phi_n\rangle\}$ is orthonormal. Thus we may write

$$c^\dagger_{k_n} = \left(\frac{2}{N+1}\right)^{1/2} \sum_{i=1}^{N} \sin(k_n z_i) c^\dagger_i \,, \tag{A.4}$$

$$c^\dagger_i = \left(\frac{2}{N+1}\right)^{1/2} \sum_{n=1}^{N} \sin(k_n z_i) c^\dagger_{k_n}. \tag{A.5}$$

We write the transfer Hamiltonian between two N-site chains as

$$H_T = -t' a_1^\dagger b_{-1} + \text{H.c} \tag{A.6}$$

$$= \frac{2t'}{N+1} \sum_{n=1}^{N} \sum_{m=1}^{N} \sin(k_n a) \sin(k_m a) a^\dagger_{k_n} b_{k_m} + \text{H.c.} \tag{A.7}$$

which may be treated as a small perturbation when $t' \ll t$.

To investigate the continuum limit, we take $a \to 0$ and $t \to \infty$ so that m and k_F remain finite. We also take $N \gg 1$. Noting that the sine functions in (A.7) can be approximated by their arguments $k_n a \lesssim k_F a \ll 1$ and that $k_{\max} = \pi/a \to \infty$, we get

$$H_T = \frac{2t' a^3}{L} \sum_{k,q>0} k\, q\, a^\dagger_k b_q + \text{H.c.} \tag{A.8}$$

This Hamiltonian is bilinear in the momenta of the electron on the right and left chain. If we were in 3D we would specify that the bilinearity refers to the momenta perpendicular to the interface plane. This Hamiltonian is analogous to that which we proposed for the continuum Bardeen theory in the case of a high barrier [see Eqs. (2.4) and (2.12)].

We may work out the corresponding Hamiltonian in real space. For that we note that, in the continuum limit, H_T in Eq. (A.6) can be expressed in terms of field operators evaluated in $z = \pm a$ (through the relationship $c_i = \sqrt{a}\,\psi(z)$ and equivalently for the creation operator). When $a \to 0$, the field operators can be expanded as

$$\psi(a) = \psi(0) + a \left.\frac{d\psi(z)}{dz}\right|_{z=0} + \mathcal{O}(a^2) \,, \tag{A.9}$$

where $\psi(0) = 0$ is a condition that results naturally from the properties of the wave functions in a chain starting in $i = 1$ or $i = -1$. For such chains, $i = 0$ is an imaginary point where the wave function necessarily vanishes; it is the place where we would locate the hard wall in a continuum description [235]. Then the tunneling Hamiltonian can be written

$$H_T = t' a^3 \left.\frac{d\psi^\dagger_R(z)}{dz}\right|_{z=0} \left.\frac{d\psi_L(z')}{dz'}\right|_{z'=0} + \text{H.c.} \tag{A.10}$$

This Hamiltonian is exactly the one-dimensional version of that in Eq. (2.24). The fact that we have derived it from a completely different set of physical arguments should be viewed as a definite proof of the adequacy of the tunneling Hamiltonians proposed in section 2.7. The Hamiltonians (A.8) and (A.10) have been obtained in the continuum limit. On the other hand, Eqs. (2.12) and (2.24) were derived for high barriers or, equivalently, low energies. Clearly, this is not a coincidence, since it is at low energies where the long wavelengths make the electron move in the chain as in continuum space.

Appendix B

Total tunneling Andreev current vs. interface radius

In this appendix we show the complete (and lengthy) expressions of the Andreev current between NS hybrid structures through a tunneling circular interface as a function of its radius, and we explain some convenient approximations in order to deal with them. This current was analyzed from a physical point of view in Sec. 2.7 of Chapter 2.

To calculate the total current as a function of the interface radius R we have to evaluate the matrix element (2.32) using hopping energies obtained from the tunneling Hamiltonian (2.25). In the resulting expression we need to integrate over the final momenta of the two electrons in the normal metal, the momentum of the intermediate virtual state consisting of a quasiparticle in the superconductor, as well as the coordinates of the points where each electron crosses the interface area. The integrations over the momenta in the final state lead to four angular integrals ($\theta_{1,2} \in [0, \pi/2]; \varphi_{1,2} \in [0, 2\pi]$), the moduli being fixed by the condition $k_B T, eV \to 0$. The integration over the superconductor excited states leads to three integrals: $\theta_s \in [0, \pi], \varphi_s \in [0, 2\pi], q \in [0, q_c]$. On the other hand, integration over the hopping points of each electron leads to two interface integrals ($r_{1,2} \in [0, R]$, $\theta_{r1,r2} \in [0, 2\pi]$), which makes four more integrals, totalling eleven real variables to be integrated. Using the symmetry property that the integrand is independent of one azimuthal angle, and solving analytically the four real space integrals, we are left with six non-reducible nested integrals of strongly oscillating functions.

We define $\vec{\kappa} \equiv \mathbf{k}/k_F$, $\vec{\varrho} \equiv \mathbf{q}/k_F$. Since the modula of the final momenta are fixed by conservation requirements, we may write $\kappa_{\|i} = \sin\theta_i$, $\kappa_{zi} = \cos\theta_i$ $(i = 1, 2)$. For the virtual states in the superconductor: $\varrho_\| = \varrho \sin\theta_s$, $\varrho_z = \varrho \cos\theta_s$.

The general, exact formula for the total current as a function of R is

$$I(R) = I_V \tau^4 \frac{(k_F R)^2}{4\pi^3} \int d\Omega_1 \int d\kappa_{2z} \kappa_{1z}^2 \kappa_{2z}^2 e^{2p_0 w[1-b(\kappa_{1z},\kappa_{2z})]} \times \left[\frac{2}{\pi} \int d\varrho \frac{\delta}{(\varrho^2-1)^2+\delta^2} \varrho^4 \int d\Omega_s e^{p_0 w[1-b(\varrho_z)]} \prod_{j=1,2} a(\kappa_{zj}, \varrho_z) J(|\vec{\varrho}_\parallel - \vec{\kappa}_{1\parallel}|, |\vec{\varrho}_\parallel + \vec{\kappa}_{2\parallel}|) \right]^2, \tag{B.1}$$

where J is a short-hand notation for

$$J(x,y) \equiv \frac{J_1(k_F R\, x) J_1(k_F R\, y)}{x\, y}. \tag{B.2}$$

The first-order Bessel functions result from the exact integration over the tunneling points $\mathbf{r}_1$ and $\mathbf{r}_2$.

For $\delta \to 0$, the Lorentzian becomes a delta function and the integral over ϱ is evaluated exactly. We get (with u still arbitrary)

$$\begin{aligned} I(R) &= I_V \tau^4 \frac{(k_F R)^2}{4\pi^3} \int d\Omega_1 \int d\kappa_{2z} \kappa_{1z}^2 \kappa_{2z}^2 e^{2p_0 w[1-a(\kappa_{1z},\kappa_{2z})]} \\ &\times \left[\int d\Omega_s e^{p_0 w[1-b(\varrho_z)]} \prod_{j=1,2} a(\kappa_{zj}, \varrho_z) J(|\vec{\varrho}_\parallel - \vec{\kappa}_{1\parallel}|, |\vec{\varrho}_\parallel + \vec{\kappa}_{2\parallel}|) \right]^2. \end{aligned} \tag{B.3}$$

For δ arbitrary and $u \gg 1$, Eq. (B.1) becomes

$$\begin{aligned} I(R) &= I_V \tau^4 \frac{(k_F R)^2}{4\pi^3} \int d\Omega_1 \int d\kappa_{2z} \kappa_{1z}^2 \kappa_{2z}^2 \\ &\times \left[\frac{2}{\pi} \int d\varrho \frac{\delta}{(\varrho^2-1)^2+\delta^2} \varrho^4 \int d\Omega_s J(|\vec{\varrho}_\parallel - \vec{\kappa}_{1\parallel}|, |\vec{\varrho}_\parallel + \vec{\kappa}_{2\parallel}|) \right]^2. \end{aligned} \tag{B.4}$$

Finally, for both $\delta \to 0$ and $u \gg 1$, we obtain

$$I(R) = I_V \tau^4 \frac{(k_F R)^2}{4\pi^3} \int d\Omega_1 \int d\kappa_{2z} \kappa_{1z}^2 \kappa_{2z}^2 \left[\int d\Omega_s J(|\vec{\varrho}_\parallel - \vec{\kappa}_{1\parallel}|, |\vec{\varrho}_\parallel + \vec{\kappa}_{2\parallel}|) \right]^2, \tag{B.5}$$

which for $k_F R \ll 1$ leads to Eq. (2.52) in the main text. This is easy to see considering that $\lim_{x\to 0} J_1(k_F R\, x)/x = k_F R/2$.

Even after making $\delta, u^{-1} \to 0$, the resulting expression (B.5) is such that a numerical integration for arbitrary R is not yet possible. In order to evaluate (B.3) and (B.5) numerically we need to introduce a set of *two approximations* which are good for $k_F R \gg 1$ and reasonable for intermediate R. To introduce the *first* approximation we go back to the original expression (2.26), where the space coordinates have not yet

been integrated. Then we shift from the two space coordinates $(\mathbf{r}_1, \mathbf{r}_2)$ to centre-of-mass and relative coordinates $(\mathbf{r}_c, \mathbf{r})$. The integration domain of the centre-of-mass coordinate $\mathbf{r}_c$ is still a circle of radius R. However, the integration region of the relative coordinate $\mathbf{r}$ is more complicated: It is eye-shaped and centred around $\mathbf{r}_c$. The first approximation consists in assuming that, for all $\mathbf{r}_c$, the integration domain of the relative coordinate is circular instead of eye-shaped. The area of such a circular region is a free parameter which can be adjusted by, e.g. comparing the approximate result with the exact calculation for those values of R for which the latter can be performed.

It is intuitive (and rigorously proved in Subsec. 2.7.2) that, because of diffraction, when $R \lesssim \lambda_F$, the parallel momentum is not conserved and, in particular, the two electrons do not leave necessarily with opposite parallel momenta [see Fig. (2.5)]. Nevertheless, as R increases the interface begins to be large enough so as to permit parallel momentum to become better conserved. A quasi-delta function $\widetilde{\delta}(\mathbf{k}_{1\parallel} + \mathbf{k}_{2\parallel})$ effectively appears. In particular we have: $\lim_{R\to\infty} J_1(k_\parallel R)/k_\parallel = 2\pi\delta(\mathbf{k}_\parallel)/R$. Thus, our *second* approximation consists in assuming that, for all $R > \lambda_F$, the quasi-delta is an exact delta: $\widetilde{\delta} \to \delta$. This is equivalent to the assumption that there is no diffraction, i.e. that we work in the ray optics limit. This approximation becomes exact as $R \to \infty$ and it is a reasonable one for finite radii. Of course, this approximation fails for $R \lesssim \lambda_F$, yielding a wrong R^4 behaviour (see discussion of Sub-subsections 2.7.1 and 2.7.1).

With the two previous approximations we can reduce the number of numerical integrals from five to three. To write the resulting expressions, let us introduce some compact notation. We define $x \equiv \cos\theta$ (where θ is the angle formed by the outgoing momentum with the direction normal to the interface), $y \equiv \cos\theta_q$ (θ_q having a similar definition within the superconductor), $\lambda \equiv k_F|\mathbf{r}_c|$, and $\mu \equiv k_F|\mathbf{r}|$.

For $\delta \to 0$ and arbitrary u we obtain

$$\begin{aligned} I(R) \;&\simeq I_V \tau^4 \int_0^1 dx\, x^3 e^{2p_0 w[1-b(x)]} \left\{ \int_0^{k_F R} d\lambda\, \frac{2\lambda}{(k_F R)^2} \int_0^1 dy \frac{r(\lambda) y^2}{x^2 - y^2} [a(x,y)]^2 e^{2p_0 w[1-b(y)]} \right. \\ &\times \left[\sqrt{1-y^2}\, J_0\Big(r(\lambda)\sqrt{1-x^2}\Big)\, J_1\Big(r(\lambda)\sqrt{1-y^2}\Big) \right. \\ &\left. \left. -\sqrt{1-x^2}\, J_0\Big(r(\lambda)\sqrt{1-y^2}\Big)\, J_1\Big(r(\lambda)\sqrt{1-x^2}\Big) \right] \right\}^2 , \end{aligned} \tag{B.6}$$

where $r(\lambda)$ is the radius of the approximate circular domain over which the relative coordinate $\mathbf{r}$ is integrated. If the circle is assumed to have the same area as the eye, we obtain

$$r(\lambda) \equiv \sqrt{\frac{8}{\pi}} \left[(k_F R)^2 \arccos\left(\frac{\lambda}{k_F R}\right) - \lambda\sqrt{(k_F R)^2 - \lambda^2} \right]^{1/2} , \tag{B.7}$$

but in practice this criterion is found to overestimate the total current. Thus we

decide to adopt the ansatz

$$r(\lambda) \equiv 2k_F R \left(1 - \frac{\lambda}{k_F R}\right)^{\alpha}, \tag{B.8}$$

where α is a parameter to be adjusted by comparison with the exact solution in those cases where it can be computed. In particular, α has been adjusted from the last two exact numerical values of each curve, i.e. from the two largest computationally possible radii. We note that both (B.7) and (B.8) satisfy the requirement $r(\lambda) \to 2k_F R$ for $\lambda \to 0$. The value $\alpha = 1$ corresponds to the case where the circle is chosen to be the maximum circle which fits within the eye-shaped integration domain. As expected, this criterion underestimates the current. The formula (B.7), which overestimates the result, can be approximated with $\alpha \approx 0.7$. Thus it comes as no surprise that the value of α obtained by comparing with the exact result (when available) is an intermediate number, namely, $\alpha = 0.84$, which has been used for the NS curves in Fig. 2.4.

For arbitrary δ and $u \gg 1$, the total current becomes

$$I(R) \simeq I_V \tau^4 \int_0^1 dx\, x^3 \left[\frac{2}{(k_F R)^2} \int_0^{k_F R} d\lambda\, \lambda \int_0^{r(\lambda)} d\mu\, \mu J_0(\mu\sqrt{1-x^2}) B(\mu)\right]^2 \tag{B.9}$$

$$B(\mu) = \left\{\frac{\sin[S(\delta)\mu)]}{\mu^3} - \frac{\sqrt[4]{1+\delta^2}\cos[\arctan\delta/2 + S(\delta)\mu]}{\mu^2}\right\} e^{-D(\delta)\mu}, \tag{B.10}$$

where

$$S(\delta) = \left(\frac{\sqrt{1+\delta^2}+1}{2}\right)^{1/2} \overset{\delta\ll 1}{\to} 1\,, \tag{B.11}$$

$$D(\delta) = \left(\frac{\sqrt{1+\delta^2}-1}{2}\right)^{1/2} \overset{\delta\ll 1}{\simeq} \frac{\delta}{2}\,. \tag{B.12}$$

Thus, for $\delta \ll 1$ we may write

$$B(\mu) \simeq \left[\frac{\sin(\mu)}{\mu^3} - \frac{\cos(\mu+\delta/2)}{\mu^2}\right] e^{-\delta\mu/2}. \tag{B.13}$$

The effect of the phase-shift $\delta/2$ is only appreciable for $\mu \lesssim \delta$, i.e. for $r \lesssim \delta\lambda_F \ll \lambda_F$, as can be seen by expanding $B(\mu)$ for small μ:

$$B(\mu) = \frac{\delta}{2\mu} + \frac{1}{3} - \frac{\delta\mu}{4} - \frac{\delta^2}{8} + \mathcal{O}(\delta^4, \mu^2). \tag{B.14}$$

The phase-shift generates a divergence for $\mu \to 0$. Although integrable thanks to the multiplying μ factor in Eq. (B.9), this divergence affects the final result. Its range

of relevance may be estimated by making $\delta/2\mu$ equal to the limiting value $1/3$ which one would obtain with $\delta = 0$. This yields a range $r_0 = (3/4\pi)\delta\lambda_F$, which will be washed out by any realistic momentum cutoff $q_c \sim k_F \ll k_F/\delta$.

Finally, we note that comparison of Eqs. (2.58) and (B.13) clearly reveals that the entangled current $I_e(r)$ given in (2.58) is essentially proportional to $B^2(k_F r)$. As discussed in Sec. 2.9, $I_e(r)$ decays faster than the prefactor obtained from momentum-independent hopping matrix elements [see Eq. (2.70)]. The current increase which results from such an unphysical approximation translates into a divergent thermodynamic limit (see again Section 2.9).

Appendix C

Probability distributions for the CH inequality

The aim of Chapter 4 is to evaluate the CH inequality of Eq. (4.20) [or Eq. (4.12)] and to see wether it can be violated. In order to do it we need to calculate single terminal and joint terminal probability distributions, which are expressed in terms of characteristic functions according to Eq. (4.14).

The most general expression for the characteristic function when spin-σ electrons are counted in lead 1 and spin-σ' electrons are counted in lead 2 is

$$\begin{aligned}\chi_E(\lambda_{1\sigma},\lambda_{2\sigma'}) = 1 &+ \left(e^{-i\lambda_{1\sigma}}-1\right)\langle\hat{N}_{\rm O}^{1\sigma}\rangle + \left(e^{-i\lambda_{2\sigma'}}-1\right)\langle\hat{N}_{\rm O}^{2\sigma'}\rangle \\ &+ \left(e^{-i\lambda_{1\sigma}}-1\right)\left(e^{-i\lambda_{2\sigma'}}-1\right)\langle\hat{N}_{\rm O}^{1\sigma}\hat{N}_{\rm O}^{2\sigma'}\rangle \end{aligned} \tag{C.1}$$

for each relevant energy range: $0 < E < \mu$ and $\mu < E < eV$. When both spin species are counted in one of the terminals, the characteristic function reads

$$\begin{aligned}\chi_E(\lambda_1,\lambda_{2\sigma'}) = 1 &+ \left(e^{-i\lambda_1}-1\right)\langle\left(\hat{N}_{\rm O}^{1\uparrow}+\hat{N}_{\rm O}^{1\downarrow}\right)\rangle + \left(e^{-i\lambda_{2\sigma'}}-1\right)\langle\hat{N}_{\rm O}^{2\sigma'}\rangle \\ &+ \left(e^{-i\lambda_1}-1\right)\left(e^{-i\lambda_{2\sigma'}}-1\right)\langle\left(\hat{N}_{\rm O}^{1\uparrow}+\hat{N}_{\rm O}^{1\downarrow}\right)\hat{N}_{\rm O}^{2\sigma'}\rangle + \left(e^{-i\lambda_1}-1\right)^2\langle\hat{N}_{\rm O}^{1\uparrow}\hat{N}_{\rm O}^{1\downarrow}\rangle \\ &+ \left(e^{-i\lambda_1}-1\right)^2\left(e^{-i\lambda_{2\sigma'}}-1\right)\langle\hat{N}_{\rm O}^{1\uparrow}\hat{N}_{\rm O}^{1\downarrow}\hat{N}_{\rm O}^{2\sigma'}\rangle \end{aligned} \tag{C.2}$$

for counting both spins in terminal 1, where we have set $\lambda_{1\uparrow} = \lambda_{1\downarrow} \equiv \lambda_1$.

Using Eqs. (4.14), (4.18) and (C.1), at zero temperature, one can calculate the single terminal probability distribution:

$$\begin{aligned}P^{\theta_1}(Q_{1\sigma}) &= \frac{1}{2\pi}\int_{-\pi}^{\pi} d\lambda_{1\sigma}\left[1+\left(e^{-i\lambda_{1\sigma}}-1\right)\langle\hat{N}_{\rm O}^{1\sigma}\rangle_S\right]^{M_\mu} \\ &\quad\times\left[1+\left(e^{-i\lambda_{1\sigma}}-1\right)\langle\hat{N}_{\rm O}^{1\sigma}\rangle_B\right]^{M-M_\mu} e^{i\lambda_{1\sigma}Q_{1\sigma}}, \end{aligned} \tag{C.3}$$

where $\langle \hat{N}_{\rm O}^{1\sigma} \rangle_{S,B} \equiv \langle \psi_{S,B}| \hat{N}_{\rm O}^{1\sigma} |\psi_{S,B}\rangle$. After integration over $\lambda_{1\sigma}$ we get

$$P^{\theta_1}(Q_{1\sigma}) = \left(1 - \langle \hat{N}_{\rm O}^{1\sigma} \rangle_S\right)^{M_\mu} \left(1 - \langle \hat{N}_{\rm O}^{1\sigma} \rangle_B\right)^{M - M_\mu - Q_{1\sigma}} \left(\langle \hat{N}_{\rm O}^{1\sigma} \rangle_B\right)^{Q_{1\sigma}}$$
$$\times \sum_{n={\rm Max}[0, Q_{1\sigma} - M + M_\mu]}^{{\rm Min}[M_\mu, Q_{1\sigma}]} \left(\begin{array}{c} M_\mu \\ n \end{array} \right) \left(\begin{array}{c} M - M_\mu \\ Q_{1\sigma} - n \end{array} \right) \left[\frac{\langle \hat{N}_{\rm O}^{1\sigma} \rangle_S (1 - \langle \hat{N}_{\rm O}^{1\sigma} \rangle_B)}{\langle \hat{N}_{\rm O}^{1\sigma} \rangle_B (1 - \langle \hat{N}_{\rm O}^{1\sigma} \rangle_S)} \right]^n . \qquad \text{(C.4)}$$

If one chooses $\mu_{\rm L} = eV$ and $\mu_{\rm R} = 0$, one obtains $\mu = \frac{eV}{2}$ and $M_\mu = \frac{M}{2}$. Therefore, in order for M_μ to be integer, M must be an even number.

Using Eqs. (4.14), (4.18) and (C.2), the single terminal probability distribution when both spin species are counted in the terminal is

$$P(Q_1) = \frac{1}{2\pi} \int_{-\pi}^{\pi} \left[1 + \left(e^{-i\lambda_1} - 1\right) \langle \hat{N}_{\rm O}^1 \rangle_S + \left(e^{-i\lambda_1} - 1\right)^2 \langle \hat{N}_{\rm O}^{1\uparrow} \hat{N}_{\rm O}^{1\downarrow} \rangle_S \right]^{M_\mu}$$
$$\times \left[1 + \left(e^{-i\lambda_1} - 1\right) \langle \hat{N}_{\rm O}^1 \rangle_B + \left(e^{-i\lambda_1} - 1\right)^2 \langle \hat{N}_{\rm O}^{1\uparrow} \hat{N}_{\rm O}^{1\downarrow} \rangle_B \right]^{M - M_\mu} e^{i\lambda_1 Q_1} d\lambda_1, \qquad \text{(C.5)}$$

where $\langle \hat{N}_{\rm O}^1 \rangle_{S,B} \equiv \langle \left(\hat{N}_{\rm O}^{1\uparrow} + \hat{N}_{\rm O}^{1\downarrow} \right) \rangle_{S,B}$. Although this is simply a single terminal probability distribution, the result of its integral is too cumbersome to be given here, no wonder what happens with joint terminal probabilities. As we mentioned in Sec. 4.3, explicit expressions of the probability distributions in terms of sums are lengthy and complicated for practical calculations.

It is possible, nevertheless, to express the result for the various probabilities in a quite simple fashion, which makes them manageable for computational analysis. The key point is to realize that the characteristic functions are nothing but polynomial functions on the variables $e^{i\lambda_i}$ of different degrees. The effect of each integral of Eq. (4.14), together with its accompanying complex exponential $e^{i\lambda_i Q_i}/(2\pi)$, is simply to select the coefficient of the characteristic function polynomial which corresponds to the power equal to Q_i. Consequently, the result of the integrals for the various probabilities can be expressed in terms of Q_i order derivatives of the characteristic function, as we show below. Note that, whenever both analyzers are present, we will choose without loss of generality: $\sigma = \uparrow$ and $\sigma' = \uparrow$. For single terminal probability distributions we will also set $\sigma = \uparrow$ for lead 1 and $\sigma' = \uparrow$ for lead 2, although resulting expressions will not depend either on the direction of the spin or on the angle of the analyzer.

For the single terminal probability distribution with analyzer we have

$$P^{\theta_1}(Q_{1\uparrow}) = \frac{1}{2\pi} \int_{-\pi}^{\pi} d\lambda_{1\uparrow} e^{i\lambda_{1\uparrow} Q_{1\uparrow}} \chi(\lambda_{1\uparrow}) = \frac{1}{Q_{1\uparrow}!} \left. \frac{d^{Q_{1\uparrow}} \chi(\lambda_{1\uparrow})}{d(e^{i\lambda_{1\uparrow}})^{Q_{1\uparrow}}} \right|_{e^{i\lambda_{1\uparrow}} \to 0}, \qquad \text{(C.6)}$$

where $\chi(\lambda_{1\uparrow})$ can be extracted from Eq. (C.1) making $\lambda_{2\uparrow} = 0$ and using Eq. (4.18). Since $\mu = \frac{eV}{2}$, we have that $M_\mu = \frac{M}{2}$, being M the total number of emitted particles

per lead or per spin. The expectation values needed in Eq. (C.1) above and below energy μ are given in Sec. C.1. The single terminal probability distribution in the absence of analyzer is

$$P(Q_1) = \frac{1}{2\pi}\int_{-\pi}^{\pi} d\lambda_1 e^{i\lambda_1 Q_1}\chi(\lambda_1) = \frac{1}{Q_1!}\left.\frac{d^{Q_1}\chi(\lambda_1)}{d(e^{i\lambda_1})^{Q_1}}\right|_{e^{i\lambda_1}\to 0}, \tag{C.7}$$

where the characteristic function can be extracted now from Eq. (C.2), setting again $\lambda_{2\uparrow} = 0$. We can get similarly the expressions for $P^{\theta_2}(Q_{2\uparrow})$ and $P(Q_2)$.

The joint probability distribution when both analyzers are present gives

$$\begin{aligned} P^{\theta_1,\theta_2}(Q_{1\uparrow}, Q_{2\uparrow}) &= \frac{1}{(2\pi)^2}\int_{-\pi}^{\pi} d\lambda_{1\uparrow} e^{i\lambda_{1\uparrow}Q_{1\uparrow}} \int_{-\pi}^{\pi} d\lambda_{2\uparrow} e^{i\lambda_{2\uparrow}Q_{2\uparrow}}\chi(\lambda_{1\uparrow},\lambda_{2\uparrow}) \\ &= \frac{1}{Q_{1\uparrow}!Q_{2\uparrow}!}\left.\frac{d^{Q_{1\uparrow}}d^{Q_{2\uparrow}}\chi(\lambda_{1\uparrow},\lambda_{2\uparrow})}{d(e^{i\lambda_{1\uparrow}})^{Q_{1\uparrow}}d(e^{i\lambda_{2\uparrow}})^{Q_{2\uparrow}}}\right|_{e^{i\lambda_{1\uparrow}},e^{i\lambda_{2\uparrow}}\to 0}, \end{aligned} \tag{C.8}$$

which only depends on the angle $\Theta \equiv (\theta_1 \pm \theta_2)/2$, as we showed in Section 4.3. When there is only one analyzer we have

$$\begin{aligned} P^{\theta_1,-}(Q_{1\uparrow}, Q_2) &= \frac{1}{(2\pi)^2}\int_{-\pi}^{\pi} d\lambda_{1\uparrow} e^{i\lambda_{1\uparrow}Q_{1\uparrow}} \int_{-\pi}^{\pi} d\lambda_2 e^{i\lambda_2 Q_2}\chi(\lambda_{1\uparrow},\lambda_2) \\ &= \frac{1}{Q_{1\uparrow}!Q_2!}\left.\frac{d^{Q_{1\uparrow}}d^{Q_2}\chi(\lambda_{1\uparrow},\lambda_2)}{d(e^{i\lambda_{1\uparrow}})^{Q_{1\uparrow}}d(e^{i\lambda_2})^{Q_2}}\right|_{e^{i\lambda_{1\uparrow}},e^{i\lambda_2}\to 0} \end{aligned} \tag{C.9}$$

and

$$\begin{aligned} P^{-,\theta_2}(Q_1, Q_{2\uparrow}) &= \frac{1}{(2\pi)^2}\int_{-\pi}^{\pi} d\lambda_1 e^{i\lambda_1 Q_1} \int_{-\pi}^{\pi} d\lambda_{2\uparrow} e^{i\lambda_{2\uparrow}Q_{2\uparrow}}\chi(\lambda_1,\lambda_{2\uparrow}) \\ &= \frac{1}{Q_1!Q_{2\uparrow}!}\left.\frac{d^{Q_1}d^{Q_{2\uparrow}}\chi(\lambda_1,\lambda_{2\uparrow})}{d(e^{i\lambda_1})^{Q_1}d(e^{i\lambda_{2\uparrow}})^{Q_{2\uparrow}}}\right|_{e^{i\lambda_1},e^{i\lambda_{2\uparrow}}\to 0}. \end{aligned} \tag{C.10}$$

However, these two last expressions are not strictly needed since one can use the relations in Eq. (4.19). Again, all the expectation values which are needed for evaluating these probabilities are given in Sec. C.1.

C.1 Expectation values for the FCS

Above we have presented convenient expressions for the single terminal and joint terminal probability distributions required to test the CH inequality of Eq. (4.20). These probabilities are expressed in terms of different expectations values, which we collect in the following subsections.

C.1.1 Setup with two additional reservoirs

Let us consider the setup depicted in Fig. 4.1, where two additional reservoirs are present. The expectation values for energies $0 < E < \mu$ as a function of transmission T, decoherence parameter α and analyzers' angle Θ are

$$\langle \hat{N}_{\rm O}^{1\uparrow} \rangle_S = \langle \hat{N}_{\rm O}^{2\uparrow} \rangle_S = \frac{2\sqrt{T}[\sqrt{T} + \alpha(2-\sqrt{T}) - \alpha^2(1-\sqrt{T})]}{[2-\alpha(1-\sqrt{T})]^2}, \tag{C.11}$$

$$\langle \hat{N}_{\rm O}^{1} \rangle_S = \langle \hat{N}_{\rm O}^{2} \rangle_S = \frac{4\sqrt{T}[\sqrt{T} + \alpha(2-\sqrt{T}) - \alpha^2(1-\sqrt{T})]}{[2-\alpha(1-\sqrt{T})]^2}, \tag{C.12}$$

$$\langle \hat{N}_{\rm O}^{1\uparrow} \hat{N}_{\rm O}^{1\downarrow} \rangle_S = \langle \hat{N}_{\rm O}^{2\uparrow} \hat{N}_{\rm O}^{2\downarrow} \rangle_S = \frac{4T\alpha[2\sqrt{T} + 2\alpha(1-\sqrt{T}) - \alpha^2(1-\sqrt{T})]}{[2-\alpha(1-\sqrt{T})]^3}, \tag{C.13}$$

$$\langle \hat{N}_{\rm O}^{1\uparrow} \hat{N}_{\rm O}^{2\uparrow} \rangle_S = \frac{4T\{[\alpha(2-\alpha) + \sqrt{T}(1-\alpha+\alpha^2)]^2 - T(1-\alpha)^2\cos\Theta\}}{[2-\alpha(1-\sqrt{T})]^4}, \tag{C.14}$$

$$\langle \hat{N}_{\rm O}^{1} \hat{N}_{\rm O}^{2\uparrow} \rangle_S = \langle \hat{N}_{\rm O}^{1\uparrow} \hat{N}_{\rm O}^{2} \rangle_S = \frac{8T[\sqrt{T} + \alpha(2-\sqrt{T}) - \alpha^2(1-\sqrt{T})]^2}{[2-\alpha(1-\sqrt{T})]^4}, \tag{C.15}$$

$$\langle \hat{N}_{\rm O}^{1\uparrow} \hat{N}_{\rm O}^{1\downarrow} \hat{N}_{\rm O}^{2\uparrow} \rangle_S = \langle \hat{N}_{\rm O}^{1\uparrow} \hat{N}_{\rm O}^{2\uparrow} \hat{N}_{\rm O}^{2\downarrow} \rangle_S = 8\sqrt{T^3}\alpha[2\sqrt{T} + 2\alpha(1-\sqrt{T}) - \alpha^2(1-\sqrt{T})]$$
$$\times \frac{[\sqrt{T} + \alpha(2-\sqrt{T}) - \alpha^2(1-\sqrt{T})]}{[2-\alpha(1-\sqrt{T})]^5}. \tag{C.16}$$

The expectation values for energies $\mu < E < eV$ are

$$\langle \hat{N}_{\rm O}^{1\uparrow} \rangle_B = \langle \hat{N}_{\rm O}^{2\uparrow} \rangle_B = \frac{2T(1-\alpha)}{[2-\alpha(1-\sqrt{T})]^2}, \tag{C.17}$$

$$\langle \hat{N}_{\rm O}^{1} \rangle_B = \langle \hat{N}_{\rm O}^{2} \rangle_B = \frac{4T(1-\alpha)}{[2-\alpha(1-\sqrt{T})]^2}, \tag{C.18}$$

$$\langle \hat{N}_{\rm O}^{1\uparrow} \hat{N}_{\rm O}^{1\downarrow} \rangle_B = \langle \hat{N}_{\rm O}^{2\uparrow} \hat{N}_{\rm O}^{2\downarrow} \rangle_B = 0, \tag{C.19}$$

$$\langle \hat{N}_{\rm O}^{1\uparrow} \hat{N}_{\rm O}^{2\uparrow} \rangle_B = \frac{8T^2(1-\alpha)^2\sin^2(\Theta/2)}{[2-\alpha(1-\sqrt{T})]^4}, \tag{C.20}$$

$$\langle \hat{N}_{\rm O}^{1} \hat{N}_{\rm O}^{2\uparrow} \rangle_B = \langle \hat{N}_{\rm O}^{1\uparrow} \hat{N}_{\rm O}^{2} \rangle_B = \frac{8T^2(1-\alpha)^2}{[2-\alpha(1-\sqrt{T})]^4}, \tag{C.21}$$

$$\langle \hat{N}_{\rm O}^{1\uparrow} \hat{N}_{\rm O}^{1\downarrow} \hat{N}_{\rm O}^{2\uparrow} \rangle_B = \langle \hat{N}_{\rm O}^{1\uparrow} \hat{N}_{\rm O}^{2\uparrow} \hat{N}_{\rm O}^{2\downarrow} \rangle_B = 0. \tag{C.22}$$

C.1.2 Setup with one additional reservoir

Let us now consider the asymmetrical setup of Fig. 4.9, where there is only one additional reservoir. For energies $0 < E < \mu$ we have that $\langle \hat{N}_{\rm O}^{1\uparrow} \rangle_S$, $\langle \hat{N}_{\rm O}^{1} \rangle_S$ and $\langle \hat{N}_{\rm O}^{1\uparrow} \hat{N}_{\rm O}^{1\downarrow} \rangle_S$ are equal to the case with two fictitious reservoirs. The other expectation

values are

$$\langle \hat{N}_{\rm O}^{2\uparrow} \rangle_S = \frac{T}{2}, \tag{C.23}$$

$$\langle \hat{N}_{\rm O}^{2} \rangle_S = T, \tag{C.24}$$

$$\langle \hat{N}_{\rm O}^{2\uparrow} \hat{N}_{\rm O}^{2\downarrow} \rangle_S = 0, \tag{C.25}$$

$$\langle \hat{N}_{\rm O}^{1\uparrow} \hat{N}_{\rm O}^{2\uparrow} \rangle_S = \frac{\sqrt{T^3}\alpha(2-\alpha) + T^2[1-\alpha+\alpha^2-(1-\alpha)\cos\Theta]}{[2-\alpha(1-\sqrt{T})]^2}, \tag{C.26}$$

$$\langle \hat{N}_{\rm O}^{1} \hat{N}_{\rm O}^{2\uparrow} \rangle_S = \langle \hat{N}_{\rm O}^{1\uparrow} \hat{N}_{\rm O}^{2} \rangle_S = \frac{2\sqrt{T^3}[\sqrt{T}+\alpha(2-\sqrt{T})-\alpha^2(1-\sqrt{T})]}{[2-\alpha(1-\sqrt{T})]^4}, \tag{C.27}$$

$$\langle \hat{N}_{\rm O}^{1\uparrow} \hat{N}_{\rm O}^{1\downarrow} \hat{N}_{\rm O}^{2\uparrow} \rangle_S = \frac{2T^2\alpha[2\sqrt{T}+2\alpha(1-\sqrt{T})-\alpha^2(1-\sqrt{T})]}{[2-\alpha(1-\sqrt{T})]^3}, \tag{C.28}$$

$$\langle \hat{N}_{\rm O}^{1\uparrow} \hat{N}_{\rm O}^{2\uparrow} \hat{N}_{\rm O}^{2\downarrow} \rangle_S = 0. \tag{C.29}$$

For energies $\mu < E < eV$ we have that $\langle \hat{N}_{\rm O}^{1\uparrow} \rangle_B$, $\langle \hat{N}_{\rm O}^{1} \rangle_B$, $\langle \hat{N}_{\rm O}^{1\uparrow} \hat{N}_{\rm O}^{1\downarrow} \rangle_B$, $\langle \hat{N}_{\rm O}^{2\uparrow} \hat{N}_{\rm O}^{2\downarrow} \rangle_B$, $\langle \hat{N}_{\rm O}^{1\uparrow} \hat{N}_{\rm O}^{1\downarrow} \hat{N}_{\rm O}^{2\uparrow} \rangle_B$ and $\langle \hat{N}_{\rm O}^{1\uparrow} \hat{N}_{\rm O}^{2\uparrow} \hat{N}_{\rm O}^{2\downarrow} \rangle_B$ are equal to the case with two additional reservoirs. The other expectation values are

$$\langle \hat{N}_{\rm O}^{2\uparrow} \rangle_B = \frac{T}{2}, \tag{C.30}$$

$$\langle \hat{N}_{\rm O}^{2} \rangle_B = T, \tag{C.31}$$

$$\langle \hat{N}_{\rm O}^{1\uparrow} \hat{N}_{\rm O}^{2\uparrow} \rangle_B = \frac{2T^2(1-\alpha)\sin^2(\Theta/2)}{[2-\alpha(1-\sqrt{T})]^2}, \tag{C.32}$$

$$\langle \hat{N}_{\rm O}^{1} \hat{N}_{\rm O}^{2\uparrow} \rangle_B = \langle \hat{N}_{\rm O}^{1\uparrow} \hat{N}_{\rm O}^{2} \rangle_B = \frac{2T^2(1-\alpha)}{[2-\alpha(1-\sqrt{T})]^2}. \tag{C.33}$$

Appendix D

Phenomenological description of inelastic scattering

Voltage probes are frequently real components of mesoscopic devices, but have also been used traditionally for phenomenological modeling purposes. The voltage probe description of inelastic scattering resorts to the addition of one or more fictitious reservoirs and leads attached to the coherent conductor under study through specific scattering matrices, around the regions where inelastic scattering is to be modeled. While being still coherent overall, the elimination of the fictitious reservoirs results in an effective description of transport such that electrons that originally scattered into the reservoirs now appear as having lost phase and energy memory completely.

We will now discuss the implementation of the voltage probe in the presence of charge relaxation and general incoming states. The whole idea of the voltage probe is to use the non-interacting scattering formalism to model inelastic electron scattering, and the crossover from coherent conductors to incoherent ones. There are two ways to do this. The simpler one assumes a static chemical potential in the probes that is computed self-consistently by fixing time-averaged current flowing into the probes to zero, as corresponds to an infinite impedance voltage probe, or to inelastic scattering. This gives a physically sound conductance value, but fails to yield reasonable shot noise predictions. The reason is that total current throughout the system should be instantaneously conserved. The more elaborate way, therefore, assumes fluctuations in the state of the probe that can compensate the current flowing into the probe(s) at any instant of time (and possibly also energy if one is modeling pure elastic dephasing [89, 90, 236]), which gives results for current fluctuations in agreement with classical arguments [95].

It is traditional to impose such constraint within a Langevin description of current fluctuations [88], whereby the chemical potential in the probe is allowed to fluctuate, but the intrinsically semiclassical formulation of this approach makes it inadequate to treat the statistics of general incoming entangled states that exhibit non-classical correlations. There seems to be no known way of how to include interference con-

tributions due to coherent superposition of current states, which are precisely the contributions we are interested in this work. The discussion to follow (and the implicit sequential scattering approximation) explicitly takes into account the precise incoming entangled state, and recovers results obtained within the Langevin approach in the case of non-entangled incoming states (see e.g. Appendix D.2).

The scattering matrix to a (two-legged) fictitious probe is given, in the bases $1, 2, 1', 2'$ (being $1', 2'$ the extra leads), by

$$S_\alpha = \begin{pmatrix} 0 & -\sqrt{1-\alpha} & i\sqrt{\alpha} & 0 \\ \sqrt{1-\alpha} & 0 & 0 & i\sqrt{\alpha} \\ i\sqrt{\alpha} & 0 & 0 & \sqrt{1-\alpha} \\ 0 & i\sqrt{\alpha} & -\sqrt{1-\alpha} & 0 \end{pmatrix}, \tag{D.1}$$

with α being the inelastic scattering probability. This should be composed together with any other scattering matrices in the system, and any other probes present. In a spinful case in which inelastic scattering does not flip spin there should be at least two of these probes, one per spin channel. Other considerations such as inelastic channel mixing in multichannel cases should be taken into account when designing the relevant fictitious probe setup. Let us first consider a general setup with a single probe for simplicity.

We will now introduce the implementation of charge conservation through the system (i.e. in the fictitious probe) which will lead to the simple result expressed in Eq. (D.16). We first make the essential approximation that the inelastic scattering time in the interacting region is much smaller than

$$\Delta t \equiv h/eV. \tag{D.2}$$

The inverse of the timescale Δt is the average rate at which the external leads inject particles into the system, in the localized wave-packet terminology [237]. We will call the scattering processes within time interval Δt a 'scattering event'. In this limit of quick scattering we can assume *sequential* scattering events, as if each Δt interval was an independent few-particle scattering problem, one for each time

$$t_j \equiv j\Delta t. \tag{D.3}$$

The overlap of the wave-packets which would in principle give contributions away from the sequential scattering approximation is assumed to have a negligible effect in the long time limit. Other works in different contexts [238] seem to support this statement. Furthermore, if one considers small transparency contacts between the electron source and the fictitious probes, the sequential scattering approximation is also exact.

The incoming state in each scattering event will be one particle in each channel of the external leads (L_1 and L_2 in the setup of Fig. 5.1), plus a certain state in the

probe's leads $1'$ and $2'$. This state injected from the probe is prepared in a way so as to compensate for excess charge scattered into the fictitious probe in all previous events, with the intention of canceling any current that has flowed into the probe in the past. The book-keeping of the probe's excess charge is done via an auxiliary slave degree of freedom $|Q\rangle$ with discrete quantum numbers $Q = 0, \pm 1, \pm 2, \ldots$ that count charge transferred to the probe. The incoming state in leads $1'$ and $2'$ injected by the probe into the system is a function of Q. The time evolution of the slave state $|Q\rangle$ is constrained so that Q always equals the total number of electrons that has entered the probe since the first scattering event. In particular, the time evolution of $|Q\rangle$ during one scattering event Δt is taken to follow the resulting net charge that was transferred to the probe during that event. This scheme effectively correlates the initially uncorrelated scattering events in order to satisfy instantaneous current conservation through the system, where by instantaneous we mean at times larger than Δt but still much smaller than the measuring time.

If the incoming state in the probe's leads is chosen correctly, the number of Q states between which $|Q\rangle$ will fluctuate during many scattering events will be bounded, and will be independent of the total number of events

$$M = eVt/h \tag{D.4}$$

in the total experiment time t. This is the underlying principle of this approach, which will guarantee that the instantaneous charge fluctuations in the probe will be bounded to a few electrons throughout the whole measurement process, i.e., the probe current will be zero and noiseless at frequencies below $eV/\hbar$.

The choice that minimizes the charge fluctuations in a single channel two-legged probe in the absence of superconductors in the system is the following: if Q at the beginning of the scattering event is 1 or 2, the probe will emit two particles, one through each 'leg', thereby losing a maximum of 2 and a minimum of 0 in that event; if Q is 0, -1 or -2 the probe will not emit any particle, thereby absorbing a maximum of 2 and a minimum of 0. The resulting fluctuations of Q are bounded in the $[-2, 2]$ range. In some cases, such as the system discussed in the main text, this range is reduced to $[-1, 1]$ since the entangler only emits one electron of each spin in each scattering event, so that the probe will never absorb 2 particles, but a maximum of 1. The relevance of this discussion will be apparent in connection with Eq. (D.11), since it will determine the dimensions of the W operator therein.

D.1 Sequential scattering scheme for the FCS

We wish to compute in a general case the characteristic function

$$\chi(\vec{\lambda}; M) = \langle e^{i \sum_n \lambda_n \Delta \hat{N}_n} \rangle = \mathrm{Tr} \left\{ \hat{\chi}(\vec{\lambda}) \rho(t) \right\} \tag{D.5}$$

after a total measuring time interval t. Number difference $\Delta\hat{N}_n \equiv \hat{N}_n^{\text{out}} - \hat{N}_n^{\text{in}}$ is defined as the number operator in channel n at time t (scattered outgoing particle number) minus the number operator at time zero, before any scattering (incoming particle number). Differentiating $\log\chi$ respect to the counting fields λ_n one obtains the different transferred charge and current cumulants, Eq. (D.18).

Let us include the fictitious probe and expand our Fock space with the slave degree of freedom $|Q\rangle$. We take the density matrix of the whole system at time zero equal to $\rho(0) = \rho^Q(0) \otimes \rho^e(0)$, the second ρ being the electronic density matrix. As we will see we do not need to specify the initial state of the slave degree of freedom $\rho^Q(0)$ since it will not affect our results in the long time limit. The density matrix is factorized in the localized wave-packet basis [237],

$$\rho(0) = \rho^Q(0) \otimes \prod_j^{\otimes} \rho_j^e, \tag{D.6}$$

with the electronic part being $\rho_j^e \equiv \rho_j^r \otimes \rho_j^p$. Each of these ρ_j^e constitutes the incoming state in each of the j scattering events corresponding to the time interval $[t_j, t_{j+1}]$. ρ_j^r, which is actually j-independent, is the density matrix of the (uncorrelated in time) electrons coming from the external reservoirs, and ρ_j^p is the density matrix of the (correlated in time-through-Q) electrons coming from the fictitious probe. As we mentioned, this matrix ρ_j^p will depend on the state of the slave degree of freedom Q at the beginning of each scattering event j.

The time evolution from 0 to t, $\rho(t) = \hat{U}_t \rho(0) \hat{U}_t^+$ is split up in the M time intervals of length Δt. The sequential scattering approximation amounts to assuming that in each event each electron group ρ_j^e scatters completely before the next one does. Therefore $\hat{U}_t = \hat{U}_{\Delta t}^M$. We defer the discussion on how $U_{\Delta t}$ operates precisely to a little later.

Since operator $\hat{\chi}(\vec{\lambda})$ will factorize into contributions for each scattering event, $\hat{\chi} = \prod_j \hat{\chi}_j$, we can rewrite equation (D.5) as

$$\begin{aligned} \chi \;\; &= \;\; \text{Tr}_Q \left\{ \text{Tr}_M \left[\hat{\chi}_M U_{\Delta t} \rho_M^e \text{Tr}_{M-1} \left[\;\cdots \right.\right.\right. \\ &\cdots \;\; \left.\left.\left. \text{Tr}_1 \left[\hat{\chi}_1 U_{\Delta t} \rho_1^e \rho^Q(0) U_{\Delta t}^+ \right] U_{\Delta t}^+ \right] U_{\Delta t}^+ \cdots \right] \right\}, \end{aligned} \tag{D.7}$$

where Tr_j stands for the trace over the ρ_j^e electron states and Tr_Q over the Q subspace. An alternative way of writing this is by induction. Defining an auxiliary operator $\hat{\Phi}^{(k)} = \sum_{QQ'} |Q\rangle \Phi_{QQ'}^{(k)} \langle Q'|$ such that

$$\hat{\Phi}^{(j)} \;\; = \;\; \text{Tr}_j \left[\hat{\chi}_j U_{\Delta t} \rho_j^e \hat{\Phi}^{(j-1)} U_{\Delta t}^+ \right], \tag{D.8}$$

$$\hat{\Phi}^{(0)} \;\; = \;\; \rho^Q(0), \tag{D.9}$$

one can see that (D.7) and (D.5) are equivalent to

$$\chi(\vec{\lambda}; M) \;\; = \;\; \text{Tr}_Q \hat{\Phi}^{(M)}. \tag{D.10}$$

After some algebra, Eq. (D.8) can be recast into the following sum over the total range of Q values,

$$\Phi^{(j)}_{Q_bQ'_b} = \sum_{Q_aQ'_a} W^{Q_aQ'_a}_{Q_bQ'_b} \Phi^{(j-1)}_{Q_aQ'_a}, \tag{D.11}$$

with the W superoperator

$$W^{Q_aQ'_a}_{Q_bQ'_b}(\vec{\lambda}) = \mathrm{Tr}_j \left[P_{Q'_bQ_b} \hat{\chi}_j(\vec{\lambda}) U_{\Delta t} \rho^e_j P_{Q_aQ'_a} U^+_{\Delta t} \right], \tag{D.12}$$

and $P_{QQ'} \equiv |Q\rangle\langle Q'|$ the generalized projector within the slave degree of freedom space. We will specify how it operates in practice a bit later, after Eq. (D.14).

Some words about the meaning of this operator W, which is a central object in this technique, are in order at this point. It is a superoperator that, for $\vec{\lambda} = 0$ simply transforms the reduced density matrix $\rho^Q(t_j) = \hat{\Phi}^{(j)}(\vec{\lambda} = 0)$ of the slave degree of freedom at time t_j to the subsequent one $\hat{\Phi}^{(j+1)}(\vec{\lambda} = 0)$ at time t_{j+1}. In Eq. (D.8) we see how $\hat{\Phi}^{(j)}$ is simply $\hat{\Phi}^{(j-1)}$ to which the incoming state ρ^e_j for event j is added, is allowed to evolve a time Δt (during which also ρ^Q evolves as dictated by the number of electrons scattered into the probe), and the scattered electrons are traced out. The result is the new evolved reduced density matrix for the slave degree of freedom. For finite $\vec{\lambda}$, the corresponding counting fields for the scattered electrons are also included into $\hat{\Phi}^{(j)}$ so as to be able to recover the desired cumulants of the traced-out electrons after time t from $\chi = \mathrm{Tr}_Q \hat{\Phi}^{(M)}$. This can be also seen as supplementing the dynamics of the system with a quantum field term $\propto \lambda_n$ in the action, in the generalized Keldysh language of Ref. [239].

By assuming without loss of generality a diagonal initial $\rho^Q(0)$ and by noting that by construction states with different Q are orthogonal, we can in general take W to be diagonal $W^{Q_aQ'_a}_{Q_bQ'_b} = \delta_{Q_aQ'_a}\delta_{Q_bQ'_b}\overline{W}_{Q_bQ_a}$, and $\Phi^{(j)}_{QQ'} = \delta_{QQ'}\Phi^{(j)}_Q$. Physically this means that sequentially taking out of the system the scattered electrons (tracing them out) forbids the Q counter to remain in a coherent superposition, since the electron that generated it has been 'measured'. Therefore (D.10) finally becomes

$$\chi(\vec{\lambda}; M) = \sum_{Q_aQ_b} \overline{W}^M_{Q_bQ_a} \rho^Q_{Q_aQ_a}(0) \tag{D.13}$$

(note the M^{th} power of the $\overline{W}$ matrix). The following alternative and useful form for (D.12) can be obtained by writing $|Q\rangle\langle Q|\rho^e_j|Q\rangle\langle Q| = |\phi^e Q\rangle\langle\phi^e Q|$, in the case of a pure incoming state in the external leads,

$$\overline{W}_{Q_bQ_a}(\vec{\lambda}) = \langle\phi^e Q_a| U^+_{\Delta t} P_{Q_bQ_b} \hat{\chi}_j(\vec{\lambda}) U_{\Delta t} |\phi^e Q_a\rangle, \tag{D.14}$$

where $|\phi^e Q\rangle$ stands now for the incoming electronic state (through all leads) that corresponds to a given value Q of the slave degree of freedom.

Let us analyze the action of the evolution operator $U_{\Delta t}$ in the above equation. Since we assume that particles scatter fully in time Δt, the action of $U_{\Delta t}$ on the electrons is written in terms of the global scattering matrix $b_n^+ = U_{\Delta t} a_n^+ U_{\Delta t}^+ = \sum_m S_{nm} a_m^+$, where a_n^+ are the electron creation operators in the different leads (including fictitious ones) of the system [1]. The effect of $U_{\Delta t}$ on the $\hat{Q}$ degree of freedom is merely to update it with the net number of electrons scattered into the fictitious leads, fixing $\hat{Q}_{t_{j+1}} - \hat{Q}_{t_j} = \Delta \hat{N}_p$, where $\Delta \hat{N}_p$ is the number of electrons absorbed by the probe in the event. This implies that $P_{Q_b Q_b}$ in Eq. (D.14), which projects on the subspace with $Q = Q_b$, can be substituted by the electron-only operator that projects over scattered electronic states that satisfy $\hat{N}_p^{\rm out} = \hat{N}_p^{\rm in} + Q_b - Q_a$, where $\hat{N}_p^{\rm out}$ is the number operator for fermions scattered into the probe, $\hat{N}_p^{\rm in}$ is the number of electrons incident from the probe into the system at the beginning of the scattering event, and Q_a is the value of Q also at the beginning of the scattering event.

As anticipated just before the beginning of this subsection, the value of $\hat{N}_p^{\rm in}$ on $|\phi^e Q_a\rangle$ is a function of Q_b, and should be chosen properly so as to compensate for a given excess probe charge Q_a at the beginning of a given scattering event. That way the fluctuations of the probe's excess charge Q will be minimum, although the precise choice does not affect the result as long as the resulting range of fluctuations of Q does not scale with measurement time t. As already discussed, for most cases the optimum choice is $N_p^{in}(Q) = g(Q)$, with

$$\begin{aligned} g(1) &= 2 \quad \text{(one electron in each lead of the probe)}, \\ g(0) &= g(-1) = 0, \end{aligned} \tag{D.15}$$

which gives $Q \in [-1, 1]$, and a 3×3 $\overline{W}$ matrix.

To finish with the discussion of Eq. (D.14), recall that $\hat{\chi_j} = e^{i \sum_n \lambda_n (\hat{N}_n^{\rm out} - \hat{N}_n^{\rm in})}$ and that a useful relation for the case of a single channel mode n in which the eigenvalues of $\hat{N}_n$ are zero and one is $e^{i\lambda_n \hat{N}_n} = 1 + (e^{i\lambda_n} - 1)\hat{N}_n$.

The whole Levitov-Lee-Lesovik formulation of FCS [201] is well defined only in the long time limit. In such limit it is clear that expression (D.14) is dominated by the biggest eigenvalues $\mu_{\rm max}$ of $\overline{W}$. All of its eigenvalues satisfy $|\mu| \leq 1$ for real values of $\vec{\lambda}$, so that those that are not close to 1 for small values of $\vec{\lambda}$ (around which we take derivatives to compute cumulants) will exponentiate to zero when $M \to \infty$. In all cases we examined only one eigenvalue $\mu_{\rm max}$ would not exponentiate to zero, although it can have finite degeneracy. In general, we have the following asymptotic property, valid for any degeneracy of $\mu_{\rm max}$,

$$\log \Big[\chi(\vec{\lambda}; M) \Big] = M \log \left[\mu_{\rm max} \right] + \mathcal{O}(1). \tag{D.16}$$

[1] Note the difference with the notation in [95]. When there is time reversal symmetry both choices are equivalent.

We can define a new generating function

$$\log \chi_I(\vec{\lambda}) = \lim_{M\to\infty} \frac{\log \chi(\vec{\lambda}; M)}{M}. \tag{D.17}$$

It can be shown that this function generates the zero frequency limit of current cumulants

$$\langle\langle I_n(\omega = 0)^k \rangle\rangle = \frac{e^{k+1}|V|}{h}(-i)^k \, \partial^k_{\lambda_n} \log \chi_I\big|_{\vec{\lambda}=0}\,, \tag{D.18}$$

being e here the electron charge and k the order of the cumulant, $k = 1$ for the average current, $k = 2$ for the shot noise, and so on.

We can identify

$$\chi_I(\vec{\lambda}) = \mu_{\max}(\vec{\lambda}). \tag{D.19}$$

This is our final result. $\mu_{\max}$ is the eigenvalue of Eq. (D.14) that equals 1 when all counting fields λ_n are taken to zero.

The generalization to multiple probes is very straightforward. Given the optimum choice of Eq. (D.15), the solution of an $N-$probe setup will involve the diagonalization of an $3^N \times 3^N$ $\overline{W}$ matrix similar to Eq. (D.14) where Q is changed to $\vec{Q}$, a vector of the N corresponding slave degrees of freedom. On the other hand, to implement charge conservation in probes with more than one channel per leg (or more than two legs), such as non-spin-conserving probes, the formalism would require a slightly different expression for Eq. (D.15) and a consequently bigger dimension for $\overline{W}$, but would otherwise remain quite the same.

We have successfully compared the present method to Langevin techniques in scenarios where the latter is applicable, obtaining identical results in all cases. Some simple examples are the FCS of a single channel wire with contact transmissions T_1 (see Appendix D.2 for a detailed calculation), the case of a Mach-Zehnder interferometer or an NS junction, for which both this and the Langevin method [88] yield identical results for χ_I.

D.2 Comparison of the method to previous techniques

In this section we will show with a simple example how the proposed method yields identical results to the ones obtained with previous Langevin technique, which we generalize here to yield the FCS, instead of current cumulants. The purpose of this section is twofold. First we wish to make a convincing case that our method actually recovers known results, and secondly, that it indeed yields the FCS in the presence of an inelastic probe, and not merely a dephasing probe as could be thought from the unusual real time sequential scattering picture.

We will do our comparison in the possibly simplest system one can think of, a zero-temperature single channel conductor for spinless fermions. We will assume symmetric contacts to the (real) reservoirs with transmission T_1. A fictitious inelastic probe will be connected between the two contacts with transmission probability α, and scattering matrix (D.1).

As discussed in detail in Ref. [95], within the Langevin approach, the current fluctuations in the presence of the probe should be corrected by the feedback due to the instantaneous fluctuations of the probes voltage, which react to cancel any current flowing into the probe. Thus the current fluctuation flowing into the right reservoir reads

$$\Delta I_2 = \delta I_2 - \frac{T_{2p}}{T_{1p} + T_{2p}} \left(\delta I_{p1} + \delta I_{p2}\right), \tag{D.20}$$

where δI_n correspond to the current fluctuations in channel n with a static potential in the probe (being $p1$ and $p2$ its two legs), and T_{nm} are the transmission probabilities between channel n and m. Note that we have used the short notation: $T_{1p} = T_{1p_1} + T_{1p_2}$ and $T_{2p} = T_{2p_1} + T_{2p_2}$. The static potential in the probe for δI_n is chosen so as to cancel any average current into the probe.

In our case, left-right symmetry implies

$$\Delta I_2 = \delta I_2 - \frac{1}{2} \left(\delta I_{p1} + \delta I_{p2}\right). \tag{D.21}$$

At this point, what one usually finds in the literature is a calculation of cumulants of certain order. It is possible however to compute them all at once and recover the FCS, as we show in the following. Define the characteristic function with a static potential $\mu_p = eV/2$ in the probe and with *two* counting fields, one (λ_2) that counts particles flowing into the rightmost reservoir, and another (λ_p) that counts particles injected from the probe into the system.

$$\chi(\lambda_2, \lambda_p) = \langle e^{i\lambda_2 \Delta N_2 - i\lambda_p(\Delta N_{p1} + \Delta N_{p2})} \rangle. \tag{D.22}$$

Since at this point there are still no probe fluctuations (each energy is independent from the rest), one can write $\chi(\lambda_2, \lambda_p)$ as the product of two characteristic functions, one for particles in the interval $[0, \mu_p]$ and another in the $[\mu_p, eV]$ [201]. We have

$$\begin{aligned} \chi(\lambda_2, \lambda_p) &= \langle 1|\hat{\chi}_2(\lambda_2)\hat{\chi}_{p1}(-\lambda_p)\hat{\chi}_{p2}(-\lambda_p)|1\rangle^{M/2} \\ &\quad \langle 0|\hat{\chi}_2(\lambda_2)\hat{\chi}_{p1}(-\lambda_p)\hat{\chi}_{p2}(-\lambda_p)|0\rangle^{M/2}, \end{aligned} \tag{D.23}$$

where $\hat{\chi}_n(\lambda) \equiv 1 + \left(e^{i\lambda_n} - 1\right)\hat{N}_n$, $|1\rangle$ is the state at an energy below μ_p (i.e., with a full state coming from the probe), and $|0\rangle$ is a state above μ_p (empty probe). Working out the algebra we get for the *current* characteristic function, Eq. (D.17),

$$\begin{aligned} \chi_I(\lambda_2, \lambda_p) &= \left\{\left[1 + (e^{i\lambda_2} - 1)T_{12} + (e^{i\lambda_2 + i\lambda_p} - 1)T_{2p}\right]\right. \\ &\quad \left. \times \left[1 + (e^{i\lambda_2} - 1)T_{12} + (e^{-i\lambda_p} - 1)T_{2p}\right]\right\}^{\frac{1}{2}}, \end{aligned}$$

where $T_{12} = T_1^2(1-\alpha)/[2-\alpha-T_1(1-\alpha)]^2$ and $T_{2p} = T_1\alpha/[2-\alpha-T_1(1-\alpha)]$.

To include the self-consistent voltage fluctuations of the probe, we return to Eq. (D.21). It is easy to see that the function

$$\chi_I(\lambda_2) \equiv \chi_I(\lambda_2, -\frac{\lambda_2}{2}) = 1 + (e^{i\lambda_2} - 1)T_{12} + (e^{i\lambda_2/2} - 1)T_{2p} \tag{D.24}$$

generates the cumulants of ΔI_2, instead of δI_2, and therefore is the proper FCS solution of the Langevin approach.

On the other hand, the method we have developed involves, in this simple system and for the same choice of $g(Q)$ as in Eq. (D.15), the following expression of the $\overline{W}$ matrix in (D.14)

$$\overline{W} = \begin{pmatrix} a & 0 & 0 \\ c & a & b \\ 0 & c & a \end{pmatrix}, \tag{D.25}$$

with $a = 1 + (e^{i\lambda_2} - 1)T_{12} - T_{2p}$, $b = e^{i\lambda_2}T_{2p}$ and $c = T_{2p}$. The highest eigenvalue of this matrix is $a + \sqrt{bc}$, which indeed equals the Langevin result (D.24).

To conclude, let us emphasize that although the generalized Langevin approach we have employed in this comparison is probably more convenient in this basic case, there seems to be no known way to apply it to systems in which the incoming state is non-locally entangled. Note also that this example clarifies the fact that the fictitious probe we are describing within our approach is inelastic since, as is evident within the Langevin approach, a particle scattered into the probe at a certain energy can abandon it at any other energy in the interval $[0, eV]$. In particular, note that the the current through the system when $T_1 = 1$ and $\alpha = 1$ is noiseless, i.e., the Fano factor as derived from Eq. (D.24) is $F = 0$, as opposed to $F = 1/4$ that would result from the quasi-elastic probe [95].

Appendix E

Anexo en castellano

Incluimos a continuación una traducción al castellano de la introducción y de las conclusiones de cada capítulo, lo cual constituye el resumen global de este trabajo, como parte de los requisitos de presentación de tesis doctorales de la Universidad Autónoma de Madrid.

E.1 Introducción

En mecánica cuántica existe un fenómeno sin análogo clásico en virtud del cual un sistema puede existir simultáneamente en una superposición de diversos estados distintos. En particular, dos o más objetos cuánticos pueden estar en un tipo especial de superposición tal que el estado del sistema global no pueda describirse como un producto de los estados de los diferentes componentes, incluso cuando los objetos estén espacialmente separados. Se dice entonces que estos objetos están mutuamente *enredados* [1, 2]. Por ejemplo, es posible preparar dos partículas con spin 1/2 en un estado cuántico puro llamado *singlete* tal que si al medir el spin de una de ellas se la encuentra en un estado de spin-arriba, la otra resultará estar en estado spin-abajo si es medida a continuación, y viceversa. Como resultado, las medidas realizadas sobre una de las partículas parecen influir instantáneamente sobre la otra partícula con la que está enredada, sin importar lo lejos que se encuentren una de otra. Esta "misteriosa acción a distancia", como la denominó Albert Einstein, está en contradicción con el principio intuitivamente obvio del *realismo local*, que afirma que los objetos físicos sufrirán la influencia únicamente de su entorno más inmediato, y de que deberán poseer sus propiedades de manera objetiva antes de que éstas sean observadas. Schrödinger acuñó el término "enredo" para describir esta peculiar conexión entre estados cuánticos en 1935 [3]. Desde entonces este concepto ha engendrado algunas de las preguntas más entretenidas y filosóficamente turbadoras sobre la interpretación de la mecánica cuántica, y permanece en el núcleo de la extrañeza del mundo cuántico.

Pero la relevancia del enredo no es meramente conceptual. Desde los años 80 en

adelante, los científicos empezaron a pensar en las correlaciones no locales de estados cuánticos enredados como un recurso físico (igual que la energía) que podría abrir la puerta a la resolución de problemas intratables dentro de la computación clásica de una manera eficiente, como por ejemplo la factorización de números enteros grandes o la simulación de la dinámica de sistemas cuánticos. Había surgido el nuevo campo de la *Información Cuántica* (QI), al que se dedicó gran interés desde diferentes sectores de la física, como la óptica cuántica, la física nuclear o la física de la materia condensada.

Hoy en día existen ya varias propuestas para construir algunos de los componentes básicos del hardware de un *ordenador cuántico*, como son los bits cuánticos o *qubits*, que son bits de información que pueden existir en un estado cualquiera de un sistema cuántico de dos niveles. Estos pares de estados pueden ser las dos polarizaciones de un fotón en una cavidad cuántica, el estado con un spin nuclear de más sobre el de otro estado en una muestra líquida dentro de un dispositivo de resonancia nuclear, el estado fundamental y primer excitado de un átomo en una trampa de iones lineal o el spin-arriba y abajo de un electrón confinado en un punto cuántico, por mencionar sólo unos pocos.

Uno de los requisitos para construir un ordenador cuántico es que el sistema elegido pueda ser escalado hasta contener un gran número de qubits. En este sentido, las arquitecturas para computación cuántica basadas en qubits de estado sólido son muy prometedoras. En particular, el uso del spin electrónico como qubit dentro de semiconductores se presenta como una opción conveniente, ya que se ha demostrado experimentalmente la existencia de largos tiempos de vida media del spin electrónico en estos sistemas, del orden de 100 nanosegundos [4, 5]. Esto implica que el transporte de spin puede permanecer coherente durante largas distancias dentro de los semiconductores. Se han observado además tiempos de coherencia incluso mayores en electrones confinados en puntos cuánticos semiconductores [6, 7].

Existe otra importante tarea para la computación cuántica, que pertenece al campo de la *comunicación* cuántica, que es la de transmitir qubits entre lugares distantes de manera fiel. Un modo de lograr esto es implementando los llamados *qubits volantes*, que son qubits que pueden ser convenientemente transportados de un lugar a otro [8]. En principio, el candidato natural para dichos qubits volantes es el fotón, con sus dos estados de polarización. Pero para evitar el problema de tener que convertir la información cuántica del spin a la luz y viveversa en un potencial ordenador cuántico basado en el spin, sería muy deseable poder implementar qubits volantes directamente mediante electrones móviles. Por este motivo, desde 1999 un gran volumen de propuestas teóricas sobre cómo construir un *enredador*, i.e., una fuente de pares de partículas enredadas de manera no local, ha aparecido dentro de la comunidad de física del estado sólido, propuestas principalmente concentradas en el grado de libertad de spin del electrón. Es éste exactamente el campo del conocimiento donde encaja la presente tesis.

En resumen, la motivación fundamental de esta tesis ha sido la de comprender diversas propiedades del enredo de spin electrónico en nanoestructuras. Es-

pecíficamente, hemos estudiado algunos aspectos de las siguientes tres importantes preguntas:

- ¿Cómo generar estados con enredo no local de spin en dispositivos de estado sólido?
- ¿Cómo describir su evolución sometida a decoherencia dentro de la nanoestructura?
- ¿Cómo detectar el enredo?

Para ahondar en la descripción del contenido de esta tesis es conveniente, llegado este punto, dar una serie de definiciones de algunos conceptos básicos en el campo de la teoría de QI. Dedicamos a ello la siguiente sección. Algunos de dichos conceptos provienen principalmente de un campo diferente del tratado en este trabajo, y no constituyen el núcleo ni el objetivo de esta tesis. Son simplemente útiles para establecer un lenguaje común y para ofrecer al lector lego un espectro más amplio del tipo de marco conceptual al que nuestro trabajo pertenece. Un lector ya familiarizado con términos como qubit, estado EPR, desigualdad de Bell, etc., puede saltar directamente a la Sec. 1.2, donde describimos en más detalle cuáles son los problemas específicos que hemos estudiado. Además de los problemas motivados por la comunicación cuántica, la dinámica del enredo electrónico ha dado lugar al estudio de otra serie de problemas interesantes dentro del campo de la materia condensada, a los que hacemos referencia en la Sec. 1.3. Concluimos esta introducción con la Sec. 1.4, donde describimos la estructura de esta memoria de tesis.

E.2 Algunos conceptos básicos de la teoría de Información Cuántica

En esta sección presentaremos algo del trasfondo histórico y algunas definiciones del campo de la QI. Esto no pretende ser una lista exhaustiva ni una descripción formal de los diferentes temas, sino un modesto resumen de los conceptos fundamentales que pueden ayudar al lector lego a hacerse una idea de la motivación y el argot de esta tesis. La mayor parte de las definiciones han sido tomadas de la Enciclopedia de Filosofía de Stanford, y de Wikipedia (la enciclopedia libre de Internet), en algunos casos de forma literal.

E.2.1 La paradoja Einstein-Podolsky-Rosen

La mecánica cuántica es probablemente una de las teorías más bellas y experimentalmente exitosas de la historia de la Ciencia, pero también una de las más antintuitivas y desconcertantes para el razonamiento humano, ya que parece violar

algunos de los principios fundamentales de la física clásica a los que estamos tan acostumbrados. Al final de los años 20 un grupo de físicos, que incluía a N. Bohr, W. Heisenberg y M. Born, hizo una propuesta sobre cómo interpretar el formalismo matemático de la mecánica cuántica basada en su estudio de la física de los átomos. Algunos de los conceptos que barajaron fueron que la función de onda no debe ser interpretada como un objeto real, sino como una herramienta matemática cuyo único significado físico es el de que nos permite calcular probabilidades para las medidas. Además, los resultados de las medidas son probabilísticos no porque reflejen nuestro conocimiento limitado de algunas propiedades de los sistemas cuánticos, sino porque la naturaleza de la medida es indeterminista de forma fundamental. También discutieron el problema de la medida, afirmando que el acto de medir causa un "colapso de la función de onda" inmediato. Este primer intento general de formular la correcta interpretación de la mecánica cuántica sería conocido como la *interpretación de Copenhagen* [9–11].

En la mecánica clásica el estado de un sistema puede ser descrito especificando un conjunto de parámetros, como por ejemplo la posición y el momento de todas las partículas que forman el sistema. La evolución de este sistema se puede calcular de acuerdo con ciertas leyes deterministas, de tal manera que es posible conocer el valor de todos esos parámetros en un tiempo futuro, y por tanto caracterizar las propiedades del sistema completamente. Pauli denominó a esta manera de describir un sistema la idealización del "observador separado". En el marco de la interpretación de Copenhagen tal descripción no es posible en el caso de sistemas cuánticos. En su lugar, el estado cuántico debe ser descrito teniendo en cuenta no sólo las propiedades del sistema, sino también la presencia o acción que ejerce un observador sobre él, y los resultados de lo que ha sido observado en el pasado [11].

En 1935 A. Einstein, que rechazaba la interpretación ortodoxa de Copenhagen de la mecánica cuántica, publicó un artículo junto con sus dos estudiantes postdoctorales B. Podolsky y N. Rosen, titulado "Puede Considerarse Completa una Descripción Mecano-Cuántica de la Realidad Física?" [12]. En la versión moderna de este experimento mental, dos observadores, denominados habitualmente en nuestros días como Alice y Bob (o A y B), realizaban medidas independientes de spin sobre un par de electrones en un estado singlete de spin. Según su razonamiento, una vez hubiera medido Alice su spin en cierta dirección, la medida que pudiese realizar Bob en el suyo en la misma dirección quedaba determinada con certeza, mientras que justo antes de la medida de Alice el resultado de Bob sólo estaba determinado estadísticamente. Por tanto, o bien los efectos de la medida podrían viajar de Alice a Bob de manera instantánea, o bien la descripción mecano-cuántica de dichos spines era una caracterización incompleta de los mismos. Para evitar "efectos a distancia" no locales e instantáneos, concluyeron que deberían existir en la naturaleza ciertos parámetros microscópicos no incluidos en la teoría que causarían correlaciones entre las partículas. A estos parámetros extra se los llaman en ocasiones *parámetros ocultos* o *variables ocultas* (aunque ellos no usaron esta terminología). Rápidamente su artículo se con-

virtió en una pieza central en el debate sobre la interpretación de la teoría cuántica, y sería conocido como la paradoja Einstein-Podolsky-Rosen (EPR) [13].

E.2.2 Desigualdades de Bell

Después de la aparición del artículo EPR la credibilidad de la mecánica cuántica quedó en una posición delicada, pues parecía que o bien era incompleta en el sentido de que no podía describir algunos elementos de la realidad física, o que violaba el principio de la velocidad de propagación finita de efectos físicos. En aquel momento la mayoría de los físicos atribuyeron las características desconcertantes del enredo cuántico al inapropiado punto de vista de "observador separado" de Einstein, y dejaron la cuestión de lado. Esto fue desafortunado, pues el estudio del enredo fue ignorado durante treinta años, hasta que aparecieron las reconsideraciones y extensiones del argumento EPR por parte de Bell en 1964 [14].

Bell volvió a abrir el debate sobre los cimientos de la mecánica cuántica examinando el problema del enredo en sistemas más simples que el caso EPR: él consideró correlaciones entre cantidades observables bivaluadas, como la polarización o el spin, de dos sistemas separados en un estado enredado. Derivó una desigualdad basada en las suposiciones de Einstein de "localidad" y "realismo", que expresó en términos de probabilidades de distribución conjuntas de los resultados de medidas realizadas simultáneamente en las dos partes separadas del sistema enredado. Estas medidas se repetían para diversas orientaciones de los aparatos de medida (por ejemplo, distintos ángulos de los polarizadores). De esta forma, Bell mostró que las correlaciones estadísticas cuánticas entre probabilidades en direcciones de los detectores distintas conllevan a la violación de la desigualdad. Esto puede ser resumido en el así llamado teorema de Bell: "Ninguna teoría física local de variables ocultas puede jamás reproducir todas las predicciones de la mecánica cuántica". La desigualdad de Bell es por lo tanto una herramienta o 'test' para distinguir entre correlaciones clásicas y correlaciones cuánticas a través de la comparación de correlaciones en direcciones distintas [15].

Los experimentos del 'test' de Bell hasta la fecha han mostrado que, de hecho, las desigualdades de Bell se violan. Esto proporciona evidencia experimental contra el realismo local y prueba la validez de la mecánica cuántica. Además, el principio de relatividad especial queda a salvo porque, aunque las dos partículas enredadas parecen estar interaccionando a través de un intervalo espacio-tiempo, no viaja información útil entre ellas, así que la causalidad no puede ser violada a través del enredo. La razón por la que es imposible que Alice pase información a Bob (o viceversa) más rápido de la velocidad de la luz tiene que ver con el *teorema de no clonación*, formulado por Wootters, Zurek y Dieks en 1982. Este teorema prohibe la creación de copias idénticas de un estado arbitrario "desconocido" sin perturbarlo. Si Alice y Bob comparten un estado enredado y fuera posible que Bob clonase su qubit varias veces, entonces Alice podría enviar bits de información de la siguiente forma. Si Alice quisiera enviar un

"1", mediría su partícula en la dirección z, colapsando de este modo el estado de Bob a spin arriba o spin abajo. Si quisiera enviar un "0", dejaría su partícula sin tocar. Por su lado, Bob crearía múltiples copias de su qubit y mediría el spin de cada una de las copias en la dirección z. Si todas sus medidas dieran el mismo resultado, él sabría de forma segura que Alice había medido su spin, obteniendo el bit de información "1". Si la mitad de las veces midiera spin arriba y la otra mitad spin abajo, Alice le habría enviado un "0". Pero el hecho es que, debido a la existencia del teorema de clonación, la inspección estadística de los estados cuánticos enredados es imposible [2, 16].

E.2.3 Información cuántica

El estudio general de las capacidades de proceso de información de los sistemas cuánticos es el tema de la teoría de QI [17]. Por definición, la información cuántica es información que hay almacenada en el estado de un sistema cuántico. Dos sistemas cuánticos en un estado enredado pueden ser utilizados como un canal de información cuántica para realizar tareas que son imposibles clásicamente. Por ejemplo, si Alice y Bob comparten dos partículas, que llamamos I (a la de Alice) y II (a la de Bob), en un estado *máximamente* enredado, Alice podrá transferir el estado exacto de una tercera partícula en su poder, digamos, por ejemplo, un átomo en un estado complejo que ella desconoce, a la partícula II de Bob, que está a una distancia arbitrariamente lejana. Para conseguirlo Alice tiene que realizar una *medida de Bell* sobre el átomo que desea "teleportar" y su partícula I del par enredado. Tras hacer esta medida el átomo habrá perdido su estado inicial, pero la información de dicho estado no habrá sido destruida, sino que habrá sido transmitida a la partícula II en virtud de su enredo inicial, aunque no de forma completa. Para completar el proceso Alice tendrá que comunicarle a Bob el resultado de su medida de manera clásica (por ejemplo mediante una llamada de teléfono), para que Bob pueda realizar una operación unitaria sobre su partícula. Hecho esto obtendrá el estado deseado. Este fenómeno es conocido como *teleportación cuántica* [18]. En 1993 C. H. Bennett et al. propusieron un método que podría en principio usarse para teleportar un objeto [19]. Este método fue verificado experimentalmente por D. Bouwmeester et al. en 1997 usando fotones [20]. También es posible usar pares enredados en *criptografía cuántica*, donde el enredo se utiliza para transmitir señales que son imposibles de espiar sin dejar trazas.

La información cuántica difiere de la clásica en diversos aspectos. Por ejemplo, no puede ser leída ni duplicada sin provocar perturbaciones (teorema de no-clonación). Es más, dado que un sistema puede estar en una superposición de varios estados simultáneos, es posible procesar información cuántica de forma "paralela", i.e., de manera exponencialmente más eficiente que la información clásica. Esto permite realizar algunas tareas difíciles de manera "eficiente", esto es, en un tiempo que crece polinómicamente con el tamaño del problema. Por el contrario, estas tareas serían ineficientes en un contexto clásico, por requerir un tiempo de cálculo que crecería exponencialmente con la complejidad del problema. Por otro lado, la información cuántica

no puede ser recuperada completamente mediante medidas de qubits o cualquier otro método. Por tanto, este *paralelismo* masivo de la computación cuántica sólo puede ser explotado mediante el uso de algoritmos inteligentes, adaptados a las peculiaridades de las leyes cuánticas.

La información cuántica, y los cambios en la información cuántica, pueden ser cuantificados mediante un análogo cuántico de la entropía clásica de Shannon, que es la entropía de Von Neumann [17].

E.2.4 Qubit and ebit

La unidad básica de información cuántica es el bit cuántico o *qubit*, que representa la cantidad de información que puede almacenarse en un sistema cuántico de dos niveles. El término se debe a Schumacher (1995) [21]. El espacio de estados de un sólo qubit puede representarse geométricamente mediante la superficie bidimensional de una esfera. Esto significa básicamente que el qubit tiene dos grados de libertad locales. De manera equivalente un registro de n qubits habita un espacio que tiene (más o menos) 2^n grados de libertad continuos. Por el contrario, el espacio de configuraciones de un registro clásico análogo es estrictamente discreto, y por tanto infinitamente más pequeño.

En el estado de un solo qubit se puede codificar una cantidad arbitrariamente grande de información clásica. Esta información puede ser procesada y comunicada pero, por las peculiaridades de la medida cuántica, el volumen de información que puede ser recuperado de un sólo qubit es igual a un bit. Es en el procesado de la información (computación cuántica) donde reside la diferencia.

Una característica importante que distingue a un qubit de un bit clásico es que múltiples qubits pueden exhibir enredo cuántico. Se dice que dos qubits en dos puntos espaciales separados A y B están enredados cuando su estado no puede ser preparado como un estado producto del qubit en A y del qubit en B mediante operaciones locales en cada qubit y comunicación clásica de bits de información entre ellos. Dos qubits en un estado *máximamente* enredado se conocen como un bit enredado, o *ebit*. Los cuatro estados enredados básicos puros que forman la base de Bell son:

$$|\Psi_{Bell_1}\rangle = \frac{1}{\sqrt{2}}\left(|\uparrow\rangle_A|\downarrow\rangle_B - |\downarrow\rangle_A|\uparrow\rangle_B\right), \tag{E.1}$$

$$|\Psi_{Bell_2}\rangle = \frac{1}{\sqrt{2}}\left(|\uparrow\rangle_A|\downarrow\rangle_B + |\downarrow\rangle_A|\uparrow\rangle_B\right), \tag{E.2}$$

$$|\Psi_{Bell_3}\rangle = \frac{1}{\sqrt{2}}\left(|\uparrow\rangle_A|\uparrow\rangle_B - |\downarrow\rangle_A|\downarrow\rangle_B\right), \tag{E.3}$$

$$|\Psi_{Bell_4}\rangle = \frac{1}{\sqrt{2}}\left(|\uparrow\rangle_A|\uparrow\rangle_B + |\downarrow\rangle_A|\downarrow\rangle_B\right), \tag{E.4}$$

donde las flechas $\uparrow, \downarrow$ representan, por ejemplo, el estado de spin arriba y el estado de spin abajo de un electrón. Un ebit también es la cantidad de información que

necesitaremos intercambiar entre dos qubits en A y B para colocarlos en un estado enredado.

El enredo es un ingrediente necesario de cualquier ordenador cuántico que no puede ser simulado eficientemente en un ordenador clásico. Una posible explicación del poder de la computación cuántica es que, mediante el enredo, el estado total de un ordenador cuántico mientras realiza una operación es una superposición de múltiples operaciones clásicas, todas ellas desarrollándose de manera simultánea.

E.2.5 Ordenadores cuánticos

Un ordenador cuántico (OC) [1, 22] es cualquier dispositivo físico que hace uso directo del enredo para realizar operaciones sobre datos. Por esta propiedad, los OC prometen un gran incremento en la eficiencia para resolver algunos problemas respecto de las posibilidades de ordenadores clásicos. Uno de estos problemas es la *factorización de números enteros*. Si un número consta de n bits (tiene n dígitos en su representación binaria), entonces un ordenador cuántico con poco más de 2n qubits puede usar el algoritmo de Shor (1994) para descomponerlo en números primos. Otro problema similar es el de los *logaritmos discretos*. Esta habilidad propia de los OC permitiría le decodificación de muchos de los sistemas criptográficos actualmente en uso, en el sentido de que existiría un algoritmo relativamente rápido (tiempo polinómico en n) para resolver tal problema. Otro problema interesante que sólo se podría resolver con un OC fue propuesto por Richard Feynman en 1982 [23]. Es el de la *simulación de la dinámica de sistemas cuánticos*. Actualmente solo se sabe de la dramática ventaja de los OC en estos tres problemas: factorización, logaritmos discretos, y la simulación de sistemas cuánticos. Aún así, no existe demostración de que la ventaja sea real: todavía es posible que se pueda descubrir un algoritmo clásico igualmente rápido, aunque se considera poco probable. Existe un problema más donde un OC tiene una ventaja (cuadrática) más pequeña, aunque aún significativa. Es el de búsquedas cuánticas en bases de datos, y puede resolverse mediante el *algoritmo de Grover*. En este caso la ventaja es demostrable. Esto establece más allá de toda duda que un ordenador cuántico (ideal) sería potencialmente superior a los ordenadores clásicos [22].

Uno de los mayores desafíos actualmente es el de implementar los elementos computacionales cuánticos básicos en un sistema físico y demostrar que pueden ser controlados de manera fiable y escalable. Ya se han realizado experimentos en los que se ejecutaron operaciones computacionales cuánticas con un número muy pequeño de qubits. En particular, en 2001 I. L. Chuang y su grupo realizaron el más complejo cálculo cuántico del mundo hasta la fecha, la factorización del número 15 usando el algoritmo de Shor en un ordenador cuántico de 7 qubits [24].

Cómo funciona un ordenador cuántico

Un ordenador clásico tiene una memoria hecha de bits, donde cada bit contiene un uno o un cero. Este dispositivo calcula manipulando estos bits, esto es, transportándolos de la memoria a *puertas lógicas* y viceversa. Por "puertas" se entiende un conjunto de transformaciones que constituyen el cálculo. La misma filosofía se aplica a un OC, pero con ciertas diferencias. En primer lugar, el OC contiene un conjunto de qubits. Como ya hemos mencionado, un qubit albergará un uno, un cero o una superposición cualquiera de ellos. Por tanto si tenemos en memoria un registro de n qubits, el estado total del OC es una superposición de hasta 2^n estados, cada uno de ellos clásicamente equivalente una sola ristra de n 1's y 0's. Igual que antes, un OC calcula mediante la manipulación de estos qubits, pero ahora los transporta de la memoria a *puertas lógicas cuánticas* y viceversa. Las puertas lógicas cuánticas actúan sobre los qubits mediante la aplicación de transformaciones unitarias (reversibles). Además trabajan con superposiciones, de manera que pueden realizar múltiples operaciones lógicas a la vez. Por motivos prácticos es conveniente elegir conjuntos de puertas cuánticas *universales*. Éstas son grupos de puertas con las cuales se puede realizar cualquier operación, o al menos aproximarla con tanta precisión como se desee. Un conjunto tal nos permitiría realizar operaciones arbitrarias sin tener que inventar un nuevo tipo de puerta cada vez. Puede demostrarse que todas las operaciones cuánticas unitarias sobre un registro de n-qubits que uno pueda imaginar pueden implementarse mediante combinaciones de una puerta unitaria sobre qubits individuales (rotación) y una puerta de dos bits de negación condicionada C-NOT. El concepto de un ordenador cuántico universal fue propuesto por primera vez en 1985 por D. Deutsch. Otra importante diferencia respecto de un ordenador clásico es que los cálculos cuánticos son probabilísticos. En un OC, al final del cálculo se realiza una medida sobre el registro de n-qubits. Por las leyes de la mecánica cuántica, esta medida resultará en una secuencia aleatoria de n-bits, y además destruirá el estado almacenado. Para poder utilizar un OC para hallar la solución de cierto cálculo, el diseño del algoritmo tiene que ser tal que la distribución de probabilidad de las medidas esté picada en torno a la solución correcta. Por tanto, para obtener la solución a un problema, en general uno tiene que repetir el cálculo varias veces y elegir el valor que resulte con mayor probabilidad.

Requisitos de un ordenador cuántico

Existen ciertos requerimientos para una implementación exitosa de un OC. D. DiVincenzo hizo una lista con los siguientes requisitos para un OC práctico [22, 26]:

- los qubits deben poder inicializarse a valores arbitrarios,
- las puertas lógicas deben operar más rápido que el tiempo de decoherencia,
- debe existir un conjunto universal de puertas lógicas,

- los qubits deben poder leerse fácilmente, y
- debe ser escalable, esto es, debe poderse agrandar el sistema hasta contener n-qubits sin dejar de cumplir los requisitos anteriores

Aparte de estos cinco criterios para un OC, existen dos criterios de conectividad en red de OCs, que son dos "desiderata" necesarias para realizar tareas de comunicación cuántica [8]. Éstas son:

- la habilidad de convertir qubits estacionarios en qubits volantes y al revés, y
- la habilidad de transmitir fielmente qubits volantes entre lugares específicos.

Propuestas para ordenadores cuánticos

Desde distintos campos de investigación se han propuesto diferentes tipos de dispositivos para ser usados como el hardware de un OC. A continuación se mencionan algunos de ellos:

- OC de iones atrapados → La primera propuesta de usar estos sistemas vino de manos de J. I Cirac y P. Zoller en 1995 [27]. Los iones, o partículas atómicas cargadas, pueden confinarse y suspenderse en el espacio libre usando campos electromagnéticos. Se dice entonces que los iones quedan atrapados en una especie de "trampa" magnética. Los qubits se almacenan en estados electrónicos estables de cada ion, y la información cuántica se puede procesar y transferir mediante el movimiento cuantizado colectivo de los iones en la trampa (que interaccionan mediante la fuerza de Coulomb). Se aplican láseres para inducir acoplos entre los estados de un qubit (para realizar operaciones a un solo qubit), o para inducir acoplos entre los estados internos de un qubit y los estados de movimiento externos (para crear enredo entre qubits). Las operaciones fundamentales de un OC ya se han demostrado experimentalmente con alta precisión en sistemas de iones atrapados, y se ha desarrollado una estrategia para escalar el sistema a un número arbitrariamente grande de qubits mediante el transporte rápido de iones dentro de una matriz de trampas de iones. Aún así, los ordenadores basados en estos sistemas tienen su velocidad limitada por la frecuencia de vibración de los modos de la trampa.
- OC basados en electrodinámica cuántica de cavidades → Para realizar un OC de este tipo se necesita una interacción coherente entre un qubit material (tal como un átomo atrapado o un punto cuántico semiconductor) y el campo cuantizado (normalmente de un solo fotón) de un resonador óptico o de microondas. Para alcanzar una dinámica coherente con un solo fotón y un átomo se emplea una cavidad pequeña, con pérdidas extremadamente bajas, que permita incrementar el campo eléctrico por fotón de manera que la frecuencia de Rabi coherente de la

interacción átomo-campo sea más rápida que la tasa de emisión espontánea del átomo y la tasa de decaimiento del campo en la cavidad. La primera propuesta de este tipo la realizó P. Domokos et al. en 1995 en la que se empleaban átomos de Rydberg en cavidades de ondas milimétricas superconductoras [28].

- OC basados en resonancia magnética nuclear (RMN) de moléculas en disolución → Los spines nucleares de moléculas en disolución pueden servir como qubits. Estos spines pueden interaccionar entre sí, programarse mediante pulsos de radiofrecuencia y detectarse mediante instrumentos de RMN similares a los habitualmente empleados en hospitales y laboratorios químicos. La primera propuesta de este tipo de sistemas vino de A. Gershenfeld y I. L. Chuang en 1997 [29]. Como resultado de diversos experimentos notables, la RMN se ha alzado como el componente más popular de la arquitectura de hardware cuántico. Sin embargo, los dispositivos de RMN sufren de una atenuación exponencial de la señal sobre ruido según crece el número de qubits del sistema.

- OC basados en superconductores (bien sea en carga o en flujo) → Las implementaciones de estado sólido de un OC serían un logro muy deseable, en particular en sistemas electrónicos nanométricos, ya que se podrían fácilmente integrar en circuitos electrónicos y así escalarlos hasta alcanzar el gran número de qubits necesarios para cálculos útiles. Entre las primeras propuestas de computación cuántica en estado sólido se encuentra la de qubits basados en uniones Josephson, propuesta por A. Shnirman, G. Schön y Z. Hermon en 1997 [30–32]. En esta propuesta existen dos clases de dispositivos, uno de ellos basado en el grado de libertad de la carga y el otro en el de fase (flujo). Las operaciones cuánticas de uno o dos qubits pueden controlarse mediante potenciales de puerta en un caso y mediante campos magnéticos en el otro. Ambos tipos de dispositivos pueden fabricarse con la tecnología existente. Existen dos problemas fundamentales que deben resolverse para que estos dispositivos puedan usarse para procesar información cuántica, el tiempo de decoherencia y la medida del estado final del sistema [31, 32].

- OC basados en el spin electrónico en puntos cuánticos → En 1998 D. Loss y D. P. DiVincenzo abrieron el campo de la computación cuántica basada en spines con la propuesta de usar como qubit el spin de un electrón atrapado en un punto cuántico [8, 33]. Para implementar las puertas lógicas de dos qubits esta propuesta se basa en la interacción de Coulomb que existe entre estos qubits de spin ya que, además de spin, poseen carga. El mayor problema de esta propuesta es la decoherencia de este tipo de qubits debido a interacciones con el entorno.

- OC ópticos → Una de las primeras propuestas para computación cuántica se basó en la utilización de los modos ópticos de un fotón para implementar un

qubit. El atractivo de esta propuesta radica en la facilidad con que es posible observar la interferencia de fotones. Pero la necesidad de interacción qubit-qubit para realizar puertas lógicas a dos qubits supone un gran desafío ya que los fotones no interacccionan directamente; medios ópticos no lineales pueden hacer de mediadores de la interacción fotón-fotón, pero resulta técnicamente difícil conseguir que estos materiales operen con la suficiente intensidad. Sin embrago, E. Knill et al. demostraron en 2001 que era posible construir un ordenador cuántico eficiente mediante óptica lineal, usando sólo divisores de haces, desfasadores, fuentes de fotones individuales y fotodetectores. Este método emplea la retroalimentación de los fotodetectores, y es robusto contra errores por pérdida de fotones e ineficiencias de los detectores [34]. Aún así, por el momento los ordenadores de fotones libres son sólo casi determinísticos (es decir, las puertas lógicas operan con menos de un 100% de éxito).

- OC de electrones libres → Las interacciones qubit-qubit son, en principio, un ingrediente crucial para la computación cuántica. La mayor parte de las propuestas y experimentos se apoyan en interacciones controladas qubit-qubit para implementar puertas lógicas universales de dos qubits. Sin embargo, Beenakker et al. [35] demostraron en 2004 que, con la utilización de medidas proyectivas junto con rotaciones de spines individuales sobre qubits electrónicos volantes, se puede alcanzar una computación cuántica eficiente y determinista. De esta forma no se requiere interacciones qubit-qubit, y se consigue computación cuántica mediante electrones libres. Para salvar cierto teorema que parecía prohibir la computación cuántica eficiente con electrones libres, estos autores aprovecharon el hecho de que las medidas de carga no afectan al qubit de spin. Sin embargo, esta propuesta, que incluye divisores de haces que polarizan el spin, no está aún al alcance de la tecnología experimental actual.

E.2.6 Decoherencia

Para que funcione un OC es necesario que las operaciones que realizan las puertas lógicas durante cada cálculo sean unitarias, es decir, reversibles. Por otro lado, los estados que se usan habitualmente como input de estas puertas deben llegar a ellas de manera efectiva en una superposición de estados concreta o en un estado enredado. Sin embargo, en el mundo real hay interacciones que destruyen el estado coherente en que deben permanecer los componentes de un OC para realizar dichas operaciones. En general, es muy difícil aislar estos dispositivos de las fuentes de decoherencia extrínsecas e intrínsecas, y por el momento los OC sólo han logrado resolver problemas triviales. Los tiempos de decoherencia para los sistemas típicos propuestos como candidatos a la computación cuántica van desde los nanosegundos a los segundos. Es necesario para que un cálculo termine con éxito que el tiempo necesario para realizarlo sea mucho menor que el tiempo de decoherencia, al menos si no se recurre

a la *corrección cuántica de errores*. La *tasa de error* se define precisamente como la razón del tiempo de operación sobre el tiempo de decoherencia. Si la tasa de error es suficientemente baja, es posible usar corrección cuántica de errores, que corrige errores debidos a la decoherencia. Una cifra muy citada (aunque algo arbitraria) para la tasa de error máxima en cada puerta es 10^{-4}. Esto implica que cada puerta debe poder realizar su operación 10000 más rápido que el tiempo de decoherencia del sistema [22].

E.3 Los problemas tratados en esta tesis

Como ya he hemos mencionado al principio de esta introducción, en los últimos siete años ha habido una actividad frenética dentro del campo de los qubits volantes en estado sólido. El estudio de la creación y medida de partículas enredadas no localmente ha atraído el interés de los físicos por su potencial uso en tareas de comunicación cuántica, como teleportación cuántica o criptografía cuántica. Además, ya existe una propuesta en la literatura [35] para construir un ordenador cuántico con qubits volantes mediante usando electrones libres. Aquí describiremos nuestra contribución al campo junto con algunas propuestas previas que han motivado nuestro trabajo y nuevas ideas de otros grupos.

E.3.1 Generación de enredo no local en dispositivos de estado sólido

Un enredador es un dispositivo que funciona como una fuente de estados enredados de forma no local. Recientemente ha habido un gran número de propuestas para construir dicho dispositivo en un medio de estado solido:

Una posibilidad es usar un superconductor convencional como una fuente natural de pares de electrones con enredo de spin que pueden ser inyectados en metales normales o ferromagnéticos [36–57]. Para obtener la separación espacial necesaria de los dos electrones al extraerlos del superconductor se han propuestos diversos mecanismos, como filtros de energía y de spin [41, 46, 49], puntos cuánticos dobles [38, 49,53], el uso de líquidos de Luttinger como terminales [45,47] o el bloqueo de Coulomb de terminales de resistencia finita [50]. El mecanismo que nosotros proponemos, como mostraremos más adelante, es un filtro angular [54].

Aparte del uso de superconductores, se han propuesto muchos otros mecanismos para generar estos pares EPR: mediante el uso de impurezas magnéticas [58], a través de un punto cuántico [59], mediante biexcitones en puntos cuánticos dobles [60], usando puntos triples [61], mediante la utilización de puntos cuánticos caóticos [62], a través de la dispersión Coulomb entre electrones en un gas bidimensional [63] o entre qubits estáticos y volantes en un nanotubo de carbono [64, 65], usando pulsos de voltaje [66], mediante osciladores nano-mecánicos [67] o por combamiento de

nanobarras [68].

Existe un grupo dentro del conjunto de mecanismos para generar pares de qubits enredados que no requiere de interacciones (en los mecanismos recién expuestos había siempre algún tipo de interacción electrón-electrón, como el apareamiento mediado por fonones en el superconductor, o la interacción de Coulomb en el punto cuántico, etc.). En ausencia de interacciones sigue siendo posible enredar el grado de libertad de spin [69–71], o el orbital [62, 72–74]. Véase la Ref. [75] para una recopilación reciente de los trabajos sobre enredo de electrones y huecos libre de interacciones.

Como explicamos a continuación, en esta tesis nosotros nos hemos concentrado en el estudio de superconductores como fuentes de pares enredados. En nuestro caso el grado de libertad que se enreda es el spin. El enredo de spin es mucho menos sensible a la decoherencia que el enredo orbital, sencillamente porque la gran mayoría de grados de libertad ambientales se acoplan al grado de libertad orbital en lugar de al spin.

Nuestras propuestas

Hemos estudiado dos tipos de enredadores en los que la fuente de pares enredados no localmente es un superconductor convencional BCS.

En el primer trabajo [51], que se describe en detalle en el Capítulo 2, nos motivó el artículo de 2001 de Recher, Sukhorukov y Loss [38]. En él investigamos teóricamente la emisión simultánea de dos electrones desde un superconductor tridimensional (3D) a dos metales normales diferentes a bajas temperaturas y voltajes (a este proceso se le suele llamar "reflexión Andreev cruzada"). Estos electrones, que forman un par de Cooper dentro del superconductor, pierden las correlaciones superconductoras cuando saltan a los metales normales (ignoramos el efecto de proximidad), pero el enredo de singlete de spin entre ellos permanece cuando alcanzan los dos cables metálicos separados, constituyendo así un ebit de información. Para describir la corriente túnel a través de una interfaz de tamaño finito como es la formada entre el superconductor 3D y los contactos distantes conectados al mismo, obtuvimos un Hamiltoniano de túnel local que depende de las derivadas normales de los campos electrónicos en cada electrodo (en lugar del habitualmente usado pero erróneo que es proporcional a los campos). Hallamos que, como función de la distancia r entre los contactos, la corriente enredada se ve truncada por un decaimiento exponencial con la longitud de coherencia del superconductor [38], y adicionalmente modulada por un prefactor geométrico ($\sim 1/r^4$) que hace que la probabilidad de extraer pares enredados decaiga muy rápido a escalas de la longitud de onda de Fermi. Por tanto, en este trabajo concluimos que el requisito de separación física entre los contactos con el superconductor supone una limitación severa en la práctica. Hacemos notar que, si los elementos de matriz de túnel se toman independientes del momento [38], entonces el factor geométrico decae más indulgentemente con la distancia ($\sim 1/r^2$). Ha habido algunas ideas en la literatura tratando de mejorar este prefactor de decaimiento. Dentro del contexto de

modelos de túnel independientes del momento, la ley de potencias cambia si el superconductor tiene baja dimensionalidad (d) [45, 49], o si es difusivo [48, 52], resultando en un prefactor r^{-d+1} y r^{-1}, respectivamente. Resta por indagar cómo cambia este comportamiento cuando se usan elementos de matriz de túnel más realistas.

Para superar las dificultades causadas por la necesidad de emitir el par de electrones enredados desde puntos distantes, proponemos un montaje experimental distinto [54], analizado en detalle en el Capítulo 3, en el que el emisor es de nuevo un superconductor BCS. La idea detrás de esta propuesta es la transmitir los electrones a través de la misma región espacial pero induciéndolos a abandonarla en direcciones distintas. Para logarlo proponemos el uso de resonancias normales y Andreev en estructuras normal-superconductor. Los niveles resonantes se ajustan para transmitir selectivamente electrones con valores específicos del momento perpendicular a la interfaz, fijando de esta manera el ángulo de salida. Cuando el metal normal es un gas electrónico bidimensional (2DEG) balístico, el mecanismo propuesto garantiza una separación espacial arbitraria de los haces de electrones emitidos desde una interfaz finita. Realizamos un estudio cuantitativo de las propiedades de transporte lineal y no lineal en algunas estructuras convenientes, teniendo en cuenta la gran diferencia de masas efectivas y longitudes de onda de Fermi entre ambos metales. Estimaciones numéricas confirman la viabilidad del método de separación de haces que proponemos. Más aún, el tipo de estructuras necesarias para este tipo de dispositivo parecen al alcance de las posibilidades experimentales actuales [76, 77].

E.3.2 Evolución de estados enredados en nanoestructuras: decoherencia

En sistemas reales los electrones están irremediablemente acoplados a grados de libertad ambientales. Como resultado surge el 'dephasing', o pérdida de memoria de fase (término que usaremos normalmente si se conserva la energía), o la decoherencia (en general), por las cuales se reduce y finalmente se destruye el enredo. Es importante entender las consecuencias de este fenómeno.

En el caso de enredo de spin, la interacción de spin-órbita y la interacción hiperfina con spines nucleares resultan ser mecanismos efectivos de 'dephasing' y relajación. Véase la Ref. [8] para encontrar una recopilación sobre decoherencia de spines electrónicos atrapados en puntos cuánticos en el contexto de la propuesta Loss-DiVincenzo [33].

En el caso de enredo orbital, las fluctuaciones electromagnéticas causadas por otras cargas inducen decoherencia (o 'dephasing' si las flutuaciones son suficientemente lentas). Se han desarrollado diversos métodos fenomenológicos para tratar sus efectos en el transporte a través de conductores mesoscópicos. En la Refs. [73, 74, 78, 79] se simuló el efecto del 'dephasing' introduciendo en la matriz densidad del estado enredado un parámetro fenomenológico que suprimía sus elementos no diagonales.

En las Refs. [72, 80] el 'dephasing' se introdujo mediante un promedio sobre una distribución uniforme de factores de fase aleatorios acumulados en cada canal de borde en una barra Hall cuántica. En las Refs. [81, 82], que de hecho describen exactamente la radiación fuera del equilibrio que actúa sobre el sistema, el 'dephasing' era inducido por un potencial clásico fluctuante. En la Ref. [83] el 'dephasing' se trató como fluctuaciones aleatorias de la fase de modos propagantes a través del conductor. Estos dos últimos métodos se han aplicado recientemente a la estadística completa de conteo (FCS) en las Refs. [84, 85].

También es posible tratar la decoherencia de forma fenomenológica como efecto de la presencia de reservas adicionales ficticias o sondas de voltaje conectadas al conductor mesoscópico considerado. Este método, que simula el efecto de procesos inelásticos, fue introducido por Büttiker hace veinte años [86, 87]. La ventaja de este modelo reside en el hecho de que los procesos inelásticos de aleatorización de fase se implementan en un marco de dispersión elástica independiente del tiempo. Idealmente, una sonda de voltaje es un terminal con flujo neto de corriente nulo, es decir, cualquier electrón que abandona el conductor a través de la sonda se termaliza por disipación e inmediatamente se devuelve al conductor. Las primeras teorías [87] usaron esta sonda de voltaje disipativa como un medio simple para analizar la transición entre conducción cuántica coherente y el límite clásico de adición de resistencias en serie. Más tarde, se generalizó para incluir conservación instantánea de corriente [88]. Se descubrió que, teóricamente, la disipación en una sonda se puede suprimir imponiendo que cada electrón que salga de la sonda sea reemplazado por un electrón incidente desde la sonda a la misma energía [89, 90]. Una sonda de 'dephasing' tal puede servir como un modelo simple para describir el 'dephasing' en procesos de conducción mesoscópica. Por otro lado, es un buen modelo para una sonda real de voltaje con impedancia infinita, un componente habitual en muchos dispositivos mesoscópicos.

Las sondas de voltaje y de 'dephasing' también juegan un importante papel en la investigación del ruido y las correlaciones de corriente en conductores mesoscópicos [85, 88–94]. La validez del modelo se ha discutido extensamente (véase Ref. [95] para una recopilación), encontrando en general un buen acuerdo cualitativo con modelos microscópicos [96–99] y experimentos [100, 101], aunque en ciertos sistemas falle a un nivel cuantitativo [82]. Recientemente se demostró que esta aproximación se volvía equivalente a técnicas de promediado de fase a nivel de la FCS en ciertos límites y sistemas [102]. Por otro lado, últimamente se ha usado para modelar dispersión con volteo de spin y decoherencia en puntos cuánticos caóticos [103, 104].

En cualquier caso, el problema de cómo aplicar tal modelo de decoherencia al caso especialmente interesante de corrientes de entrada enredadas de manera no local no ha sido discutido previamente hasta donde hemos podido comprobar. Es esto lo que nosotros hemos hecho [93, 94] y lo que resumimos a continuación.

Modelo fenomenológico para dispersión inelástica

En la Ref. [93] hemos tratado el efecto de la dispersión inelástica, producida por la presencia de reservas ficticias adicionales [86, 87], sobre un par de estados electrónicos enredados y sus consecuencias en relación con la detección del enredo. Hemos parametrizado la decoherencia mediante una probabilidad de dispersión inelástica α que afecta tanto al grado de libertad de spin como al de energía. Sin embargo, en este trabajo, presentado en el Capítulo 4, no consideramos conservación instantánea de la corriente que entra y sale de la reserva externa, sino que sencillamente fijamos su promedio a cero. En este sentido no estamos considerando una sonda de voltaje verdadera, ya que por definición debería tener una impedancia infinita, y por tanto una corriente neta instantáneamente nula.

Hemos resuelto este problema en la Ref. [94], donde desarrollamos una modificación del modelo de sonda ficticia que lo generaliza para incluir conservación instantánea de corriente en presencia de estados entrantes con enredo arbitrario. Nuestra generalización está diseñada con el objetivo de calcular la FCS de un conductor mesoscópico genérico y, mediante el uso de una sonda de voltaje distinta para cada valor del spin, conservamos el spin pero no la energía tras la dispersión. Se describe en detalle este problema en el Capítulo 5. Añadiremos en cualquier caso aquí que, en nuestro método, hay implícita una aproximación de dispersión secuencial. Si quisiéramos describir sólo 'dephasing', es decir, pérdida de memoria de fase sin intercambio de energía, entonces el problema sería de dispersión elástica y las diferentes energías se desacoplarían, pudiendo tratar cada energía por separado. Pero en presencia de dispersión inelástica esto ya no es posible. Para tratar este problema, en lugar de una representación de energías, lo que hicemos es emplear la representación de paquetes de onda en la cual los electrones llegan localizados a la sonda de voltaje en tiempos fijos. En este lenguaje, un electrón que en ausencia de dispersión inelástica llegaría a un detector en un tiempo τ_i, en presencia de dispersión inelástica se retrasa y llega en un tiempo posterior $\tau_i + \delta t$, lo cual es equivalente a una relajación de energía. Por otro lado, en nuestra aproximación ignoramos el solape de los paquetes de onda, es decir, dividimos el tiempo en intervalos de duración Δt de tal modo que cada grupo de partículas se dispersan completamente a través del sistema antes de que llegue el siguiente. Sugerimos que las contribuciones debidas al solape son despreciables en el límite de tiempos de medida largos. No demostramos esta afirmación, sólo la justificamos obteniendo con nuestro método en una serie de sistemas sin enredo incidente las mismas expresiones analíticas para la corriente y todos sus cumulantes (para la función característica) que las que se obtienen mediante un tratamiento semiclásico tipo Langevin. La dispersión inelástica se implementa en nuestro modelo a través de la memoria de cada evento que queda almacenada en un contador cuántico Q que incluimos en la sonda de voltaje, y que simula la relajación de carga. Funciona de tal modo que tiende a contrarrestar el exceso o déficit de carga que adquirió la sonda durante el evento anterior. De este modo, el contador correlaciona un intervalo de

tiempo Δt con el siguiente, y así sucesivamente. Con este modelo tratamos de describir la dispersión inelástica inducida sobre los electrones por un baño disipativo externo (no por la interacción electrón-electrón).

E.3.3 Detección del enredo

Aparte del tema de su generación, otro punto crucial es el de la detección del enredo. Mediante el uso de un divisor de haces, el enredo se puede detectar analizando cantidades como el ruido de la corriente [105–107] o cumulantes de mayor orden (FCS) [94, 108]. Más aún, la presencia de enredo puede detectarse analizando desigualdades de Bell y cantidades como la concurrencia [109], que se han expresado en términos de ruido a frecuencia cero de corrientes de spin y de carga [41, 46, 72, 73, 110–112]. La violación de una desigualdad de Bell implica que existen correlaciones cuánticas entre las partículas detectadas que no pueden ser descritas por ninguna teoría de variables ocultas. Con el mismo espíritu que ha sido hecho con el ruido, en la Ref. [113] se derivó una desigualdad de Clauser-Horne (CH) [1] [115, 116] para la FCS.

Desigualdad de Clauser-Horne y ruido de disparo en un divisor de haz

En las Refs. [93, 117] analizamos el efecto de la decoherencia en la violación de la desigualdad de CH, cuando ésta es expresada en términos de la FCS, en un conductor mesoscópico multiterminal. El sistema consiste en un enredador, que asumimos dado, que emite un flujo de electrones enredados en dos conductores caracterizados por una matriz de dispersión y sometidos a decoherencia (tal y como se describe en el apartado previo). Dado un cierto número promedio de electrones enredados emitidos, evaluamos la desigualdad de CH en función del número de partículas detectadas Q y de diversos parámetros de la matriz de dispersión. Mostramos cómo, cuando se conecta la decoherencia, la violación de la desigualdad de CH se ve reducida de forma efectiva. Una peculiaridad interesante que hallamos es la de la existencia, para ciertos parámetros del sistema, de una región protegida de valores de Q para los que la violación sobrevive para decoherencia arbitrariamente intensa. Este trabajo se presenta en el Capítulo 4.

En el Capítulo 5 presentamos los resultados de la Ref. [94], donde analizamos la robustez del método de detección de enredo mediante un divisor de haces propuesto en la Ref. [106], ante la presencia de dispersión inelástica que conserva el spin y de una probabilidad finita de retroceso para varios estados entrantes con enredo no local. Hallamos que, al diferencia del 'dephasing' elástico orbital [73], la acción de los procesos inelásticos en el divisor de haces no puede ser despreciada, ya que afectan

[1] Dada la condición $|x|, |x'|, |y|, |y'| \leq 1$, la llamada desigualdad CH (o CH74) se deriva a partir de la desigualdad algebraica $-1 \leq xy - xy' + x'y + x'y' - x' - y \leq 0$. En realidad, existe una jerarquía infinita de tales desigualdades tipo Bell, que básicamente se clasifican especificando el tipo de experimentos de correlación que involucran [114].

fundamentalmente al mecanismo físico del detector, que no es sino el hecho de que dos electrones con los mismos números cuánticos no pueden acabar ocupando el mismo canal cuántico (bloqueo de Pauli). Si la energía no se conserva, tal mecanismo de antiaglomeración ya no es perfecto, y el método de detección de enredo debe ser revisado. Sin embargo, encontramos que la detección de enredo mediante medidas de ruido de disparo sigue siendo posible incluso en condiciones muy laxas de imperfecciones en el dispositivo divisor de haces y en presencia de una dispersión inelástica considerable (hasta del 50%).

E.4 Otras motivaciones y contribuciones de esta tesis

Junto con la motivación central de esta tesis, que es la de estudiar problemas de comunicación cuántica en dispositivos de estado sólido, nos hemos enfrentado a otros temas interesantes dentro del campo de la materia condensada. Damos aquí un breve resumen de otras contribuciones de esta tesis, y de otras herramientas que hemos empleado:

- Probablemente la contribución técnica más relevante de esta tesis es la del estudio que hemos realizado en el Capítulo 2 de un Hamiltoniano local de túnel que permite investigar problemas de transporte a través de interfaces de geometría arbitraria y perfiles de potenciales de barrera arbitrarios [51]. Demostramos que, en heteroestructuras 3D o 2D, la dependencia bilineal con el momento de los elementos de matriz de túnel a baja energía se traduce en un Hamiltoniano en espacio real que queda expresado en términos de las derivadas normales de los campos electrónicos en cada electrodo. También obtuvimos esta misma forma usando una descripción de 'tight-binding'. Mostramos además que, en un metal balístico, al ignorar la dependencia del efecto túnel con el momento se incurre en una violación de la unitariedad que conlleva un límite termodinámico (de interfaz ancha) incorrecto, entre otras inconsistencias. Este Hamiltoniano local ha sido recientemente empleado en otros problemas interesantes, como el trabajo "Quantum charge fluctuations in a superconducting grain" por M. Houzet, D. A. Pesin, A. V. Andreev y L. I. Glazman en 2005 [118], y en el trabajo "Weak Localization in Metallic Granular Media" por Y. M. Blanter, V. M. Vinokur y L.I. Glazman en 2005 [119].

- También en el Capítulo 2 hemos estudiado la distribución angular de la corriente electrónica que fluye través de interfaces túnel entre un metal normal y un metal superconductor (NS) y entre dos metales normales (NN) cuando éstas poseen una forma circular de radio finito. En el caso de la corriente Andreev a través de un contacto NS, calculamos las correlaciones angulares entre haces de electrones

enredados emitidos a través de la interfaz de tamaño finito y mostramos cómo desaparecen según disminuye el radio de la interfaz.

- Hemos establecido rigurosamente la equivalencia entre la emisión de pares de Cooper y la reflexión Andreev de un hueco incidente en una interfaz NS, haciendo notar que surgen de elecciones distintas del potencial químico respecto del que se definen las cuasipartículas en el metal normal, siendo μ_S en la imagen Bogoliubov - de Gennes estándar, y μ_N en el escenario en el que se contempla la emisión de dos electrones (Capítulo 2).

- En el Capítulo 3 hemos estudiado el transporte resonante a través de barreras dobles en nanoestructuras supercondutor - semiconductor donde existe una gran diferencia en las masas efectivas y longitudes de onda de Fermi en cada lado de la interfaz. Encontramos picos a voltaje cero y voltaje finito en la conductancia diferencial vs. diferencia de voltaje que no son simétricos con respecto a inversión del signo del voltaje.

- Hemos utilizado la FCS como la cantidad observable para comprobar la violación de la desigualdad de CH. En particular, hemos considerado la distribución de probabilidad conjunta $P(Q_1, Q_2)$ de transferir un número Q_1 y un número Q_2 de cargas a dos terminales diferentes en un tiempo de observación t dado. El conteo de electrones se modeló mediante contadores selectivos de spin, que no son sino filtros de spin sin probabilidad de retroceso (Capítulo 4).

- Siguiendo la idea de la Ref. [106], en el Capítulo 5 hemos usado una rotación local de spin en uno de los terminales de un un dispositivo divisor de haces litografiado sobre un 2DEG. La rotación de spin se implementa mediante la adición de puertas extensas de voltaje encima y debajo de una cierta sección del terminal en cuestión. Aplicando un voltaje entre estas puertas se acentúa la asimetría de inversión estructural del 2DEG, induciendo un acoplo Rashba spin-órbita en esa región del 2DEG de una manera controlable sin alterar la concentración de electrones. Esto produce a su vez una precesión del spin alrededor de un eje en el plano del 2DEG que es a su vez perpendicular al momento del electrón, induciendo de esta manera una rotación del spin de un ángulo dado tras atravesar la región con las puertas. Este mecanismo permite distinguir entre diferentes estados enredados y polarizados estudiando cómo las señales de ruido de disparo cambian con el ángulo de un comportamiento de aglomeración a uno de antiaglomeración [106].

- También en el Capítulo 5 hemos generalizado el modelo fenomenológico de sonda de voltaje que simula la dispersión inelástica al caso del cálculo de la FCS de partículas con enredo no local que atraviesan un conductor mesoscópico.

E.5 Estructura de esta memoria de tesis

Esta tesis está organizada de la siguiente manera: Contiene cuatro capítulos, los dos primeros, Capítulos 2 y 3, están dedicados a intentar responder a la pregunta: *¿Cómo generar electrones con enredo de spin no local usando estructuras híbridas metal normal-superconductor?*; y los otros dos capítulos, Capítulos 4 and 5, a las preguntas: *¿Cómo describir la evolución de los estados enredados no localmente en presencia de dispersión inelástica?*, y *¿Cómo detectar enredo no local y como discriminar entre diferentes estados incidentes enredados y no enredados?*. Cada capítulo contiene una sección introductoria autocontenida del problema específico con el que lidia (donde se dan muchas referencias a trabajos relacionados), contiene además algunos resultados nuevos que nosotros hemos obtenido, y un resumen con las conclusiones fundamentales al final. Además, se incluye al final de cada capítulo una sección titulada "Experimentos relacionados". Debido a la novedad de los problemas considerados en esta tesis, el objetivo de nuestros estudios teóricos no ha sido el de describir unos experimentos que ya existían; en todo caso, ha sido el de despertar o disparar el interés de algunos grupos experimentales sobre la realización de los dispositivos propuestos. Sin embargo, con el paso de los años han aparecido en la literatura algunos experimentos relacionados con algunos de los problemas que nosotros hemos tratado aquí y que no están tan lejos de los dispositivos específicos que nosotros hemos estudiado. Éste es por ejemplo el caso del trabajo "Experimental Observation of Bias-Dependent Nonlocal Andreev Reflection" por S. Russo, M. Krough, T. M. Klapwijk y A. F. Morpurgo en 2005 [120], que describimos en el Capítulo 2, o el experimento "Shot-noise and conductance measurements of trasparent superconductor/two-dimensional electron gas junctions", por B.-R. Choi et al. en 2005 [76], descrito en el Capítulo 3. Otros experimentos son de relevancia para nosotros simplemente porque confirman la accesibilidad experimental de algunas de las cantidades que usamos en nuestra teoría. Éste el el caso de la FCS para electrones del Capítulo 4, cuya medida experimental no está tan lejana de acuerdo con el trabajo "Current measurement by real-time counting of single electrons" por J. Bylander, T. Duty y P. Delsing en 2005 [121]. Finalmente, hemos trasladado a los apéndices algunas de las discusiones y cálculos más largos que podrían haber distraído, de otra forma, del discurso principal.

E.6 Conclusiones al capítulo 2

Hemos investigado la corriente a través de una estructura túnel NS en la región de parámetros $k_BT \ll eV \ll \Delta$ donde la reflexión Andreev es el canal transmisivo dominante. Hemos establecido rigurosamente la equivalencia entre emisión de pares de Cooper y reflexión Andreev de un hueco incidente. Para describir el túnel a través de una interfaz de forma arbitraria, hemos derivado un Hamiltoniano de túnel local

truncando apropiadamente el correspondiente a una interfaz infinita. Este esquema a sido aplicado al estudio de transporte a través de una interfaz circular de radio arbitrario y a una interfaz hecha de dos contactos pequeños. En el primer caso, las correlaciones angulares entre los dos electrones emitidos han sido dilucidadas y se ha mostrado cómo se pierden a medida que el radio de la interfaz disminuye. Hemos investigado además cómo se recupera el límite termodinámico, mostrando que, debido a la interferencia destructiva entre los distintos puntos de salida, éste se alcanza para radios del orden de unas pocas longitudes de onda de Fermi. En el caso de la interfaz de dos puntos, hemos calculado la corriente enredada no local proviniente de procesos en los que cada electrón sale del superconductor a través de un agujero diferente. Hemos encontrado que, como función de la distancia entre los dos contactos, dicha corriente enredada decae rápidamente en la escala de la longitud de onda de Fermi. La interferencia entre los distintos canales de salida a dos electrones ha sido también investigada y se ha mostrado que proporciona contribuciones comparables a la corriente enredada no local. Si queremos obtener resultados físicos razonables en problemas tridimensionales que tengan que ver con el Hamiltoniano de túnel local, como el límite termodinámico, la preservación de la unitariedad, o la dependencia con la distancia de la corriente enredada no local a través de una interfaz de dos puntos, hemos encontrado que es necesario emplear elementos de matriz de 'hopping' (salto) que posean la dependencia correcta con el momento [cuya forma ha sido también obtenida a través una descripción 'tight-binding' (de ligadura fuerte)]. Una virtud importante del método que hemos desarrollado aquí es que permite el estudio sistemático de emisión de pares de Cooper a través de interfaces de túnel arbitrarias. Además, puede ser empleado como punto de partida para modelos teóricos más sofisticados y realistas donde los metales que conecta estén en régimen difusivo o existan interacciones de Coulomb, como sugieren experimentos relacionados.

E.7 Conclusiones al capítulo 3

Hemos investigado teóricamente la posibilidad de crear estructuras resonantes NS donde los dos electrones que formaban previamente un par de Cooper en el superconductor son enviados en direcciones diferentes en el metal normal. La idea central se basa en el diseño de una estructura que es transparente sólo para electrones con energía en la dirección perpendicular a la barrera dentro de la fina región de un nivel resonante. Como la energía total se encuentra próxima al nivel de Fermi, dicho filtrado de la energía perpendicular se traduce en *selección del ángulo de salida*.

Se sabe que los electrones dentro de un superconductor convencional están correlacionados de tal forma que electrones moviéndose a igual velocidad en direcciones opuestas tienden a tener spines opuestos. A bajas temperaturas y pequeños voltajes, el flujo de electrones desde el superconductor al metal normal está compuesto completamente de pares de electrones correlacionados. Estos tienen tanto spin como

momento pararelo a la interfaz opuestos, mientras que poseen la misma energía total. Si el ángulo de salida se selecciona filtrando el momento perpendicular a la interfaz, la corriente en el metal normal está formada por dos haces finos de electrones mutuamente enredados en forma de singlete. Estos haces apuntan en direcciones distintas y se separan espacialmente uno de otro a distancias de la fuente mucho mayores que la anchura de la misma.

El truco de la selección del ángulo de salida ha sido pensado para facilitar la observación del enredo no local entre haces de electrones, y este trabajo ha sido dedicado a proponer una implementación concreta de esta idea. De todas formas, hacemos notar que dicha selección de la dirección de salida puede que no sea totalmente necesaria. Si nos contentamos con medir fluctuaciones anticorrelacionadas de spin de baja energía, puede que sea suficiente con emplazar dos detectores de spin de forma simétrica con respecto a la perpendicular a la interfaz a una distancia suficientemente grande, de forma similar al dispositivo de la Fig. 3.1(a), pero con una interfaz NS normal, no con una doble barrera que selecciona el ángulo. Si su desplazamiento entre el emisor y el detector es balístico, los electrones que llegan a cada detector tienen, en media, momento paralelo opuesto y spin opuesto (la anticorrelación angular ha sido explícitamente mostrada en la Ref. [51] para el caso de una interfaz perfecta y extensa). Las fronteras del 2DEG pueden ser diseñadas para optimizar dichas correlaciones. El resultado es que los electrones que llegan a cada detector exhibirán un cierto grado de correlación de singlete de spin no local que puede ser medido.

En conjunto, concluimos que un gas de electrones bidimensional balístico proporciona un escenario ideal para investigar enredo no local entre electrones emitidos desde una interfaz de tamaño finito con un superconductor a una cierta distancia. Si la interfaz está formada por una estructura resonante que selecciona la energía perpendicular y por lo tanto la magnitud del ángulo de salida, correlaciones de spin no locales pueden ser claramente observadas si los haces salientes son dirigidos hacia detectores convenientemente emplazados.

E.8 Conclusiones al capítulo 4

En este capítulo hemos estudiado el efecto de la decoherencia en la violación de la desigualdad de CH (o CH74) cuando ésta es formulada en términos de la FCS [113]. El sistema bajo investigación (Fig. 4.1) consiste en un *enredador* ideal acoplado, a través de un par de hilos metálicos mesoscópicos e idénticos, a unos contadores selectivos de spin. Hemos asumido que la decoherencia, que ocurre de forma similar pero independiente en ambos conductores, es producida por la presencia de reservas ficticias adicionales, de acuerdo con el modelo fenomenológico de Büttiker [86,87]. La decoherencia está parametrizada por una tasa α.

Como era de esperar, la decoherencia produce una supresión de la violación de la desigualdad de CH. La magnitud de dicha supresión ha sido analizada como función

de los parámetros que caracterizan el sistema, que son: la transmisión T de los hilos, el ángulo entre los analizadores Θ, el número de pares enredados inyectados M y el número de partículas transmitidas Q_1 y Q_2 a los contadores. Primero hemos discutido la *suposición de no incremento*, una condición que necesita ser satisfecha en ambos hilos 1 y 2 para que la desigualdad de CH sea válida. Hemos encontrado que dicha condición, en un hilo determinado, se verifica para todas las transmisiones T hasta un cierto límite máximo $T_{\max}$ que depende de Q, M y, por supuesto, de α. En particular, $T_{\max}$ decrece con la tasa de decoherencia hasta un determinado valor de Q y, a partir de ahí, se incrementa. Los resultados principales pueden ser resumidos de la siguiente manera:

- La máxima violación, incluso en presencia de decohrencia, se da siempre para el mayor valor de la transmisión permitido $T = T_{\max}$ y para $Q_1 = Q_2$ (de hecho desaparece rápidamente cuando $Q_1 \neq Q_2$).

- Siempre y cuando $T = T_{\max}$, el intervalo de valores del ángulo entre analizadores para los que existe violación no depende de la tasa de decoherencia, aunque la magnitud de la violación disminuye con α.

- En ausencia de decoherencia se había demostrado que el máximo de la violación de la desigualdad de CH decaía como $1/M$ [113]. Aquí hemos encontrado que, para valores finitos de α, el parámetro $\mathcal{S}_{\mathrm{CH}}$ decrece exponencialmente con $\sqrt{M}$, en concreto, como $[f(\alpha)]^{\sqrt{M}}/M$, i.e., decae con el aumento de ambos M y α.

- El valor de Q para el que ocurre máxima violación es prácticamente independiente de M, lo que significa que las violaciones más grandes aparecen para números relativamente pequeños de las partículas transmitidas, incluso para tiempos de observación muy grandes.

- Es de interés resaltar que hemos encontrado la tasa de decoherencia máxima para la que la desigualdad de CH se viola (dentro de una tolerancia pequeña dada) presenta un máximo como función de Q. Esto significa que existen números de cargas transmitidas que están más protegidos contra la decoherencia, i.e., para los que la influencia del entorno es menos destructiva con respecto a la violación de la desigualdad de CH.

Aunque en este trabajo se asume que la decoherencia está producida por la presencia de reservas adicionales, en los sistemas mesoscópicos son posibles otras fuentes de decoherencia diferentes. Creemos en cualquier caso que este modelo captura los efectos fundamentales de la decoherencia, al menos con respecto a la violación de la desigualdad de CH, y que los resultados que encontramos en este trabajo pueden ser útiles para diseñar las mejores condiciones experimentales posibles.

Como los sistemas reales no pueden ser completamente apantallados del entorno, los temas analizados en este trabajo parecen adecuados no sólo desde un punto de

vista fundamental, sino que podrían contribuir a la compresión de las propiedades de canales cuánticos con pérdidas. En un futuro sería interesante aplicar nuestro método a sistemas realistas, como divisores de haces normales o superconductores.

E.9 Conclusiones al capítulo 5

En este trabajo hemos analizado el efecto de la dispersión inelástica, modelada por una sonda de voltaje que conserva la corriente para cada spin, en la detección de enredo a través de una geometría de divisor de haces. Hemos mostrado que, al contrario que el 'dephasing' orbital elástico [73], la acción de los procesos inelásticos en el divisor de haces no puede ser despreciada, ya que afecta directamente al mecanismo físico subyacente del detector, que es el hecho de que electrones con iguales números cuánticos no pueden ser dispersados al mismo canal cuántico. Si la energía no se conserva, este mecanismo de "antiaglomeración" deja de ser perfecto y el esquema de detección de enredo tiene que ser revisado.

Sin embargo, hemos encontrado que la detección de enredo a través de medidas de ruido de disparo sigue siendo posible incluso bajo condiciones muy laxas para las imperfecciones en el divisor de haces y una cantidad sustancial de dispersión inelástica. Incluso si no poseemos una descripción microscópica de la dispersión inelástica en la que se pueda confiar, el análisis presente sugiere que el esquema de detección es robusto hasta probabilidades de dispersión inelástica del 50%.

Hemos mostrado también que cumulantes de corriente de mayor orden no proporcionan más información acerca del enredo de las corrientes incidentes que la que proporciona el ruido. Hemos analizado en particular la asimetría de las fluctuaciones de corriente, encontrando que ésta es fuertemente afectada por una probabilidad de retroceso finita y por la dispersión inelástica. En particular, se desarrolla una asimetría positiva a medida que la transparencia del divisor de haces disminuye.

Finalmente, hemos desarrollado un método nuevo para implementar conservación de corriente en dispositivos con sondas de voltaje cuando las corrientes incidentes poseen enredo no local. Este método puede ser aplicado a una gran variedad de problemas en los que el enredo es el punto fundamental.

Bibliography

[1] "Quantum entanglement and information," *Stanford Encyclopedia of Philosophy*, 2006. http://plato.stanford.edu/entries/qt-entangle/.

[2] "Quantum entanglement," *Wikipedia*, 2006. http://en.wikipedia.org/wiki/Quantum_entanglement.

[3] E. Schrödinger, "Discussion of probability relations between separated systems," *Proceedings of the Cambridge Philosophical Society*, vol. 31, pp. 555–563, 1935.

[4] J. M. Kikkawa, I. P. Smorchkova, N. Samarth, and D. D. Awschalom, "Room-temperature spin memory in two-dimensional electron gases," *Science*, vol. 277, no. 5330, pp. 1284–1287, 1997.

[5] J. M. Kikkawa and D. D. Awschalom, "Resonant spin amplification in n-type GaAs," *Physical Review Letters*, vol. 80, no. 19, pp. 4313–4316, 1998.

[6] J. M. Elzerman, R. Hanson, L. H. W. van Beveren, B. Witkamp, L. M. K. Vandersypen, and L. P. Kouwenhoven, "Single-shot read-out of an individual electron spin in a quantum dot," *Nature*, vol. 430, no. 6998, pp. 431–435, 2004.

[7] J. R. Petta, A. C. Johnson, J. M. Taylor, E. A. Laird, A. Yacoby, M. D. Lukin, C. M. Marcus, M. P. Hanson, and A. C. Gossard, "Coherent manipulation of coupled electron spins in semiconductor quantum dots," *Science*, vol. 309, no. 5744, pp. 2180–2184, 2005.

[8] V. Cerletti, W. A. Coish, O. Gywat, and D. Loss, "Recipes for spin-based quantum computing," *Nanotechnology*, vol. 16, no. 4, pp. R27–R49, 2005.

[9] *The Description of Nature: Niels Bohr and The Philosophy of Quantum Physics*. Oxford: Clarendon Press, 1987.

[10] "Copenhagen interpretation," *Wikipedia*, 2006. http://en.wikipedia.org/wiki/Copenhagen_interpretation.

[11] "Copenhagen interpretation of quantum mechanics," *Stanford Encyclopedia of Philosophy*, 2006. http://plato.stanford.edu/entries/qm-copenhagen/.

[12] E. Einstein, B. Podolsky, and N. Rosen, "Can quantum-mechanical description of physical reality be considered complete?," *Physical Review*, vol. 47, no. 10, pp. 777–780, 1935.

[13] "The Einstein-Podolsky-Rosen argument in quantum theory," *Stanford Encyclopedia of Philosophy*, 2006. http://plato.stanford.edu/entries/qt-epr/.

[14] J. S. Bell, *Speakable and Unspeakable in Quantum Mechanics*. Cambridge, England: Cambridge University Press, 1987.

[15] "Bell's theorem," *Wikipedia*, 2006. http://en.wikipedia.org/wiki/Bell's_inequality.

[16] "No cloning theorem," *Wikipedia*, 2006. http://en.wikipedia.org/wiki/No-cloning_theorem.

[17] "Quantum information," *Wikipedia*, 2006. http://en.wikipedia.org/wiki/ Quantum_information.

[18] "Quantum teleportation," *Wikipedia*, 2006. http://en.wikipedia.org/wiki/ Quantum_teleportation.

[19] C. H. Bennett, G. Brassard, C. Crepeau, R. Jozsa, A. Peres, and W. K. Wootters, "Teleporting an unknown quantum state via dual classical and Einstein-Podolsky-Rosen Channels," *Physical Review Letters*, vol. 70, no. 13, pp. 1895–1899, 1993.

[20] D. Bouwmeester, J. W. Pan, K. Mattle, M. Eibl, H. Weinfurter, and A. Zeilinger, "Experimental quantum teleportation," *Nature*, vol. 390, no. 6660, pp. 575–579, 1997.

[21] "Qubit," *Wikipedia*, 2006. http://en.wikipedia.org/wiki/Qubit.

[22] "Quantum computer," *Wikipedia*, 2006. http://en.wikipedia.org/wiki/ Quantum_computer.

[23] R. P. Feynman, "Simulating physics with computers," *International Journal of Theoretical Physics*, vol. 21, pp. 467–488, 1982.

[24] L. M. K. Vandersypen, M. Steffen, G. Breyta, C. S. Yannoni, M. H. Sherwood, and I. L. Chuang, "Experimental realization of Shor's quantum factoring algorithm using nuclear magnetic resonance," *Nature*, vol. 414, no. 6866, pp. 883–887, 2001.

[25] J. West, "The quantum computer," 2000. http://www.cs.caltech.edu/westside/quantum-intro.html.

[26] D. P. DiVincenzo, "The physical implementation of quantum computation," *Fortschr. Phys.*, vol. 48, no. 9-11, pp. 771–783, 2000.

[27] J. I. Cirac and P. Zoller, "Quantum computations with cold trapped ions," *Physical Review Letters*, vol. 74, no. 20, pp. 4091–4094, 1995.

[28] P. Domokos, J. M. Raimond, M. Brune, and S. Haroche, "Simple cavity-QED 2-bit universal quantum logic gate - the principle and expected performances," *Physical Review A*, vol. 52, no. 5, pp. 3554–3559, 1995.

[29] N. A. Gershenfeld and I. L. Chuang, "Bulk spin-resonance quantum computation," *Science*, vol. 275, no. 5298, pp. 350–356, 1997.

[30] A. Shnirman, G. Schon, and Z. Hermon, "Quantum manipulations of small Josephson junctions," *Physical Review Letters*, vol. 79, no. 12, pp. 2371–2374, 1997.

[31] Y. Makhlin, G. Schon, and A. Shnirman, "Josephson-junction qubits with controlled couplings," *Nature*, vol. 398, no. 6725, pp. 305–307, 1999.

[32] Y. Makhlin, G. Schon, and A. Shnirman, "Quantum-state engineering with Josephson-junction devices," *Reviews of Modern Physics*, vol. 73, no. 2, pp. 357–400, 2001.

[33] D. Loss and D. P. DiVincenzo, "Quantum computation with quantum dots," *Physical Review A*, vol. 57, no. 1, pp. 120–126, 1998.

[34] E. Knill, R. Laflamme, and G. J. Milburn, "A scheme for efficient quantum computation with linear optics," *Nature*, vol. 409, no. 6816, pp. 46–52, 2001.

[35] C. W. J. Beenakker, D. P. DiVincenzo, C. Emary, and M. Kindermann, "Charge detection enables free-electron quantum computation," *Physical Review Letters*, vol. 93, no. 2, p. 020501, 2004.

[36] J. Torres and T. Martin, "Positive and negative Hanbury-Brown and Twiss correlations in normal metal-superconducting devices," *European Physical Journal B*, vol. 12, no. 3, pp. 319–322, 1999.

[37] G. Deutscher and D. Feinberg, "Coupling superconducting-ferromagnetic point contacts by Andreev reflections," *Applied Physics Letters*, vol. 76, no. 4, pp. 487–489, 2000.

[38] P. Recher, E. V. Sukhorukov, and D. Loss, "Andreev tunneling, Coulomb blockade, and resonant transport of nonlocal spin-entangled electrons," *Physical Review B*, vol. 63, no. 16, p. 165314, 2001.

[39] G. Falci, D. Feinberg, and F. W. J. Hekking, "Correlated tunneling into a superconductor in a multiprobe hybrid structure," *Europhysics Letters*, vol. 54, no. 2, pp. 255–261, 2001.

[40] R. Melin, "Superconducting cross-correlations in ferromagnets: implications for thermodynamics and quantum transport," *Journal of Physics-Condensed Matter*, vol. 13, no. 30, pp. 6445–6451, 2001.

[41] G. B. Lesovik, T. Martin, and G. Blatter, "Electronic entanglement in the vicinity of a superconductor," *European Physical Journal B*, vol. 24, no. 3, pp. 287–290, 2001.

[42] V. Apinyan and R. Melin, "Microscopic theory of non local pair correlations in metallic F/S/F trilayers," *European Physical Journal B*, vol. 25, no. 3, pp. 373–389, 2002.

[43] R. Melin and D. Feinberg, "Transport theory of multiterminal hybrid structures," *European Physical Journal B*, vol. 26, no. 1, pp. 101–114, 2002.

[44] D. Feinberg and G. Deutscher, "Using a hybrid superconducting-ferromagnetic tip as a magnetic scanning tunneling microscope," *Physica E-Low-Dimensional Systems & Nanostructures*, vol. 15, no. 2, pp. 88–93, 2002.

[45] P. Recher and D. Loss, "Superconductor coupled to two Luttinger liquids as an entangler for electron spins," *Physical Review B*, vol. 65, no. 16, p. 165327, 2002.

[46] N. M. Chtchelkatchev, G. Blatter, G. B. Lesovik, and T. Martin, "Bell inequalities and entanglement in solid-state devices," *Physical Review B*, vol. 66, no. 16, p. 161320, 2002.

[47] C. Bena, S. Vishveshwara, L. Balents, and M. P. A. Fisher, "Quantum entanglement in carbon nanotubes," *Physical Review Letters*, vol. 89, no. 3, p. 037901, 2002.

[48] D. Feinberg, "Andreev scattering and cotunneling between two superconductor-normal metal interfaces: the dirty limit," *European Physical Journal B*, vol. 36, no. 3, pp. 419–422, 2003.

[49] V. Bouchiat, N. Chtchelkatchev, D. Feinberg, G. B. Lesovik, T. Martin, and J. Torres, "Single-walled carbon nanotube-superconductor entangler: noise correlations and Einstein-Podolsky-Rosen states," *Nanotechnology*, vol. 14, no. 1, pp. 77–85, 2003.

[50] P. Recher and D. Loss, "Dynamical Coulomb blockade and spin-entangled electrons," *Physical Review Letters*, vol. 91, no. 26, p. 267003, 2003.

[51] E. Prada and F. Sols, "Entangled electron current through finite size normal-superconductor tunneling structures," *European Physical Journal B*, vol. 40, no. 4, pp. 379–396, 2004.

[52] G. Bignon, M. Houzet, F. Pistolesi, and F. W. J. Hekking, "Current-current correlations in hybrid superconducting and normal-metal multiterminal structures," *Europhysics Letters*, vol. 67, no. 1, pp. 110–116, 2004.

[53] O. Sauret, D. Feinberg, and T. Martin, "Quantum master equations for the superconductor-quantum dot entangler," *Physical Review B*, vol. 70, no. 24, p. 245313, 2004.

[54] E. Prada and F. Sols, "Divergent beams of nonlocally entangled electrons emitted from hybrid normal-superconducting structures," *New Journal of Physics*, vol. 7, p. 231, 2005.

[55] R. Melin, "Crossed conductance in ferromagnet/superconductor/ferromagnet double junctions: Role of out-of-equilibrium populations," *Physical Review B*, vol. 72, no. 5, p. 054503, 2005.

[56] R. Melin, "Contribution of weak localization to non local transport at normal metal / superconductor double interfaces," *Preprint archive cond-mat/0510837*, 2006.

[57] S. Duhot and R. Melin, "Possibility of reflectionless tunneling crossed transport at normal metal / superconductor double interfaces," *Preprint archive cond-mat/0601442*, 2006.

[58] A. T. Costa and S. Bose, "Impurity scattering induced entanglement of ballistic electrons," *Physical Review Letters*, vol. 87, no. 27, p. 277901, 2001.

[59] W. D. Oliver, F. Yamaguchi, and Y. Yamamoto, "Electron entanglement via a quantum dot," *Physical Review Letters*, vol. 88, no. 3, p. 037901, 2002.

[60] O. Gywat, G. Burkard, and D. Loss, "Biexcitons in coupled quantum dots as a source of entangled photons," *Physical Review B*, vol. 65, no. 20, p. 205329, 2002.

[61] D. S. Saraga and D. Loss, "Spin-entangled currents created by a triple quantum dot," *Physical Review Letters*, vol. 90, no. 16, p. 166803, 2003.

[62] C. W. J. Beenakker, M. Kindermann, C. M. Marcus, and A. Yacobi, "Fundamental problems of mesoscopic physics," vol. 154, (Kluwer, Dordrecht), NATO Science, Series II, 2004.

[63] D. S. Saraga, B. L. Altshuler, D. Loss, and R. M. Westervelt, "Coulomb scattering in a 2D interacting electron gas and production of EPR pairs," *Physical Review Letters*, vol. 92, no. 24, p. 246803, 2004.

[64] D. Gunlycke, J. H. Jefferson, T. Rejec, A. Ramsak, D. G. Pettifor, and G. A. D. Briggs, "Entanglement between static and flying qubits in a semiconducting carbon nanotube," *Preprint archive cond-mat/0511126*, 2005.

[65] J. H. Jefferson, A. Ramsak, and T. Rejec, "Entanglement between static and flying qubits in quantum wires," *Preprint archive cond-mat/0509010*, 2005.

[66] A. V. Lebedev, G. B. Lesovik, and G. Blatter, "Generating spin-entangled electron pairs in normal conductors using voltage pulses," *Physical Review B*, vol. 72, no. 24, p. 245314, 2005.

[67] S. Bose and G. S. Agarwal, "Entangling pairs of nano-cantilevers, cooper-pair boxes and mesoscopic teleportation," *Preprint archive cond-mat/0510676*, 2005.

[68] S. Savel'ev, X. Hu, A. Kasumov, and N. Franco, "Quantum electromechanics: Quantum tunneling near resonance and qubits from buckling nanobars," *Preprint archive cond-mat/0601019*, 2006.

[69] A. V. Lebedev, G. Blatter, C. W. J. Beenakker, and G. B. Lesovik, "Entanglement in mesoscopic structures: Role of projection," *Physical Review B*, vol. 69, no. 23, p. 235312, 2004.

[70] A. V. Lebedev, G. B. Lesovik, and G. Blatter, "Entanglement in a noninteracting mesoscopic structure," *Physical Review B*, vol. 71, no. 4, p. 045306, 2005.

[71] A. D. Lorenzo and Y. V. Nazarov, "Full counting statistics with spin-sensitive detectors reveals spin singlets," *Physical Review Letters*, vol. 94, no. 21, p. 210601, 2005.

[72] C. W. J. Beenakker, C. Emary, M. Kindermann, and J. L. van Velsen, "Proposal for production and detection of entangled electron-hole pairs in a degenerate electron gas," *Physical Review Letters*, vol. 91, no. 14, p. 147901, 2003.

[73] P. Samuelsson, E. V. Sukhorukov, and M. Buttiker, "Orbital entanglement and violation of Bell inequalities in mesoscopic conductors," *Physical Review Letters*, vol. 91, no. 15, p. 157002, 2003.

[74] P. Samuelsson, E. V. Sukhorukov, and M. Buttiker, "Two-particle Aharonov-Bohm effect and entanglement in the electronic Hanbury Brown-Twiss setup," *Physical Review Letters*, vol. 92, no. 2, p. 026805, 2004.

[75] C. W. J. Beenakker, "Electron-hole entanglement in the Fermi sea," *Preprint archive cond-mat/0508488*, 2005.

[76] B. R. Choi, A. E. Hansen, T. Kontos, C. Hoffmann, S. Oberholzer, W. Belzig, C. Schonenberger, T. Akazaki, and H. Takayanagi, "Shot-noise and conductance measurements of transparent superconductor/two-dimensional electron gas junctions," *Physical Review B*, vol. 72, no. 2, p. 024501, 2005.

[77] F. Giazotto, P. Pingue, F. Beltram, M. Lazzarino, D. Orani, S. Rubini, and A. Franciosi, "Resonant transport in Nb/GaAs/AlGaAs heterostructures: Realization of the de Gennes-Saint-James model," *Physical Review Letters*, vol. 8721, no. 21, p. 216808, 2001.

[78] P. Samuelsson, E. V. Sukhorukov, and M. Büttiker *Doga: Turkish Journal of Physics*, vol. 27, p. 481, 2003.

[79] P. Samuelsson, E. V. Sukhorukov, and M. Buttiker, "Electrical current noise of a beamsplitter as a test of spin entanglement," *Physical Review B*, vol. 70, no. 11, p. 115330, 2004.

[80] J. L. van Velsen, M. Kindermann, and C. W. J. Beenakker *Doga: Turkish Journal of Physics*, vol. 27, p. 323, 2003.

[81] G. Seelig and M. Buttiker, "Charge-fluctuation-induced dephasing in a gated mesoscopic interferometer," *Physical Review B*, vol. 64, no. 24, p. 245313, 2001.

[82] F. Marquardt and C. Bruder, "Effects of dephasing on shot noise in an electronic Mach-Zehnder interferometer," *Physical Review B*, vol. 70, no. 12, p. 125305, 2004.

[83] M. G. Pala and G. Iannaccone, "Statistical model of dephasing in mesoscopic devices introduced in the scattering matrix formalism," *Physical Review B*, vol. 69, no. 23, p. 235304, 2004.

[84] M. G. Pala and G. Iannaccone, "Effect of dephasing on the current statistics of mesoscopic devices," *Physical Review Letters*, vol. 93, no. 25, p. 256803, 2004.

[85] H. Forster, S. Pilgram, and M. Buttiker, "Decoherence and full counting statistics in a Mach-Zehnder interferometer," *Physical Review B*, vol. 72, no. 7, p. 075301, 2005.

[86] M. Buttiker, "Role of quantum coherence in series resistors," *Physical Review B*, vol. 33, no. 5, pp. 3020–3026, 1986.

[87] M. Buttiker, "Coherent and sequential tunneling in series barriers," *Ibm Journal of Research and Development*, vol. 32, no. 1, pp. 63–75, 1988.

[88] C. W. J. Beenakker and M. Buttiker, "Suppression of shot noise in metallic diffusive conductors," *Physical Review B*, vol. 46, no. 3, pp. R1889–R1892, 1992.

[89] M. J. M. deJong and C. W. J. Beenakker, "Semiclassical theory of shot noise in mesoscopic conductors," *Physica A*, vol. 230, no. 1-2, pp. 219–248, 1996.

[90] S. A. vanLangen and M. Buttiker, "Quantum-statistical current correlations in multilead chaotic cavities," *Physical Review B*, vol. 56, no. 4, pp. R1680–R1683, 1997.

[91] C. W. J. Beenakker, "Random-matrix theory of quantum transport," *Review of Modern Physics*, vol. 69, no. 3, pp. 731–808, 1997.

[92] F. Marquardt and C. Bruder, "Influence of dephasing on shot noise in an electronic Mach-Zehnder interferometer," *Physical Review Letters*, vol. 92, no. 5, p. 056805, 2004.

[93] E. Prada, F. Taddei, and R. Fazio, "Clauser-Horne inequality and decoherence in mesoscopic conductors," *Physical Review B*, vol. 72, no. 12, p. 125333, 2005.

[94] P. San-Jose and E. Prada, "Effect of inelastic scattering on spin entanglement detection through current noise," *Preprint archive cond-mat/0601365*, 2006.

[95] Y. M. Blanter and M. Buttiker, "Shot noise in mesoscopic conductors," *Physics Reports-Review Section of Physics Letters*, vol. 336, no. 1-2, pp. 2–166, 2000.

[96] P. W. Brouwer and C. W. J. Beenakker, "Voltage-probe and imaginary-potential models for dephasing in a chaotic quantum dot," *Physical Review B*, vol. 55, no. 7, pp. 4695–4702, 1997.

[97] C. Texier and M. Buttiker, "Effect of incoherent scattering on shot noise correlations in the quantum Hall regime," *Physical Review B*, vol. 62, no. 11, pp. 7454–7458, 2000.

[98] G. Kiesslich, P. Samuelsson, A. Wacker, and E. Schöll, "Counting statistics and decoherence in coupled quantum dots," *Preprint archive cond-mat/0507403*, 2005.

[99] L. E. F. Foa Torres, H. M. Pastawski, and E. Medina, "Antiresonances as precursors of decoherence," *Europhysics Letters (in press)*, 2005. Preprint archive cond-mat/0511360.

[100] G. Muller, D. Weiss, S. Koch, K. Vonklitzing, H. Nickel, W. Schlapp, and R. Losch, "Edge channels and the role of contacts in the quantum Hall regime," *Physical Review B*, vol. 42, no. 12, pp. 7633–7636, 1990.

[101] S. Oberholzer, E. Bieri, C. Schonenberger, M. Giovannini, and J. Faist, "Positive cross correlations in a normal-conducting fermionic beam splitter," *Physical Review Letters*, vol. 96, no. 4, p. 046804, 2006.

[102] S. Pilgram, P. Samuelsson, H. Forster, and M. Buttiker, "Full counting statistics for voltage and dephasing probes," *Preprint archive cond-mat/0512276*, 2005.

[103] B. Michaelis and C. W. J. Beenakker, "Voltage probe model of spin decay in a chaotic quantum dot, with applications to spin-flip noise and entanglement production," *Preprint archive cond-mat/0512465*, 2005.

[104] C. W. J. Beenakker, "Excess conductance of a spin-filtering quantum dot," *Preprint archive cond-mat/0601638*, 2006.

[105] G. Burkard, D. Loss, and E. V. Sukhorukov, "Noise of entangled electrons: Bunching and antibunching," *Physical Review B*, vol. 61, no. 24, pp. 16303–16306, 2000.

[106] J. C. Egues, G. Burkard, and D. Loss, "Rashba spin-orbit interaction and shot noise for spin-polarized and entangled electrons," *Physical Review Letters*, vol. 89, no. 17, p. 176401, 2002.

[107] G. Burkard and D. Loss, "Lower bound for electron spin entanglement from beam splitter current correlations," *Physical Review Letters*, vol. 91, no. 8, p. 087903, 2003.

[108] F. Taddei and R. Fazio, "Counting statistics for entangled electrons," *Physical Review B*, vol. 65, no. 7, p. 075317, 2002.

[109] W. K. Wootters, "Entanglement of formation of an arbitrary state of two qubits," *Physical Review Letters*, vol. 80, no. 10, pp. 2245–2248, 1998.

[110] S. Kawabata, "Test of Bell's inequality using the spin filter effect in ferromagnetic semiconductor microstructures," *Journal of the Physical Society of Japan*, vol. 70, no. 5, pp. 1210–1213, 2001.

[111] C. W. J. Beenakker, C. Emary, and M. Kindermann, "Production and detection of three-qubit entanglement in the Fermi sea," *Physical Review B*, vol. 69, no. 11, p. 115320, 2004.

[112] O. Sauret and D. Feinberg, "Spin-current shot noise as a probe of interactions in mesoscopic systems," *Physical Review Letters*, vol. 92, no. 10, p. 106601, 2004.

[113] L. Faoro, F. Taddei, and R. Fazio, "Clauser-Horne inequality for electron-counting statistics in multiterminal mesoscopic conductors," *Physical Review B*, vol. 69, no. 12, p. 125326, 2004.

[114] R. F. Werner and M. M. Wolf, "Bell inequalities and entanglement," *Preprint archive quant-ph/0107093*, 2001.

[115] J. F. Clauser and M. A. Horne, "Experimental consequences of objective local theories," *Physical Review D*, vol. 10, no. 2, pp. 526–535, 1974.

[116] L. Mandel and E. Wolf, *Optical Coherence and Quantum Optics*. Cambridge, England: Cambridge University Press, 1995.

[117] F. Taddei, L. Faoro, E. Prada, and R. Fazio, "Clauser-Horne inequality for the full counting statistics," *New Journal of Physics*, vol. 7, p. 183, 2005.

[118] M. Houzet, D. A. Pesin, A. V. Andreev, and L. I. Glazman, "Quantum charge fluctuations in a superconducting grain," *Physical Review B*, vol. 72, no. 10, p. 104507, 2005.

[119] Y. M. Blanter, V. M. Vinokur, and L. I. Glazman, "Weak localization in metallic granular media," *Preprint archive cond-mat/0504309*, 2005.

[120] S. Russo, M. Kroug, T. M. Klapwijk, and A. F. Morpurgo, "Experimental observation of bias-dependent nonlocal Andreev reflection," *Physical Review Letters*, vol. 95, no. 2, p. 027002, 2005.

[121] J. Bylander, T. Duty, and P. Delsing, "Current measurement by real-time counting of single electrons," *Nature*, vol. 434, no. 7031, pp. 361–364, 2005.

[122] A. F. Andreev, "The thermal conductivity of the intermediate state in superconductors," *Soviet Physics Jetp-Ussr*, vol. 19, no. 5, pp. 1228–1231, 1964.

[123] J. Demers and A. Griffin, "Scattering and tunneling of electronic excitations in intermediate state of superconductors," *Canadian Journal of Physics*, vol. 49, no. 3, p. 285, 1971.

[124] G. E. Blonder, M. Tinkham, and T. M. Klapwijk, "Transition from metallic to tunneling regimes in superconducting micro-constrictions - excess current, charge imbalance, and super-current conversion," *Physical Review B*, vol. 25, no. 7, pp. 4515–4532, 1982.

[125] M. Tinkham, *Introduction to Superconductivity*. New York: McGraw-Hill, 2 ed., 1996.

[126] J. M. Byers and M. E. Flatte, "Probing spatial correlations with nanoscale 2-contact tunneling," *Physical Review Letters*, vol. 74, no. 2, pp. 306–309, 1995.

[127] M. Kupka, "Modification of the Blonder, Tinkham and Klapwijk expressions for Andreev and normal reflection coefficients due to a finite-thickness barrier at the normal metal-superconductor interface," *Physica C*, vol. 221, no. 3-4, pp. 346–354, 1994.

[128] M. Kupka, "Current-voltage characteristic and differential conductance of a point contact and planar tunnel contact between an ordinary metal and superconductor in realistic three-dimensional geometry: comparison with a one-dimensional case," *Physica C*, vol. 281, no. 1, pp. 91–106, 1997.

[129] D. Beckmann, H. B. Weber, and H. von Lohneysen, "Evidence for crossed Andreev reflection in superconductor-ferromagnet hybrid structures," *Physical Review Letters*, vol. 93, no. 19, p. 197003, 2004.

[130] P. Aronov and G. Koren, "Signature of a crossed Andreev reflection effect (CARE) in the magnetic response of YBCO junctions with the itinerant ferromagnet SrRuO_3," *Physical Review B*, vol. 72, no. 18, p. 184515, 2005.

[131] P. G. de Gennes, *Superconductivity of Metals and Alloys*. Reading: Addison-Wesley, 1989.

[132] C. W. J. Beenakker, "Mesoscopic quantum physics," North-Holland, Amsterdam, 1995.

[133] J. S. Canizares and F. Sols, "Self-consistent current-voltage characteristics of normal-superconductor interfaces," *Journal of Physics-Condensed Matter*, vol. 7, no. 25, pp. L317–L323, 1995.

[134] J. SanchezCanizares and F. Sols, "Self-consistent scattering description of transport in normal-superconductor structures," *Physical Review B*, vol. 55, no. 1, pp. 531–543, 1997.

[135] R. Kummel, "Dynamics of current flow through phase-boundary between a normal and a superconducting region," *Zeitschrift Fur Physik*, vol. 218, no. 5, p. 472, 1969.

[136] F. Sols and J. Sanchez-Canizares, "Conductances in normal and normal/superconductor structures," *Superlattices and Microstructures*, vol. 25, no. 5-6, pp. 627–638, 1999.

[137] C. J. Lambert, "Generalized Landauer formulas for quasi-particle transport in disordered superconductors," *Journal of Physics-Condensed Matter*, vol. 3, no. 34, pp. 6579–6587, 1991.

[138] C. W. J. Beenakker, "Quantum transport in semiconductor-superconductor microjunctions," *Physical Review B*, vol. 46, no. 19, pp. 12841–12844, 1992.

[139] A. L. Yeyati, A. Martinrodero, and F. J. Garciavidal, "Self-consistent theory of superconducting mesoscopic weak links," *Physical Review B*, vol. 51, no. 6, pp. 3743–3753, 1995.

[140] H. Nakano and H. Takayanagi, "Second-quantization description of Andreev reflection and the relation to quasiparticle wave approaches," *Physical Review B*, vol. 50, no. 5, pp. 3139–3148, 1994.

[141] J. Sanchez-Canizares and F. Sols, "Self-consistent theory of transport in quasi-one-dimensional superconducting wires," *Journal of Low Temperature Physics*, vol. 122, no. 1-2, pp. 11–35, 2001.

[142] J. R. Kirtley, "Inelastic transport through normal-metal superconductor interfaces," *Physical Review B*, vol. 47, no. 17, pp. 11379–11383, 1993.

[143] J. Bardeen, "Tunnelling from a many-particle point of view," *Physical Review Letters*, vol. 6, no. 2, p. 57, 1961.

[144] G. D. Mahan, *Many-Particle Physics*. New York: Kluwer Academic/Plenum, 3 ed., 2000. page 561.

[145] P. V. Gray, "Tunneling from metal to semiconductors," *Physical Review*, vol. 140, no. 1A, p. A179, 1965.

[146] R. E. Prange, "Tunneling from a many-particle point of view," *Physical Review*, vol. 131, no. 3, p. 1083, 1963.

[147] A. Galindo and P. Pascual, *Quantum Mechanics*. Berlin: Springer, 1990.

[148] C. B. Duke, *Tunneling in Solids*. New York and London: Academic Press, 1969. page 218.

[149] C. J. Chen, "Tunneling matrix-elements in 3-dimensional space - the derivative rule and the sum-rule," *Physical Review B*, vol. 42, no. 14, pp. 8841–8857, 1990.

[150] E. Merzbacher, *Quantum Mechanics*. New York: John Wiley & Sons, 3 ed., 1998. Chapter 20.

[151] N. A. Mortensen, K. Flensberg, and A. P. Jauho, "Angle dependence of Andreev scattering at semiconductor-superconductor interfaces," *Physical Review B*, vol. 59, no. 15, pp. 10176–10182, 1999.

[152] R. Landauer, "Spatial variation of currents and fields due to localized scatterers in metallic conduction," *Ibm Journal of Research and Development*, vol. 1, no. 3, pp. 223–231, 1957.

[153] M. Buttiker, "4-terminal phase-coherent conductance," *Physical Review Letters*, vol. 57, no. 14, pp. 1761–1764, 1986.

[154] A. D. Stone and A. Szafer, "What is measured when you measure a resistance - the Landauer formula revisited," *Ibm Journal of Research and Development*, vol. 32, no. 3, pp. 384–413, 1988.

[155] Y. V. Sharvin, "A possible method for studying Fermi surfaces," *Soviet Physics Jetp-Ussr*, vol. 21, no. 3, p. 655, 1965.

[156] H. A. Bethe, "Theory of diffraction by small holes," *Physical Review*, vol. 66, no. 7-8, pp. 163–182, 1944.

[157] V. Ambegaokar and A. Baratoff, "Tunneling between superconductors," *Physical Review Letters*, vol. 10, no. 11, p. 486, 1963.

[158] F. W. J. Hekking and Y. V. Nazarov, "Subgap conductivity of a superconductor normal-metal tunnel interface," *Physical Review B*, vol. 49, no. 10, pp. 6847–6852, 1994.

[159] P. Samuelsson, E. V. Sukhorukov, and M. Buttiker, "Quasi-particle entanglement: redefinition of the vacuum and reduced density matrix approach," *New Journal of Physics*, vol. 7, p. 176, 2005.

[160] L. L. Chang, L. Esaki, and R. Tsu, "Resonant tunneling in semiconductor double barriers," *Applied Physics Letters*, vol. 24, no. 12, pp. 593–595, 1974.

[161] P. G. de Gennes and D. Saintjames, "Elementary excitations in the vicinity of a normal metal-superconducting metal contact," *Physics Letters*, vol. 4, no. 2, pp. 151–152, 1963.

[162] R. A. Riedel and P. F. Bagwell, "Current-voltage relation of a normal-metal-superconductor junction," *Physical Review B*, vol. 48, no. 20, pp. 15198–15208, 1993.

[163] S. Chaudhuri and P. F. Bagwell, "Andreev resonances inthe current-voltage characteristics of a normal-metal–superconductor junction," *Physical Review B*, vol. 51, no. 23, pp. 16936–16942, 1995.

[164] F. Giazotto, P. Pingue, and F. Beltram, "Coherent transport in Nb/delta-doped-GaAs hybrid microstructures," *Modern Physics Letters B*, vol. 17, no. 18, pp. 955–971, 2003.

[165] T. Akazaki, J. Nitta, and H. Takayanagi, "Single-crystal growth of Nb films onto molecular-beam epitaxy grown (001)Inas," *Applied Physics Letters*, vol. 59, no. 16, pp. 2037–2039, 1991.

[166] A. Kastalsky, A. W. Kleinsasser, L. H. Greene, R. Bhat, F. P. Milliken, and J. P. Harbison, "Observation of pair currents in superconductor-semiconductor contacts," *Physical Review Letters*, vol. 67, no. 21, pp. 3026–3029, 1991.

[167] J. R. Gao, J. P. Heida, B. J. Vanwees, S. Bakker, T. M. Klapwijk, and B. W. Alphenaar, "Low-temperature current transport of Sn-Gaas contacts," *Applied Physics Letters*, vol. 63, no. 3, pp. 334–336, 1993.

[168] C. Nguyen, H. Kroemer, and E. L. Hu, "Contact resistance of superconductor-semiconductor interfaces - the case of Nb-Inas/Alsb quantum-well structures," *Applied Physics Letters*, vol. 65, no. 1, pp. 103–105, 1994.

[169] R. Taboryski, T. Clausen, J. B. Hansen, J. L. Skov, J. Kutchinsky, C. B. Sorensen, and P. E. Lindelof, "Andreev reflections at interfaces between delta-doped GaAs and superconducting Al films," *Applied Physics Letters*, vol. 69, no. 5, pp. 656–658, 1996.

[170] S. De Franceschi, F. Giazotto, F. Beltram, L. Sorba, M. Lazzarino, and A. Franciosi, "Andreev reflection in Si-engineered Al/InGaAs hybrid junctions," *Applied Physics Letters*, vol. 73, no. 26, pp. 3890–3892, 1998.

[171] E. Toyoda, H. Takayanagi, and H. Nakano, "Systematic gate-controlled reentrant conductance of a superconductor-semiconductor two-dimensional electron gas junction," *Physical Review B*, vol. 59, no. 18, pp. R11653–R11656, 1999.

[172] I. E. Batov, T. Schapers, A. A. Golubov, and A. V. Ustinov, "Andreev reflection and enhanced subgap conductance in NbN/Au/InGaAs-InP junctions," *Journal of Applied Physics*, vol. 96, no. 6, pp. 3366–3370, 2004.

[173] H. Vanhouten, B. J. Vanwees, J. E. Mooij, C. W. J. Beenakker, J. G. Williamson, and C. T. Foxon, "Coherent electron focusing in a two-dimensional electron-gas," *Europhysics Letters*, vol. 5, no. 8, pp. 721–725, 1988.

[174] E. I. Rashba, "Properties of semiconductors with an extremum loop .1. cyclotron and combinational resonance in a magnetic field perpendicular to the plane of the loop," *Soviet Physics-Solid State*, vol. 2, no. 6, pp. 1109–1122, 1960.

[175] S. Datta and B. Das, "Electronic analog of the electrooptic modulator," *Applied Physics Letters*, vol. 56, no. 7, pp. 665–667, 1990.

[176] J. Schliemann, J. C. Egues, and D. Loss, "Nonballistic spin-field-effect transistor," *Physical Review Letters*, vol. 90, no. 14, p. 146801, 2003.

[177] O. Sauret, T. Martin, and D. Feinberg, "Spin-current noise and Bell inequalities in a realistic superconductor-quantum dot entangler," *Physical Review B*, vol. 72, no. 2, p. 024544, 2005.

[178] P. Samuelsson and M. Buttiker, "Chaotic dot-superconductor analog of the Hanbury Brown-Twiss effect," *Physical Review Letters*, vol. 89, no. 4, p. 046601, 2002.

[179] G. B. Lesovik, A. L. Fauchere, and G. Blatter, "Nonlinearity in normal-metal-superconductor transport: Scattering-matrix approach," *Physical Review B*, vol. 55, no. 5, pp. 3146–3154, 1997.

[180] J. A. Melsen and C. W. J. Beenakker, "Reflectionless tunneling through a double-barrier NS junction," *Physica B*, vol. 203, no. 3-4, pp. 219–225, 1994.

[181] S. Oh and J. Kim, "Entanglement of electron spins in superconductors," *Physical Review B*, vol. 71, no. 14, p. 144523, 2005.

[182] P. Samuelsson, "Energy dependent counting statistics in superconducting tunnel junctions," *Physical Review B*, vol. 67, no. 5, p. 054508, 2003.

[183] M. Wagner and F. Sols, "Subsea electron transport: Pumping deep within the Fermi sea," *Physical Review Letters*, vol. 83, no. 21, pp. 4377–4380, 1999.

[184] A. Altland, Y. Gefen, and G. Montambaux, "What is the Thouless energy for ballistic systems?," *Physical Review Letters*, vol. 76, no. 7, p. 1130, 1996.

[185] D. Quirion, C. Hoffmann, F. Lefloch, and M. Sanquer, "Mesoscopic proximity effect in double-barrier superconductor/normal-metal junctions," *Physical Review B*, vol. 65, p. 100508R, 2002.

[186] P. H. C. Magnee, N. Vanderpost, P. H. M. Kooistra, B. J. Vanwees, and T. M. Klapwijk, "Enhanced conductance near zero-voltage bias in mesoscopic superconductor-semiconductor junctions," *Physical Review B*, vol. 50, no. 7, pp. 4594–4599, 1994.

[187] W. Poirier, D. Mailly, and M. Sanquer, "Finite bias anomaly in the subgap conductance of superconductor-GaAs junctions," *Physical Review Letters*, vol. 79, no. 11, pp. 2105–2108, 1997.

[188] M. A. Nielsen and I. L. Chuang, *Quantum Computation and Quantum Information*. Cambridge, England: Cambridge University Press, 2000.

[189] A. Zeilinger, "Experiment and the foundations of quantum physics," *Reviews of Modern Physics*, vol. 71, no. 2, pp. S288–S297, 1999.

[190] A. Rauschenbeutel, G. Nogues, S. Osnaghi, P. Bertet, M. Brune, J. M. Raimond, and S. Haroche, "Step-by-step engineered multiparticle entanglement," *Science*, vol. 288, no. 5473, pp. 2024–2028, 2000.

[191] C. A. Sackett, D. Kielpinski, B. E. King, C. Langer, V. Meyer, C. J. Myatt, M. Rowe, Q. A. Turchette, W. M. Itano, D. J. Wineland, and I. C. Monroe, "Experimental entanglement of four particles," *Nature*, vol. 404, no. 6775, pp. 256–259, 2000.

[192] *Semiconductor Spintronics and Quantum Computation*. Series on Nanoscience and Technology, Berlin: Springer-Verlag, 2002.

[193] C. W. J. Beenakker and M. Kindermann, "Quantum teleportation by particle-hole annihilation in the Fermi sea," *Physical Review Letters*, vol. 92, no. 5, p. 056801, 2004.

[194] P. Samuelsson and M. Buttiker, "Dynamic generation of orbital quasiparticle entanglement in mesoscopic conductors," *Physical Review B*, vol. 71, no. 24, p. 245317, 2005.

[195] D. S. Saraga, B. L. Altshuler, D. Loss, and R. M. Westervelt, "Coulomb scattering cross section in a two-dimensional electron gas and production of entangled electrons," *Physical Review B*, vol. 71, no. 4, p. 045338, 2005.

[196] M. Buttiker, Y. Imry, and M. Y. Azbel, "Quantum oscillations in one-dimensional normal-metal rings," *Physical Review A*, vol. 30, no. 4, pp. 1982–1989, 1984.

[197] S. Datta, *Electronic Transport in Mesoscopic Systems*. Cambridge, England: Cambridge University Press, 1995.

[198] A. Brataas, Y. V. Nazarov, and G. E. W. Bauer, "Spin-transport in multi-terminal normal metal-ferromagnet systems with non-collinear magnetizations," *European Physical Journal B*, vol. 22, no. 1, pp. 99–110, 2001.

[199] B. A. Muzykantskii and D. E. Khmelnitskii, "Quantum shot-noise in a normal-metal superconductor point-contact," *Physical Review B*, vol. 50, no. 6, pp. 3982–3987, 1994.

[200] L. S. Levitov and G. B. Lesovik, "Charge-distribution in quantum shot-noise," *Jetp Letters*, vol. 58, no. 3, pp. 230–235, 1993.

[201] L. S. Levitov, H. Lee, and G. B. Lesovik, "Electron counting statistics and coherent states of electric current," *Journal of Mathematical Physics*, vol. 37, no. 10, pp. 4845–4866, 1996.

[202] S. J. Freedman and J. F. Clauser, "Experimental test of local hidden-variable theories," *Physical Review Letters*, vol. 28, no. 14, p. 938, 1972.

[203] A. Aspect, P. Grangier, and G. Roger, "Experimental tests of realistic local theories via Bell's theorem," *Physical Review Letters*, vol. 47, no. 7, pp. 460–463, 1981.

[204] A. Aspect, P. Grangier, and G. Roger, "Experimental realization of Einstein-Podolsky-Rosen-Bohm Gedankenexperiment - a new violation of Bell inequalities," *Physical Review Letters*, vol. 49, no. 2, pp. 91–94, 1982.

[205] A. Aspect, J. Dalibard, and G. Roger, "Experimental test of Bell inequalities using time-varying analyzers," *Physical Review Letters*, vol. 49, no. 25, pp. 1804–1807, 1982.

[206] W. Tittel, J. Brendel, H. Zbinden, and N. Gisin, "Violation of Bell inequalities by photons more than 10 km apart," *Physical Review Letters*, vol. 81, no. 17, pp. 3563–3566, 1998.

[207] G. Weihs, T. Jennewein, C. Simon, H. Weinfurter, and A. Zeilinger, "Violation of Bell's inequality under strict Einstein locality conditions," *Physical Review Letters*, vol. 81, no. 23, pp. 5039–5043, 1998.

[208] "Bell test experiments," *Wikipedia*, 2006. http://en.wikipedia.org/wiki/Bell_test_experiments.

[209] J. Tobiska and Y. V. Nazarov, "Josephson junctions as threshold detectors for full counting statistics," *Physical Review Letters*, vol. 93, no. 10, p. 106801, 2004.

[210] J. P. Pekola, "Josephson junction as a detector of poissonian charge injection," *Physical Review Letters*, vol. 93, no. 20, p. 206601, 2004.

[211] S. Gustavsson, R. Leturcq, B. Simovic, T. Ihn, P. Studerus, and K. Ensslin, "Counting statistics of single-electron transport in a quantum dot," *Preprint archive cond-mat/0510269*, 2005.

[212] I. Zutic, J. Fabian, and S. Das Sarma, "Spintronics: Fundamentals and applications," *Rev. Mod. Phys.*, vol. 76, no. 2, pp. 323–410, 2004.

[213] V. N. Golovach, A. Khaetskii, and D. Loss, "Phonon-induced decay of the electron spin in quantum dots," *Physical Review Letters*, vol. 93, no. 1, p. 016601, 2004.

[214] P. Recher, E. V. Sukhorukov, and D. Loss, "Quantum dot as spin filter and spin memory," *Physical Review Letters*, vol. 85, no. 9, pp. 1962–1965, 2000.

[215] P. G. Kwiat, K. Mattle, H. Weinfurter, A. Zeilinger, A. V. Sergienko, and Y. Shih, "New high-intensity source of polarization-entangled photon pairs," *Physical Review Letters*, vol. 75, no. 24, pp. 4337–4341, 1995.

[216] MagiQ. http://www.magiqtech.com.

[217] R. Hanson, L. M. K. Vandersypen, L. H. W. van Beveren, J. M. Elzerman, I. T. Vink, and L. P. Kouwenhoven, "Semiconductor few-electron quantum dot operated as a bipolar spin filter," *Physical Review B*, vol. 70, no. 24, p. 241304(R), 2004.

[218] H. Ohno, "Making nonmagnetic semiconductors ferromagnetic," *Science*, vol. 281, no. 5379, pp. 951–956, 1998.

[219] T. Koga, J. Nitta, H. Takayanagi, and S. Datta, "Spin-filter device based on the Rashba effect using a nonmagnetic resonant tunneling diode," *Physical Review Letters*, vol. 88, no. 12, p. 126601, 2002.

[220] Y. Kato, R. C. Myers, A. C. Gossard, and D. D. Awschalom, "Coherent spin manipulation without magnetic fields in strained semiconductors," *Nature*, vol. 427, no. 6969, pp. 50–53, 2004.

[221] J. C. Egues, B. Guido, D. S. Saraga, S. John, and L. Daniel, "Shot noise and spin-orbit coherent control of entangled and spin-polarized electrons," *Physical Review B*, vol. 72, no. 23, p. 235326, 2005.

[222] J. B. Miller, D. M. Zumbuhl, C. M. Marcus, Y. B. Lyanda-Geller, D. Goldhaber-Gordon, K. Campman, and A. C. Gossard, "Gate-controlled spin-orbit quantum interference effects in lateral transport," *Physical Review Letters*, vol. 90, no. 7, p. 076807, 2003.

[223] R. dePicciotto, M. Reznikov, M. Heiblum, V. Umansky, G. Bunin, and D. Mahalu, "Direct observation of a fractional charge," *Nature*, vol. 389, no. 6647, pp. 162–164, 1997.

[224] L. Saminadayar, D. C. Glattli, Y. Jin, and B. Etienne, "Observation of the e/3 fractionally charged Laughlin quasiparticle," *Physical Review Letters*, vol. 79, no. 13, pp. 2526–2529, 1997.

[225] X. Jehl, P. Payet-Burin, C. Baraduc, R. Calemczuk, and M. Sanquer, "Andreev reflection enhanced shot noise in mesoscopic SNS junctions," *Physical Review Letters*, vol. 83, no. 8, pp. 1660–1663, 1999.

[226] A. A. Kozhevnikov, R. J. Schoelkopf, and D. E. Prober, "Observation of photon-assisted noise in a diffusive normal metal-superconductor junction," *Physical Review Letters*, vol. 84, no. 15, pp. 3398–3401, 2000.

[227] M. Reznikov, M. Heiblum, H. Shtrikman, and D. Mahalu, "Temporal correlation of electrons - suppression of shot-noise in a ballistic quantum point-contact," *Physical Review Letters*, vol. 75, no. 18, pp. 3340–3343, 1995.

[228] A. Kumar, L. Saminadayar, D. C. Glattli, Y. Jin, and B. Etienne, "Experimental test of the quantum shot noise reduction theory," *Physical Review Letters*, vol. 76, no. 15, pp. 2778–2781, 1996.

[229] M. Henny, S. Oberholzer, C. Strunk, and C. Schonenberger, "1/3-shot-noise suppression in diffusive nanowires," *Physical Review B*, vol. 59, no. 4, pp. 2871–2880, 1999.

[230] S. Oberholzer, E. V. Sukhorukov, and C. Schoenenberger, "Crossover between classical and quantum shot noise in chaotic cavities," *Nature*, vol. 415, no. 6873, pp. 765–767, 2002.

[231] B. Reulet, J. Senzier, and D. E. Prober, "Environmental effects in the third moment of voltage fluctuations in a tunnel junction," *Physical Review Letters*, vol. 91, no. 19, p. 196601, 2003.

[232] M. Henny, S. Oberholzer, C. Strunk, T. Heinzel, K. Ensslin, M. Holland, and C. Schonenberger, "The fermionic Hanbury Brown and Twiss experiment," *Science*, vol. 284, no. 5412, pp. 296–298, 1999.

[233] W. D. Oliver, J. Kim, R. C. Liu, and Y. Yamamoto, "Hanbury Brown and Twiss-type experiment with electrons," *Science*, vol. 284, no. 5412, pp. 299–301, 1999.

[234] H. Kiesel, A. Renz, and F. Hasselbach, "Observation of Hanbury Brown-Twiss anticorrelations for free electrons," *Nature*, vol. 418, no. 6896, pp. 392–394, 2002.

[235] F. Sols, M. Macucci, U. Ravaioli, and K. Hess, "Theory for a quantum modulated transistor," *Journal of Applied Physics*, vol. 66, no. 8, pp. 3892–3906, 1989.

[236] V. S. W. Chung, P. Samuelsson, and M. Buttiker, "Visibility of current and shot noise in electrical Mach-Zehnder and Hanbury Brown Twiss interferometers," *Physical Review B*, vol. 72, no. 12, p. 125320, 2005.

[237] T. Martin and R. Landauer, "Wave-packet approach to noise in multichannel mesoscopic systems," *Physical Review B*, vol. 45, no. 4, pp. 1742–1755, 1992.

[238] A. Shelankov and J. Rammer, "Charge transfer counting statistics revisited," *Europhysics Letters*, vol. 63, no. 4, pp. 485–491, 2003.

[239] Y. V. Nazarov, "Universalities of weak localization," *Ann. Phys. (Leipzig)*, vol. 8, pp. SI–193, 1999.